TRANSACTIONS
OF THE ASME
Series B

Journal of ENGINEERING FOR INDUSTRY

August 1959

Divisions: AVIATION • MACHINE DESIGN • MANAGEMENT • PROCESS INDUSTRIES MAINTENANCE AND PLANT ENGINEERING • RAILROAD • PRODUCTION ENGINEERING MATERIALS HANDLING • RUBBER AND PLASTICS • PETROLEUM • SAFETY • TEXTILE WOOD INDUSTRIES • Research Committees: METAL PROCESSING • FLOW OF BULK MATERIALS • ELEVATORS • MECHANICAL SPRINGS

Published Quarterly by
THE AMERICAN SOCIETY OF MECHANICAL ENGINEERS

TRANSACTIONS OF THE ASME
Series B

Journal of
ENGINEERING FOR INDUSTRY

VOLUME 81 • SERIES B • NUMBER 3
August 1959

CONTENTS

187 **Factors Influencing the Performance of Grinding Wheels**
E. J. Krabacher

201 **Vibrations of Flexible Precision Grinding Spindles**
R. S. Hahn

207 **The Effect of Process Variables on Extrusion Pressures of Lead**
J. Frisch and E. G. Thomsen

217 **Approximate Solutions to a Problem of Press Forging**
S. Kobayashi and E. G. Thomsen

228 **Theory and Experiment of Press Forging Axisymmetric Parts of Aluminum and Lead**
S. Kobayashi, R. Herzog, J. T. Lapsley, Jr., and E. G. Thomsen

239 **A Three-Dimensional, Tool-Life-Equation—Machining Economics**
B. N. Colding

251 **Some Observations on the Shearing Process in Metal Cutting**
S. Kobayashi and E. G. Thomsen

263 **Observations on the Angle Relationships in Metal Cutting**
D. M. Eggleston, R. Herzog, and E. G. Thomsen

EDITORIAL DEPARTMENT

Editor, J. J. JAKLITSCH, JR.
Editor Emeritus, GEORGE A. STETSON
Consulting Editor, LEO BLODGETT
Production, JEAN NORTH
Art Editor, HENRY BALFOUR

OFFICERS OF THE ASME

President, G. B. WARREN
Secretary, O. B. SCHIER, II
Treasurer, E. J. KATES
Assistant Treasurer, H. J. BAUER

PUBLICATIONS COMMITTEE

Chairman, JOHN de S. COUTINHO
B. G. A. SKROTZKI
HENDLEY N. BLACKMON
R. D. MINDLIN
MARTIN GOLAND

Junior Representatives
A. T. WUSKA
A. S. GOLDSTEIN

REGIONAL ADVISORY BOARD

Region I, ROY L. PARSELL
Region II, GLENN R. FRYLING
Region III, F. J. HEINZE
Region IV, FRANCIS C. SMITH
Region V, H. M. CATHER
Region VI, C. R. EARLE
Region VII, M. POPOVICH
Region VIII, LINN HELANDER

Published quarterly by The American Society of Mechanical Engineers. Publication office at 20th and Northampton Streets, Easton, Pa. The editorial department is located at the headquarters of the Society, 29 West Thirty-Ninth Street, New York 18, N. Y. Cable address, "Mechaneer," New York. Price $3.00 a copy, $10.00 annually; to members, $1.50 a copy, $5.00 annually. Add 50 cents for postage to all countries outside the United States and Canada. Changes of address must be received at Society headquarters seven weeks before they are to be effective on the mailing list. Please send old as well as new address. . . . By-Law: The Society shall not be responsible for statements or opinions advanced in papers or . . . printed in its publications (B13, Par. 4). . . . Second-class mail privileges authorized at Easton, Penna. . . . This publication is authorized to be mailed at the special rates of postage prescribed by Section 132.122 . . . © Copyrighted, 1959, by The American Society of Mechanical Engineers. Reprints from this publication may be made on condition that full credit be given the Transactions of the ASME, Series B—Journal of Engineering for Industry, and the author, and that date of publication be stated.

TRANSACTIONS OF THE ASME
is indexed by the Engineering Index, Inc.

TRANSACTIONS OF THE ASME Series C

Journal of
HEAT TRANSFER
Vol. 81 • Series C • No. 3

CONTENTS FOR AUGUST, 1959

175 Heat Transfer Between Concentric Rotating Cylinders, by I. S. Bjorklund and W. M. Kays. (58—A-99)

187 Full-Scale Human-Body-Model Thermal Exchange Compared With Equational Condensations of Human Calorimetric Data, by L. P. Herrington. (58—A-181)

195 The Emissivity and Absorptivity of Parachute Fabrics, by J. P. Hartnett, E. R. G. Eckert, and R. Birkebak. (58—A-125)

202 An Experimental and Analytical Study of Vortex-Flow Temperature Separation by Superposition of Spiral and Axial Flows—Part I, by J. E. Lay. (58—SA-71)

213 An Experimental and Analytical Study of Vortex-Flow Temperature Separation by Superposition of Spiral and Axial Flows—Part II, by J. E. Lay. (58—A-90)

223 Analysis of the Aerodynamic Heating for a Re-Entrant Space Vehicle, by M. J. Brunner. (59—Av-5)

230 A Photographic Study of Boiling in the Absence of Gravity, by R. Siegel and C. Usiskin. (59—Av-37)

237 Some Radiator Design Criteria for Space Vehicles, by J. P. Callinan and W. P. Berggren. (59—Av-29)

245 Optimization of a Conventional-Fuel-Fired Thermoelectric Generator, by B. W. Swanson and E. V. Somers. (59—SA-14)

Technical Briefs

249 Heat Transfer From a Rotating Disk to Fluids of Any Prandtl Number, by E. M. Sparrow and J. L. Gregg.

251 An Approximate Treatment of Unsteady Heat Conduction in Semi-Infinite Solids With Variable Thermal Properties, by K.-T. Yang and Albin Szewczyk.

TRANSACTIONS OF THE ASME Series A

Journal of
ENGINEERING FOR POWER
Volume 81 • Series A • Number 3

CONTENTS FOR JULY, 1959

1958 Gas Turbine Progress Report

215 Introduction, by R. T. Sawyer. (58—A-46 A)

219 Materials, by A. W. Herbenar and G. R. Heckman. (58—A-46 B)

226 Turbine Cooling, by J. B. Esgar. (58—A-46 C)

234 Fuels, by A. D. Foster. (58—A-46 D)

244 Cycle Components, by P. F. Martinuzzi. (58—A-46 E)

259 Compound Piston-and-Turbine Engines, by A. L. London. (58—A-46 F)

265 Aviation, by O. E. Lancaster. (58—A-46 G)

280 Rocket Turbines, by O. E. Lancaster and C. J. Bates. (58—A-46 H)

290 Automotive, by F. L. Schwartz. (58—A-46 I)

298 Railroad, by P. R. Broadley, W. M. Meyer, D. S. Neuhart, E. L. Barlow, R. C. Bond, D. S. D. Williams, and B. W. C. Cooke. (58—A-46 J)

311 Marine, by J. W. Sawyer and H. M. Simpson. (58—A-46 K)

344 Industrial and Central Station, by B. G. A. Skrotski. (58—A-46 L)

352 Nuclear, by R. P. Godwin and E. S. Dennison. (58—A-46 M)

TRANSACTIONS OF THE ASME Series D

Journal of
BASIC ENGINEERING
Vol. 81 • Series D • No. 2

CONTENTS FOR JUNE, 1959

101 Elastic and Damping Properties of Cylindrical Journal Bearings, by B. Sternlicht. (58—Lub-3)

109 Axial, Relative Motion of a Circular Step Bearing, by L. Licht. (58—Lub-1)

118 Friction and Wear of Metals to 1000 C, by E. P. Kingsbury and E. Rabinowicz. (58—Lub-6)

123 Friction Factors for Turbulent Flow in Curved Pipes, by H. Ito. (58—SA-14)

135 Characteristics of a Self-Lubricated Stepped Thrust Pad of Infinite Width With Compressible Lubricant, by K. C. Kochi. (58—A-194)

147 Direct Measurement of Net Positive Suction Head, by R. B. Jacobs, K. B. Martin, and R. J. Hardy. (58—A-38)

153 Transitional Phenomena in Ultrasonic Shock Waves Emitted by Cavitation on Hydrofoils, by F. Numachi. (58—A-117)

167 Cavitation and NPSH Requirements of Various Liquids, by Victor Salemann. (58—A-82)

181 The Unsteady Wake Interaction in Turbomachinery and Its Effect on Cavitation, by Hsuan Yeh and J. J. Eisenhuth. (58—A-114)

190 Thermal-Stress Ratchet Mechanism in Pressure Vessels, by D. R. Miller. (58—A-129)

197 Refractory Metal Facings for Protection of Metal Surfaces Subjected to Repeated High-Temperature Pulses, by Aaron Cohen and Edward Homer. (58—A-188)

203 The Failure of Structural Metals Subjected to Strain-Cycling Conditions, by R. W. Swindeman and D. A. Douglas. (58—A-198)

213 Evaluation of Material Wear and Self-Welding in Sodium-Cooled Reactor Systems, by R. B. Jerman, R. C. Williams, and D. O. Leeser.

226 Irradiation of Haynes-25 and Inconel-X Compression Springs in High-Temperature High-Pressure Water, by R. C. Mehan. (58—A-94)

233 Energy Losses of Balls Rolling on Plates, by R. C. Drutowski. (58—A-190)

239 On the Effect of Lubricant Inertia in the Theory of Hydrodynamic Lubrication, by A. A. Milne. (58—A-195)

245 Surface Finish and Clearance Effects on Journal-Bearing Load Capacity and Friction, by F. W. Ocvirk and G. B DuBois. (58—A-134)

254 Statistical Optimization of Regulators Employing a Binary Error Criterion, by J. H. Milsum. (58—A-71)

263 An Introduction to the Time-Modulated Acceleration Switching Electrohydraulic Servomechanism, by S. A. Murtaugh, Jr. (58—A-159)

272 Discussion on previously published paper by B. Sternlicht and R. C. Elwell.

TRANSACTIONS OF THE ASME Series E

Journal of
APPLIED MECHANICS
Vol. 81 • Series E • No. 2

CONTENTS FOR JUNE, 1959

TECHNICAL PAPERS

161 Effect of a Nonisothermal Free Stream on Boundary-Layer Heat Transfer, E. M. Sparrow and J. L. Gregg. (58—A-42)

166 Visual Studies of the Wall Layers in the Turbulent Boundary Layer, S. J. Kline and P. W. Runstadler. (58—A-64)

171 Unsteady Laminar Boundary Layers Over an Arbitrary Cylinder, Kwang-Tzu Yang. (58—A-49)

179 On Journal Bearings of Finite Length With Variable Viscosity, L. N. Tao. (58—A-75)

184 Analysis of Complex Kinematic Chains With Influence Coefficients, J. Modrey. (58—A-74)

187 A Theory of Oil Whip, Yukio Hori. (59—APM-2)

199 On Critical Speeds of a Shaft Supported by a Ball Bearing, Toshio Yamamoto. (59—APM-12)

205 Root-Locus Analysis of Structural Coupling in Control Systems, R. H. Cannon, Jr. (58—A-65)

210 Normal Vibrations of Uniform Plate Carrying Any Number of Finite Masses, W. F. Stokey and C. F. Zorowski. (58—A-28)

217 Transients in Simple Undamped Oscillators Under Inertial Disturbances, Antongiulio Dornig. (58—A-58)

224 On Laterally Loaded Semicircular Plate With Clamped Edges, W. H. Jurney. (59—APM-3)

227 Direct Determination of Stresses in Plane Elasticity Problems, P. S. Theocaris. (58—A-43)

235 Stresses in a Stretched Slab Having a Spherical Cavity, Chih-Bing Ling. (58—A-45)

241 Influence Coefficients for Edge-Loaded Short, Thin, Conical Frustums, J. H. Baltrukonis

246 Upper and Lower Bounds for Special Eigenvalues, F. C. Appl and C. F. Zorowski. (59—APM-18)

251 Analysis of a Compression Test of a Model of a Granular Medium, C. W. Thurston and H. Deresiewicz. (58—A-48)

259 A Reassessment of Deformation Theories of Plasticity, Bernard Budiansky. (58—A-54)

265 Collapse Loads of Rings and Flanges Under Uniform Twisting Moment, Burton Paul. (58—A-55)

271 Creep of Thick-Walled Tubes Under Internal Pressure, F. P. J. Rimrott. (59—APM-6)

276 Strain-Hardening Solutions to Plate Problems, Nicholas Perrone and P. G. Hodge, Jr.

285 Determination of Creep Deflection of a Rivet in Double Shear, Joseph Marin. (58—A-47)

DESIGN DATA AND METHODS

290 The Frequency of Vibration of Rectangular Isotropic Plates, H. J. Fletcher

BRIEF NOTES

291 Large Deflections of a Clamped Elliptical Plate, W. A. Nash and I. D. Cooley. **293** Thermal Stresses at Spherical Cavities, A. L. Florence and J. N. Goodier. **294** Deflection of a Thick Ring in Diametral Compression, Alexander Blake. **296** The Biot-Willis Coefficients for a Sandstone, I. Fatt. **297** Circular Plates on Elastic Foundation, G. D. Galletly. **298** Frequencies of Vibration of Stiffened Plates, R. L. Thorkildsen and W. H. Hoppmann, II. **300** Design of a π Network for Heat-Flow Analog, D. G. Stephenson and G. O. Starke. **301** Stress Distribution in a Square Tube, M. A. Sadowsky and E. E. Zwicky, Jr.

DISCUSSION

303 Discussion of previously published papers by R. H. Cannon, Jr.; C. G. van Niekerk; M. Hetenyi and P. H. McDonald, Jr.; K. A. Foss; N. J. Huffington, Jr., and W. H. Hoppmann, II; T. J. Harvey; H. Tramposch and G. Gerard; C. E. Crede; C. J. Ancker, Jr., and J. N. Goodier; H. Poritsky and F. A. Fend; K. L. Johnson; J. H. Haywood and L. B. Wilson.

317 **BOOK REVIEWS**

Factors Influencing the Performance of Grinding Wheels

E. J. KRABACHER

Senior Research Supervisor, Physical Research Department, Cincinnati Milling Machine Company, Cincinnati, Ohio. Assoc. Mem. ASME

Optimum utilization of grinding wheels can best be achieved if the nature of their performance and wear characteristics, and the factors that affect these characteristics, are understood and applied. As reported in this paper, a comprehensive, continuing, grinding-research program has contributed to such an understanding.

A study of the nature of grinding-wheel wear indicates that the grinding-wheel wear curve is similar to those of other cutting tools. It demonstrates further that the type of grinding operation significantly affects the nature of wheel wear. A unique technique has been developed for very accurately measuring grinding-wheel wear. This measured wear may be translated into terms of "grinding ratio," which is the generally accepted parameter for measuring wheel wear. It is the ratio of the volume of metal removed per unit volume of wheel worn away.

Extensive studies have been carried out to determine the effect of mechanical variables on grinding ratio, power required in metal removal, and on surface finish. Experimental findings indicate that grinding ratio decreases with increased metal-removal rate and increases with workpiece diameter, decreased chip load, and increased concentration of grinding fluid. Power is found to increase with both the metal-removal rate and the amount of metal removed. It increases slightly with workpiece diameter and is affected little by work-material hardness. Surface finish is found to improve with decreased metal-removal rate and decreased chip load. It also is affected little by work diameter or work-material hardness.

Fundamental research in the mechanics of wheel wear is supplying much additional information in the study of grinding-wheel wear. The measurement of grinding forces employing a cylindrical grinding dynamometer provides the opportunity for relating the wear of grinding wheels to the basic mechanics of the process through such fundamental quantities as grinding forces, specific energy, and grinding friction.

Two additional experimental techniques for the study of chip formation in grinding have also proved to be most useful research tools. A "quick-stop" apparatus is used to freeze the grinding action by accelerating a tiny workpiece almost instantaneously to grinding-wheel speed. Another technique permits the comparison of the shape of the grinding grit and that of the contour of its path through the workpiece by a unique replicating method.

Introduction

THE GRINDING OPERATION is one of the most important means by which metal may be removed and fine finishes obtained, yet the process by which a grinding wheel wears is undoubtedly more complex than that of any other metal-cutting tool. This is true primarily because of the very complicated and indeterminate geometrical nature of the grinding wheel. Its cutting elements are not of controlled geometry as are those of the other metal-cutting tools but rather a composite random arrangement of literally thousands of tiny cutting edges of nearly as many complex geometries. Yet, these tools of vastly different shapes must perform under identical conditions to produce parts of fine finish and precision. If optimum utilization of these bonded-abrasive systems is to be achieved, it is necessary that the nature of their performance and wear characteristics and the factors that affect these characteristics be understood.

In order to investigate these problems a comprehensive, continuing grinding-research program has been undertaken within the Physical Research Department of the author's company. It provides a well integrated basic and applied approach to this very important problem of grinding-wheel wear. This paper presents some of the important results obtained and the understanding achieved to date.

Contributed by the Production Engineering Division and presented at the Semi-Annual Meeting, Detroit, Mich., June 15–19, 1958, of THE AMERICAN SOCIETY OF MECHANICAL ENGINEERS.

NOTE: Statements and opinions advanced in papers are to be understood as individual expressions of their authors and not those of the Society. Manuscript received at ASME Headquarters, March 31, 1958. Paper No. 58—SA-40.

The Grinding Wheel

The grinding wheel is a bonded abrasive body consisting usually of Al_2O_3 or SiC abrasive grain in a matrix of ceramic, resinoid, or rubber bond. Only the ceramic (vitrified) bonded wheel will be discussed here as it is the type of wheel used on the large majority of precision grinding operations.

Wheels are available in different grit size and type and in different wheel grades and structures, that is, amounts of bond and porosity, both of which affect the performance and wear characteristics of the wheel. The periphery of the wheel presents many small grits (cutting tools) to the workpiece during each revolution. As shown in Fig. 1, these grits are essentially of random geometry and remove tiny chips similar to those formed with other metal cutting tools. The character of the chips formed varies greatly depending upon the geometry of the grit which forms them, as well as other physical considerations. Fig. 2 illustrates a random chip sample which shows both excellently and poorly formed grinding chips obtained during the grinding of titanium.

The Nature of Wheel Wear

The wear of grinding wheels is both physical and chemical in nature. The relative significance of each of these types in the over-all wear depends upon the grinding-wheel work-material combination, and geometrical and mechanical conditions existing in the particular grinding operation. The nature of these wear phenomena with respect to the abrasive grit will be discussed here only in such detail as is required to explain the relationship established between wheel wear and other quantities in the experimental data presented later in this paper.

Grinding wheels have been found to wear in much the same manner as do cutting tools. However, the rate of wear of the grinding wheel with respect to the volume of metal removed is found to be approximately a million times that of a cutting tool [1].[1] The curve relating volume of wheel wear versus volume of metal removed, Fig. 3, is found to be quite similar in shape to a complete wear curve of any cutting tool. It may be seen that during the initial contact between wheel and workpiece, after dressing, the rate of wear is extremely high, while throughout the next portion of the process the rate of wear remains constant. The latter is the normal operating portion of the wheel-wear curve. As grinding proceeds and the abrasive grit makes repeated contacts with the workpiece the sharp edges are worn away producing flat areas on the grit, that is, "attritious wear." As this process continues further and the flat area on the grit increases, the force on the grit also increases until it becomes sufficient to cause it to fracture producing new cutting edges, or to rupture the bond post throwing the grit out of the wheel. This is known as "fracture wear" [2]. It is at this point on the curve, when a large percentage of the active grits reach this condition, that the wear rate increases sharply. If the bond posts are too strong or the grain is not sufficiently friable, the

[1] Numbers in brackets designate References at end of paper.

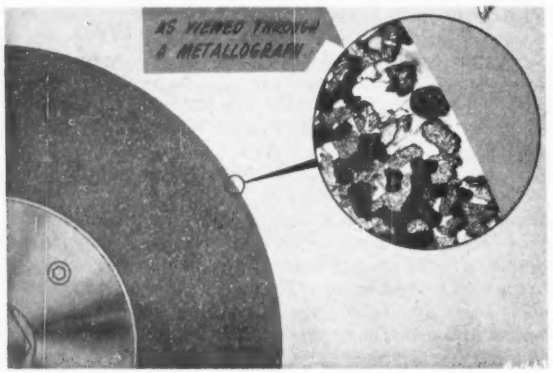

Fig. 1 Typical section indicating the nature of grit geometry existing at the periphery of the grinding wheel

Fig. 2 Random chip sample showing both excellently and poorly formed grinding chips obtained during the grinding of titanium

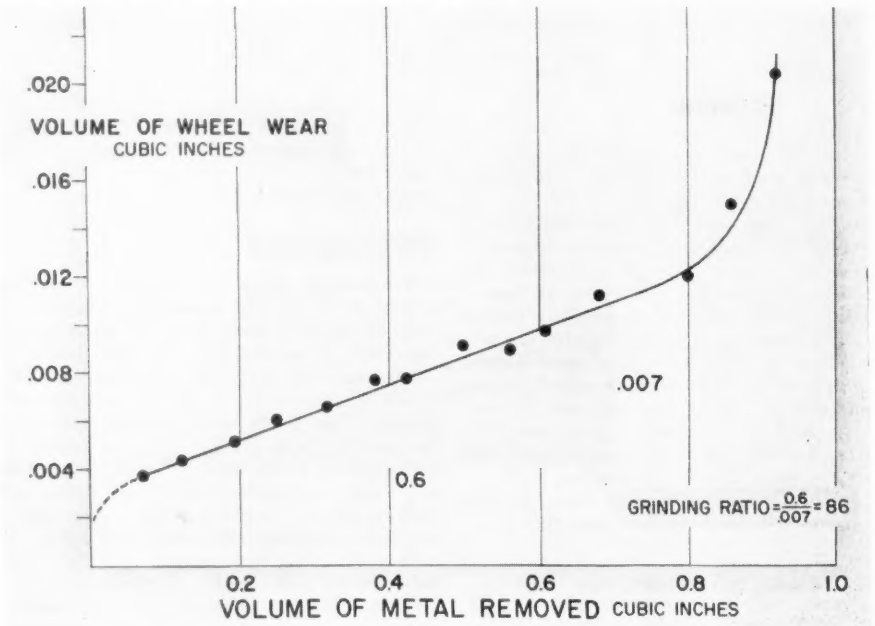

Fig. 3 Grinding-wheel wear curve indicating the nature of grinding-wheel wear

dulled grain will remain. This condition gives a glazed appearance to the wheel face and redressing of the wheel is required to restore sharpness. If, however, the wheel is properly graded and suited to the job, the nature and proportion of attritious and fracture wear will be such that the wheel will tend to be self dressing.

The grade of a wheel is a measure of the amount of bond supporting the grinding grits and is therefore a measure of bond-post strength. It follows that the harder grade wheel will permit the grits to become duller prior to bond-post rupture causing the wheel to assume a less free-cutting equilibrium condition than that of a softer wheel. Thus a wheel which is too hard will tend to glaze and eventually cause chatter while a wheel which is too soft will break down quite rapidly.

The structure of the wheel is related to the grit spacing and thus to chip-clearance space. For the same amount of bond material (same grade), a more dense wheel tends to act somewhat harder than one of open structure. In general it also requires somewhat more power, tends to load more readily, and to put more heat into the workpiece. However, too open a structure will tend to cause more rapid wheel breakdown due to heavier chip loading of the grits and will yield poorer finishes. The proper selection of wheel grade and structure is the first requirement for an efficient grinding operation.

Measurement of Wheel Wear

The generally accepted parameter of grinding-wheel wear is the grinding ratio. It is defined as the ratio of the volume of metal removed per unit volume of wheel worn away. Earlier research has indicated, however [1], that, due to the initial wheel breakdown evident in Fig. 3, a single datum point is not sufficient to establish this parameter. As the amount of metal removed increases, the ratio approaches the reciprocal of the slope of the wear curve. This reciprocal of the wear-curve slope has proved to be the useful index of grinding-wheel wear and may be obtained directly from the wear curve. An example is given in Fig. 3 where the grinding ratio as measured from the slope of this curve is found to be 86.

The method for determining the volume of grinding-wheel wear is to measure the incremental change in wheel radius for a given amount of workpiece removal. Knowing the initial wheel radius, the incremental change in this radius, and the width of wheel face, the volume of wheel wear can be computed.

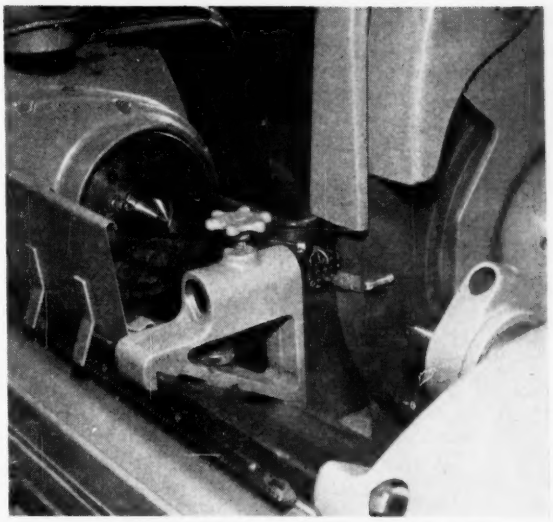

Fig. 4 Electric strain-gage transducer for measurement of grinding-wheel wear

Except for small wheels, a direct measurement of wheel diameter is an unsatisfactory method of measuring wheel wear since the change in diameter is too small a portion of the total dimension to permit sufficient accuracy. However, it has been found that, if a reference surface can be established near the outside of the wheel, the difference between the level of the wheel face and the reference surface can be measured quite accurately.

Fig. 4 shows an electric strain-gage transducer for grinding-wheel wear measurements, designed in the author's laboratories. The transducer is simply a cantilever beam with strain gages mounted at its root and a contactor at its face end. The contactor, which is a hardened steel ball with a small flat ground on it, traverses both the wheel face and the reference surface, determining the amount of radial wheel wear by measuring the change in step height between the wheel face and the reference surface. The reference surface may be either an unused portion of the wheel face, a dressed-down portion of the wheel face, or a separate surface attached to the wheel face such as the ceramic

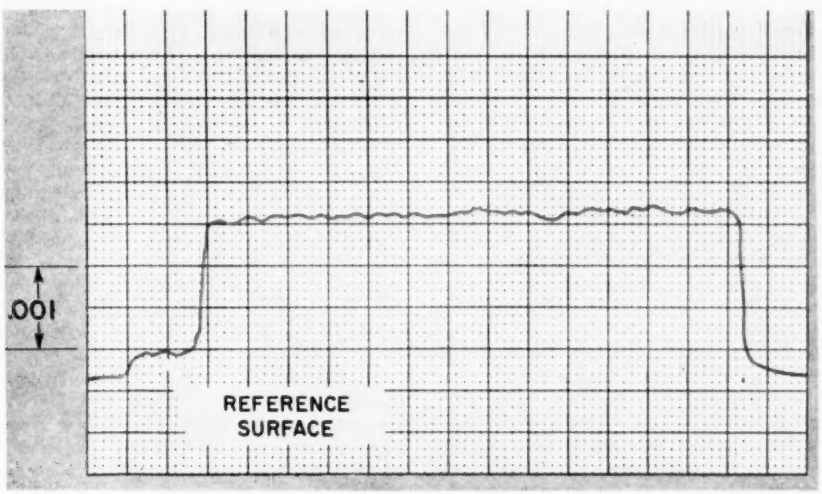

Fig. 5 Grinding-wheel wear chart

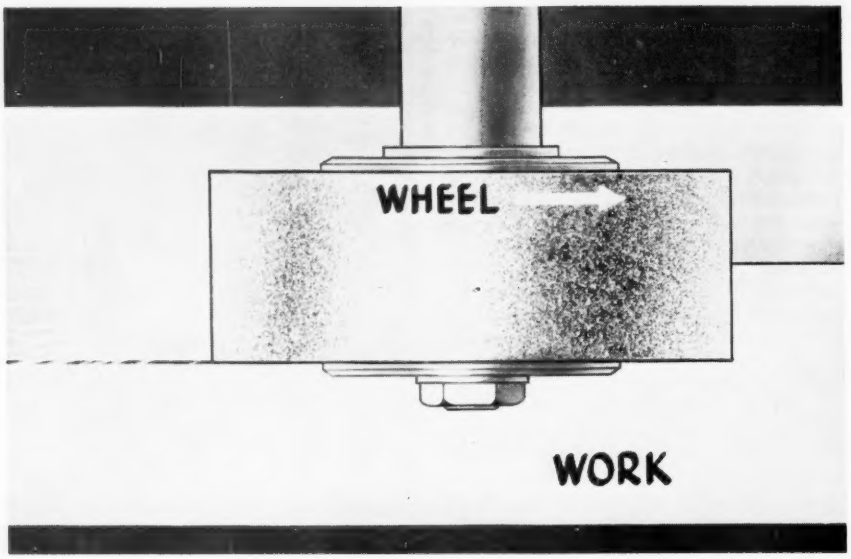

Fig. 6 Surface grinding operation

block used in Fig. 4. Reference surfaces other than those integral with the wheel face can lead to error due to thermal distortions or deflections in the spindle and its mounts as the wheel is stopped. The chart in Fig. 5 was obtained from the setup of Fig. 4. Here the wheel face is dressed initially and the ceramic reference surface is then dressed about 0.002 in. below the wheel face. A zero reading is taken and subsequent wear is found by the change in step height on the chart. This method measures radial wheel wear to an accuracy of about 0.000020 in. The profiling method also allows the analysis of such things as corner breakdown and other irregularities in the wheel-wear pattern.

Significance of the Type of Operation

The type of precision grinding operation significantly affects the mechanism by which a grinding wheel wears. Production-grinding operations may be conveniently divided into two general classifications: Plunge grinding and traverse grinding. For purposes of this discussion surface grinding is considered as interrupted plunge grinding on a workpiece of infinite radius since in both cases grinding action is the same with relative motion between wheel and work in one direction only. In the case of surface grinding, however, only a portion of the wheel face, equal to the cross feed, is working productively, see Fig. 6.

As the wheel engages the workpiece in the case of straight plunge grinding the entire active surface of the wheel face is subjected to uniformly severe grinding action. Thus the entire wheel face is similarly engaged in the process of productive metal removal. It is this factor which makes plunge grinding a much more efficient operation from the metal removal standpoint than is traverse grinding where only a portion of the wheel face is working productively at any given time. This is the reason that most production-grinding operations today are tailored to plunge grinding which permits a higher metal-removal rate. Further, it is suggested that under plunge-grinding conditions the grinding wheel is subjected to tangential and radial forces only. This effectively results in a smaller resultant force for equivalent chip load than is the case in traverse grinding. This should allow greater chip load without fracture of the grit and thus greater metal-removal rates for equivalent grinding ratios. It has been demonstrated by Backer and Merchant [3], that the mechanism of wheel wear, for plunge grinding over a wide range of mechanical variables and wheel grades, can be essentially attritious wear only, in the case where aluminum oxide and steel are the abrasive work-material pair. Since under the existing test conditions wheel wear was mechanical in nature and the forces on the grits were not great enough to cause either fracture of the grits or bond-post rupture, it is logical that neither wheel grade nor mechanical variables (machine settings) would affect the grinding ratio. These were the actual findings; attritious wheel-wear rate was found to be independent of wheel grade and mechanical variables, and varied only with the amount of metal removed, as may be seen from Fig. 7. Here is shown a wear curve with points taken at different values of wheel speed, the quantity being varied. Each of the points is taken by removing a given volume of metal at a different grinding-wheel speed with the speed increasing from left to right. The fact that the curve presented here remains linear demonstrates the independence of the rate of wheel wear of this variable. Similar tests with other varied quantities such as wheel grade or work speed give similar curves. Under conditions slightly more severe, where fracture wear did occur, the wheel wear was found to be dependent upon both mechanical variables and wheel grade as well as upon the amount of metal removed.

An investigation was conducted to determine the effect of mechanical variables on grinding ratio, power, and surface finish in the cylindrical-traverse grinding operation. Results indicate that in such grinding operations wheel wear is essentially always sensitive to both mechanical variables and wheel grade. This is so because, due to the nature of the grinding action, the wheel wears by both attrition and fracture even under what may normally be considered mild conditions. In traverse grinding only a portion of the wheel face is working productively at any given time. This portion depends on the linear inches of traverse per revolution of the workpiece (overlap) and is usually 1/3 to 1/2 the width of the wheel face. Thus as the workpiece traverses relative to the wheel, grinding action occurs only on the advance 1/3 of the wheel face (assume overlap equals 1/3 width of wheel face). If the work is being reciprocated, as is usually the case, similar action will occur on the opposite 1/3 of the wheel face when the workpiece is traveling in

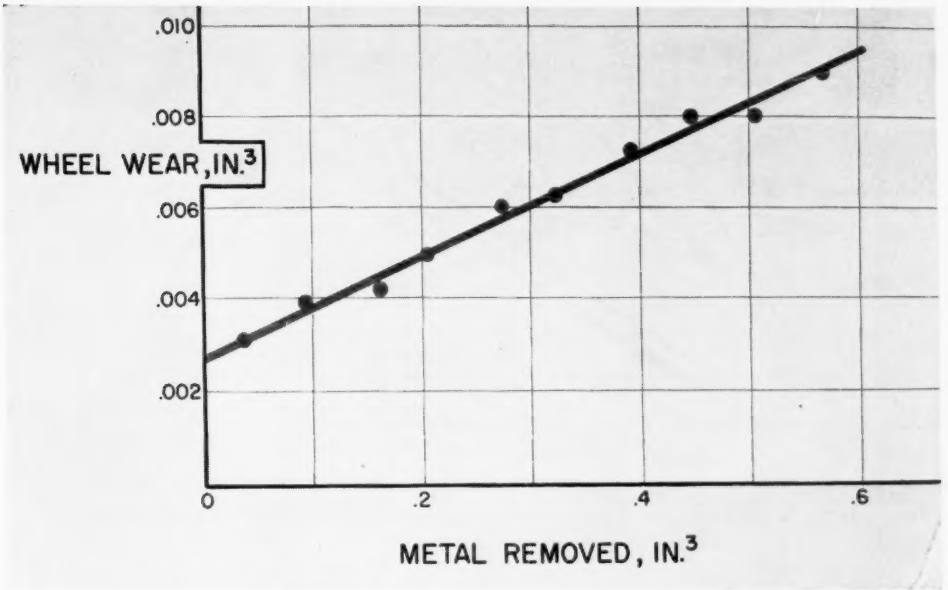

Fig. 7 Grinding-wheel wear curve. Each point is obtained by removing a given volume of metal at different grinding-wheel speeds. The linear nature of the curve indicates the independence of the rate of wheel wear of wheel speed.

the opposite direction. The central portion of the wheel face, however, does little productive work, its principal function being to size and impart fine finish to the work. As the workpiece is traversed across the wheel face, material is removed along a helical path. This helix angle imparts a third force component on the grinding wheel (in an axial direction) and therefore upon each individual active grit. While the power consumed in the traverse direction is small due to the relatively low traverse speed, the forces are known to be quite high. This axial force component therefore contributes considerably to the resultant force on the grit and therefore plays a significant part in the way in which the wheel wears.

Effect of Mechanical Variables on Grinding-Wheel Action

The extensive experimental studies previously referred to have yielded much information as to the effects of various mechanical variables on grinding ratio, power, and surface finish during cylindrical-traverse grinding, and have given considerable insight into factors affecting grinding-wheel performance and wear. The grinding conditions throughout the tests were as given in Table 1, except as specifically noted. The wheel in all cases was dressed with a sharp diamond at a traverse rate at 60 in. per min and an infeed of 0.0004 in. per pass. In order to minimize any variation in results due to possible inconsistencies in dressing of the wheels a control procedure was established.

Table 1 Experimental conditions

Grinding wheel, 2A60-J5-VN (24 × 2 × 12)
Work speed, 75 fpm
Wheel speed, 6000 fpm
Traverse rate, 60 in. per min
Work diameter, 3 in.
Work-material and hardness, AISI 81B45, 50 R_c
Infeed per pass, 0.0008 in.
Grinding fluid, water base, chemical emulsion (1:100)

This procedure was to measure the surface finish of the workpiece after the initial-traverse pass across at full depth of cut following dressing of the wheel. Experience has shown that if this initial surface finish, so produced, agreed with the standard within ±5 μ in. the influence of dressing on reproducibility of results was negligible.

A typical family of grinding-wheel wear curves relating metal removal and wheel wear as a function of one of the mechanical variables (in this case peripheral work speed) is presented in Fig. 8. The reciprocal of the slope of each curve is the grinding ratio. The linearity of the wear curves is evident and is typical of all of the data throughout these tests. The values of grinding ratio obtained here are shown as a function of work speed in Fig. 9 and are found to decrease with increasing work speed. As work speed increases power also increases and surface finish becomes poorer. These results are due primarily to the heavier chip per grit accompanying the increased metal-removal rate.

In Fig. 10, the grinding ratio is seen to increase and surface finish to improve with increased grinding-wheel speed. The increased wheel speed at a constant metal-removal rate results in a lighter chip per grit which tends to decrease the amount of fracture wear without proportionately increasing the amount of attritious wear, thus increasing grinding ratio.

However, as the grinding-wheel speed exceeds 7000 fpm, the grinding temperature becomes sufficiently high so that attritious wear increases considerably and grinding ratio falls off. The rapid increase in wear above 7000 fpm may also be due to chemical wear, as discussed later. The direct relationship between wheel speed, grinding ratio, and surface finish is immediately apparent from the similarity in the shape of the curves.

Power was found to increase with increased grinding-wheel speed up to 5000 fpm. At this speed (and resultant chip per grit) the rate of increase in power diminishes and eventually levels off, probably due to the decreased chip-grit friction known to exist at higher grinding speeds.

As traverse rate increases, the width of active wheels face (or overlap) increases and thus the metal removal rate also increases. This results in a linear increase in power, as shown in Fig. 11, but at a rate less than the rate of increase in traverse rate. This is as expected, since less wheel face remains for sizing and producing finish on the workpiece. The finish is therefore correspondingly poorer. Grinding ratio is found to de-

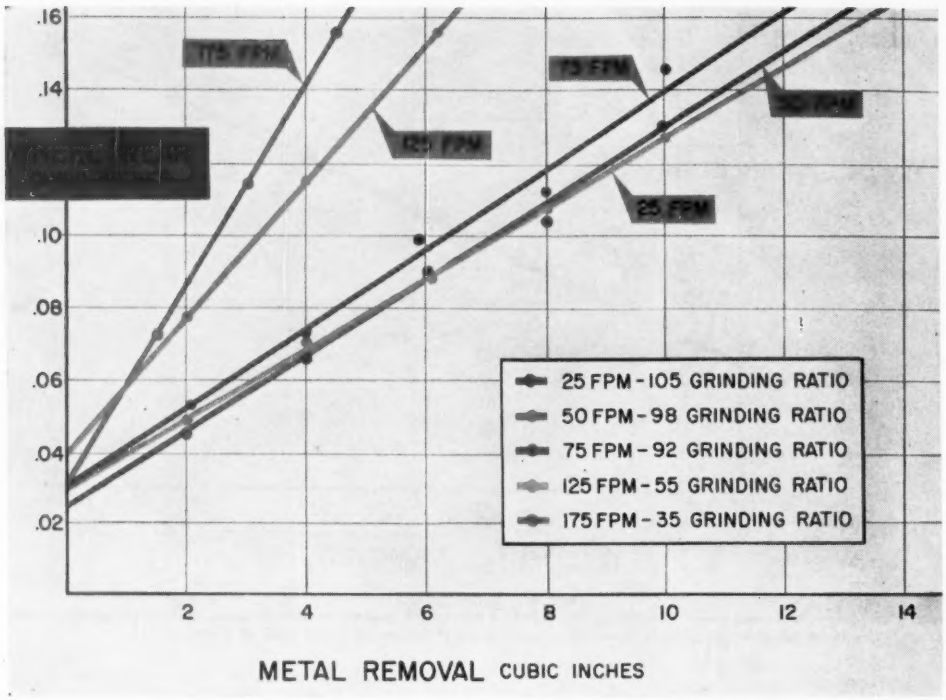

Fig. 8 Family of grinding-wheel wear curves indicating their typical linear nature

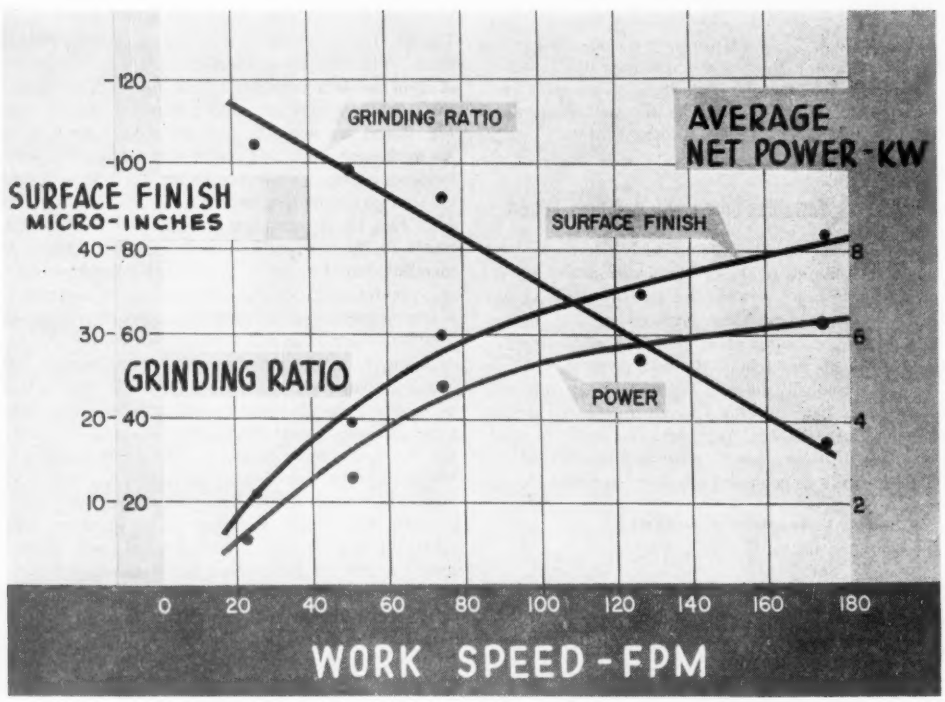

Fig. 9 Influence of work speed on grinding ratio, power, and surface finish

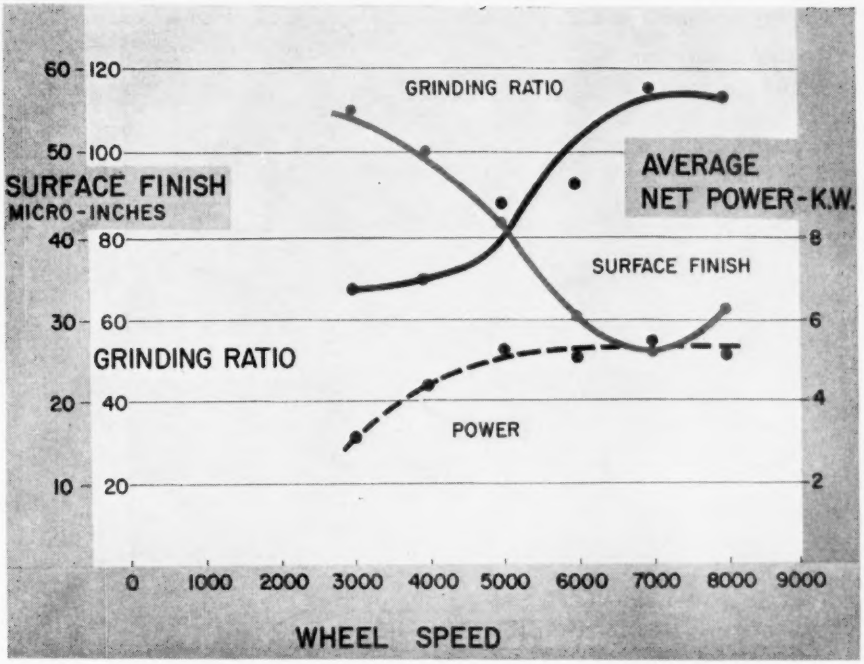

Fig. 10 Influence of grinding-wheel speed on grinding ratio, power, and surface finish

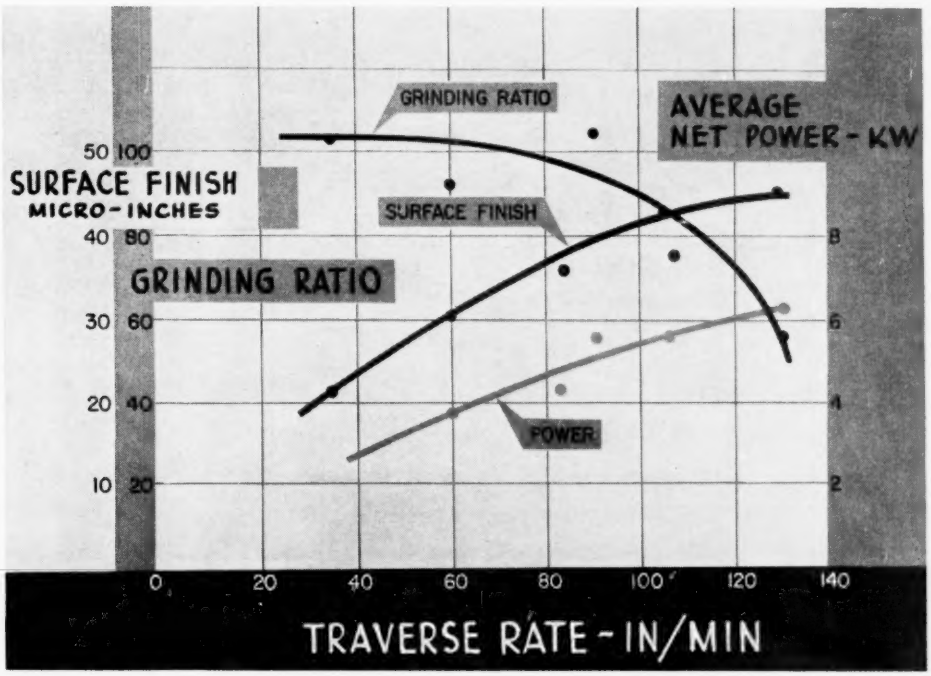

Fig. 11 Influence of traverse rate on grinding ratio, power, and surface finish

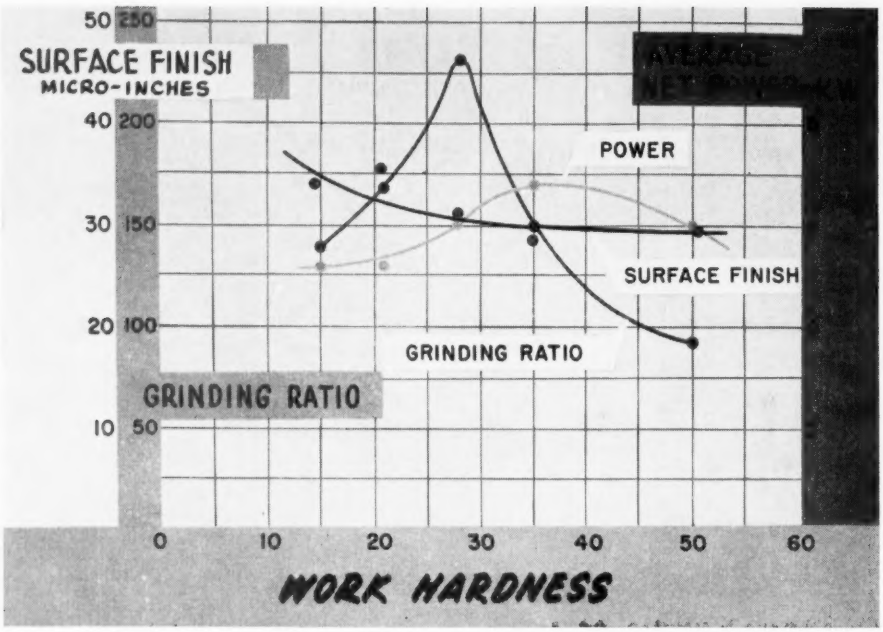

Fig. 12 Influence of work material hardness on grinding ratio, power, and surface finish

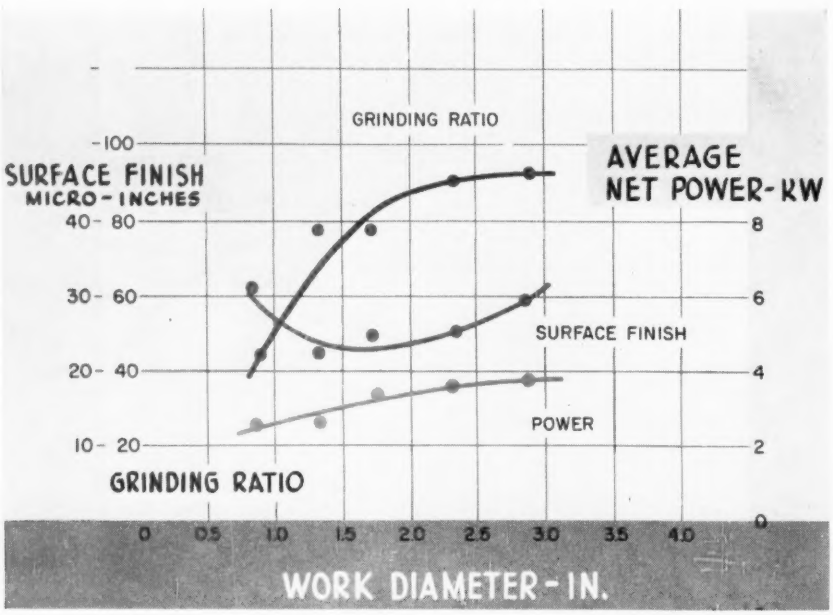

Fig. 13 Influence of workpiece diameter on grinding ratio, power, and surface finish

crease with increased traverse rate due primarily to the additional load on the grit accompanying the increase in helix angle.

In the foregoing tests, work-material hardness was found to have little effect on either power or surface finish. As indicated in Fig. 12, as the work-material hardness increases, grinding ratio first increases and then falls off. This indicates the necessity for proper grading of the wheel to suit the work-material hardness.

The small effect of hardness on power, as indicated here, has also been noted by other investigators [4] for chips of very small cross section, such as encountered in grinding.

Results presented in Fig. 13 indicate that an increase in workpiece diameter results in higher grinding ratios due to the difference in the nature of grit contact and chip formation, and to the decrease in helix angle of the grinding path which reduces the side force component on the grit. As work diameter in-

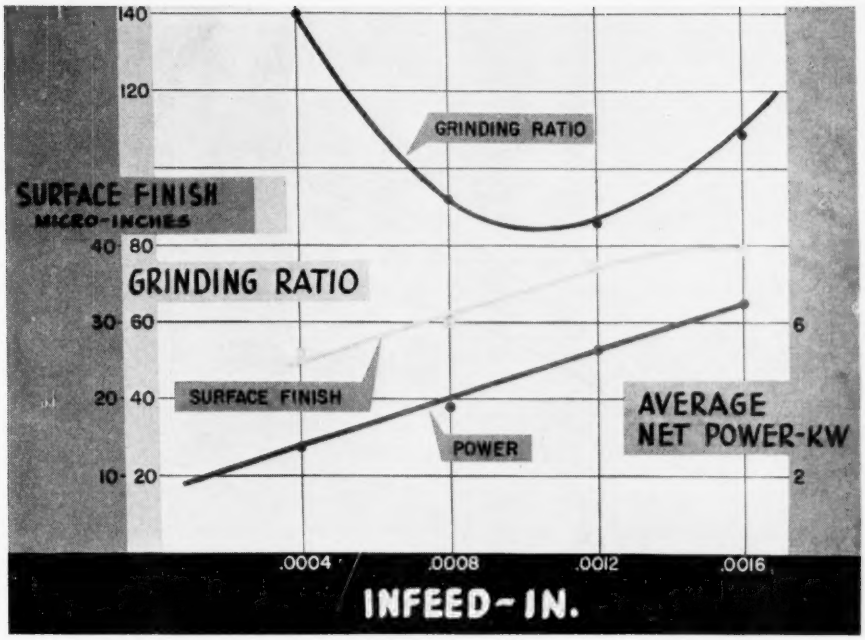

Fig. 14 Influence of infeed per traverse pass on grinding ratio, power, and surface finish

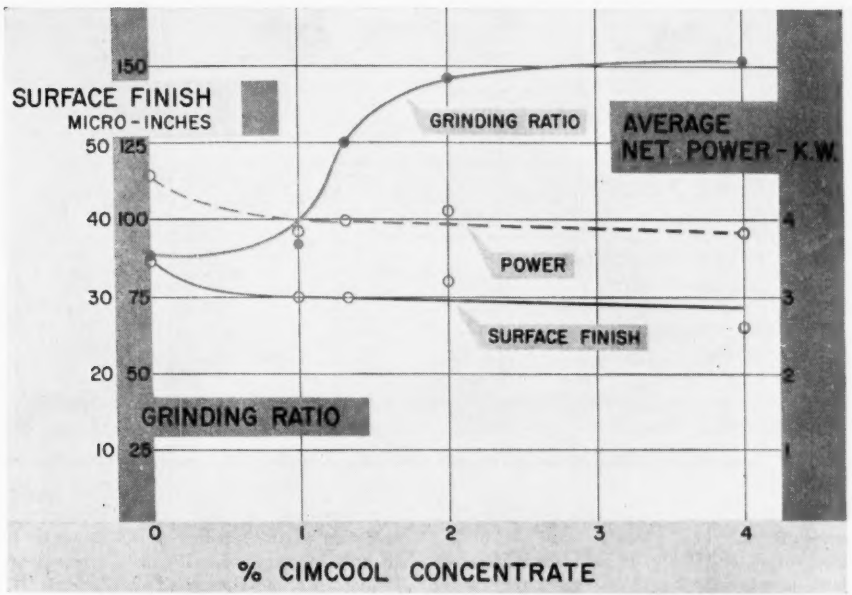

Fig. 15 Influence of grinding fluid concentration on grinding ratio, power, and surface finish

creases, the chips become thinner and longer, reducing grit load which minimizes fracture wear. Surface finish is not affected significantly, while power increases only slightly.

Increased infeed per traverse pass results in a proportionate increase in metal-removal rate and a heavier chip per grit. As shown in Fig. 14, this results in increased power and poorer surface finish. In this particular case, grinding ratio at first decreases with increased infeed, but then unexpectedly increases again. This increase in grinding ratio at the higher infeed values did not follow the usual trend of continued decrease exhibited by wheels of grades which bracket this wheel. There is no ready explanation of this effect, although it was found to be reproducible.

As shown in Fig. 15, an increase of grinding-fluid concentration resulted in a considerable improvement in grinding ratio, up to a concentration of about two per cent, in this case. However,

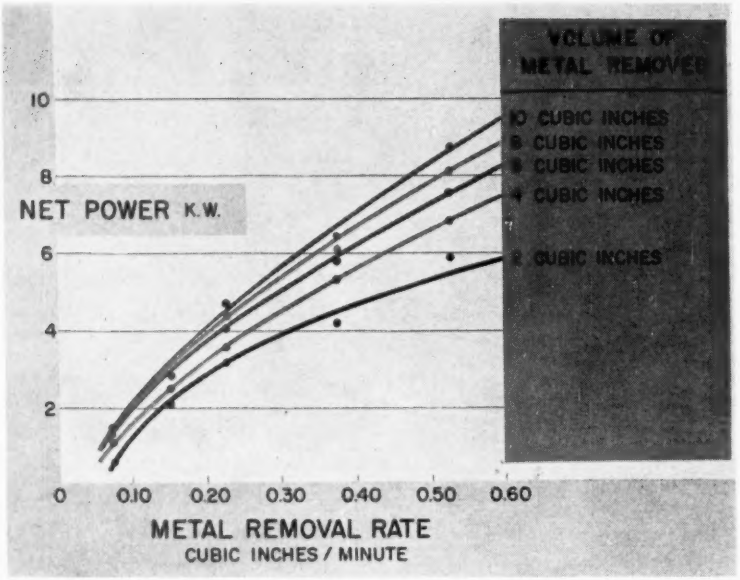

Fig. 16 Family of curves relating power, the rate of metal removal, and the amount of metal removed

	GRINDING RATIO	NET POWER	SURFACE FINISH
INCREASED METAL REMOVAL RATE	DECREASED	INCREASED	POORER
INCREASED WORKPIECE DIAMETER	INCREASED	SLIGHTLY INCREASED	NO SIGNIFICANT CHANGE
INCREASED WHEEL SPEED	INCREASED	SLIGHTLY INCREASED	IMPROVED
INCREASED CONCENTRATION OF GRINDING FLUID	INCREASED	DECREASED	IMPROVED
INCREASED WORK MATERIAL HARDNESS	*	SLIGHTLY INCREASED	IMPROVED

* OPTIMUM WORK MATERIAL HARDNESS EXISTS FOR EACH WHEEL GRADE AND SET OF OPERATING CONDITIONS.

Fig. 17 Summary of the effect of various mechanical variables on grinding ratio, power, and surface finish

increasing the concentration beyond one per cent had little effect on power and surface finish.

The family of curves plotted in Fig. 16 indicates that power increases with both metal-removal rate, as shown previously, and with the amount of metal removed. This is probably due to the individual grits in the wheel becoming dull, from attritious wear, which enlarges the flat areas and renders the grits less efficient as cutting tools.

From the experimental findings presented in the foregoing figures it is possible to draw several general conclusions. The grinding ratio is found to decrease with increased metal-removal rate; to increase with workpiece diameter, that is, decreased helix angle; to increase with decreased chip load at a given metal-removal rate, that is, increased helix angle; to increase with decreased chip load at a given metal-removal rate, that is, increased wheel speed; and to increase with increased concentration of the grinding fluid. Power is found to increase not only, as expected, with metal-removal rate, but also with the amount of metal removed after truing. It increases slightly with workpiece diameter, and is affected little by work-material hardness. Surface finish improves with decreased metal-removal rate and with decreased chip load at the same metal-removal rate, that is, with increased wheel speed. It also is affected little by work diameter or work-material hardness. These data are summarized in Fig. 17.

Chemical Wear

Chemical reactions between the abrasive grit and the work material do occur in the grinding process, and often can be the

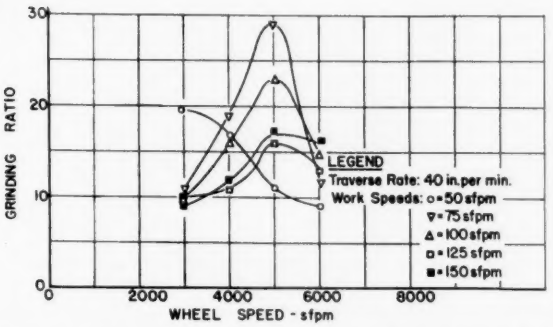

Fig. 18 Influence of wheel speed and work speed on grinding ratio when grinding titanium

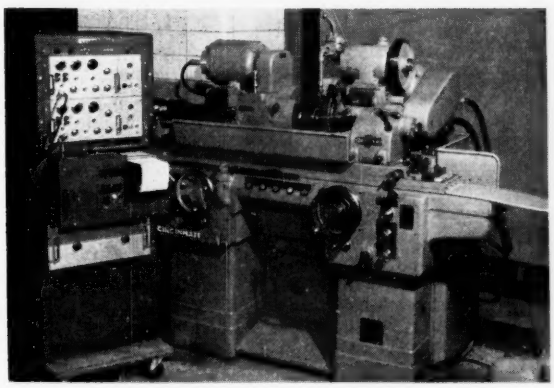

Fig. 19 Grinding dynamometer setup

cause of a large part of the total wear; however, this is not so when grinding steel with an aluminum-oxide wheel. In this case, the effect of the mechanical variables on grinding-wheel wear may be adequately explained in terms of attritious and fracture wear alone.

Chemical reactions between grit and work account for the major difficulties in the grinding of titanium; it was not until the nature of the wear phenomena here was understood that reasonable grinding of titanium was achieved through the development of effective combinations of fluids and wheels.

Fig. 18 indicates the very marked effect of grinding-wheel speed on grinding ratio in the case of titanium, as found in the course of extensive investigation on the grinding of this metal [5]. Here, as in the grinding of steel, the grinding ratio increases with increased wheel speed, but in this case only to a value of 5000 sfm, at which point performance drops off sharply due to the inability of even the specially developed grinding fluid to protect the grits from being chemically attacked by the titanium metal at the grinding temperatures reached at speeds above 5000 sfm. However, this is actually a very high wheel speed for titanium grinding. With conventional grinding fluids it is necessary to reduce the wheel speed to about 2000 sfm in order to get reasonable performance. In the case of steel, the grinding ratio continued to increase well beyond conventional grinding-wheel speeds, since the wear was primarily mechanical in nature.

Fundamental Research on the Mechanics of Wheel Wear

A thorough understanding of the grinding process could never be achieved without much research of a fundamental nature into the understanding of such things as grinding forces and chip formation. Much research has already been done in this area and brief mention will be made here of several of these phases [1, 3].

In order to measure forces in grinding and to be able to re-

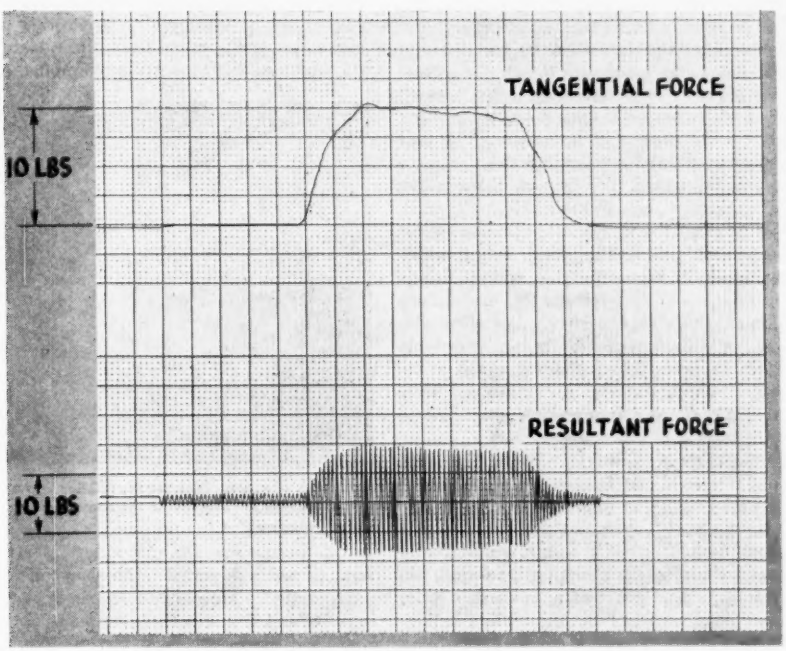

Fig. 20 Typical force recordings using grinding dynamometer

solve these forces into individual components, a strain-gage-type cylindrical-grinding dynamometer was designed and built. With this dynamometer it has been possible to measure individual force components in the cylindrical-plunge-grinding operation and to obtain information concerning grinding-force relationships, specific energy, and so forth, and to determine the effect of numerous variables on these fundamental quantities.

Fig. 19 shows the dynamometer mounted on the work head of a cylindrical grinder. The electrical connections are made by bringing the leads through the hollow headstock spindle to a set of slip rings in the back of the spindle and then into an amplifier-recorder where the tangential and resultant forces are measured. Fig. 20 shows a chart obtained during a typical cut with the grinding dynamometer. The resultant force acts sinusoidally on its sensing element because of the workpiece rotation. The workpiece rotational speed can be thought of as a carrier for the force signal.

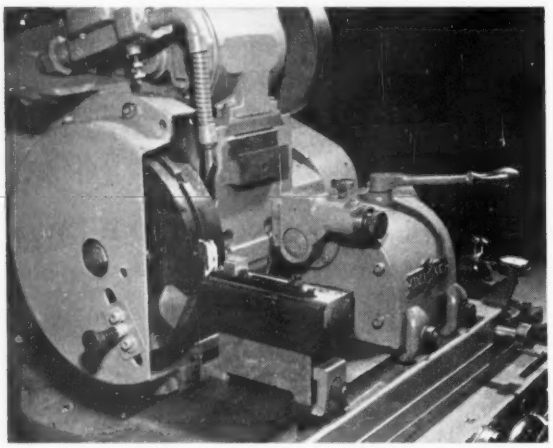

Fig. 21 View of quick-stop grinding apparatus

A technique for studying chip formation in grinding was needed to supplement the studies made with the grinding dynamometer. Such a technique has been developed in the research laboratories of the author's company, making possible the study of grinding chips during the process of formation. This was accomplished by "instantaneously" accelerating the workpiece to the speed of the grinding wheel, thus freezing the grinding action.

The test apparatus is presented in Fig. 21. It consists essentially of four components: (*a*) The wheel mount, which supports the grinding-wheel segment, the spring fingers which pick up the workpiece, and the latch and trip mechanisms which operate the spring fingers; (*b*) the trip plunger which triggers the mechanism at the desired moment; (*c*) the retractable workpiece holder which supports the specially designed workpiece during grinding; (*d*) the special variable-infeed drive unit (not shown in Fig. 21) which makes possible a wide range of positive-infeed rates.

The theory of operation of the apparatus is as follows: Initially, the spring fingers are retracted and latched below the outer surface of the grinding-wheel segment to permit grinding. The workpiece is placed in the work holder and the infeed mechanism started. At the desired instant during grinding the mechanism is triggered, permitting the spring fingers to pick the workpiece out of the work holder 3/4 of a revolution later. The workpiece is almost instantaneously accelerated to grinding-wheel speed and is held against the wheel segment by the spring fingers and revolved with it until the wheel mount is stopped.

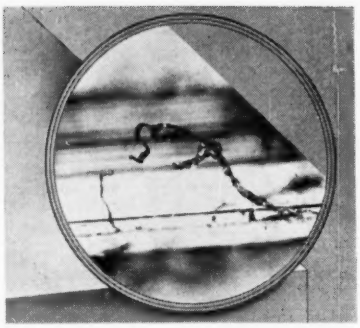

Fig. 22 Partially formed grinding chips frozen in the process of formation by the quick-stop technique

At the instant the workpiece is snatched from the fixture, the latter retracts so as to be out of the way of the revolving assembly. After accelerating the workpiece from rest up to the grinding-wheel speed almost instantaneously, and obtaining grinding chips in the process of formation, the next problem is the removal of the workpiece without breaking off the minute partially formed chips. This is done by providing another position on the latch which will permit the spring-finger arms to move out further, allowing the newly ground surface to be pushed away from the grinding-wheel segment.

The ground surfaces obtained by this technique show many partially formed chips. A typical example is shown in Fig. 22. The grinding chips of interest are oriented with respect to a reference point, and the grinding specimen is then mounted and sectioned to permit a study of the desired section through the chip-work contact area.

Recent investigations have been made with this apparatus adapted to the use of a single grinding grit of a definite preshaped geometry which permits the evaluation of the effect of grit geometry on chip formation.

Another technique has been developed here where a single selected grit on a sharply dressed corner of a grinding wheel is used to produce a single scratch in a highly polished specimen. The specimen is then sectioned to produce a cross section of the

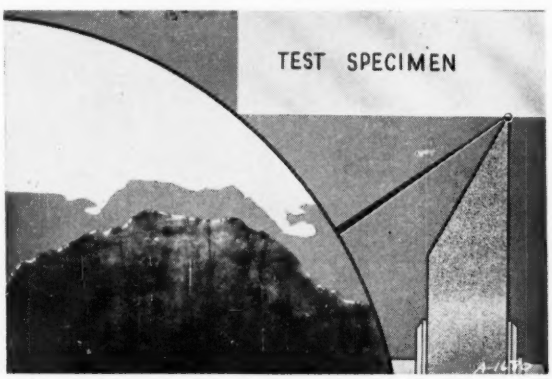

Fig. 23 A composite showing the relationship between the cross section of the grinding grit and that of the contour of the path of the grit through the test specimen

scratch, which is actually the shape of the undeformed chip cross section. A technique has been developed where first a negative and then a positive replica of the grinding grit may be made and later sectioned to give the actual cross section of the grit which produced the scratch. A composite of the scratch and

grit cross sections are shown in Fig. 23. A comparison here yields data useful in the study of the relationship between the shape of the grit and that of the undeformed chip.

Continuing investigations of this nature will yield much additional information necessary to the formulation of sound theories explaining further the nature of grinding action and grinding-wheel wear.

Summary

The nature of grinding-wheel wear has been discussed, and factors affecting it have been pointed out in an effort to develop an understanding of the process based on knowledge achieved through extensive research within this field to date at The Cincinnati Milling Machine Company. The continuing applied and fundamental research in this area will bring us to an even higher level of understanding, which will enable us to develop further a comprehensive and sound set of physical principles describing the process by which grinding wheels wear, and the factors which may be controlled to achieve minimum grinding cost.

Acknowledgment

The author wishes to express his appreciation to Dr. M. E. Merchant, Director of Physical Research, for his assistance and guidance in planning and carrying out this research. Thanks are also due Mr. C. Mehl, Senior Research Engineer, and Messrs. P. Bruns and W. B. Perkins, co-op students whose research efforts brought about the development of certain of the research techniques presented. Further, thanks are due Mr. J. Hawlik, Research Engineer, and Miss H. Conner for their assistance in preparation of the figures and manuscript.

References

1 W. R. Backer and E. J. Krabacher, "New Techniques in Metal-Cutting Research," TRANS. ASME, vol. 78, 1956, pp. 1497–1505.

2 L. P. Tarasov, "How to Grind Titanium," *American Machinist*, vol. 96, November 10, 1952, pp. 135–146.

3 W. R. Backer and M. E. Merchant, "On the Basic Mechanics of the Grinding Process," TRANS. ASME, vol. 80, 1958, pp. 141–148.

4 W. R. Backer, E. R. Marshall, and M. C. Shaw, "The Size Effect in Metal Cutting," TRANS. ASME, vol. 74, 1952, pp. 61–72.

5 E. J. Krabacher, "Fluids for the Grinding of Titanium," *Lubrication Engineering*, vol. 11, 1955, pp. 397–401.

DISCUSSION

H. B. Patterson[2]

The author mentions three classes of wheel wear; namely, grit fracture, attrition, and chemical wear. It seems that the separation of attrition and chemical wear is a very difficult one to make. To simplify matters, why not include all wear of a frictional nature in one class? Thus the total wheel wear would be made up of fracture and friction wear. Frictional wear is complex, being the result of several processes occurring simultaneously.

The statement that chemical reactions between abrasive and work do not make up a large part of the total wear when grinding steel with aluminum-oxide appears somewhat misleading. Frictional-wear properties of the various types of aluminum-oxide abrasive cover a wide range when used to grind steel. The differences in wear are due to differences in the impurity content of the aluminum oxide. It is true that the increased frictional-type wear that is noted with some of the tough abrasives may not be due to direct chemical reaction with the steel. However, the substances other than steel and aluminum oxide that are introduced as impurities do have a large effect and would have to be considered in any complete analysis of the wear process.

The fact that work hardness has little effect on the power required is again illustrated. In noting this it is easy to conclude (wrongly) that hardness has practically no effect on the grinding process. The tangential-force component (and hence the power) may remain about the same but there are large changes in the normal force component due to hardness. In other words the harder the work, the more force required to cause the abrasive grains to penetrate. The resultant force, and therefore wear by grain fracture, will increase with increasing work hardness. This is evident in Fig. 12, where grinding ratio rapidly decreases with increasing hardness.

The quick-stop mechanism appears to be a useful tool for studying the action of a grinding wheel. Another method of "freezing" grinding action is to use a single grit, lightly bonded to the periphery of a grinding wheel. At each revolution of the wheel the grit takes a cut. If the depth of cut is increased sufficiently, bond failure occurs releasing the grit while it is in the cut and leaving a partially formed chip attached to the work. This method has proved successful in studying chip formation, plastic flow, and abrasive wear.

L. P. Tarasov[3]

This paper is one of the few that deal with the effects of important grinding conditions in cylindrical traverse grinding operations. Most of the results are explained satisfactorily in terms of current grinding theory, but some points call for further consideration.

The rapid increase in wheel wear beyond the linear portion of the curve in Fig. 3 is attributed to large-scale fracture wear. It is not readily apparent whether fracture wear is considered by the author to play an important part throughout the time that the wheel wears at a constant rate, or just when it begins to break down rapidly.

This curve is similar to that for a cutting tool, and the question arises as to whether it applies to grinding operations in general or only within a certain range of conditions. Does the curve turn upward when a wheel becomes badly glazed because it is too hard for the operation? Does any substantial change occur in the wear rate when the wheel is either self-dressing or else too soft? Any data that the author might be able to provide along these lines would be of interest.

The axial-force component is stated to be quite high in traverse cylindrical grinding. It is not clear why this should be so since an individual grit cuts out a chip that is almost exactly perpendicular to the axis as a result of the high ratio of wheel to work speed. While it is in contact with the work, a grit moves perhaps 50 to 100 times as far in the circumferential as in the axial direction. Since the geometry of a grit is completely irregular, why should there be any significant axial-force component just because the chip cut out is not exactly perpendicular to the work axis?

The kind of steel that was ground is not stated, but from the grinding ratios obtained it would appear that a medium or high-carbon, low-alloy steel was involved. The author found the grinding ratio to increase to a maximum and then to decrease as the hardness of the steel went up from Rockwell C15 to C50. In a surface-grinding test performed on an oil-hardening tool steel having presumably the same general grinding characteristics, the writer found a continuous decrease in grinding ratio as the hardness of the steel was increased from C20 to C60, the grinding ratio being approximately twice as great for the former as for the latter. In a similar test with a high-vanadium, high-speed steel,

[2] Research Engineer, Bryant Chucking Grinder Company, Springfield, Vt. Assoc. Mem. ASME.

[3] Research and Development Department, Norton Company, Worcester, Mass. Mem. ASME.

AISI Type T-15, whose grindability is extremely low in the hardened condition, the grinding ratio also decreased continuously with increased hardness, but the change was far more pronounced, the grinding ratio being about 25 times greater at Rockwell C20 than at C65. Thus the effect of the hardness of the work material depends both on the material and on the grinding operation.

It is stated that the grinding ratio increased with decreased chip load at a given metal-removal rate, when the helix angle was increased, but it is not clear upon what experimental results this is based.

The type of wheel used in obtaining the titanium grinding curves in Fig. 18 is not mentioned but presumably the abrasive was silicon carbide in view of the rather high optimum wheel speed.

Attritious wear appears to be partly chemical in nature, as indicated by point-endurance tests performed on a variety of work materials including steels. It is undoubtedly also partly mechanical in nature. Thus it does not seem desirable to set up attritious wear as being distinct from chemical wear.

D. R. Walker[4]

The author is to be congratulated on his comprehensive report of the factors influencing wheel wear in traverse grinding operations. Work such as this, combined with studies of the factors affecting work damage and surface finish, should lead to important improvements in grinding operations.

Fig. 15 shows the effect of grinding-fluid richness upon grinding ratio, power, and surface finish. It would be interesting to learn if the author has obtained similar data when grinding is done dry and air is the only grinding fluid. Measurements often show that the presence of water as a grinding fluid or even in humid air can increase grinding forces over those obtained in dry grinding. Wheel wear is also often observed to be higher when grinding in the presence of water than in air because of the higher grinding forces and because of the weakening effect of water on the glass-bond posts of a vitrified wheel.

The family of power versus metal-removal-rate curves shown in Fig. 16 would appear to intersect the abscissa at a positive metal-removal rate if extrapolated toward the origin. They imply that material could be removed at a low rate with no power. The curves are thus dissimilar to those obtained for surface grinding by Marshall and Shaw.[5] A considerable change in slope would be required to make the curves pass through or to the left of the origin.

The technique of using a single grit to produce single scratches on polished workpieces is an interesting approach to the observation of the grinding process and one which has been used to study the mechanism of abrasive wear. The depth of cut in finish-type grinding has been estimated to be 10^{-5} to 10^{-4} in.[6] and is thus only 1/100 or less of the size of a 60-grit grain. Although no magnification is noted for the insert of Fig. 23, it would appear from this figure that a considerably larger portion of the grit was used in producing scratches in the author's experiments. Care must then be used in relating such results to the actual grinding process.

[4] Avco Research and Advanced Development Division, Wilmington, Mass.

[5] E. R. Marshall and M. C. Shaw, "Forces in Dry Surface Grinding," TRANS. ASME, vol. 74, 1952, pp. 51–59.

Author's Closure

The author wishes to thank Mr. H. B. Patterson, Dr. L. P. Tarasov, and Mr. D. R. Walker for the interest they have shown in this paper and for their valuable comments.

The author agrees with Mr. Patterson and Dr. Tarasov that attritious wear is comprised of both frictional (mechanical) wear and chemical wear. As was indicated under the discussion of the nature of wheel wear, two general types of wear are recognized, "attritious wear" and "fracture wear." Under the discussion of chemical wear it was desired to point out that the chemical aspect of attritious wear can, under certain conditions, play a major role in wheel wear. The author agrees further that, in his statement that chemical wear does not play a major part in wheel wear when grinding steel with an aluminum-oxide wheel, it would have been more correct to state that: "In this case, the effect of the mechanical variables on grinding-wheel wear may be adequately explained in terms of *friction* and fracture wear alone."

The linear portion of the grinding wheel wear curve of Fig. 3 is typical of the nature of grinding wheel wear in general. The rapid increase in wheel wear rate beyond the linear portion of the curve occurs when conditions become such that the amount of fracture wear including bond post rupture increases sharply. This does not mean that fracture wear does not occur along the linear portion of the curve. Under conditions where a wheel is self dressing considerable fracture wear occurs along the linear portion of the wear curve. Here, however, the wheel remains sharp and free cutting so that usually no sharp rise in wheel rate is noted.

The axial force component in cylindrical traverse grinding can be quite high even though the individual grit cuts a chip almost exactly perpendicular to the axis of the work. This axial force may be considered equivalent to the axial feeding force in a turning operation. True, the power consumed is very small because the velocity of axial motion is low, but the force can be a very significant fraction of the tangential force depending on the prevailing conditions in the cut.

All grinding during this investigation was carried out with grinding fluids. No comparison can therefore be made with conditions of dry cutting where air is the only grinding fluid.

The author believes that the family of power versus metal-removal curves shown in Fig. 16 must pass through the origin. With the exception of the lone point for 0.075 cu in. per minute metal removal rate at 2 cu in. of metal removed this would appear to be the case. Perhaps the curves should have been so drawn.

The fragment of grit shown in the insert of Fig. 23 is only a small corner of a greatly cropped No. 60 grit. The depth of the scratch is approximately 0.0002 inch.

Vibrations of Flexible Precision Grinding Spindles

R. S. HAHN

Chief Research Engineer,
The Heald Machine Company,
Worcester, Mass. Mem. ASME

The effects of pulsating forces between grinding wheel and workpiece are discussed in connection with inhomogeneous wheel wear and loading. By analysis it is shown that pulsating normal forces may be caused by rotary damping and gyroscopic effects. The influence of skew-symmetric rigidity in the spindle is also discussed and the occurrence of subharmonic resonances is pointed out.

1 Introduction

THE PROBLEM of grinding chatter has plagued precision-grinding operations for many years. In general, these vibrations between the grinding wheel and workpiece have a detrimental effect. Not only do they leave the workpiece with an untrue surface but they also may cause a reduced grinding rate.

The analysis presented here, although derived with flexible internal grinding spindles in mind, may be applied also to other flexible grinding spindles and the section on the forced vibrations of shafts with skew-symmetric rigidities is applicable to shafts supported by three or more bearings, one of which is misaligned with respect to the remainder, thereby setting up radial loads.

The objective of the work to follow is to determine the stability characteristics of the system composed of the grinding spindle and wheel and the workpiece, i.e., to determine whether small transient vibrations, which may be randomly impressed on the system, tend to grow and increase in magnitude as grinding proceeds or whether they are damped out and disappear.

2 Force Pulsations Between Wheel and Work

In precision-grinding operations it sometimes happens that vibrations build up more or less gradually as the grinding process proceeds. In internal grinding these vibrations are often the result of initially small pulsating forces between wheel and work. These small pulsating forces are sometimes caused by vibrations of the structure holding the grinding spindle. In Fig. 1, for example, it was found that the wheelhead body B was vibrating near its natural frequency as a result of the belt drive, so as to cause force pulsations in the y-direction between wheel and work. In a short time these force pulsations caused an uneven wear of the wheel which then caused greater vibrations to occur. Fig. 2 illustrates the nonhomogeneous wear of the wheel as evidenced by the blue horizontal lines on the wheel which were produced by running the used wheel in close proximity to the workpiece upon which a film of prussian blue had been smeared. The frequency of vibration corresponding to these blue lines was approximately 700 cps and essentially the natural frequency of the wheelhead body. After bracing the wheelhead body to prevent the 700 cps mode, the test was re-run and the resulting inhomogeneous wheel

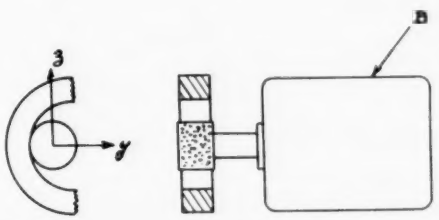

Fig. 1 Arrangement of grinding wheel and workpiece

Contributed by the Production Engineering Division and presented at a joint session with the Machine Design and Applied Mechanics Divisions at the Annual Meeting, New York, N. Y., November 30–December 5, 1958, of THE AMERICAN SOCIETY OF MECHANICAL ENGINEERS.

NOTE: Statements and opinions advanced in papers are to be understood as individual expressions of their authors and not those of the Society. Manuscript received at ASME Headquarters, August 4, 1958. Paper No. 58—A-97.

Nomenclature

m = the equivalent lumped mass of wheel and spindle
ω = rotary spindle speed
μ = static unbalance in wheel
c_u, c_v = damping strengths in the (rotating) u-v system
k_u, k_v = spring constants in the (rotating) u-v system
C_y, C_z = damping strengths in the stationary system
K_w = wheel-work spring constant
$K_w\delta$ = steady-state normal grinding force
f = "friction coefficient" between wheel and work

$$\Omega_1^2 = \frac{k_u}{m}$$

$$\Omega^2 = \frac{k_v}{m}$$

$$\nu^2 = \frac{K_w}{m}$$

$$\frac{c_u}{m} = a_1'$$

$$\frac{c_v}{m} = a_2'$$

$$\frac{C_y}{m} = b_1$$

$$\frac{C_z}{m} = b_2$$

$$h = \frac{\mu\omega^2}{m}$$

$$\alpha = a_1' - a_2' = \frac{\Delta c}{m}$$

$$\kappa = \Omega_1^2 - \Omega_2^2 = \frac{\Delta k}{m}$$

J = effective polar moment of inertia of wheel and spindle

a = see Fig. 7

$$\tau = \omega t$$

$$a_2 = \frac{\Omega_1^2 + \nu^2 - \frac{\kappa}{2}}{\omega^2} = \frac{\Omega_1^2 + \Omega_2^2 + 2\nu^2}{2\omega^2}$$

$$a_1 = \frac{\Omega_1^2 - \frac{\kappa}{2}}{\omega^2} = \frac{\Omega_1^2 + \Omega_2^2}{2\omega^2}$$

$$q = \frac{\kappa}{4\omega^2} = \frac{\Omega_1^2 - \Omega_2^2}{4\omega^2}$$

$$g = \frac{h}{\omega^2} = \frac{\mu}{m}$$

$$K = \frac{\nu^2\delta}{\omega^2}$$

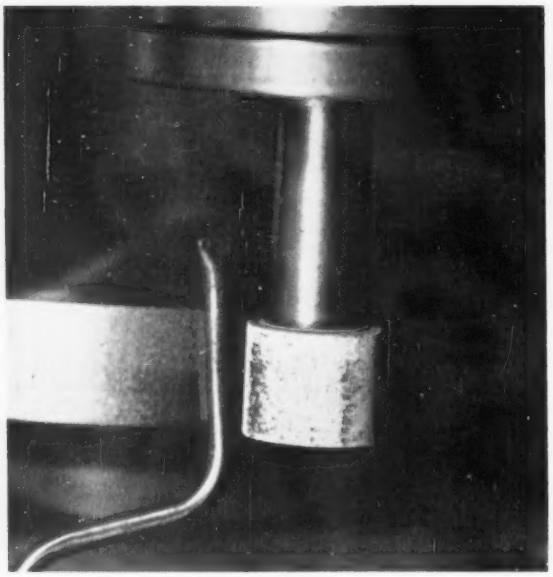

Fig. 2 Photograph showing inhomogeneous wheel wear occurring at approximately the wheelhead body natural frequency (700 cps)

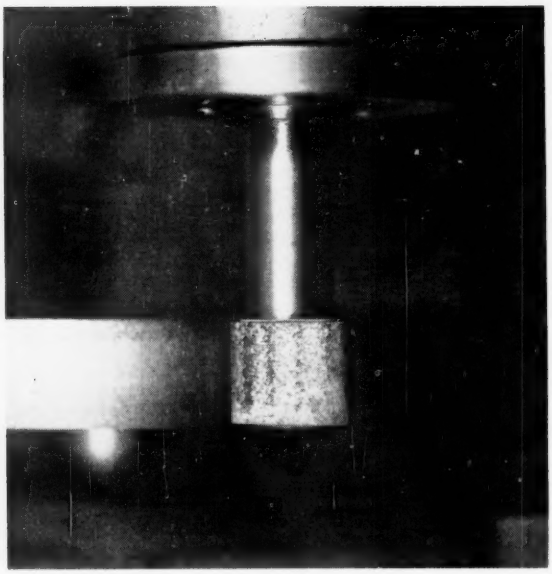

Fig. 3 Photograph showing inhomogeneous wheel wear occurring at approximately the natural frequency of the coupled wheel-work system in the z-direction

wear pattern is shown in Fig. 3. The body mode is no longer observable but instead there is a high-frequency spindle mode of approximately 3200 cps which corresponds to about 11 blue lines on the wheel. This mode was studied by pressing the wheel against the workpiece and tapping the spindle lightly while holding a vibration pickup on the spindle. In this way it was found that the vibration was essentially in the z-direction in Fig. 1. Vibration in the y-direction is greatly inhibited due to the high normal rigidity between wheel and work. It is apparent that the tangential constraint of the workpiece against the wheel is much less than the normal constraint and therefore tangential vibrations are more likely to occur. It will be shown later that vibrations in the tangential direction produce, essentially, force pulsations in the y-direction.

Additional observations have been made on wheels that have chattered in connection with loading. Not only do wheels, grinding under pulsating forces, tend to wear inhomogeneously as illustrated in Figs. 2 and 3, but loading, i.e., the packing of metal chips on and in crevasses between the grits, also occurs in an inhomogeneous manner as may be demonstrated by holding an electromagnetic velocity-type vibration pickup in close proximity to the high-speed moving surface of the wheel. The fluctuations in density of loaded metal in the wheel generate induced voltages in the pickup and in this way it has been found that the frequency corresponding to the loaded zones agrees with the vibration frequency during chatter. Oscillographic recordings of the induced voltages generated by the loaded zones ("Load-o-grams") have been made. Fig 4 shows a typical set of Load-o-grams showing the increase in inhomogeneous loading. The upper trace is the Load-o-gram while the lower trace registers the spindle orientation by the small "pip." Fig. 4(a) is a recording of a new clean wheel. Each successive picture shows the condition of the wheel at 2-second intervals during a grinding test. It may be noted that the loading pattern, once formed, stays relatively fixed and does not drift circumferentially around the wheel.

It should be remarked that the wheels tested barely show any evidence of visual loading and, judged by ordinary standards, would not be said to be loaded.

In view of the foregoing it is reasonable to conclude that pulsat-

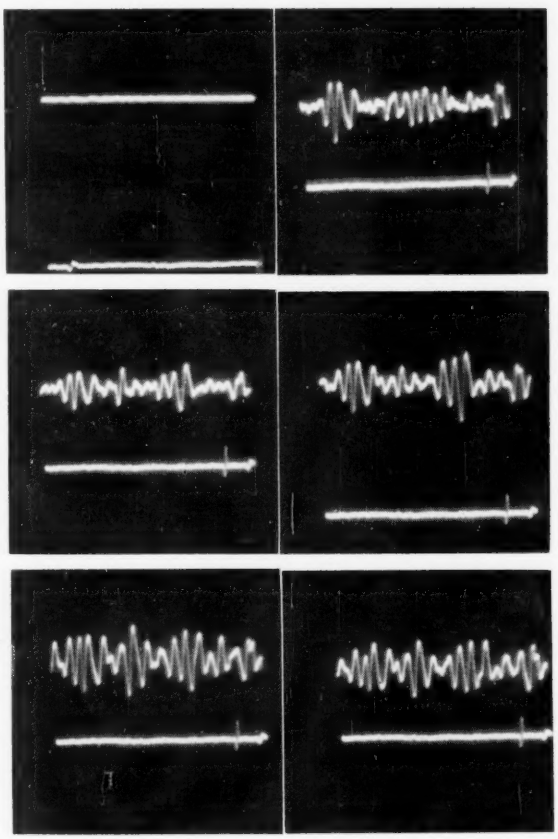

Fig. 4 Oscillograms showing inhomogeneous loading of the grinding wheel. Each successive snapshot was taken after 2-sec grinding intervals, starting from a new wheel.

ing normal forces, existing between wheel and work, tend to produce inhomogeneous wheel wear dominating with soft wheels and the inhomogeneous loading dominating with harder wheels. Because of the repeated revolutions of the wheel, this inhomogeneous wear and loading of the wheel can have a regenerative effect which causes the vibration to gradually grow stronger.

3 The Spindle-Wheel-Work System

In order to study further into the origin of pulsating forces between wheel and work the differential equations of motion of a flexible, rotating, and simultaneously vibrating spindle which is being pressed against a spring K_w, as shown in Fig. 5, will be developed. The wheel-work contact is assumed to be representable by a linear spring (for very small oscillations) whose spring constant in practice is very large. A tangential force is also taken at the wheel-work contact which is equal to the product of a constant of proportionality f and normal force. Damping forces and elastic restoring forces in the rotating spindle will be considered as well as nonrotating damping and restoring forces. Furthermore, the rigidities and constants in the rotating spindle need not be the same about all transverse axes of the spindle. In other words, the spindle rigidity and damping need not be axisymmetric. Such things as keyways, flats, out-of-round inner ball-bearing races, and out-of-round tapered socket joints may cause unsymmetrical rigidities and damping constants to occur. The gyroscopic moments on the wheel will be neglected for the time being but will be treated later in a simplified manner.

Two sets of co-ordinates are used in setting up the differential equations as shown in Fig. 6, the u-v set rotating with the spindle. In writing the dynamical equations in terms of the rotating set it is of course necessary to introduce the Coriolis and centrifugal force terms. The equations of motion are:

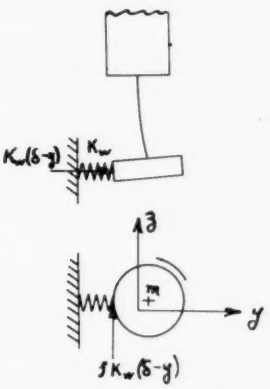

Fig. 5 Illustration of the wheel-work-spindle system

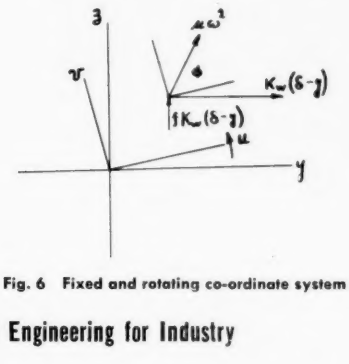

Fig. 6 Fixed and rotating co-ordinate system

$$\left.\begin{aligned} &m\ddot{u} - 2m\omega\dot{v} - m\omega^2 u + c_u\dot{u} + k_u u \\ &\quad + C_y\dot{y}\cos\omega t + C_z\dot{z}\sin\omega t - K_w(\delta - y)\cos\omega t \\ &\quad - fK_w(\delta - y)\sin\omega t = \mu\omega^2\cos\phi \\ &m\ddot{v} + 2m\omega\dot{u} - m\omega^2 v + c_v\dot{v} + k_v v \\ &\quad - C_y\dot{y}\sin\omega t + C_z\dot{z}\cos\omega t + K_w(\delta - y)\sin\omega t \\ &\quad - fK_w(\delta - y)\cos\omega t = \mu\omega^2\sin\phi \end{aligned}\right\} \quad (1)$$

Referring all terms to the stationary co-ordinates y, z by the co-ordinate transformation

$$\left.\begin{aligned} u &= y\cos\omega t + z\sin\omega t \\ v &= -y\sin\omega t + z\cos\omega t \end{aligned}\right\} \quad (2)$$

and simplifying, leads to

$$\begin{aligned} &[\ddot{y} + b_1\dot{y} + \nu^2 y]\cos\omega t - (a_1'\omega - f\nu^2)y\sin\omega t + a_1'\dot{y}\cos\omega t \\ &\quad + \Omega_1^2 y\cos\omega t + [\ddot{z} + b_2\dot{z} + \Omega_1^2 z]\sin\omega t \\ &\quad + a_1'\omega z\cos\omega t + a_1'\dot{z}\sin\omega t \\ &\quad = h\cos\phi + \nu^2\delta(\cos\omega t + f\sin\omega t) \quad (3) \end{aligned}$$

$$\begin{aligned} &-[\ddot{y} + b_1\dot{y} + \nu^2 y]\sin\omega t - (a_2'\omega - \nu^2 f)y\cos\omega t - a_2'\dot{y}\sin\omega t \\ &\quad - \Omega_2^2 y\sin\omega t + [\ddot{z} + b_2\dot{z} + \Omega_2^2 z]\cos\omega t \\ &\quad - a_2'\omega z\sin\omega t + a_2'\dot{z}\cos\omega t \\ &\quad = h\sin\phi - \nu^2\delta[\sin\omega t - f\cos\omega t] \quad (4) \end{aligned}$$

Multiplying Equation (3) by $\sin\omega t$, Equation (4) by $\cos\omega t$, and adding, gives Equation (5). Multiplying Equation (3) by $\cos\omega t$, Equation (4) by $\sin\omega t$, and substracting gives Equation (6)

$$\begin{aligned} &\ddot{z} + (b_2 + a_1' - \alpha\cos^2\omega t)\dot{z} \\ &\quad + \left(\Omega_1^2 - \kappa\cos^2\omega t + \frac{\alpha\omega}{2}\sin 2\omega t\right)z \\ &= \left(\omega a_1' - \omega\alpha\cos^2\omega t - f\nu^2 - \frac{\kappa}{2}\sin 2\omega t\right)y - \frac{\alpha}{2}\sin 2\omega t\,\dot{y} \\ &\quad + h\sin(\omega t + \phi) + \nu^2\delta f \quad (5) \end{aligned}$$

$$\begin{aligned} &\ddot{y} + (b_1 + a_1' - \alpha\sin^2\omega t)\dot{y} \\ &\quad + \left(\Omega_1^2 + \nu^2 - \kappa\sin^2\omega t - \frac{\omega\alpha}{2}\sin 2\omega t\right)y = \\ &\quad - \left(\omega a_1' - \omega\alpha\sin^2\omega t + \frac{\kappa}{2}\sin 2\omega t\right)z - \frac{\alpha}{2}\sin 2\omega t\,\dot{z} \\ &\quad + h\cos(\omega t + \phi) + \nu^2\delta \quad (6) \end{aligned}$$

These equations, with various simplifying assumptions, will be used in what follows.

4 Damping Induced Force Pulsations

Since the grinding wheel shown in Fig. 1 is readily able to execute tangential vibrations, one may suppose a small transient damped tangential vibration to occur occasionally during the grinding process. It will be shown that such a vibration will produce a pulsating normal force between wheel and work by virtue of the damping in the rotating system.

After setting $\kappa = \alpha = h = 0$ (for the present) in Equations (5) and (6) and shifting the origin to eliminate the constant terms by setting

$$z = \zeta + \zeta_0 \qquad y = \xi + \xi_0$$

there results

$$\ddot{\zeta} + (b_2 + a_1')\dot{\zeta} + \Omega_1^2\zeta = (\omega a_1' - f\nu^2)\xi \quad (7)$$

$$\ddot{\xi} + (b_1 + a_1')\dot{\xi} + (\Omega_1^2 + \nu^2)\xi = -\omega a_1'\zeta \quad (8)$$

from which it is seen that motions in the y and z-directions are

coupled by the rotary damping. A given vibratory motion in the tangential direction (ζ) is seen to produce a pulsating force in the normal direction (ξ) represented by the term $\omega a_1'\zeta$.

The possibility of self-excited vibrations in the system represented by Equations (7) and (8) can be investigated by making the substitution:

$$\zeta = Ae^{pt} + Be^{-pt}$$

$$\xi = Ce^{pt} + De^{-pt}$$

and demanding that the coefficients of e^{pt} and e^{-pt} vanish in both equations. In this way a set of four homogeneous simultaneous equations are obtained which then lead to a characteristic equation of essentially fourth order. The Routh-Hurwitz criterion [1][1] applied to this characteristic equation, assuming small damping, gives the only essential condition to be fulfilled for stability as

$$(\omega a_1')^2(f\nu^2 - \omega a_1')^2 < (\Omega_1^2 + \nu^2)\Omega_1^2(2\Omega_1^2 + \nu^2)^2 \qquad (9)$$

When $\nu = 0$, this condition, after replacing a_1' by its equivalent in terms of the logarithmic decrement δ, yields

$$\frac{\omega}{\Omega_1} < \frac{\sqrt{2}\pi}{\delta} \qquad (10)$$

which shows that, for the usual small values of δ found in ball-bearing spindles ($\delta < 0.5$), instability directly due to rotary damping occurs at speeds well over the critical speed. This is in agreement with work done on a similar system by Smith [2]. As ν increases in value the speed at which rotary damping-induced instability occurs is raised even higher. Consequently, in grinding practice, with speeds below the critical speed, instability due directly to rotary damping does not occur. However, self-excited vibrations may develop, through the regenerative effect of inhomogeneous wheel wear or loading on the wheel, which in turn may be caused by rotary damping induced normal force pulsations.

5 Gyroscopically Induced Force Pulsations

Pulsations in the normal force on a grinding wheel may be produced by gyroscopic moments in addition to those produced by rotary damping.

A complete analytical treatment, involving two differential equations for the two angular co-ordinates and Equations (5) and (6) for the displacements of the wheel center, will not be attempted here. However, an approximate simplified treatment will suffice to illustrate the cause of gyroscopically induced force pulsations between wheel and work.

It will be supposed again that the work constrains the wheel to vibrate essentially in the tangential direction as shown in Fig. 7, and also that the wheel can be represented as a thin disk on the end of a cantilever beam (admittedly a rough approximation). A tangent drawn from the wheel will intersect the spin axis at point O which forms the origin for a set of three vectors, the spin vector $\bar{\omega}$, the precession vector $\bar{\Omega}$, and the moment vector $\bar{M}$. As the wheel vibrates tangentially to the work, the precession vector $\bar{\Omega}$ reverses its direction and its magnitude varies sinusoidally. The moment vector $\bar{M}$ will have its largest value when $\bar{\Omega}$ is largest. From the theory of the simple gyroscope

$$\bar{M} = J\bar{\Omega} \times \bar{\omega} \qquad (11)$$

If the wheel is vibrating tangentially

$$|\bar{\Omega}| = \frac{1}{a}\frac{dz}{dt} \qquad (12)$$

and since the pulsating moment $M = \Delta F_n a$, the pulsating normal force ΔF_n is

[1] Numbers in brackets designate References at end of paper.

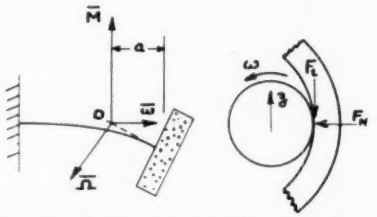

Fig. 7 Illustration showing gyroscopically produced normal force pulsations due to tangential vibrations

$$\Delta F_n = J\frac{\omega}{a^2}\frac{dz}{dt} \qquad (13)$$

and the pulsating tangential force is

$$\Delta F_t = Jf\frac{\omega}{a^2}\frac{dz}{dt} \qquad (14)$$

where f is the "coefficient of friction." It may be seen from Fig. 7 that an upward movement of the wheel causes a reduction or unloading of F_n and F_t and on the downward stroke an increase in F_n and F_t. If the wheel encounters a diminishing force, $-\Delta F_t$, as it moves up and an increasing force, $+\Delta F_t$, as it moves down, it is clear that the possibility of self-excited vibration exists. Consequently, since ΔF_t is proportional to the velocity and acts in the same direction as the velocity, the following differential equation, for the tangential motion alone, results

$$m\frac{d^2z}{dt^2} + \left[c - \frac{Jf\omega}{a^2}\right]\frac{dz}{dt} + Kz = 0 \qquad (15)$$

and the system is stable as long as

$$\frac{Jf\omega}{a^2} < c \qquad (16)$$

where c is the total effective damping. It can be seen from inequality (16) that high speeds and low damping encourage instability. Furthermore, higher modes of vibration, yielding smaller values of a may become unstable.

Assuming condition (16) to be satisfied, it is clear that, even though the system is stable in regard to direct gyroscopic action, tangential vibrations will produce force pulsations between wheel and work which, as before, through a regenerative effect involving wheel wear or inhomogeneous loading or dulling, may lead to a build-up of vibration.

If the wheel is vibrating tangentially to the workpiece at frequency p, the gyroscopic force pulsation is in phase with the velocity and rotary damping-induced force pulsation is in phase with the displacement. Consequently the total force pulsation can be expressed in the form

$$\Delta F = (F_d^2 + F_g^2)^{1/2}\sin(pt + \phi) \qquad (17)$$

where F_d and F_g are the force pulsations due to rotary damping and gyroscopic moment respectively.

6 Effect of Unsymmetrical Spindle Rigidities

In addition to these effects, the question naturally arises as to what effect small differences in rigidity of the spindle have and whether or not instabilities can occur as a result of this rigidity variation. In Equations (5) and (6), κ represents the difference in rigidity about two mutually perpendicular principal axes. For the present, assume all damping constants to vanish ($a_1' = b_1 = b_2 = a = 0$) and $\phi = 0$. Then Equations (5) and (6) become, after introducing $\tau = \omega t$ and using the symbols defined in the nomenclature,

$$\frac{d^2z}{d\tau^2} + (a_1 - 2q\cos 2\tau)z = \left(-\frac{fp^2}{\omega^2} - 2q\sin 2\tau\right) y + g\sin\tau + Kf \quad (18)$$

$$\frac{d^2y}{d\tau^2} + (a_2 + 2q\cos 2\tau)y = -2q\sin 2\tau\, z + g\cos\tau + K \quad (19)$$

In these equations the terms K and Kf represent the normal and tangential grinding forces and the terms involving g represent the unbalance. If the dimensionless rigidity difference q is small compared to K and g, one of the coupling terms may be neglected and there results

$$\frac{d^2z}{d\tau^2} + (a_1 - 2q\cos 2\tau)z = -\frac{fp^2}{\omega^2} y + g\sin\tau + Kf \quad (20)$$

$$\frac{d^2y}{d\tau^2} + (a_2 + 2q\cos 2\tau)y = g\cos\tau + K \quad (21)$$

which form a pair of inhomogeneous Mathieu equations.

The problem of forced vibrations in systems yielding an inhomogeneous Mathieu equation has been treated by Kotowski [3], whose results will be applied here to discuss the nature of the solutions of Equations (20) and (21).

Since Equations (20) and (21) are linear differential equations with periodic coefficients they possess solutions of the form

$$y = y_r + y_p$$

where y_r is the general solution of the reduced equation and y_p is a particular solution depending on the forcing function. Also, if the forcing function consists of two or more frequencies as Equations (20) and (21) do, the constant term being essential and of frequency zero, the corresponding particular solutions may be superimposed due to the linearity of the equations.

The solutions of the reduced Equation (21)

$$\frac{d^2y}{d\tau^2} + (a_2 + 2q\cos 2\tau)y = 0 \quad (22)$$

have been thoroughly investigated [4]. As is well known, periodic solutions of this equation exist only for certain values of a and q. Unbounded solutions, representing unstable operations, exist for certain other values of a and q as shown in Fig. 8.

It has been shown that the particular solution of the inhomogeneous Equation (21) possesses an infinite number of frequencies in contrast to the usual theory of forced vibrations in linear systems with constant coefficients, where only the forcing frequency itself appears in the particular solution. Consequently, instead of having one resonance condition, there are many in this case. The points of resonance found in the aq plane will be discussed shortly after describing the locus of the point aq as the spindle speed is changed.

It will be noted that both a and q vary with the spindle speed ω but that a/q is independent of ω. Therefore, for a given spindle or fixed values of Ω_1, Ω_2, and ν, the point a, q moves along a straight line, such as OA in Fig. 8, having the slope a/q and intersecting the origin. If q is considered positive in Equation (20) then the one in Equation (21) is negative; hence the line OA is drawn in the area for $q < 0$ and corresponds to Equation (21), while line OB corresponds to Equation (20). It will further be observed that a is essentially the reciprocal of the square of the critical speed ratio, i.e., when running at 1/2 the critical $a = 4$, etc. Starting with low spindle speeds and increasing them corresponds to moving along OA in the direction toward O.

The driving function $g\cos\tau + K$ in Equation (21) is even and as has been shown [3] will have resonant points on the even a_n-curves of Fig. 8 corresponding to the "cosine-elliptic" Mathieu functions. Resonant points due to the K term occur at the intersections of OA with the a_2, a_4, a_6, . . ., curves while the unbalance term causes resonances at the intersection of OA with a_1, a_3, a_5, . . ., curves. Consequently, a spindle may exhibit vibrations in the neighborhood of 1/2, 1/4, 1/6, . . . of the critical speed due to the grinding force K and vibrations in the neighborhood of 1/3, 1/5, 1/7, . . . of the critical speed due to unbalance, the lower speed resonances being of less importance.

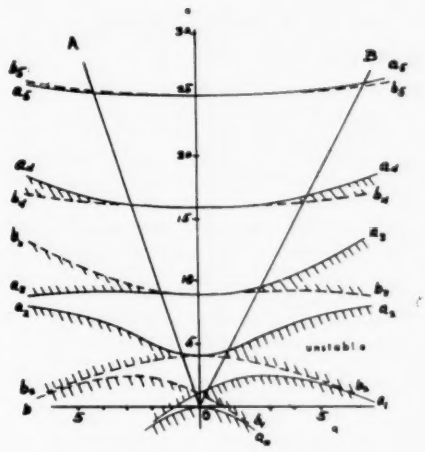

Fig. 8 Mathieu stability chart

Since y may be considered small at speeds other than those just mentioned, Equation (20) degenerates into one similar to Equation (21) by dropping the y coupling term. In this case, as already mentioned, the line OB applies, and again there are resonant points at the intersections of OB with the a_2, a_4, . . . curves caused by the tangential force Kf and resonant points at the intersections with the b_1, b_3, b_5, . . . curves caused by the unbalance term $g\sin\tau$.

In view of the fact that Equations (18) and (19) are actually coupled it is to be expected that large vibrations in the y-direction will cause large vibrations in the z-direction. Since $a_1 \neq a_2$, there will be two sets of speeds where vibrations may appear. For example, suppose a spindle has an average natural frequency, tangential to the workpiece, of say 1000 cps and 1600 cps normal to the workpiece. Then rough operation is likely to occur at spindle speeds of: 500, 333, 250, 200, . . ., due to a_1 and 800, 533, 400, 320, . . ., due to a_2.

Conclusion

On first thought it might be supposed that a grinding wheel should grind smoothly irrespective of the rigidity and damping characteristic of the spindle. However, it is apparent that there are many factors which may contribute to rough and undesirable operation of high-speed precision-grinding equipment.

References

1 E. J. Routh, "Advanced Dynamics of a System of Rigid Bodies," sixth edition, Dover Publications, Inc., New York, N. Y., 1955.

2 D. M. Smith, "The Motion of a Rotor Carried by a Flexible Shaft in Flexible Bearings," *Proceedings, Royal Society (London)*, vol. 142, series A, pp. 92–118.

3 G. Kotowski, "Lösungen der inhomogenen Mathieuschen Differential gleichung mit periodischer Störfunction beliebiger Frequenz (mit besonderer Berücksichtigung der Resonanzlösungen)," *Zeitschrift für angewandte Mathematik und Physik*, vol. 23, no. 4, 1943, pp. 213–229.

4 N. W. McLachlan, "Theory and Application of Mathieu Functions," The Clarendon Press, Oxford, England, 1947.

DISCUSSION

J. E. Plainevaux[2]

The author has presented an excellent pioneering paper on the vibrations of grinding spindles with two degrees of freedom.

Recently, attention has been devoted to the study of tool vibrations with two degrees of freedom. The problem of single-point tools has been examined in a particular case by Saljé[3] and in more general cases by two Czech engineers: J. Tlustý and L. Špaček.[4] There is no doubt that studies applied to the more difficult problem of grinding spindles will give also interesting results.

In the case of the force pulsations introduced through dampings, the main condition, equation (9) of the paper, to be fulfilled for stability seems to have to be

$$2(2\Omega_1^2 + \nu^2)(b_1 + a_1')^2 + \nu^4 > 4\omega a_1'(\omega a_1' - f\nu^2)$$

with $b_1 = b_2$.

If $\nu = 0$, relation (10) of the paper becomes:

$$\frac{\omega}{\Omega_1} < 1 + \frac{b_1}{a_1'}$$

[2] Lecturer of Technology, University of Brussels, Brussels, Belgium.

[3] Ernst Saljé, "Self-Excited Vibrations of Systems With Two Degrees of Freedom," TRANS. ASME, vol. 78, 1956, pp. 737-748.

[4] J. Tlustý and L. Špaček, "Samobuzené kmity v obrábecích strojích," 378 pages. The writer suggests that a translation of this book in a more accessible language would be welcome.

in agreement with the paper of D. M. Smith [2], in which there is a misprint in the corresponding relation.

The part devoted in the paper to the effects of unsymmetrical spindle rigidities is of striking interest. The simplified mechanical problem is familiar to electrical engineers due to the analogy with the self-excitation of a salient-pole alternator on a purely capacitive load.

Fortunately for us, rotors (and their bearings) have important damping and only little anisotropy for a complete instability is to be encountered, not at determined speeds, but in intervals of speeds, even for an unsymmetrical perfectly balanced rotor with some damping. Possibly, this phenomenon could explain the difficulties encountered in building two-pole turbogenerator rotors like ordinary salient-pole rotors (with a view to avoiding the patent of Charles Brown for round-rotor machines).

For grinding spindles, we think that increasing the damping will increase the quality of the surface finish.

Author's Closure

The author wishes to thank Mr. Plainevaux for his remarks. In connection with the section on Damping Induced Force Pulsations the stability of the system is governed by four conditions which are obtained by the Routh-Hurwitz criteria. These conditions are rather unwieldy and are being studied further.

If Mr. Plainevaux will qualify the last statement in his discussion by limiting the damping of grinding spindles to nonrotary damping the author will agree that better surface finishes may in some cases be attained.

J. FRISCH

Associate Professor of Mechanical Engineering, University of California, Berkeley, Calif. Assoc. Mem. ASME

E. G. THOMSEN

Professor of Metal Processing, University of California, Berkeley, Calif. Mem. ASME

The Effect of Process Variables on Extrusion Pressures of Lead

Billets of commercially pure lead, 2 in. diam × 3 in. long were extruded at room temperature through five different die contours at ram speeds up to 50 ipm. It was found that, for the direct and indirect extrusions, with good lubrication (white lead in oil) and with good cylinder-wall finish, the extrusion pressure-displacement diagrams were essentially the same. The concentric and eccentric single-bar and multibar extrusions at constant extrusion ratio required approximately the same pressures when extruded at identical speeds. The extrusion pressures over the wide range of speeds investigated showed approximate linearity when plotted on log-log co-ordinates.

THE commercial extrusion of metals is a process in which a billet is squeezed through an orifice into a variety of industrial shapes usually having uniform cross sections. Two common methods of extrusion are the direct and indirect methods shown schematically in Figs. 1(*a* and *b*), respectively. In the direct method, the ram of the extrusion press pushes the billet to be extruded toward the stationary die from which it emerges as the extruded product. Consequently, relative motion between billet and cylinder wall results. In the indirect extrusion process, the billet remains fixed in the cylinder and the die is forced into the billet imparting a movement to the extruded product which is opposite in direction to the die motion. In the latter case, the so-called dead-metal region, which in practice usually exists in the region of the metal entrapped between cylinder wall and die, prevents relative motion between cylinder and billet from taking place. Both processes are used in practice but the direct process is the more common.

While extrusion practice is well advanced, it is still more an art than a science. As in other metal-working processes, the art appears to be far ahead of the theory so that the theory gives some information *a posteriori* about what is already known from practice. However, it is generally believed, as stated so well by Bishop [1][1] in his comprehensive account of the theory, that even an incomplete and late theory is of material assistance in permitting a more informed, semiempirical approach in dealing with practical problems.

A survey of the literature reveals that a great deal of theoretical as well as experimental work is in progress abroad, notably in Great Britain. This seems to point up the fact that there the extrusion process is not only considered to have scientific interest, but also that the process may offer excellent opportunities for study of the mechanics of metal deformation under complex stressing. This has been the point of view of the authors in their work on extrusion, and the paper will deal with another facet of the extrusion problem which apparently serves this dual function. In what follows, no attempt will be made to give a complete account of the published literature. Hence the reader is referred to two recent articles by Bishop [1] and Watkins, et al. [2] where a

Contributed by the Metal Process Activity of the Production Engineering Division and presented at the Annual Meeting, November 30–December 5, 1958, New York, N. Y., of THE AMERICAN SOCIETY OF MECHANICAL ENGINEERS.

NOTE: Statements and opinions advanced in papers are to be understood as individual expressions of their authors and not those of the Society. Manuscript received at ASME Headquarters, July 2, 1958. Paper No. 58—A-109.

[1] Numbers in brackets designate References at end of paper.

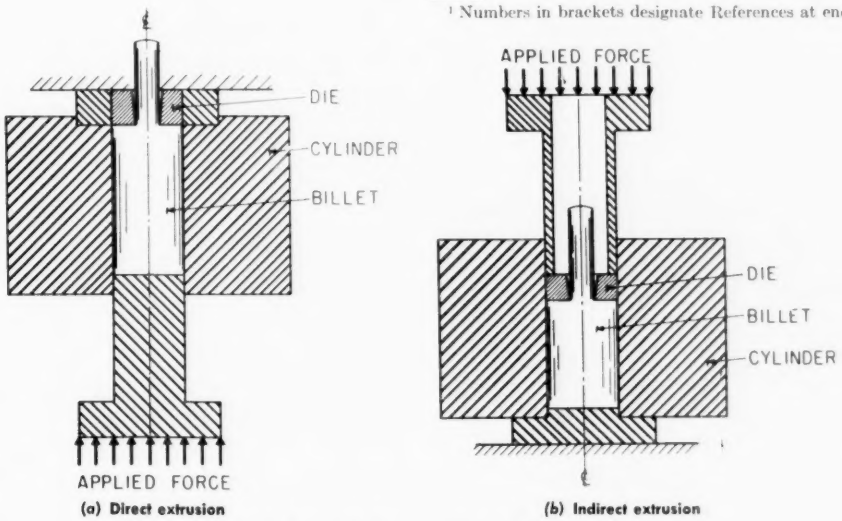

(*a*) Direct extrusion (*b*) Indirect extrusion

Fig. 1 Schematic diagrams of extrusion processes

reasonably complete survey of the published literature is reported. In addition, these papers are worth studying, inasmuch as Bishop gives an excellent account of the present status of the theory, while Watkins, et al., give a comprehensive survey of results from recent extrusion experiments.

Dodeja and Johnson [3, 4] have recently published two articles on extrusions covering both theoretical and experimental investigations on multiple-bar extrusions with lead and other metals. These investigators used 1-in. billets at a relatively low ram speed of 0.1 ipm in a direct extrusion process. It was found that the pressure, at the instant of formation of cavities (coring) at the bottom end of the billets when the extrusion ratio was held constant, increased with the number of bars extruded. This appears to be in agreement with experimental results reported by Pearson [5], but is contrary to those found by Watkins, et al. [2]. In addition, Dodeja and Johnson [3, 4] determined possible slip-line solutions for multihole, sharp-edged dies and concluded that the theoretical extrusion pressures should remain nearly constant. It is the purpose of the paper to give additional results on direct and indirect extrusions of lead for several bar eccentricities as well as multibar extrusions at higher rates of deformation than were reported by the afore-mentioned investigators.

Experimental Technique

The 2-in-diam × 3-in-long commercially pure (99.9 per cent) lead billets, forged and annealed at room temperature before machining, were extruded through sharp-edged circular dies with cross sections as shown in Fig. 2. The resulting cylindrical extrusions shown in Fig. 3, for each of the five different die shapes, had a total extruded cross-sectional area such that the ratio of extrusion area to billet area remained essentially constant. The A_0/A ratio selected was the same as the one used with 4.3-in-diam billets reported previously [6]. The direct and indirect extrusion methods used in this investigation and shown schematically in Fig. 1, were performed in a 40-ton hydraulic press shown in Fig. 4. In the direct method, the cylinder was suspended from the crosshead of the press as shown in Fig. 5, while during the indirect extrusion tests the cylinder rested on the platen of the ram as seen in Fig. 6. White lead in oil was used in making friction negligible during extrusion of the 40 specimens listed in Table 1.

During each test the instantaneous extrusion loads as well as ram displacements and corresponding ram velocities were recorded on a Sanborn two-channel amplifier-recorder. Load calibration of the hydraulic press was done by means of the calibrated compression bar in spherical seats shown in Fig. 4. The pressure variations were sensed with a Baldwin SR-4 fluid pressure cell connected between the hydraulic system of the press and the Sanborn recorder. For the purpose of illustration, Fig. 7 shows autographic records of load displacement for the direct and indirect extrusion of specimen I in Fig. 3 at a steady-state ram velocity of 36 ipm. For recording instantaneous ram displacements, i.e., billet reductions and corresponding velocities, a 200-point circular electric contact switch was mounted on the ram platform. The switch was rotated through a pinion by a rack attached to the press frame. Calibration of the beginning and end of contact of each switch position and corresponding amounts of ram displacement were done with a 0.001-in. dial indicator showing the instantaneous ram positions. During each test the switch signaled the ram displacement, i.e., the amount of billet reduction, to the Sanborn recorder, and was plotted together with a 1-sec interval time marker on the recording tape. Translation of the switch signals into inches of billet reduction together with the time-interval recording made it possible to obtain the velocities at which the extrusion tests were performed.

The experimental tests for each of the 5 extrusion patterns were divided into two groups; namely, direct extrusion and indirect extrusion. Four different ram velocities within the capacity of the hydraulic press were selected for each group, the extremes being a minimum velocity of 2.65 ipm and a maximum velocity of 49 ipm. The resultant experimental data are shown in Table 1. Additional tests at ram velocities ranging from 0.05 to 0.2 ipm were made in a hydraulic testing machine, in order to compare extrusion pressures of 2-in-diam billets with those of 4.3-in-diam billets obtained in earlier tests [6, 7].

Results and Discussion

Examining the autographic diagrams of the direct and indirect

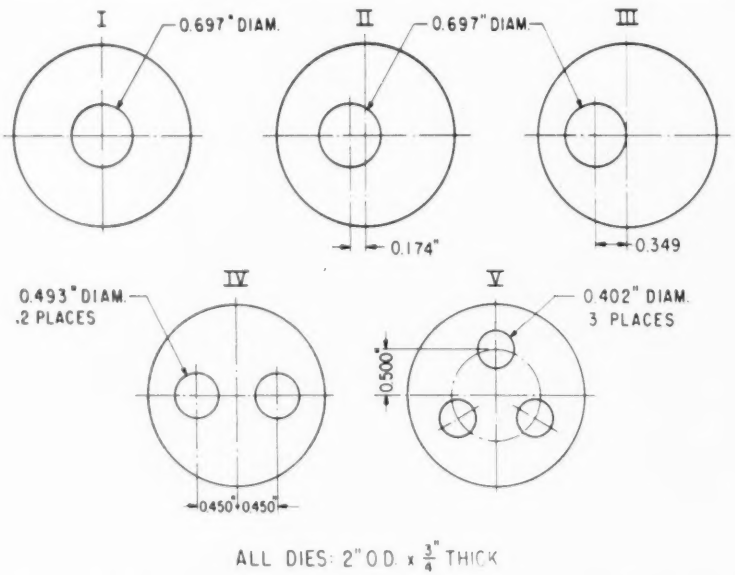

Fig. 2 Configuration of the five sharp-edged dies used in experiment at constant extrusion ratios

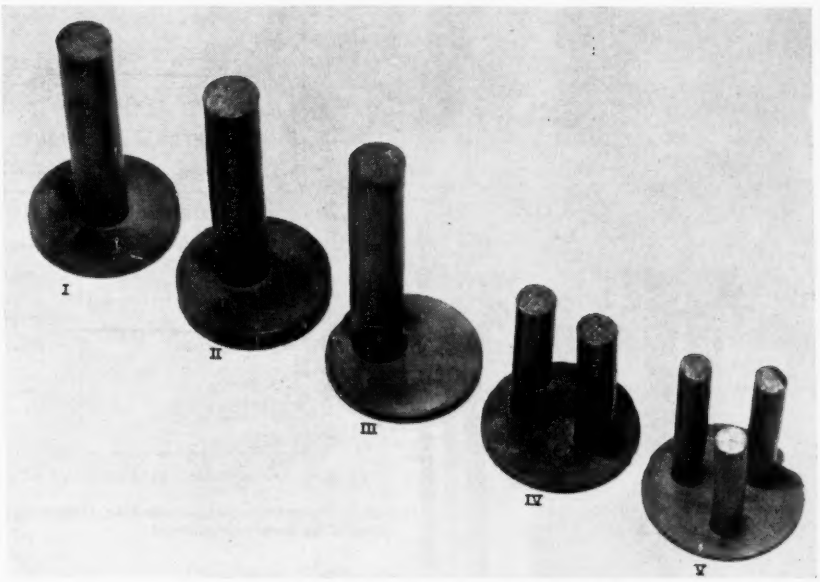

Fig. 3 Short segments of extruded bars still attached to billet

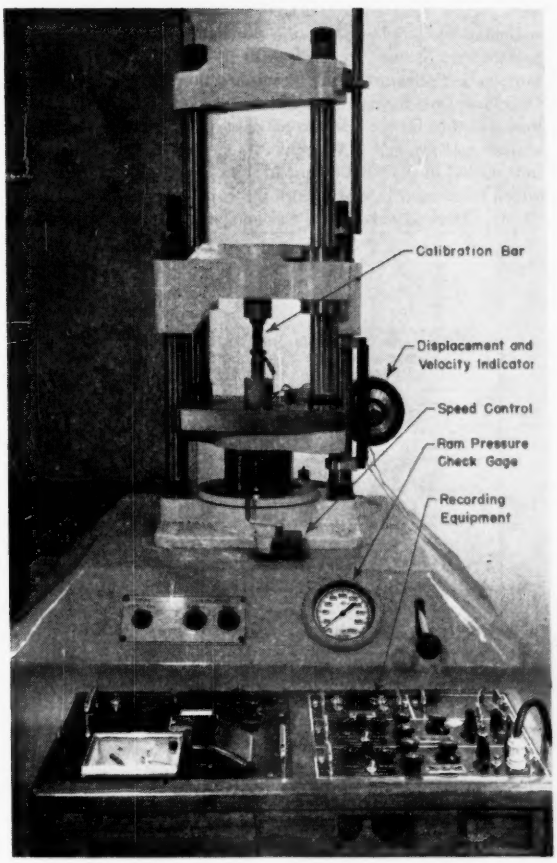

Fig. 4 High-speed hydraulic press and Sanborn recording equipment

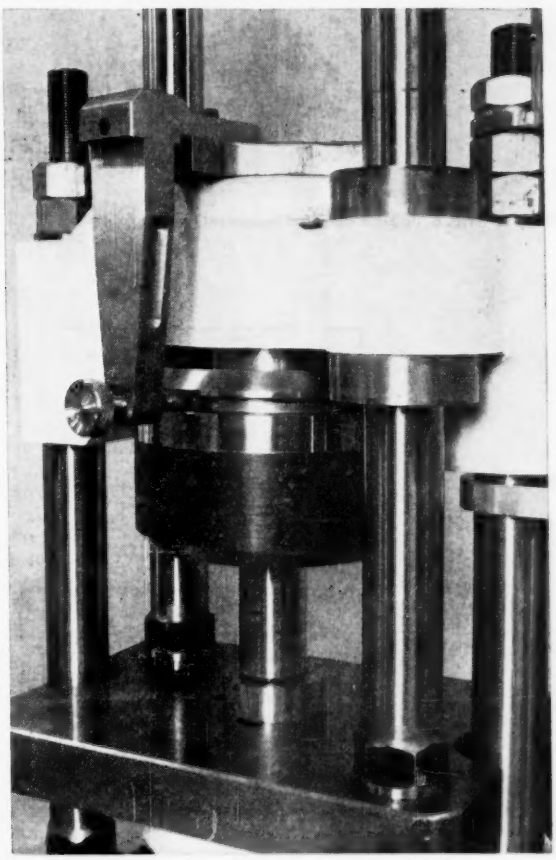

Fig. 5 Direct extrusion equipment in place for testing

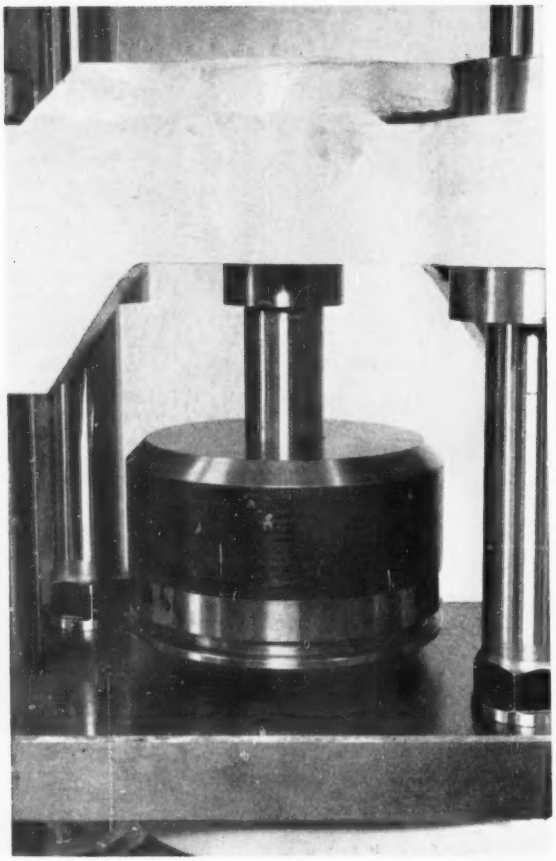

Fig. 6 Indirect extrusion equipment in place for testing

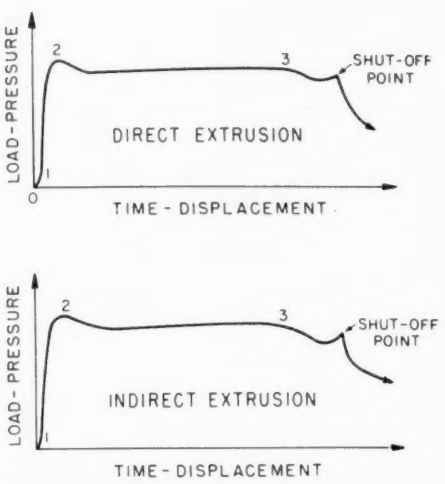

Fig. 7 Typical autographic extrusion load-displacement diagrams as recorded by Sanborn equipment

extrusion of the 2-in-diam × 3-in-long lead billets shown in Fig. 7, it may be seen that the curves are nearly identical. This demonstrates the fact that good lubrication and a good surface finish can reduce wall friction to a negligible value. It may be seen further that each diagram consists of several portions as indicated by numbers. In the portion 0–1, the billet is compressed and is made to conform to the cylinder cavity. In the portion 1–2 the load rises to initiate flow through the orifice. Ordinarily, the maximum extrusion load occurs at point 2. The load will then decrease to a somewhat lower value as steady-state extrusion is reached. At point 3 unsteady state sets in and the bottom end of the billet begins to show the formation of a cavity, which is referred to as the coring point by Dodeja and Johnson [3, 4]. Beyond this point, the load first decreases and subse-

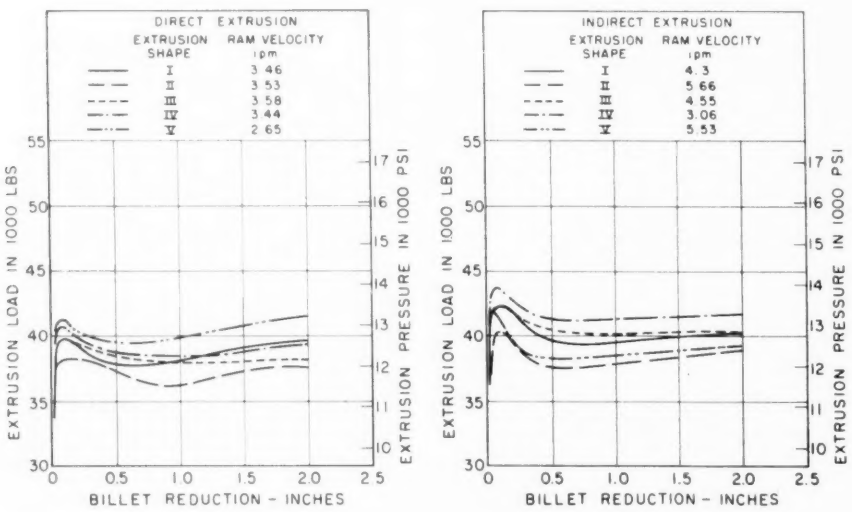

(a) Direct extrusion

(b) Indirect extrusion

Fig. 8 Load versus ram displacement diagrams for ram velocities from 2.65 to 5.66 ipm

Table 1 Extrusion pressures

Specimen Type	Description	A_o/A	Direct Extrusion								Indirect Extrusion							
			a		b		c		d		e		f		g		h	
			V_m ipm	P_{max} / P_{min}	V_m ipm	P_{max} / P_{min}	V_m ipm	P_{max} / P_{min}	V_m ipm	P_{max} / P_{min}	V_m ipm	P_{max} / P_{min}	V_m ipm	P_{max} / P_{min}	V_m ipm	P_{max} / P_{min}	V_m ipm	P_{max} / P_{min}
I	Single bar extrusion 0.694" diam. Axial symmetric	8.31	3.46	12,600 / 12,000	18.6	14,200 / 12,650	36.5	15,400 / 14,000	42.0	14,700 / 13,100	4.30	13,400 / 12,500	8.45	13,700 / 12,700	37.9	16,300 / 14,700	48.9	14,700 / 13,850
II	Single bar extrusion 0.691" diam. 0.174" eccentricity	8.38	3.53	12,200 / 11,500	19.0	14,200 / 13,100	34.5	15,500 / 14,000	43.2	13,800 / 13,400	5.66	12,800 / 11,900	10.0	14,100 / 12,900	37.7	16,200 / 14,600	49.0	15,500 / 14,100
III	Single bar extrusion 0.691" diam. 0.349" eccentricity	8.38	3.58	12,600 / 12,100	19.8	14,200 / 12,900	36.2	15,400 / 14,350	42.6	14,700 / 13,700	4.55	13,300 / 12,800	9.60	13,800 / 12,950	37.2	15,500 / 14,600	48.7	15,500 / 14,200
IV	Two bar extrusion 0.490" diam.	8.33	3.44	13,000 / 12,300	20.15	14,700 / 13,100	37.1	15,700 / 14,300	42.6	15,000 / 13,700	3.06	13,900 / 13,100	9.00	14,100 / 13,100	37.5	15,700 / 14,400	48.3	16,000 / 14,850
V	Three bar extrusion 0.396" diam.	8.50	2.65	12,800 / 12,550	20.6	14,700 / 13,150	37.2	15,800 / 14,300	42.6	16,000 / 14,300	5.53	13,300 / 12,200	8.76	14,400 / 13,400	35.7	16,200 / 15,000	47.4	16,300 / 15,680

V_m = Ram velocity, inches per minute
P_{max} = Maximum extrusion pressure, psi.
P_{min} = Minimum extrusion pressure, psi.
A_o = Billet area, in^2
A = Sum of extruded bar areas, in^2
A_o/A = Extrusion ratio

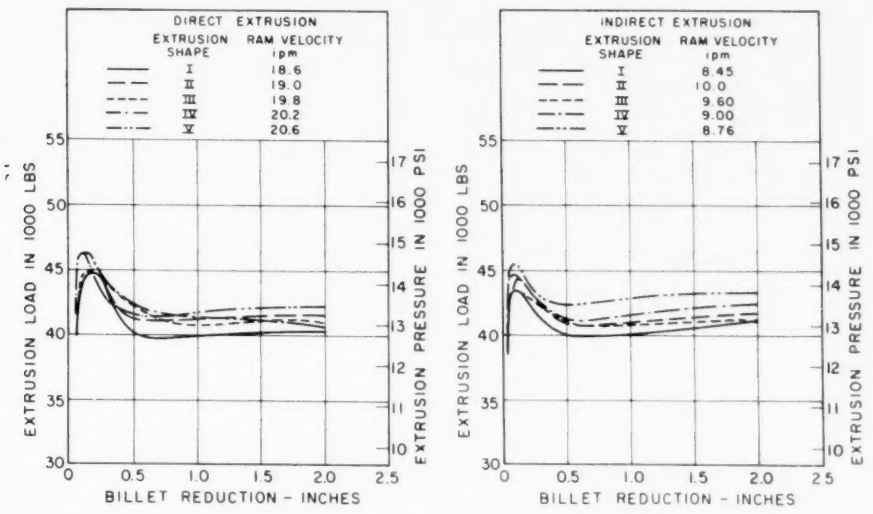

(a) Direct extrusion (b) Indirect extrusion

Fig. 9 Load versus ram displacement diagrams for ram velocities from 8.45 to 2.06 ipm

quently increases to a relatively large value, as the thickness of the billet reduces to the thickness of a thin disk. In practice, friction is usually encountered, hence the maximum extrusion load in direct extrusions (point 2 on the diagram) is higher than that for indirect extrusions. The magnitude of the maximum load is dependent on the length of the billet, but both curves tend to merge into one near the end of the stroke.

From the foregoing it is evident that the extrusion pressure as defined by the load divided by the billet area is not constant during an extrusion process. In order to size extrusion equipment, it appears that the maximum pressure, point 2 of Fig. 7, is obviously the critical value which needs to be known. For comparison with an extrusion theory, however, some other pressure may serve better. The extrusion pressure being influenced by wall friction in the direct extrusion process but not in the indirect prompted Dodeja and Johnson [3, 4] to choose the coring point as the pressure at which comparison between theory and experiment should be made. This method has the disadvantage that the

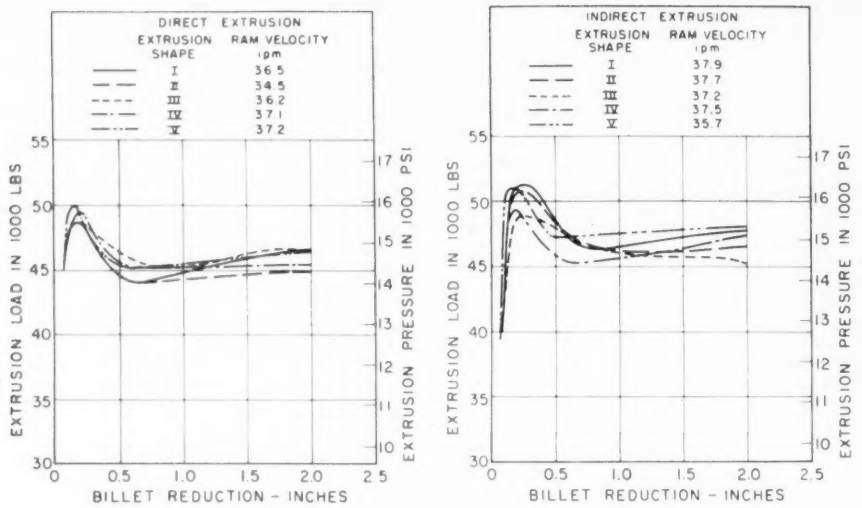

(a) Direct extrusion (b) Indirect extrusion

Fig. 10 Load versus ram displacement diagrams for ram velocities from 34.5 to 37.9 ipm

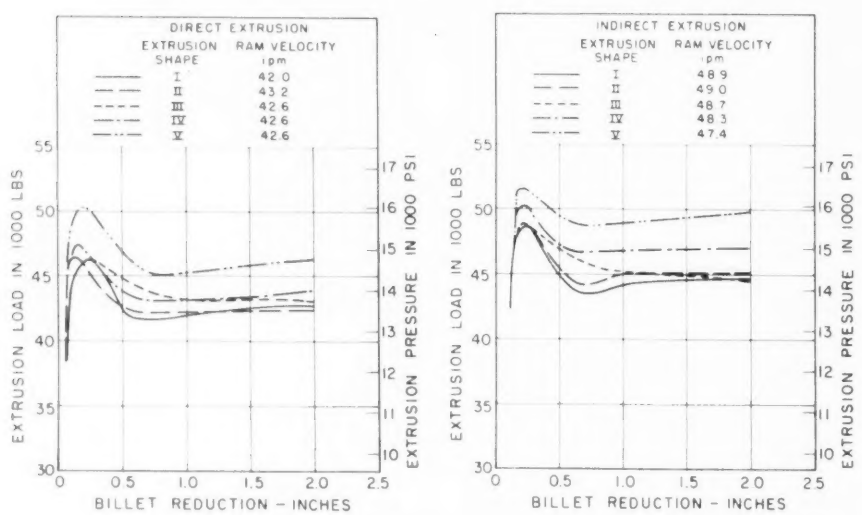

(a) Direct extrusion (b) Indirect extrusion

Fig. 11 Load versus ram displacement diagrams for ram velocities from 42.0 to 49.0 ipm

coring point is not readily observed at high ram speeds. In fact, in the present experiments it was difficult to obtain a positive shutoff of the hydraulic press near the coring point, so that the coring point was indeterminate. Furthermore, since the direct and indirect extrusion processes gave similar load-displacement diagrams, it was decided to compare only maximum and minimum extrusion pressures (load/billet area). These values are shown in Table 1 and have been obtained from the diagrams of Figs. 8–11, inclusive. It should be noted that the diagrams have been terminated arbitrarily at a billet reduction of 2 in., since the remainder of the curves varied, depending on where in the ram travel the load happened to be released. It may be seen from these curves that, generally speaking, eccentricity has no influence on the extrusion pressure, while the number of rods extruded may have a slight but not consistent effect on the extrusion pressure.

The minimum and maximum extrusion pressures are summarized as functions of speed in Figs. 12 to 15, inclusive. It is seen that the pressures are but slightly influenced by speed, i.e., rise with increasing speed except at the highest speeds investigated, but are essentially independent of eccentricity and rod diameter for the same extrusion ratios. Hence these experiments tend to confirm the theoretical predictions based on slip-line theory for plane strain extrusions given by Dodeja and Johnson [3, 4].

Fig. 16 shows a log-log plot of the minimum and maximum pressures as function of ram velocity. Some additional slow-speed data were obtained with 2-in-diam billets, while those

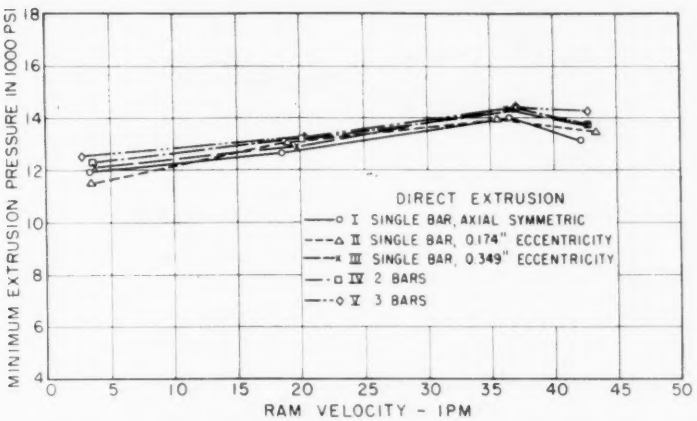
MINIMUM EXTRUSION PRESSURE IN 1000 PSI
RAM VELOCITY - IPM
DIRECT EXTRUSION
I SINGLE BAR, AXIAL SYMMETRIC
II SINGLE BAR, 0.174" ECCENTRICITY
III SINGLE BAR, 0.349" ECCENTRICITY
IV 2 BARS
V 3 BARS

Fig. 12 Minimum extrusion pressures versus ram velocities during direct extrusion at an approximately constant extrusion ratio of 8.4

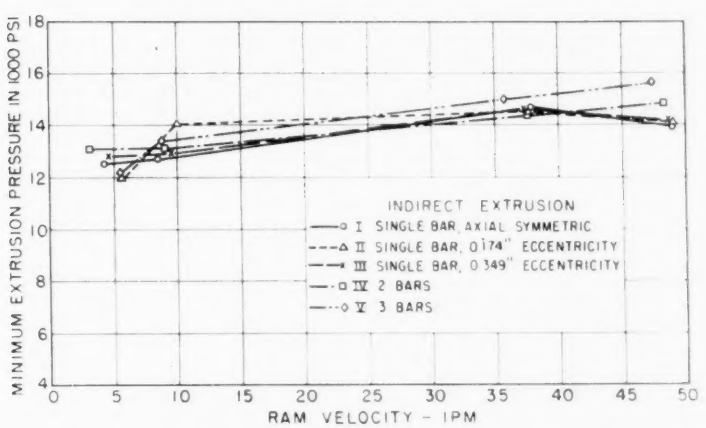
MINIMUM EXTRUSION PRESSURE IN 1000 PSI
RAM VELOCITY - IPM
INDIRECT EXTRUSION
I SINGLE BAR, AXIAL SYMMETRIC
II SINGLE BAR, 0.174" ECCENTRICITY
III SINGLE BAR, 0.349" ECCENTRICITY
IV 2 BARS
V 3 BARS

Fig. 13 Minimum extrusion pressures versus ram velocities during indirect extrusion at an approximately constant extrusion ratio of 8.4

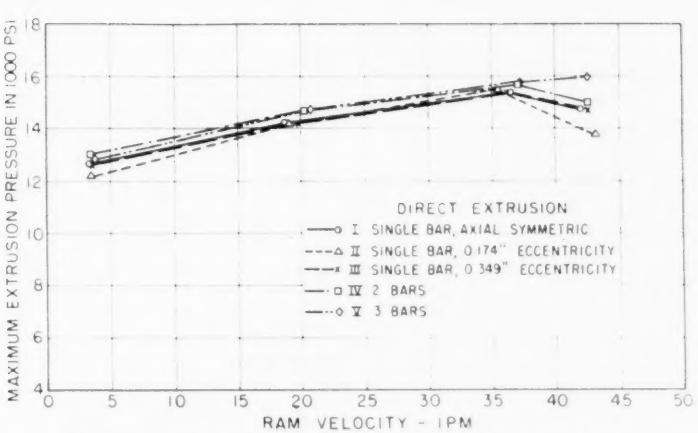
MAXIMUM EXTRUSION PRESSURE IN 1000 PSI
RAM VELOCITY - IPM
DIRECT EXTRUSION
I SINGLE BAR, AXIAL SYMMETRIC
II SINGLE BAR, 0.174" ECCENTRICITY
III SINGLE BAR, 0.349" ECCENTRICITY
IV 2 BARS
V 3 BARS

Fig. 14 Maximum extrusion pressures versus ram velocities during direct extrusion at an approximately constant extrusion ratio of 8.4

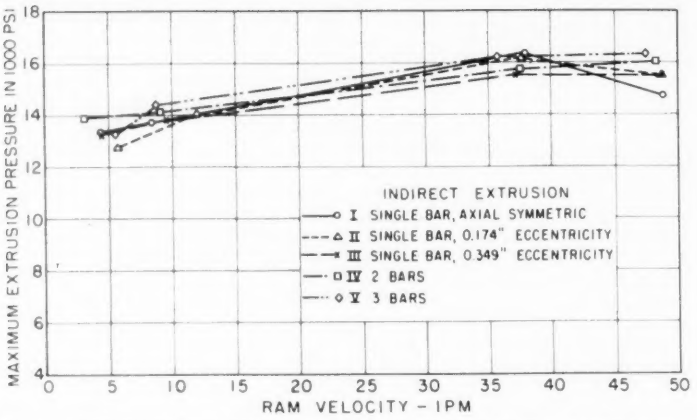
MAXIMUM EXTRUSION PRESSURE IN 1000 PSI
RAM VELOCITY - IPM
INDIRECT EXTRUSION
I SINGLE BAR, AXIAL SYMMETRIC
II SINGLE BAR, 0.174" ECCENTRICITY
III SINGLE BAR, 0.349" ECCENTRICITY
IV 2 BARS
V 3 BARS

Fig. 15 Maximum extrusion pressures versus ram velocities during indirect extrusion at an approximately constant extrusion ratio of 8.4

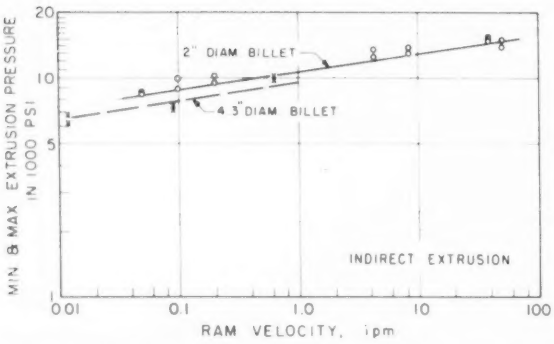

Fig. 16 Minimum and maximum extrusion pressures versus ram velocities of centrally located single rods during indirect extrusion of 2-in-diam and 4.3-in-diam billets with 8.3 and 8.2 extrusion ratios, respectively

with 4.3-in-diam billets were taken from earlier tests [6, 7]. All extrusions, however, had approximately the same extrusion ratios as shown in the figure. It is seen that the experimental points fall on approximate straight lines for each billet diameter. These data support the contentions of Watkins and his collaborators [2] that there is little or no size effect and that, for lead, the extrusion pressures plotted on log-log co-ordinates are essentially linear over a wide range of ram velocities.

Conclusions

1 With good lubrication and good cylinder-wall finish, the extrusion pressures for 2-in-diam × 3 in-long commercially pure lead billets are essentially identical when extruded at room temperature at an approximate extrusion ratio of 8.4.

2 Eccentricity of a single bar or multiple bars up to three, extruded at the same extrusion ratio, do not appear to influence the extrusion pressure.

3 Extrusion pressures appear to be influenced but little by size effect for 4.3 and 2.0-in-diam billets.

4 Extrusion pressures for the wide range of extrusion speeds investigated were approximately linear when plotted on log-log co-ordinates.

Acknowledgments

The authors wish to thank the National Science Foundation for its support of the present investigation by its Grant G-2957 to the University of California. They also wish to thank the University of California and the Division of Industrial Engineering for the use of their facilities, and Messrs. Lockrem and Gohl for the construction of the extrusion equipment and high-speed hydraulic press. They further wish to acknowledge the assistance given in testing and reduction of data by Messrs. Eggleston, Wolff, and Thometz, students in Engineering, as well as Mr. Kot, Mrs. Brewer, and Miss Matsumoto for preparing the manuscript.

References

1 J. F. W. Bishop, "The Theory of Extrusion," *Metallurgical Reviews*, vol. 2, 1957, pp. 361–390.

2 M. T. Watkins, K. Ashcroft, and J. McKenzie, "Some Aspects of the Cold Extrusion of Metals," Paper 47 (advance copy), presented at the Conference on Technology of Engineering Manufacture arranged by The Institution of Mechanical Engineers, London, England, March 25–27, 1958, pp. 1–13.

3 L. C. Dodeja and W. Johnson, "On the Multiple Hole Extrusion of Sheets of Equal Thickness," *Journal of Mechanics and Physics of Solids*, vol. 5, 1957, pp. 267–280.

4 L. C. Dodeja and W. Johnson, "The Cold Extrusion of Circular Rods Through Square Multiple Hole Dies,", *Journal of Mechanics and Physics of Solids*, vol. 5, 1957, pp. 281–295.

5 C. E Pearson, "The Extrusion of Metals," John Wiley & Sons, Inc., New York, N. Y., 1944, p. 136.

6 E. G. Thomsen and J. Frisch, "Experimental and Theoretical Pressures and Velocity Fields for Various Lead Extrusions," TRANS. ASME, vol. 80, 1958, pp. 117–123.

7 J. Frisch and E. G. Thomsen, "An Experimental Study of Metal Extrusions at Various Strain Rates," TRANS. ASME, vol. 76, 1954, pp. 599–606.

DISCUSSION

John L. Alden[2]

Some notes on a series of tests conducted in 1931 incidental to a 10-year program directed toward the development of a continuous extrusion machine for lead-cable sheath may serve to amplify this interesting paper. Lead containing $2^1/_2$ per cent antimony was extruded by the direct-extrusion method through a $^1/_4$-in. round die. Four cylinder diameters were employed, $^{13}/_{16}$, $1^1/_8$, $1^3/_8$, and $1^5/_8$ in. The extrusion ratios were approximately 10.5, 20.2, 30.2, and 42.2, respectively. The billets, 4 in. long, were cast directly in the cylinders.

Friction of the billet against the cylinder walls was an important element of the extrusion pressure and was found to be in direct

[2] Consultant, Maplewood, N. J.

proportion to the ratio of the cylinder circumference to its cross-sectional area. Extrusion pressures rose rapidly as the extrusion speed increased but tended to flatten out between about 50 and 120 ipm, the highest speed employed.

The effect of temperature was almost linear within the practical working range of 300 to 600 F. Thus, at 80 ipm with a circumference-to-area ratio of 2.0, the extrusion pressure at 300 F was 16,000 psi, at 450 F 10,000 psi, and at 600 F 5000 psi. At a ratio of 4.0 and at the same temperatures the respective pressures were 25,000, 18,000, and 12,000 psi.

To visualize flow patterns and profiles within the cylinder, thin layers of wax, dyed with contrasting colors, were cast in the cylinder. The results were useful qualitatively in demonstrating the presence of the dead area at the intersection of the cylinder wall with the plane of the die.

Excellent visualization of the flow lines within the cylinder and at the approach to the die orifice was obtained by filling the cylinder with lead shot which were then pressed and extruded. After extrusion was under way the press was stopped and the resulting slug carefully pressed out in reverse. Each pellet retained its individuality and the transition from approximate sphericity to filamentary form was dramatically exhibited.

J. M. Alexander[3]

The authors are to be commended for having carried out such a precise experimental investigation and for their clear presentation of the resulting data and details of the equipment used. It is most interesting to observe that the extrusion pressure for lead is substantially unaffected by the precise manner in which a given reduction is achieved. Since lead behaves almost exactly as a perfectly plastic material and since slip line field solutions predict the behavior found, the implication is that slip line field theory does give a good indication of behavior in general three-dimensional systems.

Johnson[4] recently proposed upper-bound solutions for the extrusion problem, under plane-strain conditions. The writer suggested in his discussion on Johnson's paper that these upper-bound techniques can be extended to problems of rotational symmetry. The use of such methods in conjunction with lower-bound techniques gives promise for solving complicated extrusion problems of the type under discussion here. Experimental researches of the type carried out by the authors are invaluable from the point of view of giving a sound basis of comparison for such theories, and serve to keep the theoretical plastician's "feet on the ground."

In this connection, one small criticism of the paper is that the authors have not included the basic yield-stress curve for the material used in their experiments. This will render it difficult to make the comparisons just suggested between theory and experiment, and it would be most helpful if the authors could include such a graph in their reply to the discussion. The effect of strain rate on this basic yield-stress curve could be estimated from the data given in Fig. 16.

[3] Reader in Plasticity, Imperial College of Science and Technology, University of London, South Kensington, London, England.

[4] W. Johnson, "Estimation of Upper-Bound Loads for Extrusion and Coining Operations," presented at a meeting of The Institution of Mechanical Engineers, London, England, October 31, 1958.

C. T. Yang[5]

The authors give very valuable information in their paper and are to be congratulated. There are several points on which the writer wishes to comment:

1 The authors found extruding either single bar or multiple bars (up to 3) with the same extrusion ratio does not influence the extrusion pressure. This furnishes strong evidence that friction on the extrusion die is very small. In that case, the equation for deformation pressure,

$$p = \beta \bar{\sigma}_0 \log_e \frac{A_0}{A}$$

where

β = shear factor
$\bar{\sigma}_0$ = yield strength
A_0/A = extrusion ratio

can be applied not only to single but to multiple-bar extrusions also, as long as the reduction ratio is kept constant.

2 In Fig. 7 of the paper, the pressure versus displacement curves are identical for both direct and indirect extrusion. This is rather unusual because it shows the wall friction on the direct extrusion chamber is negligible and the lubricant used is ideal. Generally, in the direct-extrusion process, the extrusion pressure drops as the displacement of the ram increases.

3 The authors show that the ram speed or strain rate has little effect on extrusion pressure with lead as the billet. This agrees

[5] University of Michigan, Ann Arbor, Mich.

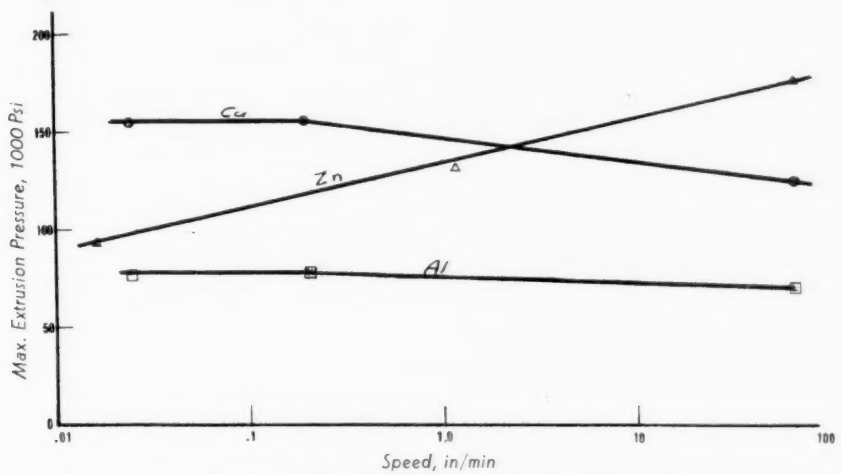

Fig. 17 Maximum extrusion pressure versus speed curve

partly with the research data from Professor Fukui, et al,[6] Tokyo University. They found the backward extrusion pressure versus strain-rate curves as shown in Fig. 17.

Fig. 17 indicates that Cu and Al behave in a similar manner to lead, which is shown in the paper; that is, insensitive to strain rate at slow speed. However, Zn is very sensitive to speed effect. The writer believes this is due to the fact that Zn is HCP in lattice structure. The number of slip mechanisms for Zn is only three compared with Cu and Al, both are FCC and each has 12 slip mechanisms.

Also in Fig. 17, at a speed of about 16.5 ipm, the pressure drops. This could be attributed to the temperature increase in the billet at high speed. If the speed is high, the process is close to adiabatic. The temperature in the billet could reach the recrystallization temperature, and annealing effect counteracts the strain-rate effect. The pressure drop, however, is not shown in Fig. 15 in the paper. This could be due to the fact that the recrystallization temperature of lead is the room temperature. Concerning the curve for Zn, the writer believes that pressure also will drop eventually, if high speed is reached.

Authors' Closure

The authors are taking this opportunity to thank Mr. Alden and Professors Alexander and Yang for their kind discussions.

Mr. Alden's description of earlier research in extrusion of lead and the methods employed to visualize flow patterns are most interesting. However, since then the authors have successfully employed the method of visioplasticity described in previous papers [6, 7]. In this method both rectangular and polar co-ordinate grid patterns were inscribed on the meridian plane of axial symmetrical extrusion billets of lead and aluminum. Not only was flow visualization obtained by tracing the movements of grid intersections but studies of stress-strain distributions in the billet at various strain rates as well as comparisons with theory were successfully performed.

To make the comparisons between theory and experiment suggested by Professor Alexander the average effective-stress effective-strain curves for commercially pure lead at various strain rates are shown in Fig. 18. These curves, which were also published in another paper,[7] were obtained with 1-in. high × 1-in. diam cylindrical specimens using white lead in oil lubricant in grooves at both end surfaces of the specimens. Since the effective stress no longer depends on strain at and above an effective strain of 1.0 in./in. a cross plot of effective stress versus effective strain rate is shown in Fig. 19 for an effective strain of 1.0 in./in. Comparison of the slope of the curve in Fig. 19 with the slopes of the extrusion pressure versus ram velocity curves in Fig. 16 shows essentially identical values thereby demonstrating the good agreement between theory and experiment. Johnson's[8] paper, referred to by Professor Alexander, deals with cases for which straight-edged dies have been assumed. However, another as yet unpublished paper[8] by the same author on upper bound

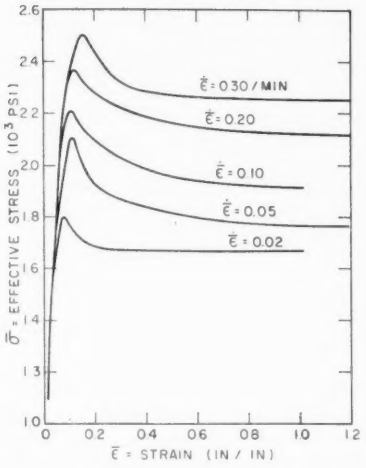
$\bar{\sigma}$ = EFFECTIVE STRESS (10³ PSI)
$\bar{\epsilon}$ = STRAIN (IN / IN)
$\dot{\bar{\epsilon}}$ = 0.30 / MIN
$\dot{\bar{\epsilon}}$ = 0.20
$\dot{\bar{\epsilon}}$ = 0.10
$\dot{\bar{\epsilon}}$ = 0.05
$\dot{\bar{\epsilon}}$ = 0.02

Fig. 18 Average effective-stress effective-strain curves of commercially pure lead in compression for various strain rates

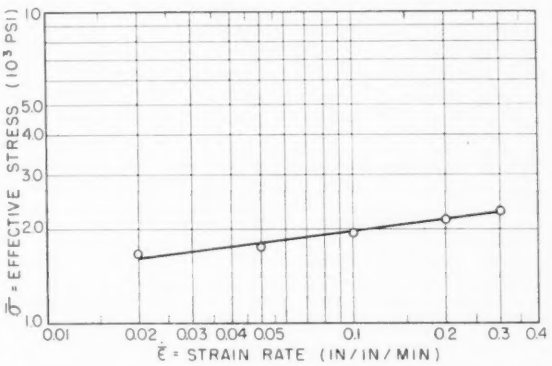

Fig. 19 Average effective-stress strain-rate curve of commercially pure lead in compression at an effective strain of 1.0 in./in.

loads for extrusion of circular shaped dies would serve well in comparing his graphical estimates of loads with the experimental values presented here.

Professor Yang's suggestion to apply the equation for deformation pressure in single extrusions to multiple bar extrusions assuming a constant extrusion-ratio is valid only for ideal lubrication condition and particular ram speeds. As demonstrated by the authors' experiments the effect of ram velocity, i.e., strain rate, however slight, is still a parameter which must be considered.

The maximum extrusion pressure versus speed curves for Cu, Zn, and Al shown in Fig. 17 together with Professor Yang's comment that the shape of the curves is influenced by the lattice structures and slip mechanisms of the respective materials, shows the need for further research in this area particularly with regard to establishing structural indexes.

[6] S. Fukui, H. Kudo, and J. Seino, "Study on Impact Extrusion Method for Nonferrous Metals," Report of the Institute of Science and Technology, University of Tokyo, Tokyo, Japan, vol. 11, 1957.

[7] S. Kobayashi, R. Herzog, J. T. Lapsley, Jr., and E. G. Thomsen, "Theory and Experiment of Press Forging Axisymmetric Parts of Aluminum and Lead," published in this issue, pp. 228–238.

[8] W. Johnson, "Upper Bound Loads for Extrusion of Circular Shaped Dies," *Applied Scientific Research*, to be published.

S. KOBAYASHI[1]

Assistant Professor,
Doshisha University,
Kyoto, Japan

E. G. THOMSEN

Professor of Metal Processing,
University of California,
Berkeley, Calif. Mem. ASME

Approximate Solutions to a Problem of Press Forging

The velocity vectors in the flash and body of a press forging of commercially pure lead having axial symmetry were obtained experimentally from incremental displacements in stepwise forging operations. It was found that the velocities are in excellent agreement with those derived with the aid of a simple disk theory, where it was assumed that all deformation is concentrated in a fictitious disk. Comparison with velocities derived from certain slip-line solutions also shows that substantial agreement exists here between theory and experiment.

Calculated average forging pressures, which were obtained by the approximate disk and slip-line theories, are in approximate agreement and the local pressure distributions are similar. These results seem to clarify the role which the flash height and friction in the die-lands play in achieving a good impression of the die cavities.

Press forging in closed impression dies is presently an important manufacturing process which is extensively used in the chipless shaping of metals into useful objects. The art of this process is well advanced, seemingly having been brought to near perfection, but the mechanics of the process are neither generally nor completely understood. Consequently, present-day engineering practice essentially still consists of trial-and-error methods for obtaining solutions to forging problems, a procedure which at its best is costly and inefficient.

Kobayashi, et al. [1],[2] in a companion paper show that experimental forging pressures, when press forging axisymmetric parts of commercially pure lead and aluminum, were in good agreement with a simplified theory. This simplified theory, as shown schematically in Fig. 1, assumes that in the finishing operation no plastic deformation occurs in the metal contained in the upper and lower die halves. This they justified by the fact that in an actual forging operation only minor readjustments are required in order that the metal conform to the die contours while changing its shape from the blocked forging to the finished forging. This concept apparently is different from that envisioned by previous investigators, as is revealed by a literature survey (bibliography of [1]). It was considered reasonable to assume further, that all plastic deformation is restricted to the flash and the metal of the forging, shown in Fig. 1 by dotted lines, from which the flash is formed. As a first approximation, therefore, it was assumed [1] that the final or finish-forging process consists of deforming a fictitious disk of height h under variable surface friction.

Their final equation (19), equation (6) of the present paper, as derived for the dimensionless press-forging pressures [1] is shown graphically by the solid curves in Fig. 2 for several μ (coefficients of friction) between flash and die as a function of $m = h/h_0$. It was assumed in the derivation that Coulomb friction exists in the fictitious disk between the flash and the die-land interfaces, but that metal shearing occurs on the remainder of its interfaces which remain permanently attached to the main body of the forging. In spite of these simplifying assumptions the experimentally determined dimensionless pressures $p_a/\bar{\sigma}$ agree well with the theoretical values, except at the beginning of a forging test, when excessive bulging occurs in the flash; this latter departure of the theory from experiment, however, is of no practical significance, because final and not initial pressures are of importance in practice. The solid circles shown in Fig. 2 represent the experimentally determined dimensionless pressures

$$p_a/\bar{\sigma} = \frac{\text{total forging load}}{\text{total projected area} \times \text{flow stress}}$$

for commercially pure lead. The dimensionless ratios $m = h/h_0$ (or by volume constancy, $m = [r_d/r_f]^2$) given in this figure were evaluated from measured r_f (flash radius), in order to eliminate the effect of bulging. In the remainder of the curves presented by Kobayashi, et al. [1], however, the values of m were based on instantaneous h (height of flash) measurements and hence in-

[1] At present, Graduate Student in Mechanical Engineering, University of California, Berkeley, Calif.

[2] Numbers in brackets designate References at end of paper.

Contributed by the Metal Process Section of the Production Engineering Division and presented at the Annual Meeting, New York, N. Y., November 30-December 5, 1958, of THE AMERICAN SOCIETY OF MECHANICAL ENGINEERS.

NOTE: Statements and opinions advanced in papers are to be understood as individual expressions of their authors and not those of the Society. Manuscript received at ASME Headquarters, August 4, 1958. Paper No. 58—A-140.

Nomenclature

σ_x, σ_y = normal-stress components in x and y-directions, respectively, psi

τ_{xy} = shearing-stress component on plane normal to x-axis and in direction of y-axis, psi

$\bar{\sigma}$ = effective stress, psi

p_a = average forging pressure, (load/total area), psi

h, h_0 = instantaneous and initial flash height, in.

r_d, r_f = radius of body (or die) and flash of forging, respectively, axial symmetry, in.

l_d, l_f = length of body only and combined length of body and flashes of forging subjected to plane-strain deformation

$m = h/h_0$ = flash-height ratio and from constancy of volume = r_d/h_0 for axial symmetry and $l_d/2h_0$ for plane strain

μ = coefficient of friction

u, U = instantaneous velocities of forging dies and exit velocity of flash edge, fpm

k = constant maximum shearing stress at yielding for ideal solid

p = mean pressure during deformation of ideal plastic solid

θ = angle measured from y-axis in counterclockwise direction to first shear line, deg

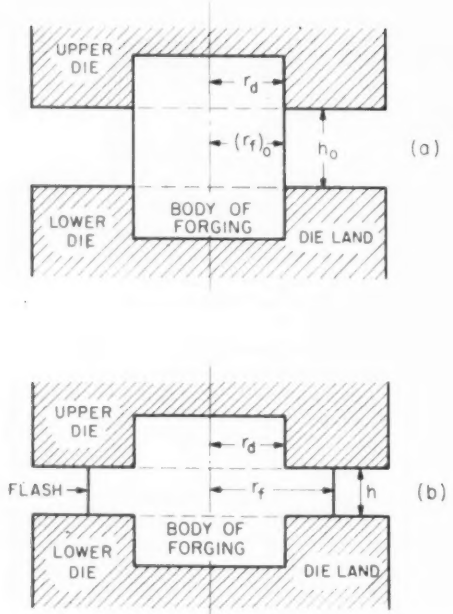

Fig. 1 Schematic diagram of ideal press forging. (a) Before deformation; (b) during deformation, showing formation of flash.

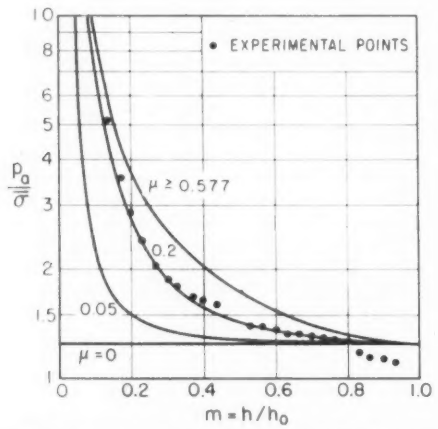

Fig. 2 Average dimensionless axially-symmetric forging pressures as function of $m = h/h_0$ for various coefficients of friction μ in die lands. (a) Solid curves are based on disk theory; (b) solid circles are experimental points using commercially pure lead: $r_d/h_0 = 0.65$, $h_0 = 1.50$ in., $r_d = 31/32$ in.

volve errors due to bulging when determining the variable m. It should be observed further that all experimental points were calculated by dividing the instantaneous load per unit area by the instantaneous flow stress $\bar{\sigma}$ (effective stress) as determined from independent compression tests under variable strain rates equivalent to those encountered in the forging. The coefficient of friction $\mu = 0.2$, which was used for the theoretical curve, also was determined independently with an experimental friction tester under similar operating conditions as were encountered in the forging: the details of the results of the friction tests are described in the same paper [1]. From these preliminary results it appears that the forging theory is valid for axisymmetric forgings of lead and aluminum. It appears, therefore, of theoretical as well as practical interest to obtain additional experimental confirmation and to compare the present theory with those based on slip-line theories in plane strain. Hence the purpose of this paper is to present this additional information, which was obtained after the preparation of the previous forging paper.

Flow Patterns in a Forging

The experimentally determined velocity vectors of an axially symmetric lead forging are shown in Fig. 3. The velocity vectors were obtained relative to a stationary center line by determining direction and displacement of marked particles on a central plane during incremental forging steps. This was accomplished by marking particles on this plane in the form of intersections of grid lines and following the displacements of these particles during incremental forging steps.

Fig. 4 shows hodographs (velocity diagrams) of particle velocity vectors corresponding to the assumed simplified theory previously discussed in which a forging is treated as a fictitious disk. The velocity u is the die velocity relative to the center line and U is the exit velocity at the end of the flash. At a particular instance, when the flash height is h, continuity demands that

$$u\pi r_f^2 = U\,2\pi r_f \frac{h}{2}$$

or

$$U = u\frac{r_f}{h}, \quad \text{and} \quad U_r = u\frac{r}{h} \tag{1}$$

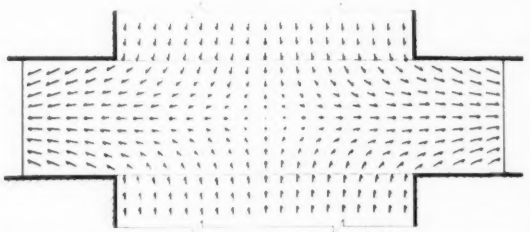

Fig. 3 Instantaneous velocity vectors for commercially pure lead obtained from a stepwise, axially-symmetric press-forging process; $r_d = 31/32$ in., $h = 0.75$ in., $r_f = 1.57$ in.

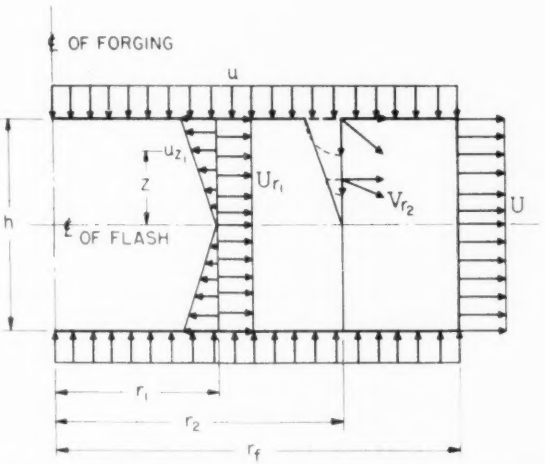

Fig. 4 Hodograph of an axially-symmetric press forging based on the fictitious disk theory

Hence equation (1) gives the radial velocity component U_r at any r of the desired velocity vector V_r in terms of the die velocity u. To obtain the velocity vector V_r, however, it is necessary to calculate the normal component u_z, which is u at the surface of the disk, but decays to zero at the center line. This can be accomplished by making a material balance at any r and z, namely

$$u_z \pi r^2 = U_r 2\pi r z, \quad \text{or} \quad u_z r = 2 z U_r \tag{2}$$

Substituting for $U_r = ur/h$ from equation (1),

$$u_z = \frac{2z}{h} u \tag{3}$$

is obtained which shows that u_z must be linear with respect to z. In the hodograph at r_1, the vertical components u_z have been shown pointed in a backward direction in order to show how these velocity components decay as r decreases. The manner in which the vector components combine to yield the velocity V_r is shown at r_2. The theoretical velocity vectors V, computed from equations (1) and (2) are shown in Fig. 5 and may now be compared with the experimental velocity vectors of Fig. 3. It is at once evident that the theory is good and that the theoretical velocities nearly agree with the experimental velocities. Other comparisons with slip-line solutions will be made also but are deferred to a subsequent section of the paper.

Approximate Forging Pressures

In order to compare the axially symmetric solutions with those in plane strain, let us first restate the former in summary form. The derivations of the equations to follow which apply to axially symmetric forgings are taken from the companion paper [1].

The local dimensionless axial compressive stress acting on the die is given by

$$\frac{-\sigma_z}{\bar{\sigma}} = e^{\frac{2\mu}{h}(r_f - r)}, \quad \text{when} \quad r_d \le r \le r_f$$

$$\frac{-\sigma_z}{\bar{\sigma}} = \frac{2}{\sqrt{3}\, h}(r_d - r) + e^{\frac{2\mu}{h}(r_f - r_d)}, \quad \text{when} \quad 0 \le r \le r_d \tag{4}$$

as long as sliding occurs in the flash, where $\bar{\sigma}$ is the effective stress and is equal to the instantaneous true stress in a tension or compression test which must be evaluated at the same strain or strain rate as occurs in the forging. The selection of $\bar{\sigma}$, however, depends on whether the material is affected by strain, strain rate, or both. The total dimensionless average forging pressure $p_a/\bar{\sigma}$ can then be shown to be

$$\frac{p_a}{\bar{\sigma}} = \frac{1}{2}\left(\frac{h}{\mu r_f}\right)^2 \left[\left(\frac{2\mu r_d}{h} + 1\right) e^{\frac{2\mu}{h}(r_f - r_d)} - \frac{2\mu r_f}{h} - 1\right] + \left(\frac{r_d}{r_f}\right)^2 \left[e^{\frac{2\mu}{h}(r_f - r_d)} + \frac{2\sqrt{3}}{9}\frac{r_d}{h}\right] \tag{5}$$

or

$$\frac{p_a}{\bar{\sigma}} = \frac{m^3}{2\mu^2 n^2}\left[\left(\frac{2\mu n}{m} + 1\right) e^{2\mu n\left(m^{-3/2} - \frac{1}{m}\right)} - 2\mu n m^{-3/2} - 1\right] + m\left[e^{2\mu n\left(m^{-3/2} - \frac{1}{m}\right)} + \frac{2\sqrt{3}}{9}\frac{n}{m}\right] \tag{6}$$

where $m = \dfrac{h}{h_0} = \left(\dfrac{r_d}{r_f}\right)^2$ and $n = \dfrac{r_d}{h_0}$

In the event that sticking or welding occurs in the flash between r_0 and r_d, where r_0 is the critical value of the radius at which sticking begins and is given by

$$r_0 = r_f - \frac{h}{2\mu} \ln\left(\frac{1}{\mu\sqrt{3}}\right)$$

then equations (4) and (5) reduce to the following:

$$\left.\begin{aligned} \frac{-\sigma_z}{\bar{\sigma}} &= e^{\frac{2\mu}{h}(r_f - r)}, \quad \text{when} \quad r_0 \le r \le r_f \\ \frac{-\sigma_z}{\bar{\sigma}} &= \frac{2}{h\sqrt{3}}(r_0 - r) + \frac{1}{\mu\sqrt{3}}, \quad \text{when} \quad 0 \le r \le r_0 \end{aligned}\right\} \tag{4*}$$

and

$$\frac{p_a}{\bar{\sigma}} = \frac{1}{2}\left(\frac{h}{\mu r_f}\right)^2 \left[\left(\frac{2\mu r_0}{h} + 1\right) e^{\frac{2\mu}{h}(r_f - r_0)} - \frac{2\mu r_f}{h} - 1\right] + \left(\frac{r_0}{r_f}\right)^2 \left[\frac{1}{\mu\sqrt{3}} + \frac{2\sqrt{3}}{9}\frac{r_0}{h}\right] \tag{5*}$$

For the case of plane strain, the forging becomes a fictitious slab of height h, having width in the z-direction, taken to be unity, which will not change during the progress of the forging operation. By transforming the variables, Fig. 1, as follows:

$$r \to x, \quad r_d \to \frac{l_d}{2}, \quad r_f \to \frac{l_f}{2}$$

$$\sigma_z \to \sigma_y, \quad \sigma_r \to \sigma_x$$

$$\sigma_\theta \to \sigma_z = \frac{\sigma_x + \sigma_y}{2} \quad \text{for plane strain}$$

$$\frac{h}{h_0} = \left(\frac{r_d}{r_f}\right)^2 \to \frac{h}{h_0} = \frac{l_d}{l_f}$$

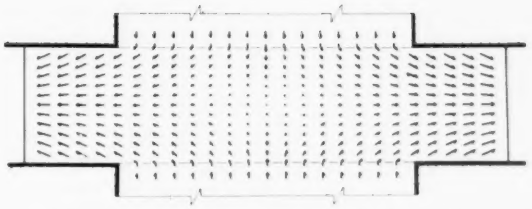

Fig. 5 Direction and magnitude of velocities of an axially-symmetric press forging based on fictitious disk theory

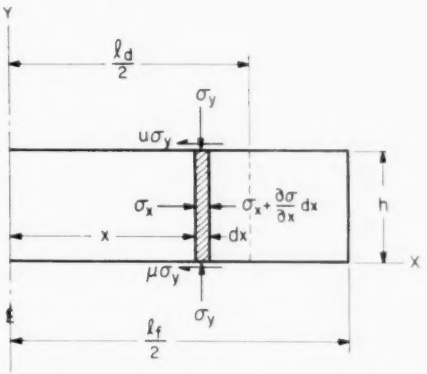

Fig. 6 Idealized stress distribution in a press forging in plane strain

and making a stress analysis on the slab shown in Fig. 6, in a manner similar to that used previously on the disk [1] for the axially symmetric forging, the following equations are obtained for the case of no sticking:

$$\left.\begin{aligned} \frac{-\sigma_y}{\bar{\sigma}} &= \frac{2}{\sqrt{3}} e^{\frac{2\mu}{h}\left(\frac{l_f}{2}-x\right)}, \quad \text{when} \quad \frac{l_d}{2} \le x \le \frac{l_f}{2} \\ \frac{-\sigma_y}{\bar{\sigma}} &= \frac{2}{h\sqrt{3}}\left(\frac{l_d}{2}-x\right) \\ &\quad + \frac{2}{\sqrt{3}} e^{\frac{2\mu}{h}\left(\frac{l_f}{2}-\frac{l_d}{2}\right)}, \quad \text{when} \quad 0 \le x \le \frac{l_d}{2} \end{aligned}\right\} \tag{7}$$

$$\frac{p_a}{\bar{\sigma}} = \frac{2}{\sqrt{3}}\left[\left(\frac{h}{\mu l_f}+\frac{l_d}{l_f}\right) e^{\frac{\mu}{h}(l_f-l_d)} + \frac{l_d^2}{4hl_f} - \frac{h}{\mu l_f}\right] \tag{8}$$

$$\frac{p_a}{\bar{\sigma}} = \frac{2}{\sqrt{3}}\left[\left(\frac{m^2}{2\mu n}+m\right) e^{2\mu n\left(m^{-2}-\frac{1}{m}\right)} + \frac{n}{2} - \frac{m^2}{2\mu n}\right] \tag{9}$$

where $$m = \frac{h}{h_0} = \frac{l_d}{l_f} \quad \text{and} \quad n = \frac{l_d}{2h_0}$$

Again, if sticking occurs in the flash between x_o and $l_d/2$, where x_o is the critical distance from the center line of the forging at which sticking begins and is given by

$$x_0 = \frac{l_f}{2} - \frac{h}{2\mu}\ln\frac{1}{2\mu} \ge \frac{l_d}{2}$$

then

$$\left.\begin{aligned} \frac{-\sigma_y}{\bar{\sigma}} &= \frac{2}{\sqrt{3}} e^{\frac{2\mu}{h}\left(\frac{l_f}{2}-x\right)}, \quad \text{when} \quad x_0 \le x \le \frac{l_f}{2} \\ \frac{-\sigma_y}{\bar{\sigma}} &= \frac{2}{h\sqrt{3}}(x_0-x) + \frac{1}{\mu\sqrt{3}}, \quad \text{when} \quad 0 \le x \le x_0 \end{aligned}\right\} \tag{7*}$$

and $$\frac{p_a}{\bar{\sigma}} = \frac{2}{\sqrt{3}}\frac{h}{\mu l_f}\left[\frac{\left(1+\frac{2\mu x_0}{h}\right)^2+1}{4\mu} - 1\right] \tag{8*}$$

It may be noted that the average forging pressures $p_a/\bar{\sigma}$, for plane strain and axial symmetry are not the same, because of the fact that different areas are involved, on which the forging pressures act. This may be seen readily by comparing equation (5) with (8) or equation (6) with (9). The local axial pressures, however, differ by only a small amount as will be shown later.

Slip-Line Solutions of Press Forging

There is no evidence to indicate that slip-line techniques have been used extensively by metal-processing engineers in the solution of practical problems. This is probably due to the fact that experimental verification is lacking and that solutions are often too general to apply to a particular problem, unless the metal-processing engineer is able to obtain the slip lines readily himself. This, however, is now possible because, among others, a graphical method [2] was proposed recently and has been used on a number of forming problems. This method is rapid and for all practical purposes is sufficiently accurate.

Before comparing possible slip-line solutions of forgings, which were obtained by this graphical method, with approximate solutions and with experimental results discussed earlier, it will be necessary to restate briefly what they are and how they can be used in calculating forging loads, stress distribution, and particle velocities. For a more complete discussion the reader is referred to the literature, in particular to books on this subject by Hill [3] and Prager and Hodge [4].

The slip lines are lines of maximum shear and are the characteristics of the hyperbolic differential equations, which must satisfy static equilibrium and continuity in an ideal solid subjected to plastic deformation in plane strain. It is assumed that the critical shearing stress k, of the ideal solid, which is required to cause plastic deformation, is constant and that a state of stress outside of the plastic zone will not produce any deformation whatsoever. This, in effect, means that the material beyond this zone is rigid, which is equivalent to stating that the modulus of elasticity is infinite. A solution obtained is often called a par-

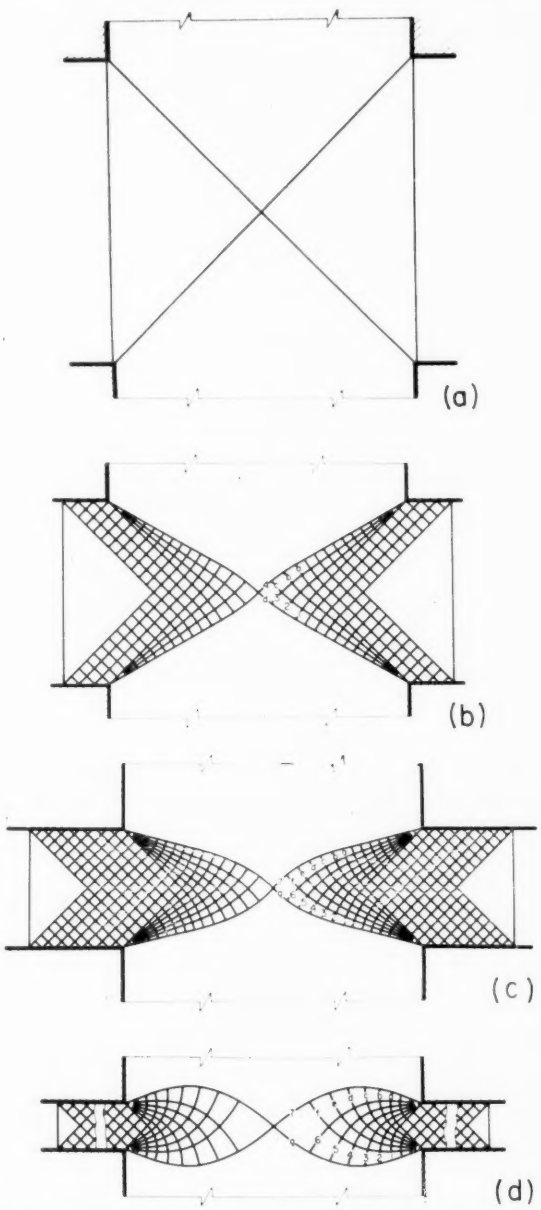

Fig. 7 Possible slip-line solutions for press forgings in plain strain without friction in die lands. See Table 1 for conditions.

tial solution, since usually no attempt is made to check if the so-called rigid material has an elastic boundary which is satisfied simultaneously by the plastic boundary.

Fig. 7 shows four possible slip-line solutions which were obtained graphically. These solutions correspond to the four instantaneous flash heights given in Table 1 under columns a to d for both axial symmetry and plane strain. Friction between flash metal and die land was assumed to be zero: i.e., $\mu = 0$. The slip lines given numbers are first slip lines, while those lettered are second slip lines, in accordance with the convention used by Prager and Hodge [4]. The equations which satisfy equilibrium along these maximum shear lines are

$$\begin{aligned} p + 2k\theta &= C_1 = \text{constant along first shear line} \\ p - 2k\theta &= C_2 = \text{constant along second shear line} \end{aligned} \tag{10}$$

and the stress components are

$$\sigma_x = -p + k \sin 2\theta, \quad \sigma_y = -p - k \sin 2\theta \tag{11}$$

The convention used is shown in Fig. 8 and is as follows: The angle θ is the angle of turn-off and is measured counterclockwise from the y-axis to the first shear line. This holds irrespective of whether we are evaluating stresses on a first or on a second shear line. The stress components are σ_x and σ_y, the maximum shearing stress to initiate or maintain plastic deformation is k, and is assumed constant along any slip line, and finally, $p = -\frac{1}{2}(\sigma_x + \sigma_y)$ is the mean pressure. If a centered fan-type solution applies, such as the example in Fig. 8, the slip lines 1 and a originating at the die corners are limiting slip lines up to their point of intersection at the center line and bound the region of plastic deformation. These limiting slip lines may, however, be displaced as a series of parallel lines into the flash as shown in Fig. 7(d) requiring a constant state of stress in this region. In this event, plastic deformation may extend to the last slip lines marked 1 and a, as for example, in Fig. 7(d), but the solid becomes rigid beyond these limiting lines. The limiting slip lines 1 and a are also the starting lines of a graphical solution and must be so located that θ will satisfy the boundary condition $\sigma_x = 0$, since there are no forces acting in the x-direction on the outer edge of the flash. Inasmuch as $\sigma_x = 0$, the x and y-directions must be principal directions and hence a Mohr's circle of radius k would show that

$$\sigma_y = -2k \quad \text{and} \quad p = -\frac{1}{2}(\sigma_y + 0) = k$$

Hence introducing these conditions into equation (11) determines $\theta = 45$ deg, which could also have been obtained directly from a Mohr's circle diagram. The state of stress $\sigma_x = 0$ is shown on infinitesimal elements of the solid marked A and B on the first and second shear lines, respectively. The first shear line is chosen to be that line which contains shearing stresses on the faces of the element C parallel to the shear line, which tends to rotate the element clockwise. Thus, as shown by element D, negative shearing stresses exist on these faces on second shear lines. Inasmuch as friction is assumed to be zero at the die land and flash interface, shear lines must meet the solid boundary of the die at 45 deg which satisfies the condition that shearing stresses are zero at that point.

The remaining shear lines, shown by way of example in Fig. 8, are obtained by a graphical or wedge technique [2], assuming that a discontinuity in stress occurs at the die corners. All slip lines preferably are located with constant angles between them, i.e., equiangular where $\Delta\theta = \text{const}$, except the last slip lines marked 4 and d, respectively, of Fig. 8. These last slip lines are also limiting slip lines and divide the rigid solid in the body of the forging from that in the plastic zone. They are located by satisfying the condition of symmetry, which dictates that no shearing stresses can exist along the center line; hence the center line is a principal direction and the slip lines must meet here at angles of 45 deg inclined toward the center line.

If the slip line field has been constructed it is a simple matter now to calculate the local forging pressure which is the y-component of stress $-\sigma_y$ along the limiting lines, as for example, line d. This is accomplished by first calculating p along slip line 1 with the help of equation (10) $p + 2k\theta = C_1$. The constant

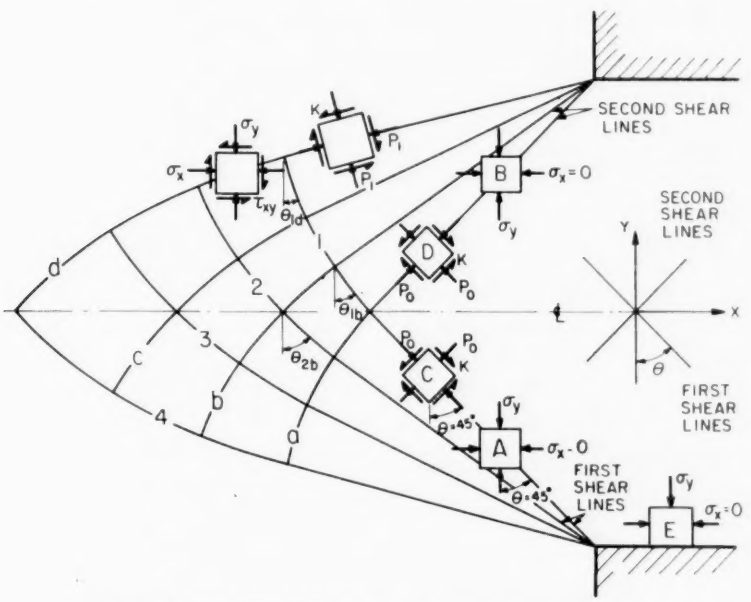

Fig. 8 Schematic stress distributions along first and second shear lines

C_1 is determined by the known condition illustrated by element C in Fig. 8. Thus the pressures along slip line 1 up to and including the point of intersection with slip line d can be determined. Hence, knowing p and θ at this point, the constant C_2 of equation $p - 2k\theta = C_2$ can be determined and hence, as θ changes along slip line d, the mean pressure p can be evaluated. The local pressure $-\sigma_y$ can next be evaluated, since p and θ are now known at every point along line d, and finally the total average forging pressure can be obtained by summing up the local y-components of stress multiplied by increments of cross-sectional areas on which they act and by dividing this sum by the total area; or symbolically in integral form, neglecting shearing stresses,

$$p_a \cong -\frac{1}{A}\int_{A=0}^{A} \sigma_y \, dA \tag{12}$$

While it has been said [4] that slip-line solutions are not necessarily unique, i.e., other slip-line fields may apply to a particular problem, as for example those proposed by Green [5] for smooth wedges, we will assume that the fields of Fig. 7 are possible solutions. Inspection of these figures reveals that the extent of the plastic zone depends on the flash height h and that the pressure on the limiting lines increases with decreasing h because of the fact that θ is increasing with decreasing h.

Boundary Conditions for Construction of Slip-Line Fields

The flash metal, during the forging process, is subjected to two boundary conditions; namely, the condition that $\sigma_x = 0$ at the free outer edge of the flash metal which has already been referred to in the previous section, and the condition of sliding along the die surfaces, which may be assumed to involve Coulomb friction between die land and flash metal.

Referring to Fig. 9, the limiting lines $\overline{OA}$ and $\overline{O'A}$ along which $\sigma_x = 0$, are drawn as before and intersect at the stress-free edge $\overline{OO'}$ at an angle of 45 deg. The intersections of two boundary surfaces, i.e., die land and flash edge, demand that O and O' be singular points, since the state of stress at O or O', as is derived from one boundary condition, is different from the other (except in the frictionless case). This suggests that slip-line patterns, starting from this limiting line, form centered fan-type solutions with O and O' as centers.

The condition of friction along the die surface determines the angle at which slip lines intersect this boundary. Let it be assumed now that Coulomb friction along the flash-die interface is given by a constant coefficient of friction μ_0. The slip line $\overline{AB}$ can then be extended to the boundary surface with a straight line $\overline{BC}$. This satisfies the condition that the coefficient of friction μ along $\overline{OC}$ be constant. The angle θ_0 at which the slip lines intersect with the boundary, i.e., the die surface, is uniquely determined for a given coefficient of friction μ_0 in the following manner as was suggested by Hoffman and Sachs [6]. Let the state of stress at the die surface be represented by the point Y on Mohr's diagram shown in Fig. 10. At Y

$$\left.\begin{aligned} \sigma_x &= -p + k \sin 2\theta_0 \\ \sigma_y &= -p - k \sin 2\theta_0 \\ \tau_{xy} &= -k \cos 2\theta_0 \end{aligned}\right\} \tag{13}$$

and the coefficient of friction along the die surface μ_0 is given by

$$\mu_0 = \tan \rho = \frac{k \cos 2\theta_0}{p + k \sin 2\theta_0}, \quad \text{for} \quad 0 \leq \theta_0 \leq 45 \text{ deg} \tag{14}$$

Equation (14) is the relationship between μ_0 and the corresponding angle θ_0 and p can be evaluated from the slip lines as described earlier.

Fig. 11 shows the variation of interfacial friction along the die land $\overline{OC}$ for various intersecting angles. It may be seen from this figure that for the condition of no friction $\mu_0 = 0$, the slip line intersects the boundary surface at 45 deg and when slip lines are tangent to the surface $\theta_0 = 0$, it corresponds to $\mu_0 = 0.39$. Therefore, for $0 \leq \mu_0 \leq 0.39$, the possibility exists that the construction of slip lines can be extended toward the center of the body of the forging from the initial slip lines which are so drawn that these slip lines satisfy both the stress-free edge condition and the friction condition at the die-flash interface. In these cases θ_0 for a given μ_0 must be uniquely determined by equation (14).

For the condition when $\mu_0 > 0.39$, i.e., the so-called perfectly rough surface, slip lines may be tangent to the die surface in a similar manner, as for the case when $\mu_0 = 0.39$. However, the present boundary condition, in which it is assumed that a stress free edge exists in the flash, apparently cannot be satisfied.

A probable slip-line pattern for the condition of high friction, $\mu_0 = 0.39$, is shown in Fig. 12 (see column c of Table 1) and is the same type of solution first proposed by Prandtl [7] and later improved upon by Hill, et al. [8] and others [9, 10].

Hodographs

The hodographs corresponding to the slip-line fields of Fig. 7 are given in Fig. 13. These diagrams depict the metal flow during an assumed pseudosteady-state condition. These lines are transformed slip lines and satisfy the assumed continuity conditions, while the slip lines, as already mentioned, satisfy the equilibrium conditions for the stresses. The hodographs can be constructed in a manner similar to the slip lines, but for the sake of brevity they will not be discussed in detail here. Let it suffice to say that the pole of these figures is the origin from which the instantaneous particle velocities are scaled off. Each intersection of lettered and numbered lines is identified on these diagrams as the corresponding intersection of numbered and lettered lines in the slip-line fields of Fig. 7. In order to obtain the particle velocity at any such intersection, it is merely necessary to connect the pole to the intersection of the lines with a straight line. Its direction and magnitude can then be scaled off. The velocity vectors in Fig. 14 were obtained in this manner. It should be noted, however, that these velocity fields do not agree with the experimentally determined velocity field shown in Fig. 3. This is due to two principal reasons; namely:

1 The velocity field of Fig. 3 was obtained with a forging having axial symmetry and cannot be compared with those in plane strain directly. This is so because continuity demands that for a given die velocity u, the exit velocity at the die edge U for plane strain must be twice as large as that for axial symmetry.

2 The slip-line solution of Fig. 7 and the corresponding hodographs and velocity diagrams of Figs. 13 and 14, respectively, were obtained by considering the dies as remaining in a fixed position. This, in effect, means that material is assumed to enter the fixed plastic zone bounded by the limiting shear lines in the body of the forging at velocity u under steady-state conditions. Hence the velocity patterns are in reality those which correspond to a sidewise extrusion rather than those of a forging. While it appears possible, at least in principle, to construct other slip lines more appropriate for forgings, the solutions given here are probably not far from the truth.

The hodograph, velocity diagrams, and the slip-line pattern Fig. 12, for a rough surface, i.e., $\mu = 0.39$, are given in Fig. 15. This solution unlike those of $\mu = 0$, does not require the assumption of a stationary die. Hence the instantaneous velocity vectors, except for magnitude due to plane-strain condition and a difference in the coefficient of friction, should agree more closely with the experimental patterns given in Fig. 3.

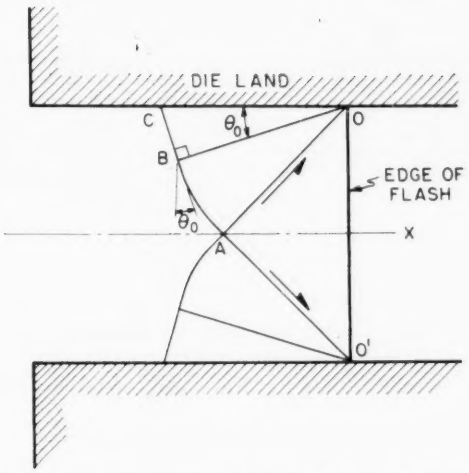

Fig. 9 Possible construction of shear lines in flash with $\mu > 0$

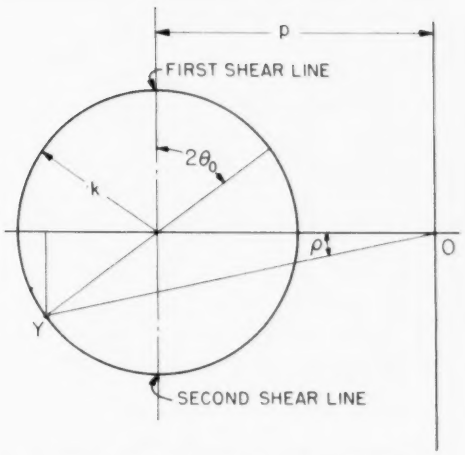

Fig. 10 Mohr's circle diagram for shear lines shown in Fig. 9

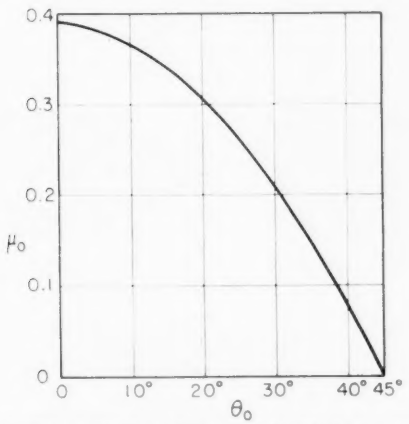

Fig. 11 Coefficient of friction μ_0 between die land in flash as function of angle of intersection between die land and a second shear line

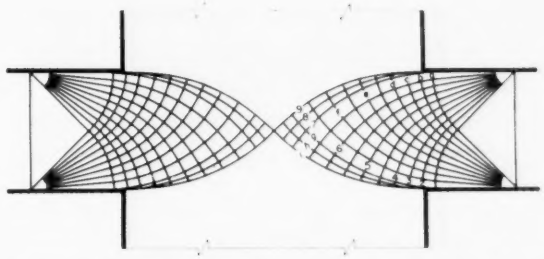

Fig. 12 Slip-line field for a press forging in plane strain with rough die lands ($\mu = 0.39$)

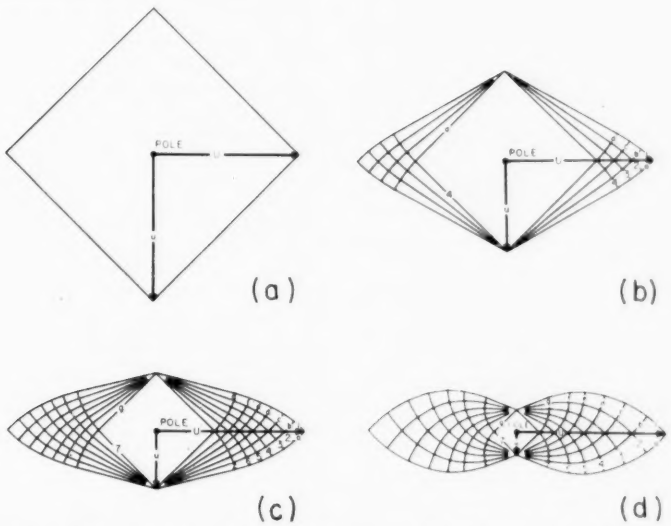

Fig. 13 Hodographs of press forgings in plane strain based on slip-line theory. See Table 1 for conditions.

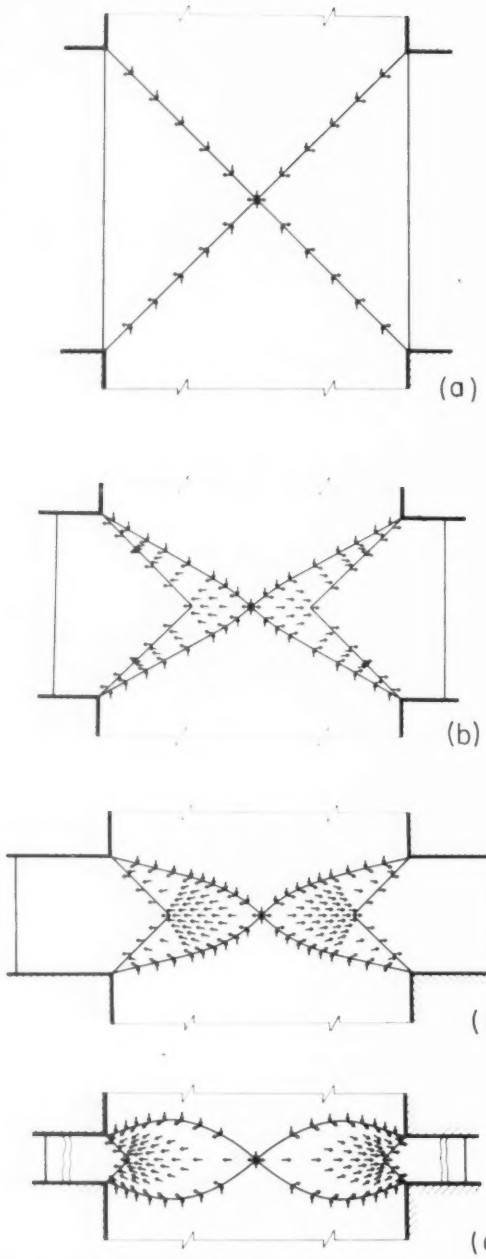

Fig. 14 Direction of velocity vectors of a press forging in plane strain based on slip-line theory. See Table 1 for conditions.

Discussion

In order to get a close comparison between experiment and theories, the velocity fields are brought together in Fig. 16. It is at once evident that the slip-line solution overestimates the extent of the rigid material, but that on the whole either theory gives a good estimate of the velocity distribution in the body and flash of a press forging.

For purposes of comparing the pressures from the approximate

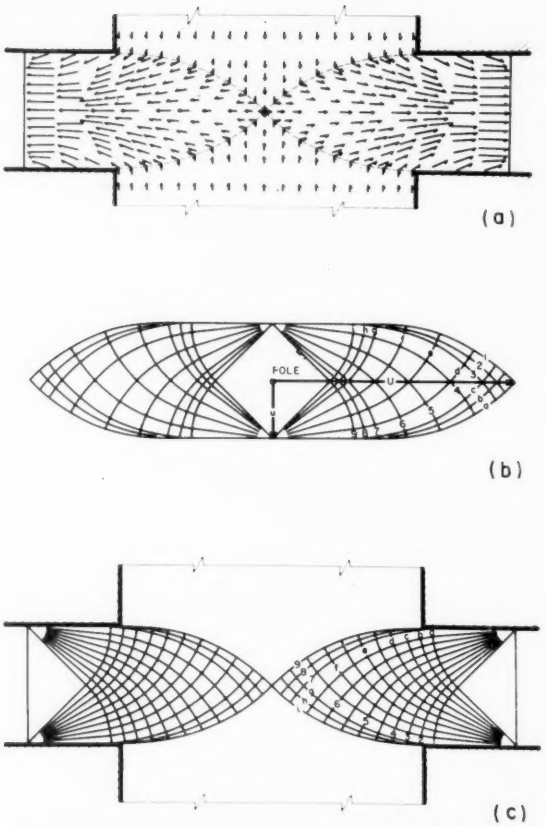

Fig. 15 Slip-line solutions for a press forging in plane strain with rough die lands ($\mu = 0.39$). (a) Direction and magnitude of velocities; (b) hodograph; (c) slip-line field. See column c of Table 1 for conditions.

solution with those calculated from the slip-line solutions, the local components of stress $-\sigma_y$ were calculated with the aid of equation (7) and with the slip-line solutions of Figs. 7 and 12, respectively. The results are given in Figs. 17 and 18. The critical shearing stress was taken as $k = \bar{\sigma}/\sqrt{3}$ for the slip-line solution which for the case of $\mu = 0$ requires that both solutions yield the same value of $-\sigma_y$ at the edge of the flash, where $x/(l_f/2) = 1$. It is seen that both solutions predict a constant pressure $-\sigma_y$ in the flash region and that the pressure rises to a maximum at the center of the forging. In all cases, it is evident that the slip-line solutions yield slightly lower stress distributions than those of equation (7). It also may be observed that the slip-line solutions show some discontinuities at the die edges as well as some constant-pressure regions within the body of the forgings. In spite of these differences, however, the same trend in the pressure distributions exists for both theories. For the case when the coefficient of friction μ is not equal to zero, equation (7) predicts a rising pressure in the flash as one travels from the edge toward the center. The proposed slip-line solution for this particular configuration, on the other hand, gives constant local pressures in the flash region but these pressures appear to increase with increasing friction.

In order to compare slip-line solutions with axial symmetric pressure distributions, equation (4) was used in the calculation of approximate pressures. These results are shown in Fig. 19 for several coefficients of friction μ. It is to be noted that these curves are nearly identical to the plane-strain pressure distribu-

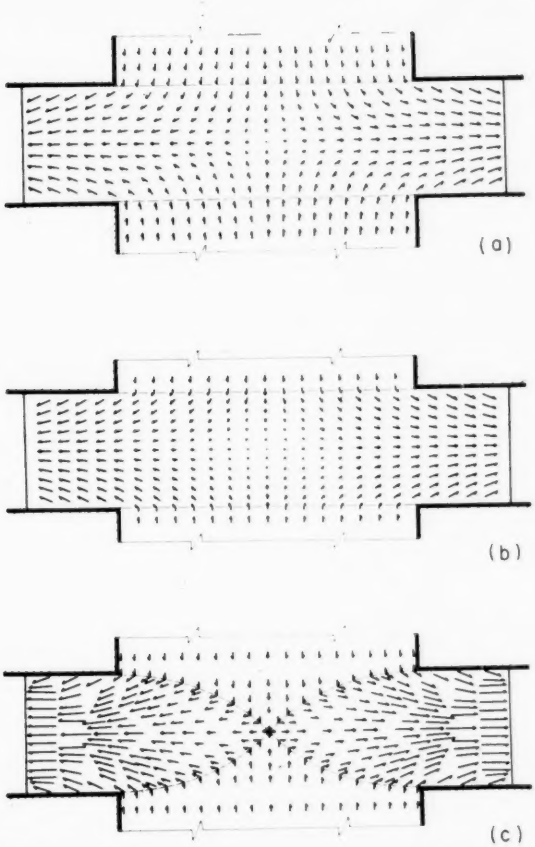

Fig. 16 Comparison of particle velocities in a press forging. (a) Experiment with lead, axial symmetry; (b) theoretical fictitious disk theory, axial symmetry; (c) slip-line theory, rough die ($\mu = 0.39$), plane strain.

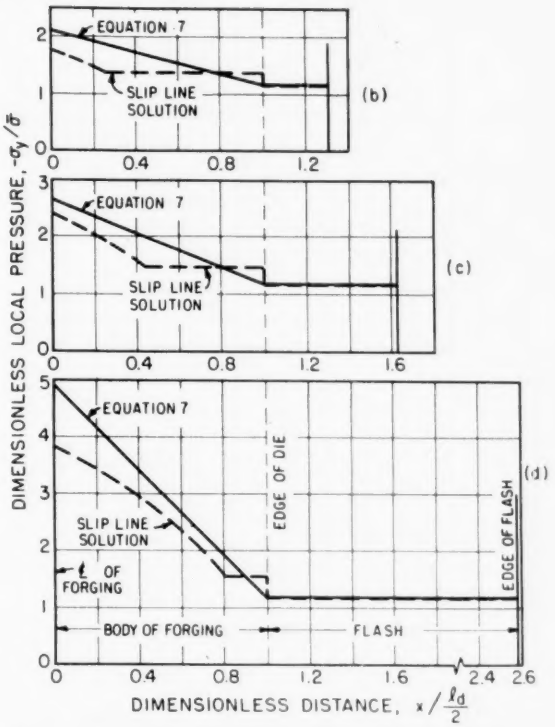

Fig. 17 Theoretical local dimensionless forging pressure distributions for several stages in a press forging in plane strain with zero friction between die land and flash. See Table 1 for conditions. Values of h are (b) 1.178 in., (c) 0.751 in., (d) 0.297 in.

tion except that the axially symmetric curves are slightly lower. This is due to the fact that in the plane-strain problem greater restraint exists as, for example, at the die edge. Hence for the plane-strain case the value of $-\sigma_y$ must be equal to $2\bar{\sigma}/\sqrt{3}$, in order to initiate plastic deformation, which in the axial-symmetric case requires $-\sigma_z$ to be equal to $\bar{\sigma}$. This difference in stress at the die edge is 15.5 per cent and changes but slightly the curve of the pressure distribution as a function of r/r_d.

Let it be assumed now that the slip-line field in plane strain can be applied to a problem in axial symmetry, providing that the proper boundary conditions are satisfied. This requires for the case of frictionless sliding in the flash region $\mu = 0$, that the local pressure $-\sigma_z$ be the same as in the approximate solution, since both are under the influence of zero restraint. Hence it is required that the maximum critical shearing stress for the slip-line solutions take on values of $k = \bar{\sigma}/2$. Referring to the figures, it is again seen that the pressure distributions show the same trends as for plane strain but do not exactly reproduce each other, for the reasons already discussed.

Figs. 20 and 21 show the average forging pressures which were computed using equations (9) and (6), respectively, for the approximate solutions and by a graphical integration using equation (12) and the respective local pressure distributions from the slip-line solutions. The values for the slip-line solutions for the same $m = h/h_0$ are also compared with the approximate solutions in Table 1. It is to be noted that a direct comparison for the case of variable friction was made only for the values given in column c of Table 1 for both plane strain and axial symmetry. This is due to the fact that the configuration of body and flash of a forging on the central plane must be the same, in order to permit direct comparison. It is to be noted that the slip-line theory predicts slightly lower forging pressures than the approximate solution for all conditions investigated, but that both theories predict lower average forging pressures for plane strain than for axial symmetry.

In order to obtain good reproducibility and filling of the die cavity by the body of the forging, it seems desirable that the local forging pressure be approximately constant over the cross section of the forging. Let us, therefore, investigate the function of the flash in a forging, with respect to the local pressure. Referring to Fig. 17, it is seen that for the case when $\mu = 0$, increasing the flash length results in a higher local pressure in the center of the body of the forging, but does not affect the local pressure near the die edge. Hence an increased flash radius or length merely increases the total forging load without yielding any real benefit in the ability to obtain a uniformly good impression. If the die lands are roughened, on the other hand, the local pressure in the body tends to a higher but more uniform distribution. This should tend to produce a better impression in the forging. Increased flash length is helpful, but it appears possible that a flash may be made to flow from the body of the forging in such a way that restraint and friction are induced, without raising the forging load unnecessarily high. Further investigations will be required to explore this possibility.

Conclusions

1 Experimentally determined velocity patterns of an axi-

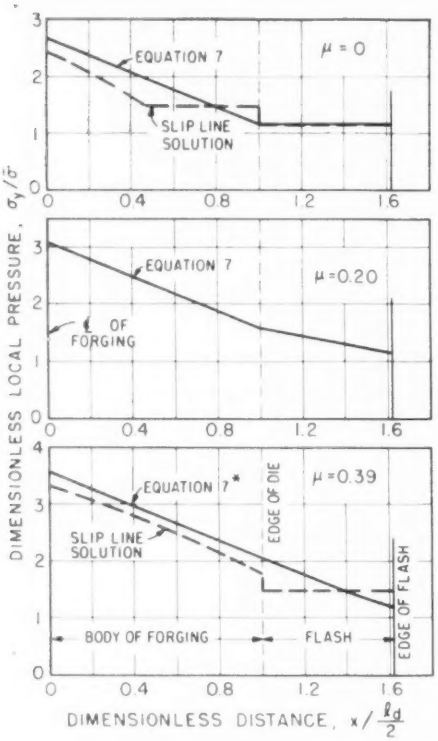

Fig. 18 Theoretical local dimensionless forging pressure distributions in a press forging in plane strain with variable friction between die land and flash. See column c in Table 1 for conditions.

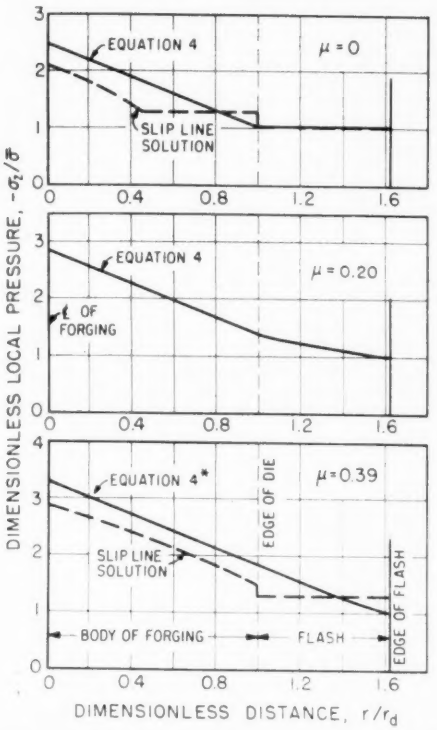

Fig. 19 Theoretical local dimensionless forging pressure distributions in a press forging with axial symmetry with varying friction between die land and flash. See column c in Table 1.

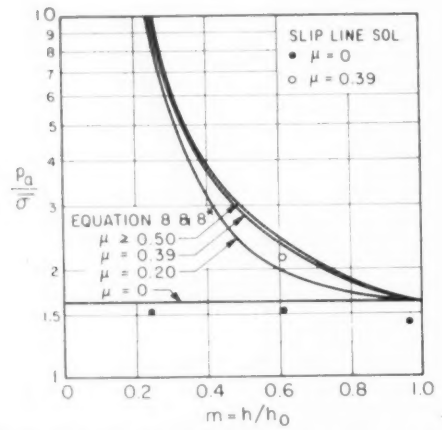

Fig. 20 Comparison of theoretical dimensionless average forging pressures in a press forging in plane strain. See column c in Table 1 for conditions.

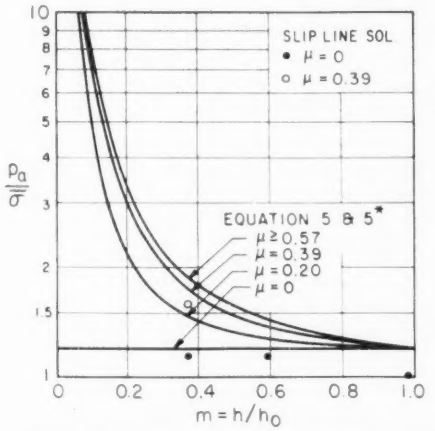

Fig. 21 Comparison of theoretical dimensionless average forging pressure in a press forging having axial symmetry. See column c in Table 1 for conditions.

Table 1 Comparison of slip-line solutions with approximate solutions

		(A) Axial symmetry $r_d = \frac{31}{32}$ (= 0.96875 in.) $h_0 = 2.00$ in. $n = r_d/h_0 = 0.480$				(B) Plane strain $\frac{l_d}{2} = \frac{31}{32}$ (= 0.96875 in.) $h_0 = 1.22$ in. $n = l_d/2\,h_0 = 0.793$			
		a	*b*	*c*	*d*	*a*	*b*	*c*	*d*
h, in.		1.937	1.178	0.751	0.297	1.937	1.178	0.751	0.297
r_f and $l_f/2$, in.		0.983	1.26	1.57	2.50	...	1.005	1.57	3.98
$m = h/h_0$		0.969	0.589	0.376	0.149	...	0.965	0.615	0.243
r_f/h and $l_f/2h$		0.507	1.07	2.09	8.42	...	0.853	2.09	13.4
		$p_a/\bar{\sigma}$				$p_a/\bar{\sigma}$			
Slip-line theory	$\mu = 0$	1.00	1.12	1.13	1.13	...	1.42	1.51	1.51
Disk theory	$\mu = 0$	1.18	1.18	1.18	1.18	...	1.61	1.61	1.61
Slip-line theory	$\mu = 0.2$	...	...	...	...	...	...	...	...
Disk theory	$\mu = 0.2$	...	...	1.45	...	...	...	1.96	...
Slip-line theory	$\mu = 0.39$	...	...	1.56	...	...	...	2.16	...
Disk theory	$\mu = 0.39$	...	...	1.77	...	...	...	2.30	...

NOTE: 1 Slip-line patterns are the same for axial symmetry, and plane strain when $r_f/h = l_f/2h$.

2 $\bar{\sigma} = 2k$ for axial symmetry, $\bar{\sigma} = \sqrt{3}k$ for plane strain.

symmetric lead forging seem to confirm that the plastic zone is concentrated in a narrow region, which can be approximated by a disk.

2 Theoretical magnitudes and directions of velocities based on the disk model are in nearly exact agreement with experimental velocities, while the velocities derived from slip-line solutions are in substantial agreement, but the solution for high friction underestimates the extent of the plastic region.

3 The theoretical local pressure distributions and average forging pressures show the same trends, but the pressures calculated from the slip lines are slightly lower than those obtained using the approximate solutions.

4 From the theoretical analysis, it appears that the local pressures near the die edge do not increase materially with flash width nor flash height for the case when little or no friction exists between the die land and flash surfaces. It appears that the pressure may be increased, however, by increasing the frictional resistance to flow between these surfaces and thereby improving the over-all ability to obtain a good impression of the die cavity in all parts of the body of the forging.

Acknowledgment

The authors wish to thank the National Science Foundation for its Grant NSF-G-2957 in support of the present investigation. They also wish to thank the University of California and especially the Division of Industrial Engineering for continued support of the projects. Special thanks are also given to Messrs. Miller, Schlegel, and Goodman for their assistance in preparation of the report and Mr. Petersen, senior mechanician of the Production Laboratory, for his assistance in constructing the forging dies.

References

1 S. Kobayashi, R. Herzog, J. T. Lapsley, Jr., and E. G. Thomsen, "Theory and Experiment of Press Forging Axisymmetric Parts of Aluminum and Lead," published in this issue, pp. 228–238.

2 E. G. Thomsen, "A New Method for the Construction of Hencky-Prandtl Nets," *Journal of Applied Mechanics*, vol. 24, TRANS. ASME, vol. 79, 1957, pp. 81–84.

3 R. Hill, "The Mathematical Theory of Plasticity," Clarendon Press, Oxford, England, 1950.

4 W. Prager and P. G. Hodge, "The Theory of Perfectly Plastic Solids," John Wiley & Sons, Inc., New York, N. Y., 1951.

5 A. P. Green, "A Theoretical Investigation of the Compression of a Ductile Material Between Smooth, Flat Dies," *Philosophical Magazine*, series 7, vol. 13, 1951, pp. 900–919.

6 O. Hoffman and G. Sachs, "Introduction to Theory of Plasticity for Engineers," McGraw-Hill Book Company, Inc., New York, N. Y., 1953.

7 L. Prandtl, "Anwendungsbeispiele zu einem Henckyshen Satz über das Plastische Gleichgewicht," *Zeitschrift für Angewandte Mathematik und Mechanik*, vol. 3, 1923, pp. 401–406.

8 R. Hill, E. H. Lee, and S. J. Tupper, "A Method of Numerical Analysis of Plastic Flow in Plane Strain and Its Application to the Compression of a Ductile Material Between Rough Plates," *Journal of Applied Mechanics*, vol. 18, TRANS. ASME, vol. 73, 1951, pp. 46–52.

9 J. M. Alexander, "The Effect of Coulomb Friction in the Plane-Strain Compression of a Plastic Rigid Material," *Journal of the Mechanics and Physics of Solids*, vol. 3, 1955, pp. 233–245.

10 J. F. W. Bishop, "On the Effect of Friction on Compression and Indentation Between Flat Dies," *Journal of the Mechanics and Physics of Solids*, vol. 6, 1958, pp. 132–144.

S. KOBAYASHI[1]
R. HERZOG[2]
J. T. LAPSLEY, JR.[3]
E. G. THOMSEN[4]

Theory and Experiment of Press Forging Axisymmetric Parts of Aluminum and Lead

The mechanics of finishing in a press-forging operation were analyzed. It was concluded that the metal in the die, as well as that contained in the flash, could be treated as a fictitious disk which is subjected to compression between flat surfaces under variable surface friction. Comparison of experimental average pressures with those predicted by the foregoing simplified theory showed good agreement.

Press forging in closed dies is one of the important operations in the shaping of metals and their alloys into useful objects. While hammer forging appears to have had its beginning in prehistoric times [1],[5] closed-die forging may be considered to have started in the 1850's, when the Colt Arms Company in the United States produced firearms on a drop hammer [2]. It was not until 1861, however, that press forging was apparently first applied when the Englishman John Haswell developed in Austria a successful hydraulic press for the production of locomotive parts [3, 4]. Thus press forging, the process of relatively slow squeezing of metals in closed dies into finished and semifinished products, was born less than a century ago.

While press forging as a manufacturing technique since its inception in the middle of the past century has undergone a fruitful period of development, the mechanics of this process are still incompletely known. Hence press forging is yet more an art than it is a science, and the functional relationships of the forging variables are not known completely. Much of the prediction of metal movement and forming loads in new applications of press forging is obtained by relatively inaccurate calculations, trial-and-error methods, or empiricisms—often involving guesses based on past performance of similar design of product and material. Hence a better understanding of the forging mechanism leading to more precise methods of prediction of the forming variables, notably the forming pressure, appears to be a goal worth achieving.

Following the formulation of the mathematical relationships of plastic behavior of metals subjected to combined stresses which resulted in theories of plasticity, several notable attempts have been made to analyze the press-forging process. Prandtl [5] analyzed the compression of an ideal plastic solid in plane strain between rough dies and obtained a rigorous solution for the stress distribution and average forging pressure. This case was later reconsidered by Hill [6], also Green [7], Alexander [8], and Bishop [9]. Other more approximate solutions which are based on simpler states of stress were proposed by Siebel [10], Nadai [11], Sachs [12], Schroeder and Webster [13], Hoffman and Sachs [14], and Stone [1]. In these latter cases, however, the forging consists of a flat plate or solid disk and the results apparently are applicable to the metal contained in the flash of a press forging rather than the forging itself. Dietrich and Ansel [15], recognizing this fact, applied some of the foregoing analyses to various portions of a real and rather complex forging and found a composite solution. These authors claimed that their solution was confirmed by experiment with an accuracy of ±20 per cent in spite of the fact that plane-strain conditions were assumed, an estimated constant coefficient of friction was used, and the metal flowing from a larger section to a smaller section was treated as an extrusion in determining back pressures.

The purpose of this paper is to reanalyze the forging process for a press forging having axial symmetry and to compare the solutions with new experimental data.

[1] Assistant Professor at Doshisha University, Kyoto, Japan. At present, Graduate Student in Engineering at University of California, Berkeley, Calif.
[2] Student in Engineering, University of California, Berkeley, Calif.
[3] Associate Professor of Industrial Engineering, University of California, Berkeley, Calif.
[4] Professor of Metal Processing, University of California, Berkeley, Calif. Mem. ASME.
[5] Numbers in brackets designate References at end of paper.

Contributed by the Production Engineering Division and presented at the Annual Meeting, New York, N. Y., November 30–December 5, 1958, of The American Society of Mechanical Engineers.
Note: Statements and opinions advanced in papers are to be understood as individual expressions of their authors and not those of the Society. Manuscript received at ASME Headquarters, August 5, 1958. Paper No. 58—A-154.

Nomenclature

$\epsilon_z, \epsilon_\theta, \epsilon_r$ = plastic-strain components in z, θ, r cylindrical co-ordinate directions, respectively

$\epsilon, \dot{\epsilon}$ = effective plastic strain and plastic-strain rate, respectively

$\sigma_z, \sigma_\theta, \sigma_r$ = normal stress components in z, θ, r cylindrical co-ordinate directions, respectively, psi

τ_{zr} = shear-stress component on the z-plane and in the r co-ordinate direction

τ_{cr} = critical instantaneous shearing stress, psi

$\bar{\sigma}$ = effective stress, psi

r_f = flash radius, in.

r_d = die radius, in.

r = instantaneous radius anywhere in flash or body of forging, in.

$\delta r, dr$ = small increment and infinitesimal quantities of radius, in.

h, h_0 = instantaneous and initial flash height, in.

l_0 = initial length of forging

n, m = dimensionless ratios of r_d/h_0 and h/h_0, respectively

L = forging load, lb

p_a = average forging pressure, psi

μ = coefficient of friction, F/N

F = force due to internal stresses (subscripts refer to direction), lb

$\delta\alpha$ = angle of annulus of segment of fictitious ring, deg

Theory of Forging

Press forging usually requires a number of preliminary operations such as edging, fullering, and blocking in which the forging progressively is brought closer to its final size. After the blocking operation, the rough forging nearly fits the finishing die and a close impression is obtained by squeezing the excess metal of the rough forging into a flash through the space between the closing dies. The finishing operation determines the quality of the forging since it is here that the rough forging is made to fit the die and assume its final dimensions. The flash, which will be removed from the forging later by a trimming operation, will attain a certain thickness which is determined by the final height (flash height) between the closing die halves when the finishing operation is completed. It is in this last operation that appreciable metal flow occurs in the region of the flash opening as the metal is discharged into the flash from the die cavity; the metal in the forging itself, however, only undergoes minor deformations in filling the die cavity. This operation, too, requires the greatest forging force, since that force will be determined by the total projected area of the flash land and the die cavity and by the pressure distribution over this area. The following analysis on press forging will be restricted to the finishing operation.

Let Fig. 1 represent a press forging at a particular stage of deformation. Assume also that the forging has been blocked and that the operation in question is a finishing operation. Consequently, to at least a first approximation, it may be assumed that the metal in the body of the forging is rigid and that all plastic deformation occurs in a fictitious disk of thickness h. This assumption is approximately confirmed by consideration of a probable slip-line field in plane strain. It is possible, therefore, to treat an axisymmetric press forging as a disk having thickness equal to the instantaneous flash height h of a real forging.

The fictitious disk in the press forging is subjected to variable friction on its surfaces, as follows:

(a) Friction below the rigid metal in the forging itself which is due to metal shearing.

(b) Friction in the flash which is due to metal sliding over the die surface and depends on the friction characteristics of these surfaces.

Let Fig. 2(a) represent the disk in the body of the forging before commencement of deformation and Fig. 2(b) the disk corresponding to that stage of deformation shown in Fig. 1. It is assumed that the edge of the disk remains square, i.e., barreling is absent, and further that the stresses are principal stresses and that the stress ratios during the entire deformation remain constant. Under these conditions the finite plastic strains, ϵ_z, ϵ_θ, and ϵ_r in cylindrical co-ordinates may be determined for any elemental volume in the disk at distance r from the axis; namely

$$\left.\begin{aligned} \epsilon_z &= \ln \frac{h}{h_0}, \\ \epsilon_\theta &= \ln \frac{2\pi r}{2\pi r_0} = \ln \frac{r}{r_0}, \\ \epsilon_r &= \ln \frac{\delta r}{\delta r_0} \end{aligned}\right\} \qquad (1)$$

However, since for each elemental volume, constancy of volume deformation must be satisfied, therefore

$$h_0 \pi r_0 \delta r_0 = h \pi r \delta r,$$

or

$$1 = \frac{h}{h_0} \frac{r}{r_0} \frac{\delta r}{\delta r_0},$$

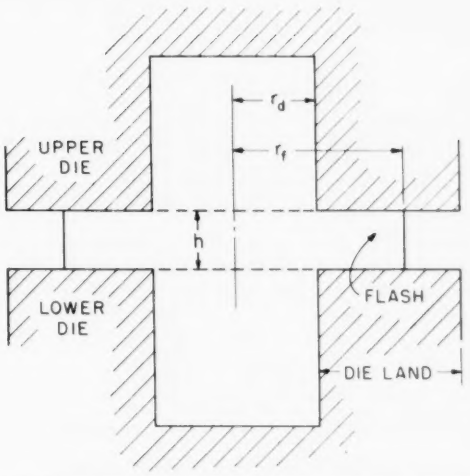

Fig. 1 Diagrammatic sketch of press forging with axial symmetry

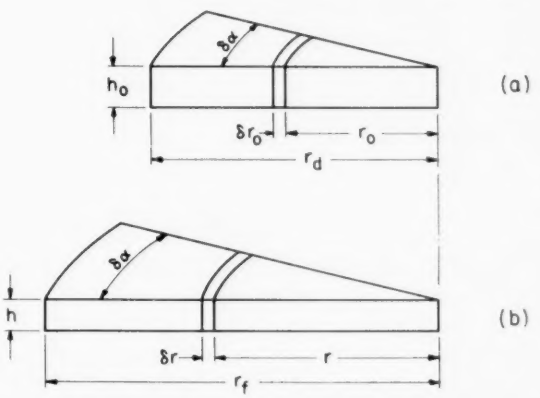

Fig. 2 Fictitious wedge in a press forging before and after deformation

and

$$\ln \frac{h}{h_0} + \ln \frac{r}{r_0} + \ln \frac{\delta r}{\delta r_0} = \epsilon_z + \epsilon_\theta + \epsilon_r = 0 \qquad (2)$$

Under the condition of absence of barreling, each element in the disk must deform as the disk as a whole deforms. Since

$$\pi r_0^2 h_0 = \pi r^2 h,$$

therefore

$$\frac{h_0}{h} = \left(\frac{r}{r_0}\right)^2$$

and

$$\ln \frac{h_0}{h} = -\epsilon_z = 2 \ln \frac{r}{r_0} = 2\epsilon_\theta \qquad (3)$$

Hence, substituting equation (3) into the constant-volume equation (2) results in

$$\epsilon_\theta = \epsilon_r, \qquad (4)$$

from which the plastic strains in terms of flash height are given by

$$\left.\begin{aligned} \epsilon_z &= \ln \frac{h}{h_0}, \\ \epsilon_r = \epsilon_\theta &= -\frac{1}{2}\,\epsilon_z = -\frac{1}{2} \ln \frac{h}{h_0}. \end{aligned}\right\} \tag{5}$$

Substituting these values into the expression for effective strain yields $-\epsilon_z = \bar{\epsilon}$, where

$$\bar{\epsilon} = \frac{2}{3}\left[\frac{(\epsilon_z - \epsilon_\theta)^2 + (\epsilon_\theta - \epsilon_r)^2 + (\epsilon_r - \epsilon_z)^2}{2}\right]^{1/2} \tag{6}$$

The fact that the deformation mechanism in the foregoing analysis was oversimplified will be readily seen later, when the roll-out or unfolding of the flash in the early stages of deformation is shown. Consider now the force system resulting from the uniform stress distribution due to normal stresses and shearing stresses on the faces of a sector of an annulus of thickness δr, height h, and angle $\delta\alpha$, as shown in Fig. 3. The forces in terms of stresses are given by

$$\left.\begin{aligned} F_1 &= \sigma_r r h \delta\alpha, \\ F_2 &= \sigma_r r h \delta\alpha + \frac{\partial}{\partial r}(\sigma_r r h \delta\alpha) dr, \\ F_3 &= \mu\sigma_z \delta\alpha r dr, \\ F_4 &= \sigma_\theta h dr, \end{aligned}\right\} \tag{7}$$

where the force F_3 results from the frictional drag on the top and bottom surfaces of the sector, due to the coefficient of friction μ, which is given by

$$\mu = \frac{F}{N} = \frac{\tau_{zr}\delta\alpha r dr}{\sigma_z \delta\alpha r dr} = \frac{\tau_{zr}}{\sigma_z}. \tag{8}$$

Equilibrium in the radial direction demands that the sum of the forces in the radial direction be zero; namely,

$$\Sigma F_r = -\frac{\partial}{\partial r}(\sigma_r \delta\alpha r h) dr + 2\sigma_\theta h dr \sin\frac{\delta\alpha}{2} - 2(\mu\sigma_z \delta\alpha r dr) = 0. \tag{9}$$

If h and $\delta\alpha$ are not functions of r and if $\delta\alpha \to 0$, then equation (9) will reduce to

$$r\frac{d\sigma_r}{dr} + \sigma_r - \sigma_\theta + \frac{2\mu\sigma_z r}{h} = 0. \tag{10}$$

Since the assumed deformation is symmetrical when $\epsilon_\theta = \epsilon_r$, therefore the plasticity equations demand that $\sigma_r = \sigma_\theta$, and thus equation (10) reduces to the following differential equation:

$$\frac{d\sigma_r}{dr} + \frac{2\mu\sigma_z}{h} = 0. \tag{11}$$

The friction stress $\mu\sigma_z$ can take on different values in the disk. If the disk is within the die, the metal forms a continuous structure and, in order that the disk may move, the friction force must be sufficient to permit shearing on both of its faces. On the other hand, if a portion of the disk has left the body in the form of a flash, then the friction force on this part of the disk will depend on the degree of lubrication between flash and disk and, unless welding occurs, will be less than would be required for metal shearing. Before integrating equation (11) under the foregoing boundary conditions it can be transformed as follows: Inasmuch as the effective stress, which is the instantaneous flow stress under the assumption of absence of shear stresses is given by

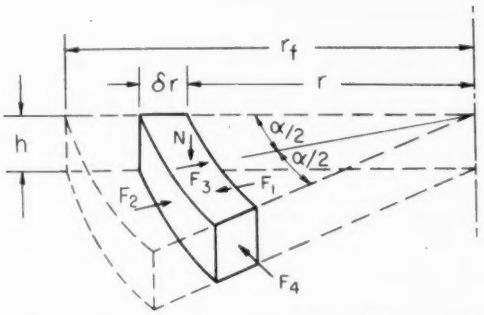

Fig. 3 Forces acting on a sector of small annulus in fictitious wedge of a press forging

$$\bar{\sigma} = \left[\frac{(\sigma_z - \sigma_\theta)^2 + (\sigma_\theta - \sigma_r)^2 + [\sigma_r - \sigma_z)^2}{2}\right]^{1/2},$$

which reduces, for the case when $\sigma_r = \sigma_\theta$, to

$$\sigma_r - \bar{\sigma} = \sigma_z, \tag{12}$$

hence the differential equation (11) takes the following form:

$$\frac{d\sigma_r}{\sigma_r - \bar{\sigma}} = -\frac{2\mu}{h} dr = \frac{d\sigma_z}{\sigma_z} \tag{13}$$

For the portion of the sector of the disk contained within the forging die, i.e., $0 \le r \le r_d$, the restraining force on the surfaces of the sector is equal to the critical stress of the metal τ_{cr}, multiplied by twice the projected area of the forging on which it acts. This shearing stress is assumed to act on small surface layers of the disk, on which the normal stress $-\sigma_z$ is a hydrostatic pressure; i.e., $\sigma_z = \sigma_r = \sigma_\theta$. Hence $\bar{\sigma} = (3\tau_{zr}^2)^{1/2}$, or $\tau_{zr} = \mu\sigma_z = -(1/\sqrt{3})\,\bar{\sigma}$. Substituting this relationship into equation (13) results in the differential equation,

$$d\sigma_z = \frac{2}{\sqrt{3}}\frac{\bar{\sigma}}{h} dr. \tag{14}$$

Under the assumption that $\bar{\sigma}$ is not a function of r, equation (14) can be integrated and the boundary condition, $\sigma_z = (\sigma_z)_{r_d}$ at $r = r_d$, can be substituted, hence

$$-\sigma_z = \frac{2}{\sqrt{3}}\frac{\bar{\sigma}}{h}(r_d - r) - (\sigma_z)_{r_d}. \tag{15}$$

For the flash of the forging, which is represented by the metal between $r = r_d$ and $r = r_f$, the coefficient μ is assumed to be constant, but less than that required to cause plastic deformation. Hence integration of equation (13), using the boundary condition that $\sigma_r = 0$ at $r = r_f$ and hence $-\sigma_z = \bar{\sigma}$, yields

$$-\sigma_z = \bar{\sigma} e^{\frac{2\mu}{h}(r_f - r)}. \tag{16}$$

The total load in the forging, at any stage of deformation, is given by

$$-L = 2\pi \int_0^{r_d}\left[\frac{2}{\sqrt{3}}\frac{\bar{\sigma}}{h}(r_d - r) - (\sigma_z)_{r_d}\right] r dr + 2\pi \int_{r_d}^{r_f} \bar{\sigma} e^{\frac{2\mu}{h}(r_f - r)} r dr. \tag{17}$$

Integrating equation (17) again under the assumptions that h, $\bar{\sigma}$, and μ are not functions of r and dividing through by the total

projected area and the flow stress $\bar{\sigma}$, the following equation for the average dimensionless forging pressure is obtained:

$$\frac{p_a}{\bar{\sigma}} = \frac{1}{2}\left(\frac{h}{\mu r_f}\right)^2\left[\left(\frac{2\mu r_d}{h}+1\right)e^{\frac{2\mu}{h}(r_f-r_d)} - \frac{2\mu r_f}{h} - 1\right] + \left(\frac{r_d}{r_f}\right)^2\left[e^{\frac{2\mu}{h}(r_f-r_d)} + \frac{2\sqrt{3}}{9}\frac{r_d}{h}\right] \quad (18)$$

Equation (18) can be used for computation of the maximum forging pressure for any practical case, when the flash radius r_f, for example, becomes the radius of the flash-relief trough and takes on a fixed value in any particular die design. However, for our present purpose of comparing experimental pressures during continuous forging tests with the theory, where r_f is a variable, it will be more convenient to transform equation (18) to read

$$\frac{p_a}{\bar{\sigma}} = \frac{m^3}{2\mu^2 n^2}\left[\left(\frac{2\mu n}{m}+1\right)e^{2\mu n\left(m^{-3/2}-\frac{1}{m}\right)} - 2\mu n m^{-3/2} - 1\right] + m\left[e^{2\mu n\left(m^{-3/2}-\frac{1}{m}\right)} + \frac{2\sqrt{3}}{9}\frac{n}{m}\right] \quad (19)$$

where

$$m = h/h_0 \text{ and } n = r_d/h_0$$

However, when the coefficient μ is equal to or greater than that required to cause plastic deformation, i.e., when the shear stress at $r = r_d$ computed by equation (16) is equal to or greater than the shear strength of the material, then sticking occurs in the flash. In this case the process becomes one of press forging of a disk, and equations (15), (16), and (18) reduce to those of Schroeder [13], where r_0 is the limiting radius beyond which metal sliding occurs; namely,

$$\frac{-\sigma_z}{\bar{\sigma}} = e^{\frac{2\mu}{h}(r_f-r)}, \quad \text{when} \quad r_0 \le r \le r_f \quad (20)$$

$$\frac{-\sigma_z}{\bar{\sigma}} = \frac{2}{h\sqrt{3}}(r_0 - r) + \frac{1}{\mu\sqrt{3}}, \quad \text{when} \quad 0 \le r \le r_0 \quad (21)$$

$$\frac{p_a}{\bar{\sigma}} = \frac{1}{2}\left(\frac{h}{\mu r_f}\right)^2\left[\left(\frac{2\mu r_0}{h}+1\right)e^{\frac{2\mu}{h}(r_f-r_0)} - \frac{2\mu r_f}{h} - 1\right] + \left(\frac{r_0}{r_f}\right)^2\left[\frac{1}{\mu\sqrt{3}} + \frac{2\sqrt{3}}{9}\frac{r_0}{h}\right] \quad (22)$$

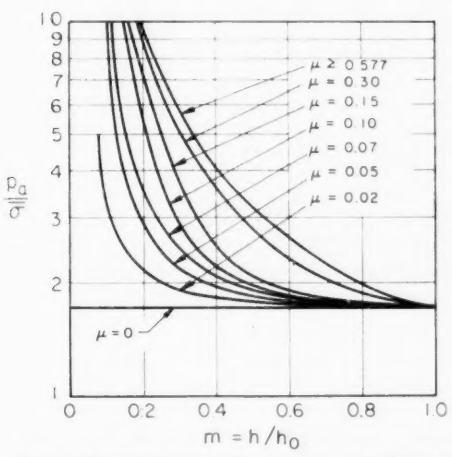

Fig. 4 Average dimensionless press-forging pressures ($p_a/\bar{\sigma}$) as functions of dimensionless flash-height ratios (h/h_0), for various coefficients of friction μ and for ratio of die radius to flash height (r_d/h_0) = 1.93

where

$$r_0 = r_f - \frac{h}{2\mu}\ln\left(\frac{1}{\mu\sqrt{3}}\right)$$

The functional relationship between the dimensionless forging pressure and m for various coefficients of friction and one parameter n are given in Fig. 4. The limiting conditions between which any experimental data must lie are indicated by the curves $\mu = 0$ and $\mu = 1/\sqrt{3} = 0.577$.

Experimental Apparatus and Technique

In order to test the applicability of equation (19) to press forging, the following experiments were carried out: Commercially pure lead and commercially pure aluminum (1100-0) were selected as representative examples of materials which could be hot-forged (lead) and cold-forged (aluminum), respectively, at room temperature. Cylindrical forging specimens having a $1^{15}/_{16}$-in. diameter, were varied in length from 3.5 to 5 in., to permit variation in initial flash height. The specimens were prepared as follows: Pig lead was cast into 4-in. molds and extruded into 2-in. cylindrical bars, prior to being machined into test specimens. Annealing was done at room temperature. Aluminum specimens were prepared from 2-in. rolled bars in the F-condition, annealed at 650 F in an electric furnace, and then machined. The forging dies consisted of hardened die rings having cylindrical die cavities ground to a diameter of $1^{15}/_{16}$ in. The dies, specimen, closing plates, and spacers are shown assembled in Fig. 5.

It may be seen that the forging apparatus was constructed in such a manner that a number of forging variables could be investigated, as for example, effects of flash-land width, die-filling ability, and others. In the present experiments, however, all tests were performed with solid die spacers and for the present the only variable investigated was the initial flash height h_0, which was obtained by varying the length of the specimens. The forging tests were carried out at essentially constant crosshead speeds of the hydraulic testing machine, which resulted in varying strain rates in the flash of the forging easily determinable from the instantaneous crosshead speed and flash height h.

The plastic-flow properties of the lead and aluminum, required

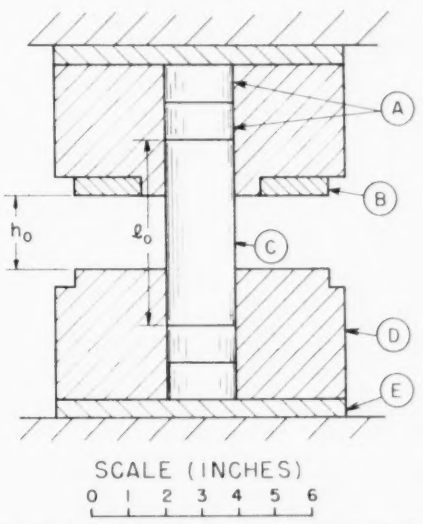

Fig. 5 Forging dies and specimen in position for testing. A—die spacers, B—land ring, C—specimen, D—die, E—backup plate.

to evaluate $\bar{\sigma}$ of equation (19), were obtained from 1-in-diam × 1-in-long cylindrical specimens in compression tests between lapped flat dies. The ends of the specimens were grooved and lubricated to prevent barreling, [16, 17, 18]. All tests were carried out in such a manner that the strain rates remained essentially constant. This was accomplished by adjusting the crosshead speed of the testing machine continuously during each test as a function of instantaneous specimen height. Typical effective-stress effective-strain and effective strain-rate curves are given in Figs. 6 to 8, inclusive. It is again seen that while aluminum, Fig. 8, showed no effects of strain rate on the flow stress for the low strain rates investigated [18], lead, on the other hand, shows a strain-rate effect as well as a strain effect.

Undulating stress-strain curves similar to those of Fig. 6 were observed earlier [17], and it was suggested that the effect was possibly due to a combined effect of work-hardening and recrystallization. In order to permit the evaluation of the flow stress of lead under various conditions of strain and strain rate, the average curves of Fig. 7 were drawn through the experimental points. From these an approximate flow stress $\bar{\sigma}$ could be evaluated by cross plotting the data for any condition of strain and strain rate encountered in the present forging tests. No strain-rate effects needed to be considered for the aluminum forging tests, as may be seen from Fig. 8, since $\bar{\sigma}$ can be uniquely determined by the effective strain alone.

It is of interest to note that the aluminum test data gave the same equation, $\bar{\sigma} = C\bar{\epsilon}^{(0.285)}$, as was obtained with earlier compression tests in connection with extrusion studies [18], except that the magnitude of the constant in the present case is only 25,800, while in the former it was 32,000. This anomaly was thought to be due to incomplete annealing as a result of relatively low strains in the 6-in. aluminum extrusions, from which the compression specimens in the earlier tests were machined.

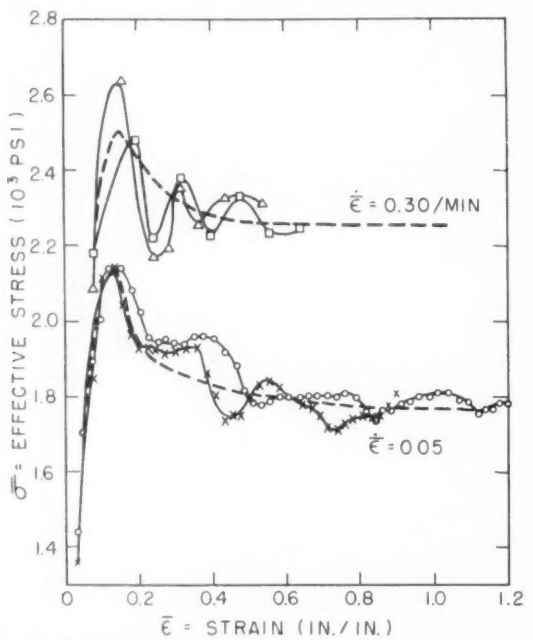

Fig. 6 Typical effective-stress effective-strain curves of commercially pure lead in compression at constant strain rates

Test conditions: 1-in-high × 1-in-diam cylindrical specimens
Lubricant: White lead in grooves at ends of specimens

○—specimen 5, × —specimen 2 } $\dot{\bar{\epsilon}}$ = 0.05/min
□—specimen 10, △—specimen 9 } $\dot{\bar{\epsilon}}$ = 0.30/min

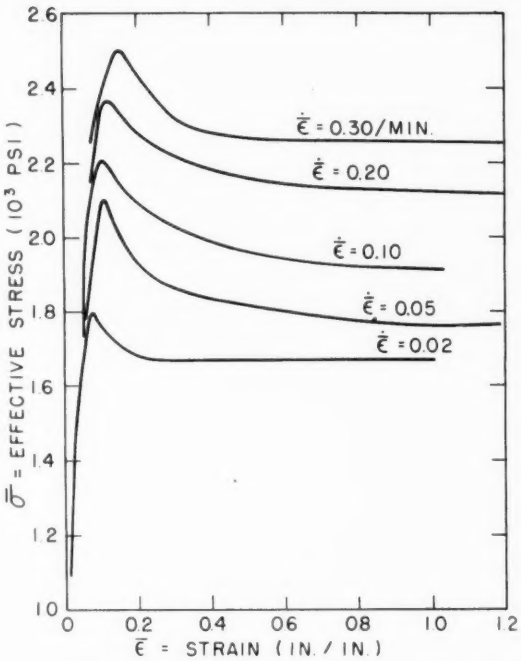
$\bar{\sigma}$ = EFFECTIVE STRESS (10^3 PSI)
$\bar{\epsilon}$ = STRAIN (IN./ IN.)
$\dot{\bar{\epsilon}}$ = 0.30/MIN.
$\dot{\bar{\epsilon}}$ = 0.20
$\dot{\bar{\epsilon}}$ = 0.10
$\dot{\bar{\epsilon}}$ = 0.05
$\dot{\bar{\epsilon}}$ = 0.02

Fig. 7 Average effective-stress effective-strain curves of commercially pure lead in compression at various strain rates

Test conditions: 1-in-high × 1-in-diam cylindrical specimens
Lubricant: White lead in grooves at ends of specimens

To evaluate the friction characteristics of the metals in the flash sliding over the forging dies, some friction studies also were made. These were performed in the friction apparatus shown schematically in Fig. 9. Cylindrical specimens of lead and aluminum were machined to predetermined diameters in order that various strains could be realized when the specimens were subjected to compression loading. As a result of the plastic deformation the specimens then fitted the pusher shown in Fig. 9. The surfaces of the specimens and the lapped and parallel surfaces of the friction apparatus were then cleaned (after removal of load) and provided with fresh lubricant. Following this, the specimens were replaced in the apparatus, reloaded to the former load before removal for cleaning, and the force required for steady-state sliding was determined. The results of this preliminary study are shown in Table 1.

Experimental Results and Discussion

The results of the press-forging tests are given in Figs. 10 to 16, inclusive. The solid lines are the theoretical curves, equation (19), while the symbols represent the experimental data of one or more continuous forging tests. The dimensionless pressure ratios were obtained by dividing the actual average pressures observed in the experiments by the flow stresses $\bar{\sigma}$ at the same strains and strain rates used in the compression tests as those which were maintained in the actual forging tests. Under these conditions it is at once evident that agreement between theory and experiment is good but not perfect. The experimental points of lead and aluminum appear to be nearly parallel with the theoretical curves at moderately high strains; i.e., low values of h/h_0, with $\mu \approx 0.2$.

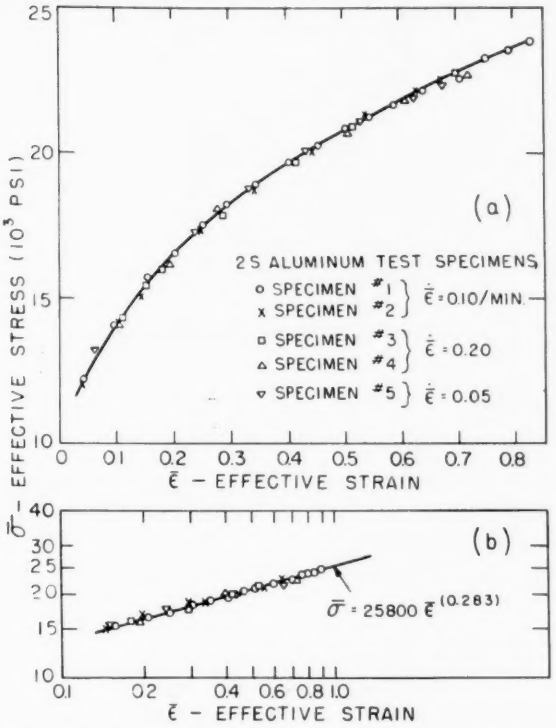

Fig. 8 Effective-stress effective-strain curves of commercially pure aluminum (1100-0) in compression at various strain rates

Test conditions: 1-in-high × 1-in-diam cylindrical specimens
Lubricant: Graphite in oil in grooves at ends of specimens

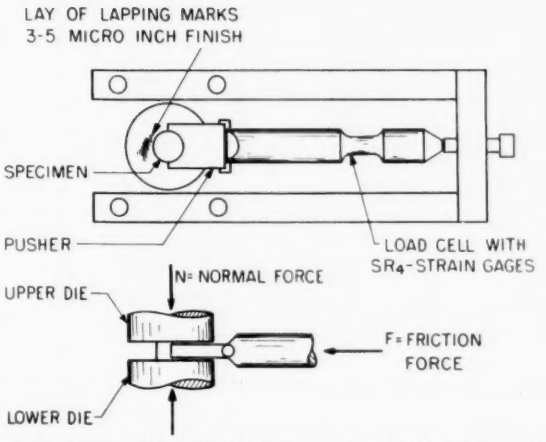

Fig. 9 Diagrammatic sketch of friction apparatus for determination of coefficients of friction

The extent of deformation achievable in the forging tests of aluminum was lower than that with lead, because of the fact that the forging load was limited by the 400,000-lb testing machine available. Consequently a check between theory and experiment with aluminum was possible only for a relatively short range of deformation as indicated by the figures.

Figs. 10 to 16 also reveal that all experimental points at the beginning of each forging test fall below the theoretical curves. This departure of experiment from theory is apparently due to two major causes:

1 The increase in the area of the flash in actual contact with the land of the die is smaller, due to barreling, than would be calculated from constant-volume relationships.

2 Shearing of the metal is not confined to a thin layer of metal

Table 1 Some preliminary friction studies with commercially pure lead and commercially pure aluminum (1100) between flat dies

Material	Test no.	Diameter of cylind. specimen, in.	Effective strain $\bar{\epsilon}$	Normal force, lb.	Friction force, lb	Coeff. of friction	Condition of ends of specimens	Lubrication of dies and specimens
Lead	1	1.12	0.23	1300	200	0.08	Spiral grooves	White lead in oil. Thick film applied
	2	1.35	0.60	1370	210	0.08	Spiral grooves	White lead in oil. Thick film applied
	3	1.12	0.23	1310	100	0.04	Plain	White lead in oil. Thick film applied
	4	1.35	0.60	1290	150	0.05	Plain	White lead in oil. Thick film applied
	5	1.12	0.24	1350	575	0.21	Plain	None
	6	1.35	0.60	1400	590	0.21	Plain	None
Aluminum	10	1.12	0.12	17400	640	0.02	Spiral grooves	Graphite in oil. Thick film applied
	11	1.13	0.14	17350	990	0.03	Plain	Graphite in oil. Thick film applied
	12	1.12	0.47	19200	800	0.02	Plain	Graphite in oil. Applied then wiped clean
	13	1.12	0.47	19200	5500	0.14	Plain	None
	14	1.11	0.44	18200	8000–18500	0.22 Start 0.50 End	Plain	None—dies were covered with some smear metal at start of test

NOTE: All specimens were compressed to strains indicated at an approximate strain rate of 0.1 to 0.2 in/in per min. Dies and ends of cylindrical specimens were washed in CCl_4 before each test. Lubrication was then applied as indicated. All coefficients of friction were evaluated during short movements of the specimens of approximately $^1/_8$ to $^1/_4$ in. at a slow constant speed of approximately 2–4 ipm. The dies were finish-lapped to 3–4 microin. roughness and the specimens were moved perpendicular to the lay of the lapping marks.

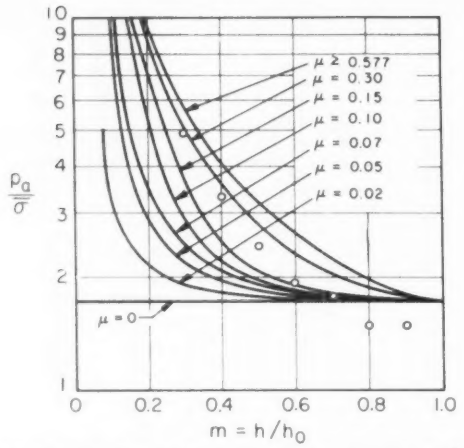

Fig. 10 Average dimensionless press-forging pressures ($p_a/\bar{\sigma}$), as functions of dimensionless flash height (h/h_0), for commercially pure lead forged at room temperature, with ratio of die radius to initial flash height (r_d/h_0) = 1.94

Test conditions: $h_0 = 0.50$ in.
$r_d = {}^{31}/_{32}$ in.
Lubricant: White lead in oil

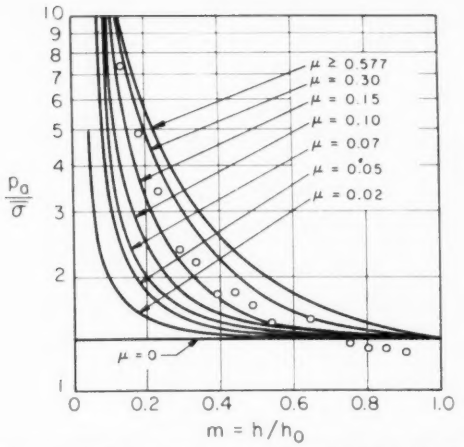

Fig. 11 Average dimensionless press-forging pressures ($p_a/\bar{\sigma}$), as functions of dimensionless flash height (h/h_0), for commercially pure lead forged at room temperature, with ratio of die radius to initial flash height (r_d/h_0) = 0.99

Test conditions: $h_0 = 0.98$ in.
$r_d = {}^{31}/_{32}$ in.
Lubricant: White lead in oil

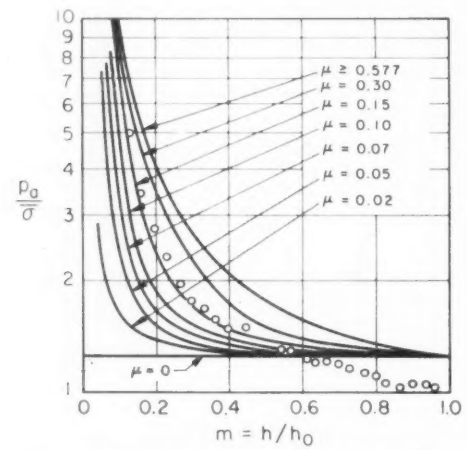

Fig. 12 Average dimensionless press-forging pressures ($p_a/\bar{\sigma}$), as functions of dimensionless flash height (h/h_0), for commercially pure lead forged at room temperature with ratio of die radius to initial flash height (r_d/h_0) = 0.65

Test conditions: $h_0 = 1.50$ in.
$r_d = {}^{31}/_{32}$ in.
Lubricant: White lead in oil

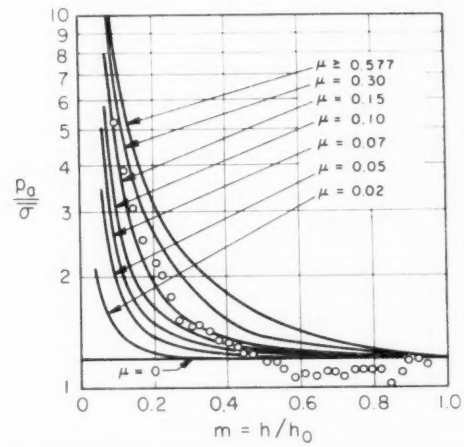

Fig. 13 Average dimensionless press-forging pressures ($p_a/\bar{\sigma}$), as functions of dimensionless flash height (h/h_0) for commercially pure lead forged at room temperature with ratio of die radius to initial flash height (r_d/h_0) = 0.48

Test conditions: $h_0 = 2.00$ in.
$r_d = {}^{31}/_{32}$ in.
Lubricant: White lead in oil

of the forging in contact with the die, but in the initial stage of deformation occurs throughout the flash metal.

The nonideal behavior of deformation actually taking place is illustrated in Fig. 17. It is evident that the neglect of shearing stresses in the initial stages of deformation is incorrect, since severe barreling of the flash metal contained in the initial right circular cylinder of height h_0 takes place. Hence the constant-volume relationship, $h/h_0 = (r_d/r_f)^2$, cannot be used in calculating the area over which the pressure p_a acts. However, a simple partial correction of p_a is possible, by measuring the actual contact area of the flash and dividing the observed load by this area. This has been done to the data shown in Fig. 12 and the results are given in Fig. 18. It is seen that the theoretical curves in the initial stages of deformation are now in closer agreement with the experimental points, but that the corrections do not eliminate completely the nonideal behavior of the flash metal, at magnitudes of h/h_0 near unity, which is caused by internal shearing.

In order to study the effects of lubrication on the forging pressures some preliminary tests were made with lead for various surface conditions. The results are shown in Fig. 19. It is seen that lead evidently has little tendency to weld to the die surfaces and that a dry surface causes no greater friction than a well-lubricated one. It apparently shows also that a copious supply of lubricant appears to be ineffectual, since the flash, in squeezing itself through the flash opening, wipes the die surfaces clean. Hence the metal flowing from the forging into the flash space, except for the initial folding, consists of unlubricated nascent metal. The coefficient of friction in forging, therefore,

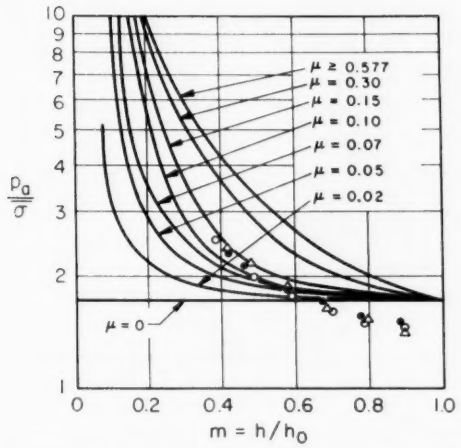

Fig. 14 Average dimensionless press-forging pressures ($p_a/\bar{\sigma}$), as functions of dimensionless flash height (h/h_0), for commercially pure aluminum (1100-0) forged at room temperature with ratio of die radius to initial flash height (r_d/h_0) = 2.00

Test conditions: $h_0 = 0.48$ in.
$r_d = {}^{31}/_{32}$ in.
Lubricant: Graphite in oil
△—specimen 6
●—specimen 9
○—specimen 11

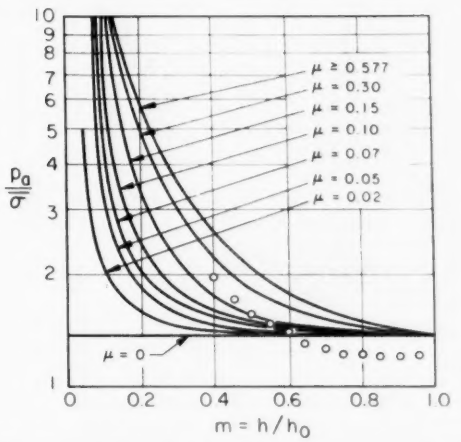

Fig. 15 Average dimensionless press-forging pressures ($p_a/\bar{\sigma}$), as functions of dimensionless flash height (h/h_0), for commercially pure aluminum (1100-0) forged at room temperature with ratio of die radius to initial flash height (r_d/h_0) = 0.97

Test conditions: $h_0 = 1.00$ in.
$r_d = {}^{31}/_{32}$ in.
Lubricant: Graphite in oil

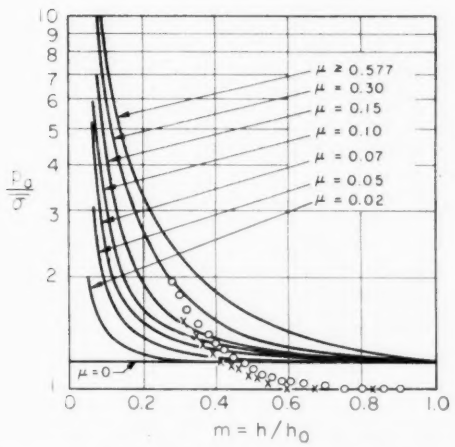

Fig. 16 Average dimensionless press-forging pressures ($p_a/\bar{\sigma}$), as functions of dimensionless flash height (h/h_0), for commercially pure aluminum (1100-0) forged at room temperature with ratio of die radius to initial flash height (r_d/h_0) = 0.48

Test conditions: $h_0 = 2.00$ in.
$r_d = {}^{31}/_{32}$ in.
Lubricant: Graphite in oil
×—specimen 20
○—specimen 22

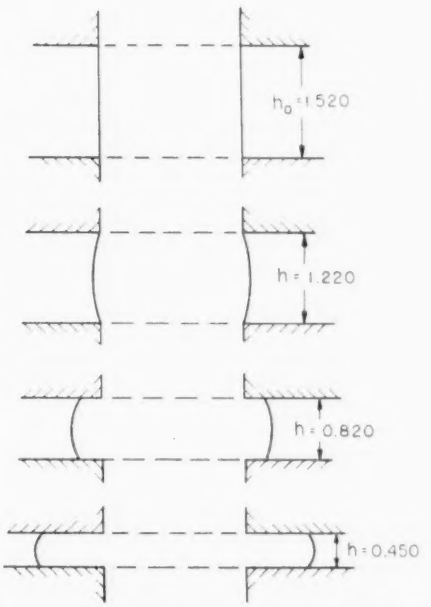

Fig. 17 Typical actual shapes of flash of commercially pure lead test specimen at various stages of forging test at room temperature as determined from photographs taken during test (r_d/h_0) = 0.65

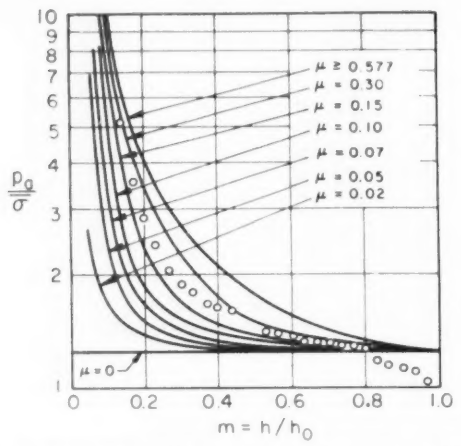

Fig. 18 Average dimensionless press-forging pressures ($p_a/\bar{\sigma}$), as functions of dimensionless flash height h/h_0, for commercially pure lead forged at room temperature and for ratio of die radius to initial flash height (r_d/h_0) = 0.65. Forging pressures computed by using corrected areas as obtained from photographs taken during test.

Test conditions: h_0 = 1.50 in.
r_d = $^{31}/_{32}$ in.
Lubricant: White lead in oil

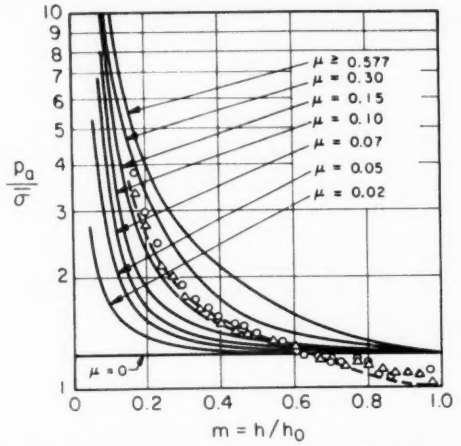

Fig. 19 Effect of various types of lubrication on average dimensionless press-forging pressures ($p_a/\bar{\sigma}$), as functions of dimensionless flash height (h/h_0), for commercially pure lead forged at room temperature with ratio of die radius to initial flash height (r_d/h_0) = 0.65

Test conditions:
○—specimen 22—cleaned with CCl_4, no lubricant
△—specimen 23—wiped with white lead in oil
– – – data from Fig. 12; die and specimen copiously coated with white lead in oil

should approach that of sliding of dry surfaces. Referring to Table 1, it is seen that an average coefficient of friction of approximately 0.2, inferred from the forging tests, agrees quite well with those for dry friction, when little or no pickup of metal occurs on the die surfaces.

Conclusions

1 The idealized deformation mechanism assumed in a simplified theory of axisymmetric press forging yields forging pressures which are in good agreement with experiments on commercially pure lead and aluminum.

2 Departure of the theory from the experimental observations at the beginning of the forging operations is believed to be due to the idealization that shear takes place only in a thin surface layer of the flash.

3 Coefficients of friction observed in the forging tests between die and flash are approximately 0.2 for both lead and aluminum.

4 Lubrication of flash lands of dies appears to be ineffectual, because of the wiping action of the nascent metal of the forging as it enters the flash space.

Acknowledgments

The authors wish to thank the University of California for making available laboratory space and equipment, and the National Science Foundation for its grant No. NSF-G-2957 in support of the present investigation.

They also wish to thank Mr. Petersen of the Division of Industrial Engineering, for preparing the forging dies, and Messrs. Miller, Eggleston, Kerr, and Dailey for assisting with the experiments.

References

1 M. D. Stone, "Design and Construction of Large Forging and Extrusion Presses for Light Metals," TRANS. ASME, vol. 75, 1953, pp. 1493–1512.

2 W. Naujoks and D. C. Fabel, "Forging Handbook," American Society for Metals, Cleveland, Ohio, 1939, p. 8.

3 "Hydraulische Presse zum Schnellschmieden (Haswell System)," *Zeit. Vereines Deutscher Ingenieure*, vol. 7, 1863, pp. 287–290.

4 W. P. Blake, "Hydraulic Forging," Reports United States Commissioners Vienna International Exhibition, 1873, vol. 4, 1876, Washington, D. C., Section E, pp. 257–274.

5 L. Prandtl, "Anwendungsbeispiele zu einem Henckyschen Satz über das Plastische Gleichgewicht," *Zeit. für Angewandte Mathematik und Mechanik*, vol. 3, 1923, pp. 401–406.

6 R. Hill, "The Mathematical Theory of Plasticity," Clarendon Press, Oxford, England, 1950, pp. 226–236.

7 A. P. Green, "A Theoretical Investigation of the Compression of a Ductile Material Between Smooth Flat Dies," *Philosophical Magazine*, series 7, vol. 42, 1951, p. 900.

8 J. M. Alexander, "The Effect of Coulomb Friction in the Plane-Strain Compression of Plastic-Rigid Material," *Journal of Mechanics and Physics of Solids*, vol. 3, 1955, pp. 233–245.

9 J. F. W. Bishop, "On the Effect of Friction on Compression and Indentation Between Flat Dies," *Journal of Mechanics and Physics of Solids*, vol. 6, 1958, pp. 132–144.

10 E. Siebel, "The Plastic Forming of Metals," *Steel*, vol. 94, January–June, 1953, April 23, pp. 40–45, April 30, pp. 39–42.

11 A. Nadai, "The Forces Required for Rolling Steel Strip Under Tension," *Journal of Applied Mechanics*, vol. 6, TRANS. ASME, vol. 61, 1939, p. A-54.

12 G. Sachs (unter Mitwirkung von W. Eisbein, W. Kuntze, and W. Linicus), "Spanlose Formung der Metalle," *Mitteilungen der Deutscher Material Prüfungsanstalten*, Supplement 16, Kaiser Wilhelm Institut für Metall Forschung, Julius Springer, Berlin, Germany, 1931, p. 93.

13 W. Schroeder and D. A. Webster, "Press-Forging Thin Sections: Effect of Friction, Area, and Thickness on Pressure Required," *Journal of Applied Mechanics*, vol. 16, TRANS. ASME, vol. 71, 1949, pp. 289–294.

14 O. Hoffman and G. Sachs, "Introduction to Theory of Plasticity for Engineers," McGraw-Hill Book Company, Inc., New York, N. Y., 1953, pp. 240–248.

15 R. L. Dietrich and G. Ansel, "Calculation of Press Forging Pressures and Application to Magnesium Forgings," *Trans. ASM*, vol. 38, 1947, pp. 709–728.

16 N. Loizou and R. B. Sims, "The Yield Stress of Pure Lead in Compression," *Journal of the Mechanics and Physics of Solids*, vol. 1, 1953, pp. 234–243.

17 E. G. Thomsen, C. T. Yang, and J. B. Bierbower, "An Experimental Investigation of the Mechanics of Plastic Deformation of Metals," University of California Publications in Engineering, vol. 5, 1954.

18 E. G. Thomsen and J. Frisch, "Stresses and Strains in Cold-Extruding 28-O Aluminum," TRANS. ASME, vol. 77, 1955, p. 1343.

DISCUSSION

C. T. Yang[6]

The writer believes this paper to be valuable in both theoretical and practical aspects. He wishes to discuss a few points in the following:

1 In Fig. 1 of the paper, the authors assume that the plastic flow occurs only in the fictitious disk of thickness h. The metal in the die with radius r_d is assumed to be plastic rigid. This assumption is a bit difficult to justify as far as the energy of deformation is concerned. It is well known that the energy of deformation for press forging and other plastic deformation is related to volume in the following equation:

$$W = v \int \bar{\sigma} d\bar{\phi} \tag{23}$$

where

W = total work done
V = total volume of billet or work
$\bar{\sigma}$ = effective stress
$\bar{\phi}$ = effective strain

Under the authors' assumption, the volume involved is the fictitious disk of height h and this volume is very different compared with the actual total volume of the specimen. Hence the pressure of press forging derived from the deformation energy is very different in these two cases.

2 In Equation (14) of the paper, the authors assume that $\bar{\sigma}$ is not a function of r so that Equation (14) can be integrated. This assumption seems to be a little drastic. It is well known that in the following equation,

$$\bar{\sigma} = \left[\frac{(\sigma_r - \sigma_\theta)^2 + (\sigma_\theta - \sigma_z)^2 + (\sigma_z - \sigma_r)^2}{2}\right]^{1/2} \tag{24}$$

$\bar{\sigma}$ is a function of σ_r and in forging it is understood that σ_r is a function of r.

3 To avoid the foregoing difficulty, the writer believes the following equation (the yielding criterion) can be used instead of Equation (12) in the paper:

$$\sigma_r - \sigma_z = \bar{\sigma}_0 \tag{25}$$

where $\bar{\sigma}_0$ = yield strength (psi) of the specimen.

In the case of sliding, Equation (11) in the paper would become

$$\frac{d\sigma_r}{\sigma_r - \bar{\sigma}_0} = -\frac{2\mu}{h} dr \tag{26}$$

which can be integrated easily.

In the case of sticking, $\mu\sigma_z = -\mu p = \hat{\tau}_{zr}$, where p = forging pressure, and $\hat{\tau}_{zr}$ = maximum shear stress. Also, we have:

$$\hat{\tau}_{zr} = \bar{\sigma}_0/2 \tag{27}$$

By substituting Equation (27) into Equation (11) in the paper, the following equation yields:

$$\frac{d\sigma_r}{dr} - \frac{\bar{\sigma}_0}{h} = 0 \tag{28}$$

which also can be integrated directly.

Regarding boundary conditions:

1 In the case of sliding, that is, when $r_d < r < r_f$,

$$\sigma_r = 0, \quad \text{at} \quad r = r_f$$

2 In the case of sticking, i.e., when $0 < r < r_d$, σ_r at $r = r_d$ is the same for both sliding and sticking.

The writer is interested to know if the foregoing checks with the experimental results.

[6] Associate Professor, Department of Mechanical Engineering, University of Michigan, Ann Arbor, Mich.

Authors' Closure

The authors greatly appreciate the comments offered by Professor Yang and the evident detailed consideration he has given the paper.

Concerning the first comment, the neglect of plastic deformation work absorbed by the forging proper is believed to be a reasonable idealization which need not depart markedly from practice. Under the assumptions of the analysis, the forging die cavity is considered completely filled and the material constituting the forging proper is plastic rigid with stress condition of hydrostatic pressure. Plastic deformation is thus restricted to the flash which is here treated as a fictitious disk. The experi-

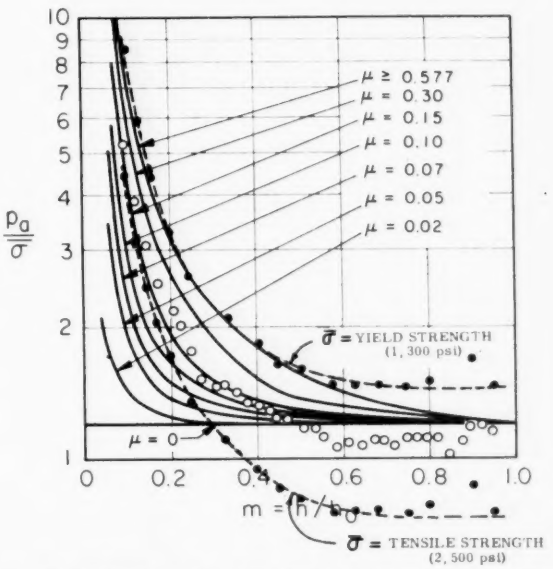

Fig. 20 Lead forging, $r_d/h_0 = 0.48$. Ratios based upon yield and tensile strength criteria compared with instantaneous effective stress criterion results of paper, Fig. 13.

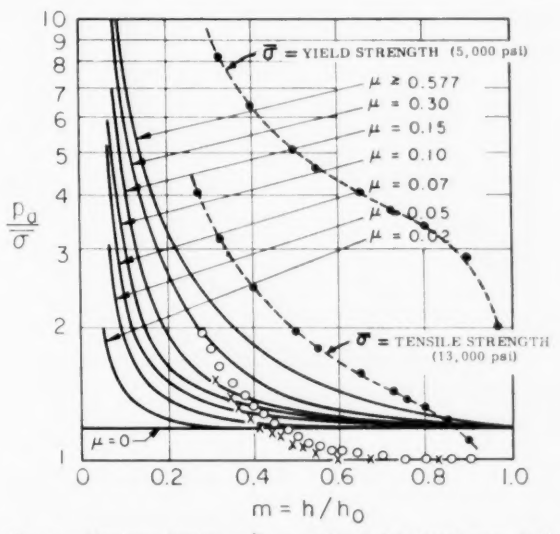

Fig. 21 Aluminum forging, $r_d/h_0 = 0.48$. Ratios based upon yield and tensile strength criteria compared with instantaneous effective stress criterion results of paper, Fig. 16.

mental tests performed in the investigation conformed to this condition. The analyses and tests thus approximate a final sizing operation in press forging where previous blocking operations have shaped the rough forging to conform nearly to the final die cavity. In practice, the forging proper would experience some plastic deformation leading to complete filling of the die cavity. The extent of such plastic deformation would be very small relative to that occurring in the flash.

Professor Yang's second comment suggesting use of the tensile yielding criterion, $\bar{\sigma}_0$, rather than the instantaneous effective stress, $\bar{\sigma}$, was applied to both lead and aluminum for the test condition $(r_d/h_0) = 0.48$ reported in Figs. 13 and 16 of the paper. In addition to yield strength, analysis also was made with tensile strength as the criterion. Values for representative materials as reported in literature were used for computation as follows: Lead $\bar{\sigma}_0 = 1300$ psi, 2500-psi tensile strength; aluminum $\bar{\sigma}_0 = 5000$ psi, 13,000-psi tensile strength. Ratios determined for the alternative analyses are shown in Figs. 20 and 21 along with those of the initial analysis based on effective stress, Figs. 13 and 16.

In the case of lead, Fig. 20, results based on yield and tensile criteria bracket those obtained from the effective stress analysis and which most closely approximate predicted variation. In the complete absence of strain-hardening a general agreement might be anticipated. In the present instance, the simultaneous strain-hardening and recrystallization effects observed for lead complicate the comparison.

However, for aluminum, Fig. 21, both yield and tensile strength criteria results depart markedly from predicted behavior. The yield criterion, showing greatest deviation, neglects the effects of strain-hardening whereas the tensile criterion which incorporates this effect partially is in better agreement with prediction. The much closer agreement of results obtained from the analysis of the paper would indicate the most appropriate criterion to be that of instantaneous effective stress.

A Three-Dimensional, Tool-Life Equation—Machining Economics

BERTIL N. COLDING

Research Supervisor, Physical Research Department, The Cincinnati Milling Machine Company, Cincinnati, Ohio

In Part 1 of this paper, two tool-life equations are derived, one limited equation and one general tool-life equation, between the variables cutting speed, chip equivalent, and tool life. The chip equivalent, introduced by Woxén, is a well-defined function of feed, depth of cut, nose radius, and side-cutting-edge angle. The limited equation takes into account the variation of Taylor's exponent n with the value of the chip equivalent, but the equation is only valid within certain limits of cutting speed and chip equivalent. A general equation is then derived on the basis of the limited equation. In Part 2 an expression called the productivity is derived. This relationship is valid for either maximum production or minimum cost and, combined with the general, hyperbolic, tool-life equation, it is used to investigate the optimum combination of tool-life, cutting speed, and chip equivalent.

1 TOOL-LIFE RELATIONSHIPS

MANY INVESTIGATIONS in the field of metal cutting have been carried out since the time of F. W. Taylor [1],[1] resulting in abundant data. These data, however, refer often only to the special conditions of the tests and are not correlated. The progress made in recent years should enable one to deduce from these tests generalized tool-life equations. Such equations have been suggested by Woxén [2], Kronenberg [3], Gilbert [4], and others. However, the generalized "Taylor" equations are derived on the basis of a constant exponent n, in Taylor's well-known relation

$$VT^n = C \tag{1}$$

Although, for practical purposes it is quite convenient to work with a constant n-value, one realizes the importance of the n-variation when dealing with metal-cutting problems of a more scientific character.

Many investigations show very peculiar tool-life curves when plotted against cutting speed, indicating deviations from the straight line resulting when Equation (1) is plotted on a log-log graph paper even in the region of high cutting speeds where Equation (1) is usually assumed to hold.

In the following an approximate relation between tool-life, cutting speed, feed, depth of cut, nose radius, and side-cutting-edge angle will be derived. This equation takes into account the variation of the exponent n. A closer examination of this equation in connection with experimental data gives rise to the question whether Taylor's experimental relation is really the funda-

[1] Numbers in brackets designate References at end of paper.

Contributed by the Metal Processing Activity of the Production Engineering Division and presented at the Annual Meeting, New York, N. Y., November 30–December 5, 1958, of THE AMERICAN SOCIETY OF MECHANICAL ENGINEERS.

NOTE: Statements and opinions advanced in papers are to be understood as individual expressions of their authors and not those of the Society. Manuscript received at ASME Headquarters, August 4, 1958. Paper No. 58—A-123.

Nomenclature

A_0 = cross-sectional area of "chip" before removal from workpiece
L = contact length of part of tool edge engaged in cutting
$q = L/A_0$ = chip equivalent
t = feed
b = depth of cut
r = nose radius of cutting tool
C_s = side-cutting-edge angle
V = cutting speed
T = tool life
C = constant in Taylor's equation
n = exponent of T, in Taylor's equation
m = exponent of q, in limited tool-life equation
A = constant in limited tool-life equation
T_*, C_W, c_W, q_0 = constants in Woxén's equation
k = thermal conductivity of work material
(ρ_c) = volume specific heat of work material
$K = k/\rho_c$ = thermal diffusivity of work material
E = electromotive force generated in chip-tool and work-tool interface
B, U, a_0, l, β = dimensionless quantities
$\phi(x, y, z)$ = general hyperbolic, tool-life equation, where $x = \log_e q$, $y = \log_e V$, $z = \log_e T$
a, b, c = semiaxes of hyperbolic tool-life surface
x_0, y_0, z_0 = location of center of hyperbolic tool-life surface
H = constant in hyperbolic tool-life equation
N = normal vector on hyperbolic tool-life surface
P = cost of machine and operator including overhead per unit time
R = average cost to regrind tools per part
Q = total cost per part
T_c = cutting time per part
T_i = idle time per part
T_d = down time per part
T_{avg} = average time to produce one part
W_p = volume work material removed per part
W = volume work material removed per unit time
γ = time, equivalent to sum of down time T_d and ratio R/P
$F(x, y, z)$ = productivity function
f = productivity
p = productivity per unit length of cutting edge

mental one in the metal-cutting field. Another equation is proposed having the geometrical configuration of an axisymmetric surface. The equation is shown to fit very well with experimentally obtained tool-life curves of different feeds and depths of cut in the linear tool-life region as well as in the nonlinear case. The equation holds for a great number of combinations of tool and work materials. This equation is then applied to machining economics, raising the question whether machine tools should be designed to allow larger feeds rather than increasing cutting speeds.

The Chip Equivalent

To obtain the afore-mentioned equations use is made of the so-called chip equivalent (a direct English translation of the Swedish term in turning, suggested by Woxén [2] in 1931), defined by

$$q = L/A_0 \tag{2}$$

The inverse value of the chip equivalent is known in German literature as "Bogenspandicke" [5], in French literature as "epaisseur du coupeau equivalent" [6].

The chip equivalent, q, is a physical quantity which, together with cutting speed, V, and material properties, determines the temperature in the cutting edge. Woxén first assumed [2] and later showed [7] the following by a theoretical treatment of the heat balance in the cutting process:

1 That the actual area of cut $A_0 \cong bt$ (b = depth of cut, t = feed) is a measure of the heat quantity generated at a certain cutting speed.

2 Also that the engaged cutting-edge length L is a measure of the heat quantity carried off by chip, tool, and workpiece.

From Fig. 1 it is readily seen that an approximate value of the chip equivalent q is given by

$$q \cong \frac{\dfrac{b - r(1 - \sin C_s)}{\cos C_s} + \dfrac{(90 - C_s)}{180}\pi r + (t/2)}{bt} \tag{3}$$

valid for $b \geq r(1 - \sin C_s)$, where

b = depth of cut
t = feed
r = nose radius
C_s = side-cutting-edge angle

Woxén showed by the use of the tool-work thermocouple method and tool-life data:

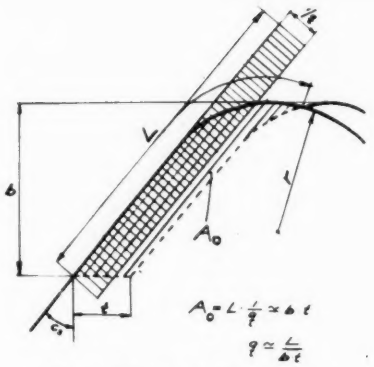

Fig. 1 Definition of chip equivalent

1 That the same temperature was obtained, if feed, depth of cut, nose radius, and side-cutting-edge angle were combined so that the values of the chip equivalent were equal, the cutting speed being constant.

2 For a constant value of chip equivalent the temperature rises with increased cutting speed.

3 For the same cutting speed the temperature rises with a diminished chip equivalent.

4 A generalized tool-life equivalent may be written

$$V = \left(\frac{T_*}{T}\right)^n C_W \frac{q + q_0}{1 + c_W q} \tag{4a}$$

where

V = cutting speed
T = an arbitrary tool life
T_* = a certain tool life; e.g., 60 min
n = exponent in Taylor's equation (1), (constant)
C_W = a constant determined by workpiece and tool
q = chip equivalent
c_W, q_0 = constant

By applying Fourier's differential equation to the conduction of heat going to the work, the chip, and the cutting tool, Woxén obtained an equation, analogous to Equation (4a). In deriving this equation he showed that the specific cutting energy or the specific cutting force is approximately a linear function of q.

The close dependence of cutting speed and chip equivalent shown by Woxén also can be seen from cutting data published by this Society [8], which were converted into q-values and represented in Fig. 2, where V_{60} (cutting speed corresponding to 60-min

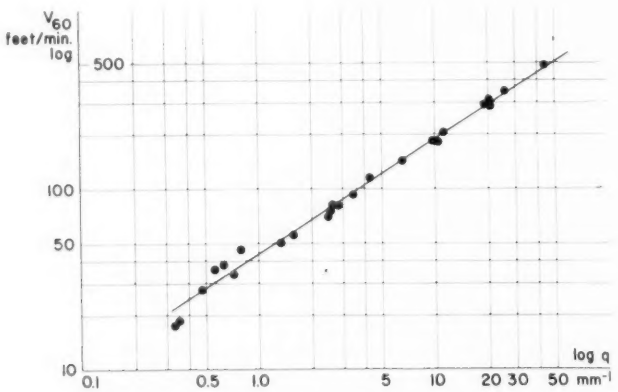

Fig. 2 Relation showing dependence of V_{60} on chip equivalent

tool life) is plotted against q in a double logarithmic scale. The data represent turning of SAE X1335 with HSS tools of two different nose radiuses (0 and 1.6 mm) and a side-cutting-edge angle of 0 deg, feeds from 0.05–3.18 mm, depths of cut from 0.79–25.4 mm. All the data fall very close to a straight line. The dimension of the chip equivalent is mm^{-1}.

Dimensional Analysis

A Limited Tool-Life Equation. Dimensional analysis has proved to be a very handy method in many fields of engineering. To perform such an analysis it is most important to know the fundamental physical quantities affecting the cutting process. Previous investigations have shown the importance of temperature, thermal properties of work material, energy per unit volume of metal removed, chip equivalent (or feed and depth of cut), and cutting speed on tool life [7, 9, 10, 11]. There also seems to be general agreement that tool life is a direct function of temperature in the region where Taylor's equation is valid. Therefore, in a dimensional analysis aiming at a generalization of Taylor's original equation (1), temperature should not be included in the analysis, but the thermal properties of the workpiece. To take into account the specific energy u necessary to cut the metal, the chip equivalent, being a function of u, might very well take care of this variable for a constant combination of work and tool material. As q in particular takes care of feed, depth of cut, nose radius, and side-cutting-edge angle, q therefore would be a variable as important as the cutting speed V. In Table 1 the quantities regarded essential for the analysis are tabulated.

Table 1 Quantities affecting tool life

Physical quantity	Symbol	Dimension
Tool life	T	(T)
Cutting speed	V	(LT^{-1})
Chip equivalent	q	(L^{-1})
Thermal conductivity	k	($MLT^{-3}\theta^{-1}$)
Volume specific heat	ρ_c	($ML^{-1}T^{-2}\theta^{-1}$)
Thermal diffusivity	$K = \frac{k}{\rho_c}$	(L^2T^{-1})

An application of the principles of dimensional analysis to the quantities T, V, q, and K yield either

$$VTq = f\left(\frac{V^2T}{K}\right) \tag{5}$$

or

$$KTq^2 = \phi(VTq) \tag{6}$$

In an attempt to establish the law governing the relations (5) and (6), a convenient way is often to plot actual data on a log-log graph paper, as also Taylor's equation (1) is guiding one in this sense. However, owing to lack of temperature, diffusivity, and tool-life data for corresponding cutting speeds, and so on, the investigation has to be limited to plotting the relations (5) and (6) for varying q and V-values, holding T constant. As T is assumed to depend entirely on temperature, then K also must assume a constant value for constant T. In doing so it is found that equation (5) gives curves while (6) yields reasonably straight lines. For convenience KTq^2 is plotted against $(VTq)^{1/2}$ in Fig. 3, where three test series covering HSS tool cutting of 0.60 C, 0.45 C, and Cr-Ni steel, and two test series for carbide tools cutting carbon and Cr-Ni steels are represented. As the values of K are unknown, K was set = 1. Also the relative displacements between the relations for $T = 60$ and $T = 1$ min has no meaning; only the slopes are of importance. The latter are different for the two T-values chosen as well as between different materials. It is seen

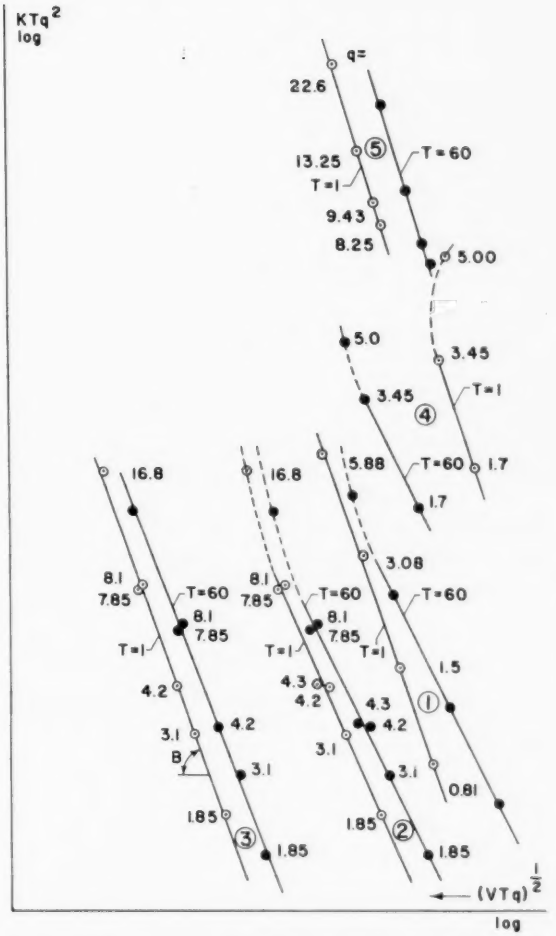

Fig. 3 Relation between dimensionless quantities KTq^2 and $(VTq)^{1/2}$. [1 = HSS − 0.60 C (18), 2 = HSS − 0.45 C (15), 3 = HSS − Cr Ni (15), 4 = carbide U − Cr Ni (14), 5 = carbide TT3 − St. 50.11 (13).]

that over a large range of q-values the relations are essentially straight. This coincides with observations of Woxén, who used different values of the constants q_0 and c_W Equation (4a) in the regions of $q \leq 4 - 5$ and $q \geq 4 - 5$, termed rough cutting and finish cutting, respectively.

To test further the validity of the assumption of the dependence of tool life on temperature, tests by Colding [12] using the work-tool-thermocouple method are plotted in Fig. 4, assuming a relation equivalent to Equation (6):

$$KEq^2 = \psi(VEq)^{1/2} \tag{7}$$

where E is the electromotive force (emf). The plotted relations valid for two different carbide grades and 0.60 carbon and Cr-Ni steel, are of the same shape and slope as those in Fig. 3. The straight-line dependence is neither valid for large values of q when based on emf measurements nor when based on tool-life data. This observation is of importance, since it confirms the great dependence of tool life upon temperature and chip equivalent. The relations shown in Figs. 3 and 4 indicate that a straight-line approximation seems justified in the q-region corresponding to rough machining, but also the data from Hucks obtained for $8 \leq q \leq 23$ indicate a straight-line relation. Thus, together with

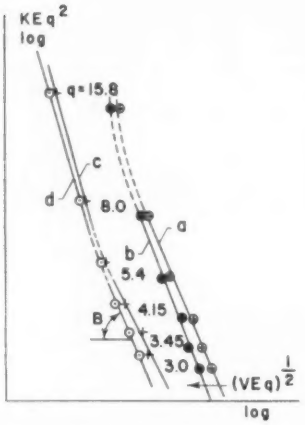

Fig. 4 Relation between quantities KEq^2 and $(VEq)^{1/2}$. (E = 10 mv for a and b, E = 12 mv for c and d, a = carbide U—Cr Ni, b = carbide S3 — Cr Ni, c = carbide U — 0.60 C, d = carbide S3 — 0.60 C.)

Woxén's conclusions regarding Equation (4a), it may be assumed that a relation of the form

$$KTq^2 = U(VTq)^{B/2}$$

or (8)

$$V_T = (\Omega_T)^{\beta_T} T^{\beta_T - 1} q^{2\beta_T - 1}$$

may be applied in either the region of rough cutting or finishing. In Equation (8) U is a dimensionless constant, B is the slope in Figs. 3 and 4 corresponding to a certain tool life T,

$$\Omega_T = \frac{K_T}{U_T}, \quad \beta_T = \frac{2}{B}, \quad \text{and} \quad V_T$$

is the corresponding cutting speed.

In Taylor's equation $VT^n = C$, the constant C is defined as the cutting speed V_1 for a tool life $T = 1$ min. From Equation (8)

$$V_1 = (\Omega_1)^{\beta_1} q^{2\beta_1 - 1} = C \tag{9}$$

Equations (1) and (9) then yield

$$VT^n = (\Omega_1)^{\beta_1} q^{2\beta_1 - 1}$$

or

$$VT^n = Aq^m \tag{10}$$

where $A = (\Omega_1)^{\beta_1}$ and $m = 2\beta_1 - 1$ are constants valid for the particular combination of tool, work, and tool angles considered. Equation (10) is found to be valid to a good degree of approximation in some cases investigated while less good in some others when applied to either the region of rough cutting or finishing. It is of interest to get some idea of the meaning of the constant $C = V_1$ in Equation (9). The thermal diffusivity, K_1, maintains a constant value, no matter what the value of q is. Hence C is entirely dependent on the chip equivalent for a constant combination of tool and work material, and so on, in the case where Equation (10) is valid. The variation of the exponent n is obtained by introducing Equation (8) into Equation (10):

$$T^n = A\Omega_T^{-\beta_T} T^{1-\beta_T} q^{m-2\beta_T+1} \tag{11}$$

Choosing a particular value of T, for example $T = 60$ min, one obtains

$$e^{a_0 n} = Bq^{(m-1)} \tag{12a}$$

where

$$a_0 = \log 60$$

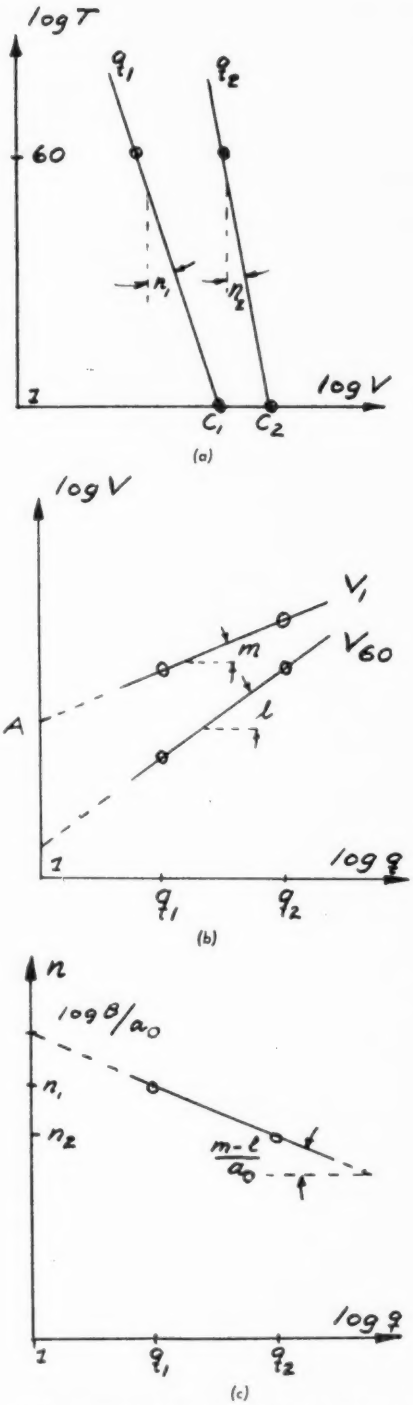

Fig. 5 Principles to determine a limited tool-life equation for arbitrary q on basis of two experimental curves

$$l = 2\beta_{60} - 1$$

$$B = \frac{A}{(\Omega_{60})^{\beta_{60}}} 60^{1-\beta_{60}}$$

Rewriting Equation (12*a*)

$$n = \frac{1}{a_0} \left[\log Bq^{(m-l)}\right] \tag{12b}$$

The determination of the constants A, B, m, and l is done most conveniently from graphs on the basis of two accurately determined tool-life relations; e.g., $q = 1$ and $q = 3$, or $q = 10$ and $q = 15$. In Fig. 5(*a*) there is a schematic representation of two tool-life curves for $q = q_1$ and $q = q_2$, giving the slopes n_1 and n_2 and the constants C_1 and C_2. In Fig. 5(*b*), V_1 and V_{60} are plotted against q, yielding the values of m, l, and A. Hereby Equation (10) is determined, except for the variation of n with q. By plotting the values of n_1 and n_2 from Fig. 5(*a*) versus q_1 and q_2 as is done in Fig. 5(*c*), Equation (12) is established.

Equations (10) and (12) constitute a generalized approximate tool-life equation for V, T, q. It has the advantage over other such equations as, for example, the type $VT^{n_1}l^{a_1}b^{\epsilon} = C$ and Equation (4*a*), in that it takes into consideration the variation of the exponent n, here shown to depend solely on the chip equivalent. Estimates of obtainable tool lives for other chip equivalents and cutting speeds can thus be made from two known tool-life curves simply by proceeding in the way indicated in Fig. 5.

A General Tool-Life Equation. Equations (10) and (12) yield approximate relations between tool life, cutting speed, and chip equivalent, if a distinction is made between the regions of rough cutting, $q \leq 5 - 8$, and the finishing region, $q \geq 5 - 8$. This is somewhat equivalent to stating that Taylor's Equation (1) is valid above a certain cutting speed or below a certain tool life. Below a particular speed or above a particular tool life, Taylor's equation is neither valid at all or the exponent n may assume an entirely different value. In Figs. 6(*a–d*) are shown four different types of families of tool-life curves plotted versus cutting speed, all of which are represented in the way they are interpreted by different investigators. The author found no curve being verified all over the speed region considered, so the curves shown are usually curves extrapolated toward shorter or longer tool lives. The general pattern of the four types seems to be generally applied to whether the life criterion is total destruction, a predetermined wear land, or a certain wear rate; e.g., the time it takes to wear off 1 mg of tool material from clearance or rake side (radioactive tests) [14]. A closer examination of the test points obtained in the straight parts of the curves in Fig. 6(*a–d*) reveals very often a certain curvature, so that a smooth curve can be fitted to the points. Woxén states:[2] "In many investigations it is found first, that not a straight line but a slightly bent curve is obtained; secondly, that this line or curve has a different slope at different chip equivalents q, so that the slope diminishes with an increased value of the chip equivalent." He also found that a more general equation than equation (4*a*) would be of the form

$$V = \left[\left(\frac{T_*}{T}\right)^n + c_1 T\right] C_\omega \frac{q + q_0(T)}{1 + c_\omega q} \tag{4b}$$

[2] Reference [2], p. 50.

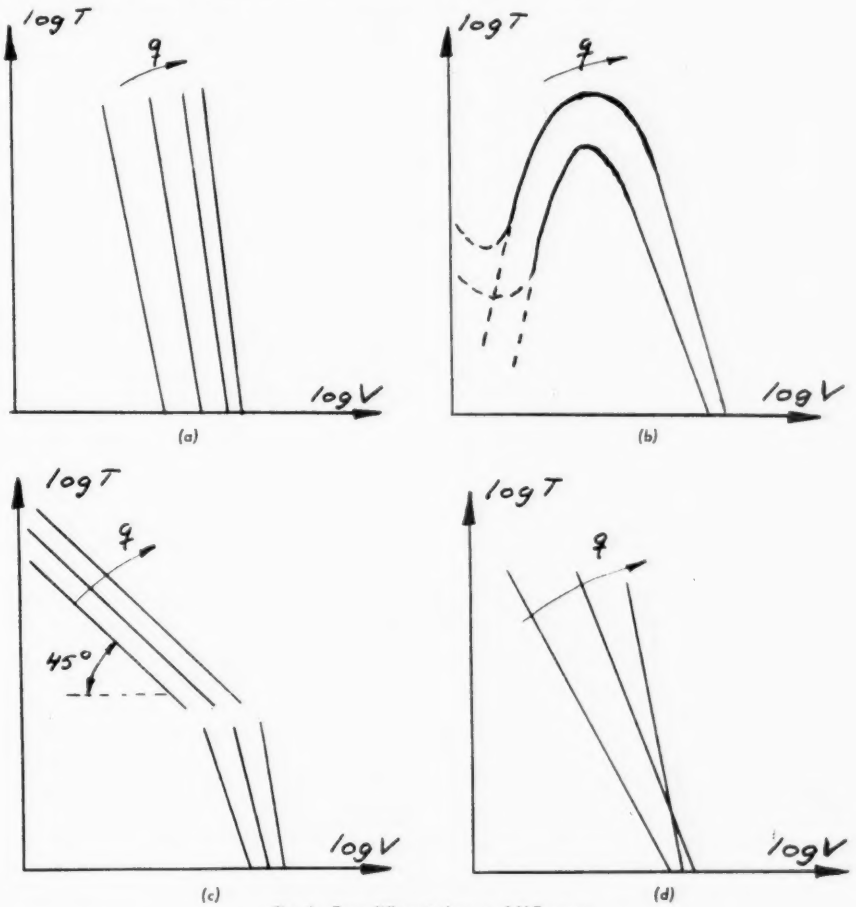

Fig. 6 Four different shapes of V-T-curves

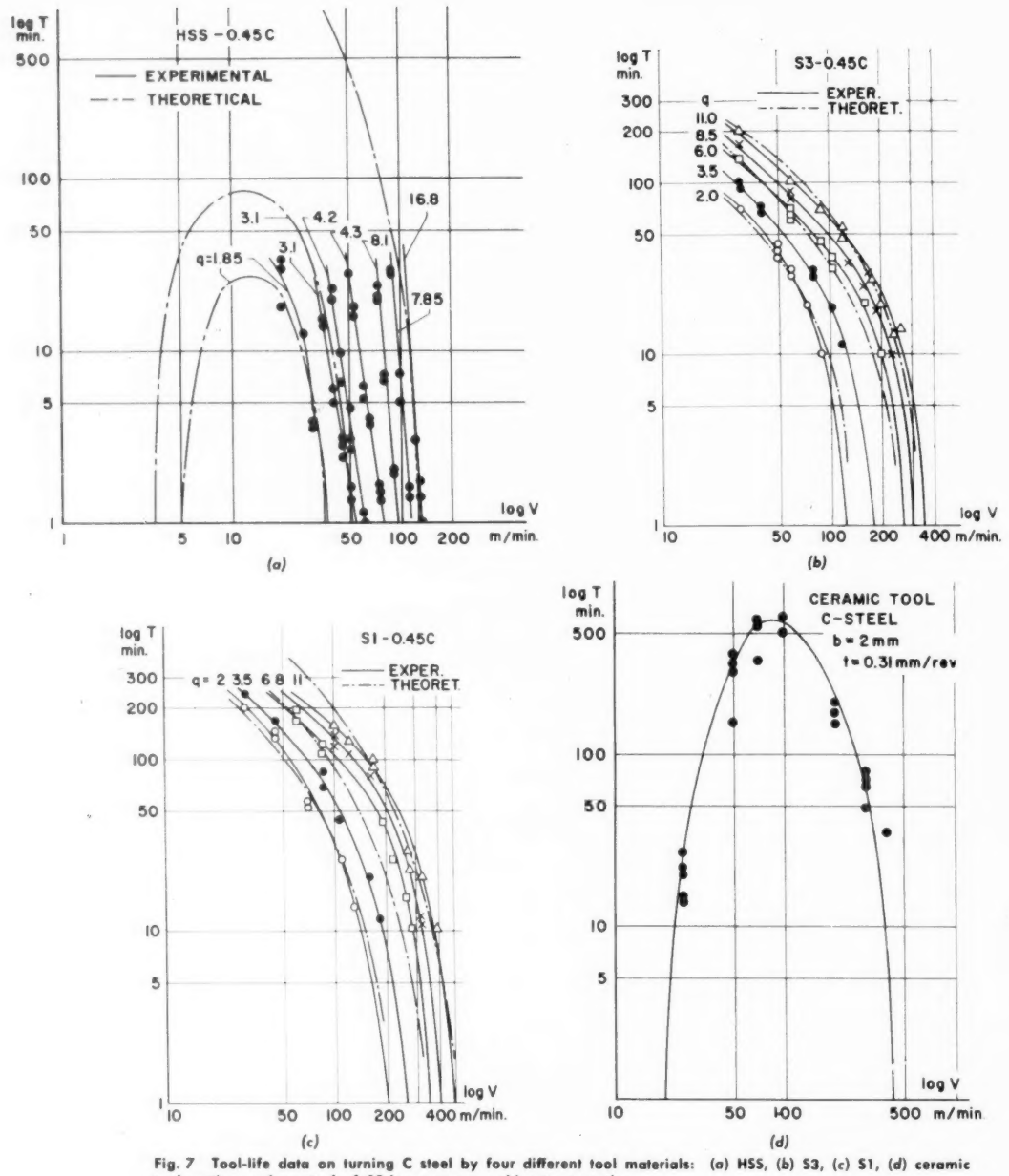

Fig. 7 Tool-life data on turning C steel by four different tool materials: (a) HSS, (b) S3, (c) S1, (d) ceramic tool cutting carbon steel of 80-kg-per-sq-mm ultimate strength

The author also found by radioactive tests that data, obtained when tool life is very short, give a shorter tool life than an extrapolation of a straight line toward the V-axis would yield [19]. Data of type Fig. 6(*c*) are presented by Svahn [15], who shows thirteen graphs for different combinations of tool materials and work materials or more than 40 relations corresponding to different q-values. Svahn's curves were obtained in milling tests as well as in turning tests. He interpreted the lines drawn according to Fig. 6(*c*) as Taylor relations, where the exponent $n \cong 1$ for the families of lines with the smaller inclination. Figs. 7(*a*, *b*, *c*) are Svahn's test points in the case of turning 0.45 carbon steel with HSS tools and two carbide grades S3 and S1. The HSS data show a definite curvature for $q = 1.85$. If the carbide data (interpreted by Svahn as in Fig. 6(*c*), all of which are smooth curves, are tentatively extrapolated toward short tool lives (dashed curves in Figs. 7(*b* and *c*), it would certainly be possible to represent each dashed curve with a Taylor relation in that region.

Plots of data on double-logarithmic graph paper is in many cases of great value as many functions are linearized that way and are easy to use. However, when such linearized functions are used in combination with other well-defined functions in theoretical investigations, the conclusions drawn may be quite wrong. Turning to Fig. 3 and replotting these data in the form V_{60} and V_1 as functions of q as is done on log-log graph paper in Fig. 8, where also

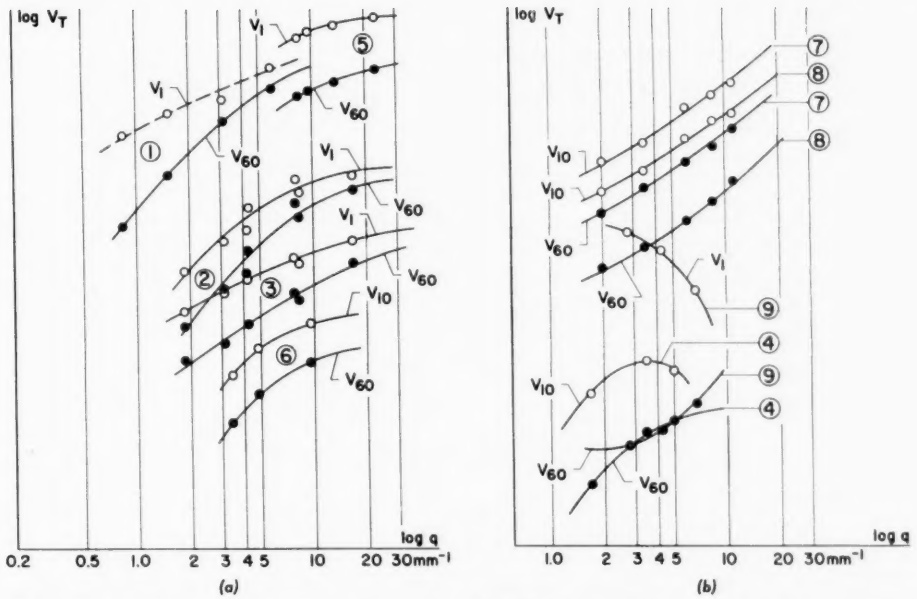

Fig. 8 Different shapes of VT-q-curves. (1 = HSS — 0.60 C [18], 2 = HSS — 0.45 C [15], 3 = HSS — Cr Ni [15], 4 = carbide U — Cr Ni [14], 5 = carbide TT3 — St 50.11 [13], 6 = carbide K2S — Ti-alloy [19], 7 = carbide S1 — 0.45 C [15], 8 = carbide S3 — 0.45 C [15], 9 = carbide L3 — C45 [17].)

data from other investigations are plotted, it is seen that smooth curves may be fitted to the points. These curves are either concave or convex to the q-axis or practically straight lines.

From the foregoing diagrams and discussions it may be assumed that the basic tool-life relation is *never* of the type $VT^n = C$. It would be of interest to investigate if a simple geometric relation may be obtained between V, T, q, which is valid at least for the region of practical interest.

Writing Equation (10) in the form

$$-mx + y + nz - D = 0 \tag{13}$$

where $x = \log q$, $y = \log V$, $z = \log T$, $D = \log A$, then Equation (13) represents a plane in the xyz-co-ordinate system, for each value of m, n, and D. Obviously, Equation (13) is also the mathematical form of a *tangent* plane to a surface $\phi(x, y, z) = 0$ at the point x, y, z, on ϕ. At that point assume

$$\frac{\delta\phi}{\delta x} = -mx, \quad \frac{\delta\phi}{\delta y} = y, \quad \frac{\delta\phi}{\delta z} = nz \tag{14}$$

If the assumption (14) is correct then the normal vector at (x, y, z) is

$$\bar{N} = -mx\bar{i} + y\bar{j} + nz\bar{k} \tag{15}$$

Of the parameters m and n in Equation (15), m is seen to vary by only a few per cent when x and y vary 100 per cent, Fig. 7, while n's variation, known from a number of tool-life curves, is of the same order of magnitude as that of m. Therefore, on a certain area of ϕ, the normal vector $\bar{N}$ can be considered dependent on x, y, and z only. In such a case the curl of $\bar{N}$ ($\nabla x\bar{N}$) is zero. This means that ϕ is an equipotential surface.

The determination of ϕ is done by integration of Equation (15):

$$\phi(x, y, z) = -\frac{(x - x_0)^2}{a^2} + \frac{(y - y_0)^2}{b^2} + \frac{(z - z_0)^2}{c^2} = H \tag{16}$$

A hyperboloid of one sheet for $H = 1$
A hyperboloid of two sheets for $H = -1$
A cone for $H = 0$

To check the validity of Equation (16) many test points of Figs. 7(a, b, c) were taken and a, b, c, x_0, y_0, z_0 were calculated and found to be constants:

HSS—0.45 C steel:

$$-\frac{(x + 2.60)^2}{6.05} + \frac{(y - 2.57)^2}{1.305} + \frac{(z - 0.106)^2}{15.54} = -1$$

(hyperboloid of two sheets).

Carbide S1—0.45 C steel:

$$-\frac{x^2}{15.1} + \frac{y^2}{27.7} + \frac{z^2}{44.8} = 1$$

(hyperboloid of one sheet).

Carbide S3—0.45 C steel:

$$-\frac{x^2}{14.0} + \frac{y^2}{25.0} + \frac{z^2}{31.0} = 1$$

(hyperboloid of one sheet).

In Figs. 7(a–c) the curves represented by the foregoing equations are drawn for different values of q. The agreement with the experimental data is seen to be reasonably good. Fig. 7(d) shows a case where, for a constant q, actual test data over a large range of speeds can be approximated with half an ellipse according to Equation (16). The data are taken from Russian tests with ceramic tools [20].

In Figs. 9(a, b) the two types of hyperboloids, represented by Equation (16), are shown. It is seen that planes parallel to the x-y-plane yield hyperbolas symmetrical around the y_0 or x_0-axis. Comparing the curves in Fig. 8 with those of intersecting planes for z = const, the pattern of the materials 1, 2, 3, 5, 6 correspond to that of Fig. 9(b), while 7, 8 correspond to Fig. 9(a). For the material combinations in Fig. 8 with the exception of the unusual cases 4 and 9, either Fig. 9(a) or Fig. 9(b) is applicable.

The calculation of the constants in Equation (16) is theoretically possible from knowing only six points on the surface;

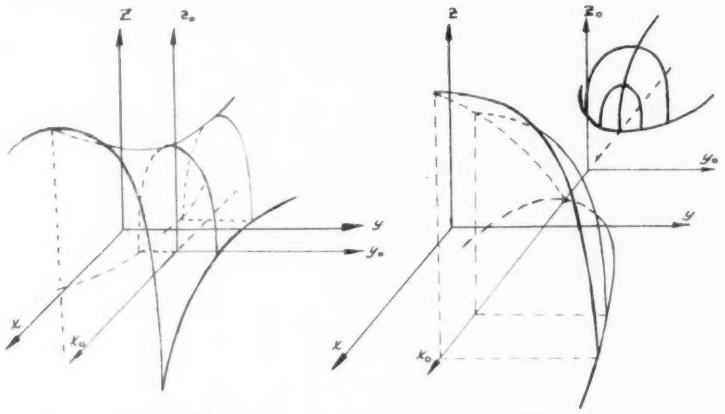

(a) (b)

Fig. 9 Three-dimensional representation of tool-life data: (a) Hyperboloid of one sheet, (b) hyperboloid of two sheets (x = log q, y = log V, z = log T)

i.e., only six tool-life values for six different q and V-values would be necessary. If Equation (16) really represents a general equation, then tool-life testing could be limited to a comparatively small number of actual tests. Furthermore, the intricate question of the influence of material properties, tool angles, and so on, may be attacked in a more systematic way than hitherto has been possible. The three-dimensional pictures of the variation of tool life with cutting speed and chip equivalent in Fig. 9 indicate the possibilities of obtaining longer tool lives when q is made very small (very heavy feeds), when one operates, for example, on the negative side of the z-y-plane. The Russian tool design by Kolesov makes very heavy feeds possible, corresponding to q-values sometimes smaller than 1; i.e., $x < 0$. Tool lives are reported to be in the conventional range, even longer than for those obtained by a conventional tool using the same depth of cut but, for example, 10 times smaller feed [16].

The reason why tool life decreases with reduced feed (increased q), as for V_1 of material 9 and for V_{10} of material 4 in Fig. 8 while V_{60} in both cases follows the pattern of hyperbolas in Fig. 9, cannot be anticipated. However, the relations V_1 and V_{10} as functions of q for these materials are based on extrapolated tool-life curves of the type $VT^n = C$, so a certain uncertainty is associated with their drawing.

Owing to the assumption expressed by Equation (14) the surface ϕ would be an equipotential surface for each combination of tool and work, and so forth. This problem is associated with the presently very limited knowledge of the fundamentals of the wear process on clearance and rake face of a tool and will therefore not be discussed in this connection.

2 MACHINING ECONOMICS

In choosing the operating variables to be used in any machining operation one is usually interested in obtaining either the lowest possible cost per part (minimum cost) or the shortest possible time per part (maximum production).

In computing the machining cost per part, four items should be considered:

1 Cost of machine and operator including overhead P for time to make cut T_c.

2 Cost of machine and operator during time required to change workpieces (idle time T_i).

3 Cost of machine and operator during down time T_d necessary to replace worn tools.

4 Average cost to regrind work tools R.

The total cost per part Q is readily shown to be

$$Q = PT_c\left(1 + \frac{T_d}{T} + \frac{R}{P}\frac{1}{T}\right) + PT_i$$

or

$$Q = PT_c\frac{T+\gamma}{T} + PT_i \tag{17}$$

where $\gamma = T_d + R/P$, T = tool life.

A similar expression valid for maximum production is

$$T_{avg} = T_c\frac{T+T_d}{T} + T_i \tag{18}$$

where (T_{avg}) is the average time to produce one part. The two expressions (17) and (18) should be differentiated ultimately with respect to tool life T and the result equated to zero to find the extreme values. Instead of expressing T_c as a function of cutting speed, feed, axial length of work, and work diameter as is often done, a more general expression of T_c is introduced; namely, the material volume to be removed per part W_p

$$W_p = T_cW \tag{19}$$

where $W = Vtb$ is the volume removed per unit time, V is cutting speed, t is feed, b depth of cut.

Introducing the value of T_c from Equation (19) into Equations (17) and (18)

$$Q = \frac{W_pP}{Vtb}\frac{T+\gamma}{T} + PT_i \tag{20}$$

$$T_{avg} = \frac{W_p}{Vtb}\frac{T+T_d}{T} + T_i \tag{21}$$

It is seen from the similarity of Equations (20) and (21) that in economic analysis of a cutting process the following expression should be investigated:

$$f = Vtb\frac{T}{T+\gamma} = L\frac{V}{q}\frac{T}{T+\gamma} \tag{22}$$

where $\gamma = T_d + R/P$, Equation (20), or $\gamma = T_d$, Equation (21), and f may be called the "productivity function."

A maximum of f will yield a minimum Q and T_{avg}. The idle time T_i has no influence on the economic computations.

The commonly found form (when t and b are kept constant) of

the economic tool life, T_{econ}, is also obtained from Equation (22) using $VT^n = C$

$$T_{econ} = \gamma\left(\frac{1}{n} - 1\right) \tag{23}$$

Determination of Optimum Values of Productivity

Equations (22) and (16) can be used to investigate the simultaneous extreme values of T, V, and q, but the fact that the product tb is expressed as a function of q and L is a function of b, t, C_s, and r, in itself complicates the solution. Therefore consider two cases:

1 Keeping depth of cut, nose radius, and side-cutting-edge angle constant. Then the feed is

$$t = \frac{k/b}{q - \dfrac{1}{2b}}$$

and

$$bt = \frac{k}{q - \dfrac{1}{2b}}$$

where k = constant depending on b, r, and C_s.

2 Keeping L constant when q varies. One way of doing this is to vary depth of cut to compensate for the variation of L with feed.

Taking the logarithm of Equation (22), the following expressions are obtained according to points 1 and 2 in the foregoing:

$$F(x, y, z) = \log k - \log\left(q - \frac{1}{2b}\right) + y + z - \log(e^z + \gamma) \tag{22a}$$

$$F(x, y, z) = \log L - x + y + z - \log(e^z + \gamma) \tag{22b}$$

where

$$F(x, y, z) = \log f, \quad x = \log q, \quad y = \log V, \quad z = \log T$$

These expressions should combine with Equation (16) to solve the economic problem. The term $\log [q - 1/(2b)]$ will complicate the solution of the problem, however. A series expansion of it shows $\log [q - 1/(2b)] \cong \log q = x$, provided $1/(2b)$ is reasonably smaller than q. For example, the error in x when $b = 2$ mm is ≤ 2 per cent when $q \geq 6$; for $b = 5$ mm the error is ≤ 3 per cent when $q \geq 3$. The nose radius was here set = 1 mm and the side-cutting-edge angle 0 deg. Thus, choosing q bigger than a certain value depending on b, the second expression of $F(x, y, z)$, Equation (22b), also can be used when depth of cut is constant (point 1). However, when the practical problem is to take away a certain amount of volume when depth of cut can be chosen within a rather large range, then the second expression of F can be used as an exact expression considering either point 1 or point 2.

The problem is seen to consist of investigating extreme values of the function

$$F(x, y, z) = y - x + z - \log(e^z + \gamma) \tag{24}$$

when

$$\phi(x, y, z) = -\frac{(x - x_0)^2}{a^2} + \frac{(y - y_0)^2}{b^2} + \frac{(z - z_0)^2}{c^2} - H = 0$$

where $H = \pm 1, 0$.

The possible extreme values of Equation (24) may occur when

$$(x - x_0)^2 = \frac{\left[H - \dfrac{(z - z_0)^2}{c^2}\right] a^4}{b^2 - a^2} \tag{25a}$$

$$(y - y_0)^2 = \frac{\left[H - \dfrac{(z - z_0)^2}{c^2}\right] b^4}{b^2 - a^2} \tag{25b}$$

$$\left[1 - \frac{e^z}{e^z + \gamma}\right]^2 = \frac{\dfrac{b^2 - a^2}{c^2}}{H \dfrac{c^2}{(z - z_0)^2} - 1} \tag{25c}$$

In Fig. 10 the left-hand side of Equation (25c) is plotted against z for the quantity $\gamma = 10$ and 100. The intersections of these curves with the corresponding plot of the right-hand side of Equation (25c) yield the extreme values. From the values of a, b, c, H, and z in the generalized equations of the data of Fig. 9 the right-hand side of Equation (25c) is also plotted in Fig. 10. The intersection points yield the possible tool lives. The corresponding values of cutting speed and chip equivalent are calculated from Equations (25a, b) in Table 2.

Table 2 Economic extreme values of q, V, T for data of Fig. 9

	$\gamma = 10$			$\gamma = 100$		
Material	q, mm^{-1}	V, m min^{-1}	T, min	q, mm^{-1}	V, m min^{-1}	T, min
HSS-0.45 C	2.3	28.0	20	6	34	135
	0.002	6.3	20	0.001	5	135
S3-0.45 C	37	640	18	18	190	60
	0.027	0.0016	18	0.055	0.0053	60
S1-0.45 C	42	950	25	22	290	100
	0.024	0.001	25	0.046	0.0035	100

To investigate whether the data of Table 2 correspond to real maxima or minima or other characteristic points of the surface

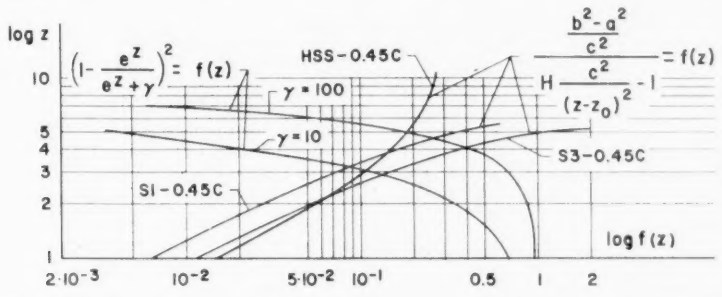

Fig. 10 Graphical determination of possible economic tool lives for materials in Figs. 7(a-c)

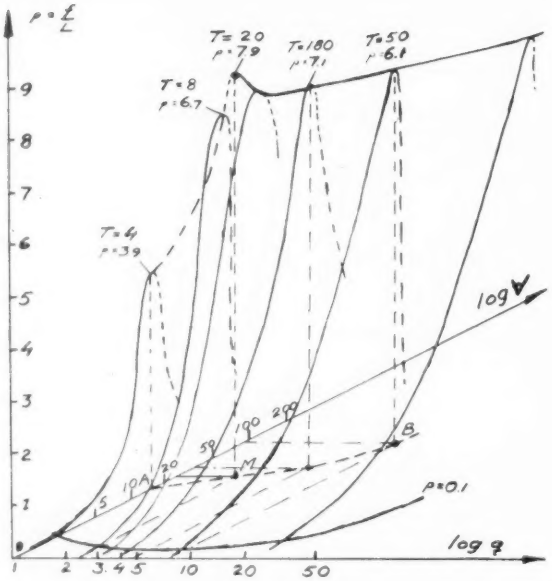

Fig. 11 Productivity as function of chip equivalent and cutting speed for HSS — 0.45 C (hyperboloid of two-sheet case)

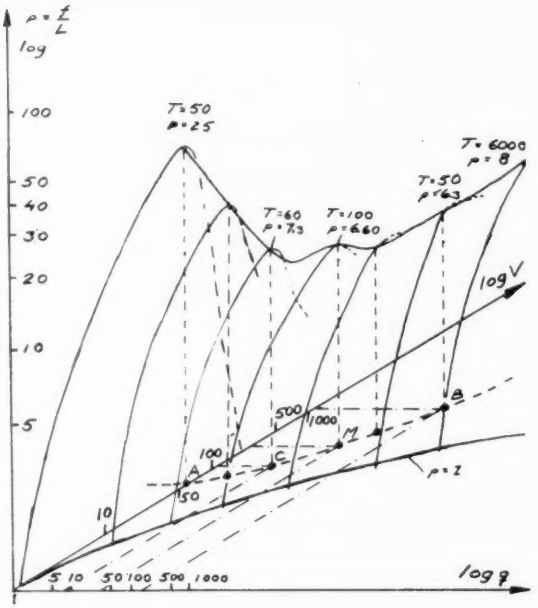

Fig. 12 Productivity as function of chip equivalent and cutting speed for carbide S1 — 0.45 C (hyperboloid of one-sheet case)

$F(x, y, z)$ or $(f/L)(v, T, q)$, the shape of the surfaces for HSS—0.45 C and $\gamma = 10$ and carbide S1—0.45 C and $\gamma = 100$ were determined and drawn in Fig. 11 and Fig. 12, respectively, where the productivity $f/L = p$ is expressed as a function of cutting speed V and chip equivalent q. The productivity p and the corresponding values of V, T, and q are indicated for interesting points in Figs. 11 and 12. The calculated tool life 20 min of Table 2, corresponds to an absolute maximum, Fig. 11, yielding $p_{max} = 7.9$ cu cm of material removed per min and per mm engaged cutting-edge length. It is seen that if cutting speed and chip equivalent are varied along the curve MB in the log q-log V-plane (AB is the projection curve of the maximum values of p) the productivity decreases very slowly, while rapidly when moving along MA. However, p is very sensitive to combinations of V, q on both sides of the curve AB; in particular, on the high-cutting-speed side of it.

The calculated tool life $T = 100$ min for carbide grade S 1 turning 0.45 C steel corresponds to a maximum as seen in Fig. 12, but it occurs in the saddle-type region. The productivity increases rapidly for decreasing values of V and q along the curve CA, from 7.3 at $V \cong 150$, $q \cong 8$ to 25 at $V \cong 70$, $q \cong 1$. The productivity increases further upon a reduction of q below the value $q = 1$. On reducing the value of q, Fig. 12 shows the importance of choosing the cutting speed so that it does not deviate too much from curve CA in order to obtain an increase of productivity. It is not known whether the relation derived between V, T, q, Equation (16), is valid for very small values of q. For this reason the productivity surfaces were not investigated in the regions of other possible extreme values given in Table 2.

Conclusions

The general pattern of the curves for $V_T = V_T(q)$ in Fig. 8, corresponding to the two types of hyperboloids, shown in Fig. 9, suggests the following conclusions:

1 When tool-life data can be expressed as a hyperboloid of two sheets then there exists an absolute economic optimum combination of V, T, q.

2 When tool-life data can be expressed as a hyperboloid of one sheet then the economic optimum represents the smallest q obtainable. This means that the largest feed possible should be used depending on strength of tool, maximum feed of the machine tool, surface finish, and so on.

3 The maximum possible productivity ($f_{max} = Lp_{max}$) expressed as material removed per unit time is obtained by using a maximum cutting-edge length L, determined by $q_{max}\, bt = L$.[3] Here either b or t can be regarded as fixed values or maximum values determined by other considerations. The maximum value of L is then determined by combining nose radius, side-cutting-edge angle, and b or t such that the expression for L given by Equation (3) attains a maximum value. In this connection practical considerations may, for example, fix the values for nose radius and side-cutting-edge angle.

4 The value of the quantity γ has no influence on the general shape of the productivity surface $p = p(V, T, q)$, but a reduction of γ increases p.

5 The extreme sensibility of the productivity p to the value of q in particular, in the vicinity of the maximum value of p, shows the great importance that should be paid to machining-economics determinations.

The foregoing conclusions emphasize the great need for having a reasonably general relation between V, T, q in an economic analysis. The author performed the same kind of analysis as outlined on the basis of the Taylor type Equations (10) and (12) for the material combinations in Fig. 8, assuming a straight-line approximation was valid for $q \leq 5$–6. All the maximum productivities calculated corresponded to very small values of q ($q \ll 1$), except in the case of material 6, yielding a maximum in the practical region of q. The reason for errors committed may be shown in the following manner: The assumption of straight-line relations in Fig. 8 may be illustrated by a surface ϕ, Equation (16), in the form of a cone ($C = 0$). The x-y-plane cuts the cone along straight lines ($z = 0$ corresponds to $T = 1$), if the z_0-co-ordinate of the apex lies in the x-y-plane. If also $z_0 = 0$ then an eco-

[3] q_{max} refers to the maximum value of productivity per unit length of cutting edge, p_{max}, and not to the maximum value of q.

nomic tool life may be expected in the practical region, as tool life approaches zero in the neighborhood of the apex. On the other hand, if the x_0-co-ordinate of the apex lies sufficiently far away from the origin on the negative axis, then a maximum production rate may be expected for very small values of q. The apex co-ordinates depend on the slope m and the value A in Fig. 5(*b*). Further examples of the limitations of using equations of type $VT^nf^ab^s = C$ in economic considerations are given in the author's discussion of Brewer's paper [21].

References

1 F. W. Taylor, "On the Art of Cutting Metals," TRANS. ASME, vol. 28, 1907, pp. 31–279 plus 24 folded plates.

2(*a*) R. Woxén, "Teknisk Tidskrift," *Mekanik*, H. 4, Stockholm, Sweden, April, 1931, pp. 43–44.

2(*b*) R. Woxén, "A Theory and an Equation for the Life of Lathe Tools," *Ingeniörs Vetenskaps Akademien*, Handlingar 119, Stockholm, Sweden, 1932.

3 M. Kronenberg, "Grundzüge der Zerspanungslehre," Springer Verlag, Berlin/Göttingen/Heidelberg, Germany, 1954.

4 W. W. Gilbert, "Economics of Machining," in "Machining—Theory and Practice," American Society for Metals, Cleveland, Ohio, 1950, pp. 465–485.

5(*a*) W. Leyensetter, "Die Schnittgeschwindigkeit beim Zerspanungsvorgang," *Werkzeugmaschine*, vol. 35, 1931, pp. 363–367 and 392–395.

5(*b*) W. Leyensetter, "Prüfverfahren der Zerspanung," BKW-Veroff, Nr. 114, Teubner-Verlag, 1938.

6 E. Hausler, "Etude des Lois de la Coupe des Métaux et Leur Application Pratique aux Travaux d'Usinage," Session de l'Outil, Liège, Belgium, 1944.

7 R. Woxén, "Tool-Life and Balance of Heat in Lathe Work," *Ingeniörs Vetenskaps Akademien*, Handlingar Nr. 142, Stockholm, Sweden, 1937.

8 "Manual on Cutting of Metals With Single-Point Tools," second edition, ASME, New York, N. Y., 1952.

9 M. Kronenberg, "Math Cuts Cost of Machining Studies," *American Machinist*, vol. 93, September 22, 1949, pp. 104–106.

10 K. J. Trigger and B. T. Chao, "An Analytical Evaluation of Metal-Cutting Temperatures," TRANS. ASME, vol. 73, 1951, pp. 57–68.

11 E. G. Loewen and M. C. Shaw, "On the Analysis of Cutting-Tool Temperatures," TRANS. ASME, vol. 76, 1954, pp. 217–231.

12 B. Colding, "EMK-mätningar med enstålsmetoden" (EMK-Measurements With the Tool-Work Method), Report, Swedish State Council of Technical Research, Stockholm, Sweden, 1953.

13 H. Hucks, "Schneidentemperaturen und Standzeitverhalten spanabhebender Werkzeuge," *Technische Mitteilungen*, Bd. 45, H. 9/10, 1952.

14 B. Colding, "Testing of Machinability by Radioactive Methods," *Acta Polytechnica Scandinavica*, (Acta P. 243/1958) Mechanical Engineering Series 1, Stockholm, Sweden, February, 1958, 42 pp. + Figs.

15 O. Svahn, "Machining Properties and Wear of Milling Cutters," *Tekniska högskolan Avhandling* 55, Stockholm, Sweden, 1948.

16 M. C. Shaw, "Machine Tool Requirements of the Future," *Tool Engineer*, vol. 37, August, 1956, pp. 105–111.

17 G. Weber, "Spanentstehung und Standzeitverhalten beim Drehen von Stahl mit Hartmetall," *Industrie-Anzeiger*, Nr. 45, vol. 7, June, 1955.

18 A. Svensson, thesis, Royal Institute of Technology, Stockholm, Sweden, 1939.

19 M. C. Shaw, P. A. Smith, B. Colding, and N. H. Cook, "Machining Titanium II," prepared by Metals Processing Division, Department of Mechanical Engineering, Massachusetts Institute of Technology, February, 1957.

20 V. I. Schicharen, "The Use of Ceramic Tools in Machining," *Stankii Instr.* No. 2, 1956.

21 R. C. Brewer, "On the Economics of the Basic Turning Operation," TRANS. ASME, vol. 80, 1958, pp. 1479–1489.

DISCUSSION

R. C. Brewer[4]

The author is to be congratulated for taking another step forward in a field of machining which has, so far, been neglected by comparison with the more fundamental aspects of the machining process.

This discussion will not, in general, be directed to the analysis itself but rather to the question of the validity of it, i.e., to the assumptions on which it is based and to the conclusions which may be drawn from it.

In the section headed The Chip Equivalent, an account is given of Woxén's work; the references, unfortunately, are not easily accessible outside Sweden and the conclusions must be accepted rather blindly. Some of these conclusions are merely observations (from graphs) of trends of one variable relative to another, but others are statements of equality, the correctness of which is important, e.g., it is stated that the area of cut is a measure of the heat generated at a given speed and that the length of engagement is a measure of the heat in the chip, tool, and workpiece. Since Woxén's work is almost thirty years old, it would be very helpful if the author would amplify his comments a little, especially as the original publications are so difficult to consult.

Again, a generalized tool-life equation [Equation (4*a*)] is given with no indication of its derivation. However, if one assumes it to be true, then it may be written, for a tool-life of 60 minutes, as:

$$V = \mu + \lambda q,$$

where μ and λ are constants.

Evidently, Fig. 2 does not agree with this although it does indicate a dependence of V_{60} on the chip equivalent. Without more data, particularly for other tool lives, it is not possible to deduce from Fig. 2 an equation similar to (4*a*). Also, it is most desirable that any relationship which replaces the previously accepted one (viz, $VT^nd^af^b$ = constant) should be demonstrated to be valid for more than one set of results.

Turning to conclusions which may be drawn from the analysis, it is seen that, whether the relationship between V, T, and q be a hyperboloid of one or two sheets, curves of constant x are ellipses, i.e., the curve relating V and T is an ellipse. This is shown in Fig. 7(*d*), in which the author has given his interpretation of Zhikharev's results. Since the data refer to a ceramic tool, the decrease in tool life at lower cutting speeds is to be expected since the criterion of tool life can no longer be the amount of flank wear but must, in the circumstances, be the crumbling of the cutting edge, i.e., since there has been a change of criterion, one would not expect the same "Taylor" law to hold.

A more serious aspect of the ellipse as a V-T relationship is its complete interpretation. What significance, for example, has the other half of the ellipse shown in Fig. 7(*d*)? My own opinion is that it has no significance because it does not exist. The author might put this another way by saying that the upper half of the ellipse is a representation of experimental data—a better representation than the Taylor line with slope "n." With this in mind, I feel it necessary to stress that the closing section of Part I of the paper is still empirical; although the author has not, in any way, attempted to give any other impression, I feel that the paper is rather comprehensive and that it would be very easy, after a mathematical analysis such as the author has given, to think subconsciously that the whole subject had been put on a fundamental rather than empirical basis.

I think it would be fair to summarize Mr. Colding's discussion of my paper (reference [21] of the paper) by saying that he criticized me for an analysis which was too far ahead of the knowledge about the justifications for the assumptions made. I think I would make the same criticism of this paper and suggest that, before any more papers are written, the fundamentals of the tool-life equation should be settled. I think enough has been said already to indicate that the answer is not so self-evident as has been assumed.

[4] Lecturer in Production Engineering, Imperial College of Science and Technology, University of London, London, England.

Author's Closure

The author thanks Mr. Brewer for his kind remarks about the paper, and for his detailed discussion of some of the conclusions of the analysis.

Unfortunately, there was originally a misprint as to Equation (4*a*) where the term $(1 + C_w q)$ reads $(1 + C_w q_0)$. Hence Mr. Brewer's expression $V = \mu + \lambda q$ and his discussion of the dependence of V_0 on the chip equivalent are directly related to this misprint. Woxén deduced Equation (4*b*) for the dependence of V_{60} on the chip equivalent on the basis of numerous temperatures as well as tool-life measurements. However, because of the complicated nature of Equation (4*b*), realizing that the simplicity of a tool-life equation is very important when used in the shop, he introduced the simplified Equation (4*a*) or, when selecting $T = T_w = 60$ min·

$$V_{60} = C_w \cdot \frac{q + q_0}{1 + c_w q} \tag{4c}$$

Out of numerous tool-life tests Woxén concluded that in *rough-turning* of steel—low q-values—

$$V_{60} = C_w(q + q_0) \tag{4d}$$

and in *finishing* turning of steel and *rough-turning* of cast iron

$$V_{60} = C_w \cdot \frac{q}{1 + c_w \cdot q} \tag{4e}$$

Although C_w was found to be a function of the Brinell hardness and specific values of the constants in Equation (4*c*) were given by Woxén, it is particularly interesting for the present discussion to see that Woxén used two different types of equations [Equations (4*d*) and (4*e*)], one in the rough-machining range, and the other in the finishing range. The present author's Equation (10) is to be compared with Equations (4*d*) or (4*e*) for $T = 60$, when assigning different values of the exponent m in the two mentioned regions of cutting. Furthermore, although Equation (10) agrees with the data of Fig. 2 over a wide range of q-values, it is not generally true as seen by Fig. 8. Instead, the hyperbolic relationships, given by Equation (16) when $Z = \ln T$ = constant, were found to be more general than either Equation (4*c*) or Equation (10). In particular, on a log-log graph paper a straight line of the form given by Woxén's Equation (4*d*) for rough turning is represented by a line of slope 1. It is therefore not surprising when examining the data for V versus q in Fig. 8 to find that the slope is approximately unity for q being less than about 5. Consequently the author's Equation (10) yields Woxén's Equation (4*d*) as a special case. Finally, as Equation (10) was found to be too inaccurate, the present derivation showed Equation (16) to be a general tool-life equation superior to any of the previous equations.

Turning to Mr. Brewer's discussion of Fig. 7(*d*) it should be emphasized that the half of the ellipse valid for small values of cutting speed is of no practical significance. It is not generally true that the occurrence of an ellipse such as in Fig. 7(*d*) is due to crumbling of the cutting edge. The most fundamental measure of wear rate in tool-life testing should not be a geometrical quantity such as flank wear, crater depth, failure, etc., but the amount of wear on flank or face of tool measured by weight or volume. This can be done by radioactive tests provided the cutting edge is ground properly prior to the test [14]. In the fundamental studies of the tool-wear process made by the author [14] at the Royal Institute of Technology in Stockholm, Sweden, and at Massachusetts Institute of Technology, U. S. A., he found several examples of ellipses of the kind shown in Fig. 7(*d*). These radioactive tests tend to show that the tool-wear process may basically be described by a comparatively simple law rather than by different types of functions depending on the region of q or V in question. Equation (16) is found to constitute a good approximation of reality which is particularly well-suited for economic analysis of the turning process. In order to determine the constants in Equation (16) accurately and quickly, use is made of an automatic digital computer.

Some Observations on the Shearing Process in Metal Cutting[1]

S. KOBAYASHI[2]

Assistant Professor,
Doshisha University,
Kyoto, Japan

E. G. THOMSEN

Professor of Metal Processing,
University of California,
Berkeley, Calif. Mem. ASME

It was found that shearing forces on the shear plane were linear functions of the area on which they acted. This was observed for all materials investigated; for SAE 1112 steel, 2024-T4, and 6061-T6 aluminum alloys, and alpha-brass, and also is in agreement with data taken from the literature. Furthermore, all data examined showed that the straight line of shear force F_S versus area A_S intercepted the ordinate at a positive force value. This was interpreted to mean that the intercept part of the shearing force was used up in overcoming workpiece deformation or friction at the flank of the tool and was not available for chip deformation. Accepting this concept, it can then be shown that the average shearing stress on the shear plane for SAE 1112 is constant and is independent of normal stress, cutting speed, or strain rate, extent of deformation or finite strain, and extent of prior deformation. The shearing stresses for the other materials tested or examined were also constant for the limited range of variables available.

In contrast to the shearing stress, the normal stress on the shear plane was not constant and appears to be a yet unknown function of the mechanism of friction on the tool face.

The shearing stresses calculated from the metal-cutting data showed good correlation with flow stresses at the same finite strains which were obtained from static compression tests. The reason for the uniqueness of the finite strains at which correlation is achieved is not as yet clear.

It seems to be reasonably well established that the principal plastic-deformation process in orthogonal metal cutting with single-point cutting tools and continuous chip formation is one of shear deformation. Detailed studies of photomicrographs of sectioned chips, as well as visual examinations of the cutting process, reveal that this deformation process is confined to an extremely narrow region. This latter phenomenon is the reason that the shear zone is referred to simply as the shear plane.

The deformation process on the shear plane takes place under some unusual conditions, such as, high normal pressures on the shear plane, extremely high strain rates, large finite strains, and high temperatures. These conditions are normally not all encountered simultaneously in other typical metal-forming processes nor in the usual testing procedures of engineering materials. It is largely for these reasons that it is difficult unequivocally to establish the relationship between the plastic-flow properties of a material and its plasticity condition in metal cutting.

Merchant [1][3] in his basic analysis of the mechanics of metal cutting examined the properties of the work material in terms of metal-cutting data and came to the conclusion that the shearing stress on the shear plane was a linear function of the normal stress on this same plane. He developed his machining constant from this concept. Merchant thought he found support for his hypothesis in the high-pressure experiments of Bridgman [2]. Unfortunately, however, Bridgman noted an effect with drill rod only but not with mild steel. Hence, it appears that the Merchant hypothesis for ductile metals is not well supported by experiment and, in fact, is contrary to the usual concepts of plastic deformation assumed in theories of plasticity.

Other investigators, as for example, Chao and Bisacre [3], Chao and Trigger [4], Creveling, et al. [5], observed that the shearing stress on the shear plane appeared to be constant, except at low feeds, while Kececioglu [6] insists that the shear-flow stress is a function of the mean shear-plane temperature. However, Kececioglu's hypothesis was not well supported since his data showed such a general scatter that any trend, if it existed, was not in evidence. Thus the plasticity condition apparently has not

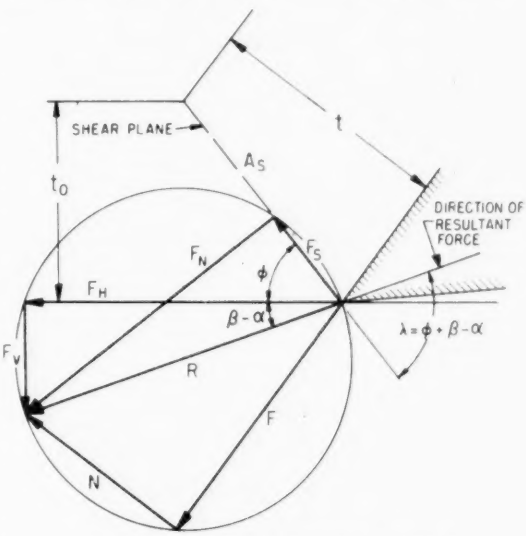

Fig. 1 Force system in orthogonal metal cutting

[1] This paper is the result of an investigation sponsored by the machinability program located at Rock Island Arsenal under Contract DA-11-070-508-ORD-605 with the University of California.

[2] Graduate student in Mechanical Engineering at University of California, Berkeley, Calif.

[3] Numbers in brackets designate References at end of paper.

Contributed by the Metal Processing Section of the Production Engineering Division and presented at the Annual Meeting, New York, N. Y., November 30–December 5, 1958, of The American Society of Mechanical Engineers.

Note: Statements and opinions advanced in papers are to be understood as individual expressions of their authors and not those of the Society. Manuscript received at ASME Headquarters, August 4, 1958. Paper No. 58—A-139.

been established. It is the purpose of the present paper to present new experimental data and to examine the condition for plastic flow on the shear plane in metal cutting.

Shearing Stress on Shear Plane

The force system applicable to orthogonal metal cutting is shown in Fig. 1. The forces F_H and F_V are determinable from a two-component dynamometer and are the components of the force vector R. This force vector R may be decomposed into the two force components F_S and F_N, which are parallel with and normal to the shear plane A_S, respectively. The force components F_S and F_N can be calculated as follows:

$$\begin{aligned} F_S &= R\cos\lambda = F_H\cos\phi - F_V\sin\phi \\ F_N &= R\sin\lambda = F_H\sin\phi + F_V\cos\phi \end{aligned} \tag{1}$$

where ϕ is the shear angle, $\lambda = \phi + \beta - \alpha$, $R = (F_H^2 + F_V^2)^{1/2}$, α is the rake angle, and $\beta = \tan^{-1}\{(F_V + F_H\tan\alpha)/(F_H - F_V\tan\alpha)\}$ is the angle between the friction force and normal force on the tool face and is called the friction angle.

The shear angle ϕ is given by the equation

$$\phi = \tan^{-1}\left(\frac{r\cos\alpha}{1 - r\sin\alpha}\right) \tag{2}$$

in which $r = t_0/t = l/l_0$ is the cutting or chip ratio and can be determined from chip measurements [1, 7, 8]. The shear area A_S on which the force components F_S and F_N act, can be determined from the thickness t_0 and width w_0 of the layer of metal removed. This layer transforms into the chip of thickness t and width w under constant volume and plane-strain conditions so that $w_0 = w$. The shear-plane area is then given by

$$A_S = \frac{t_0 w_0}{\sin\phi} \tag{3}$$

Hence F_S, F_N, and A_S can be determined when r, α, F_H, and F_V are available from metal-cutting tests.

The shearing force F_S and shearing areas A_S were calculated for SAE 1112 steel tested in the as-received (cold-rolled) condition. The results and testing conditions are shown in Fig. 2. It is seen that at the cutting speed of 90.8 fpm the data points lie on a straight line with a scatter band which is only slightly greater than that for 10 reproducibility data points shown by a solid bar.

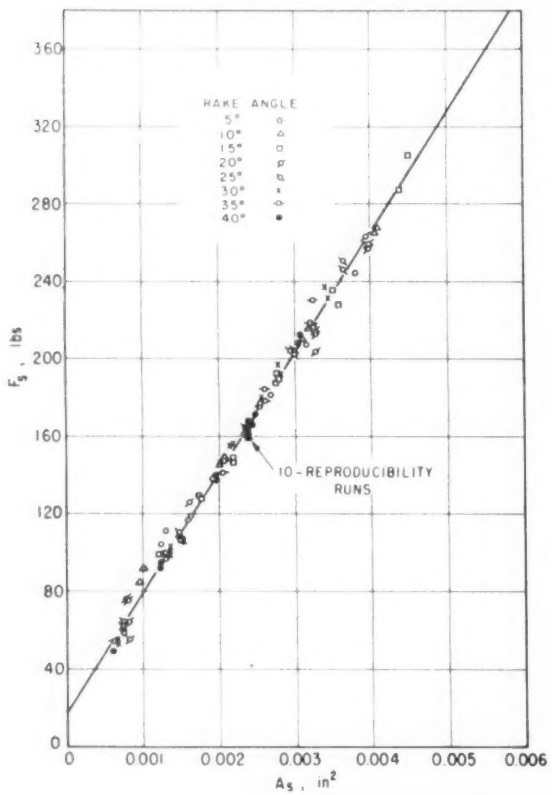

Fig. 2 Shear force, F_S, as function of shear-plane area, A_S, on which force acts for SAE 1112 steel as-received (cold-rolled)

Cutting condition:

Tool = 18-4-1 high-speed steel, 3 deg end clearance
End cutting of tubular specimen
Mean cutting speed = 90.8 fpm
Feed = 0.002 – 0.010 ipr
Width of cut = 0.200 in.
Cutting fluid = air

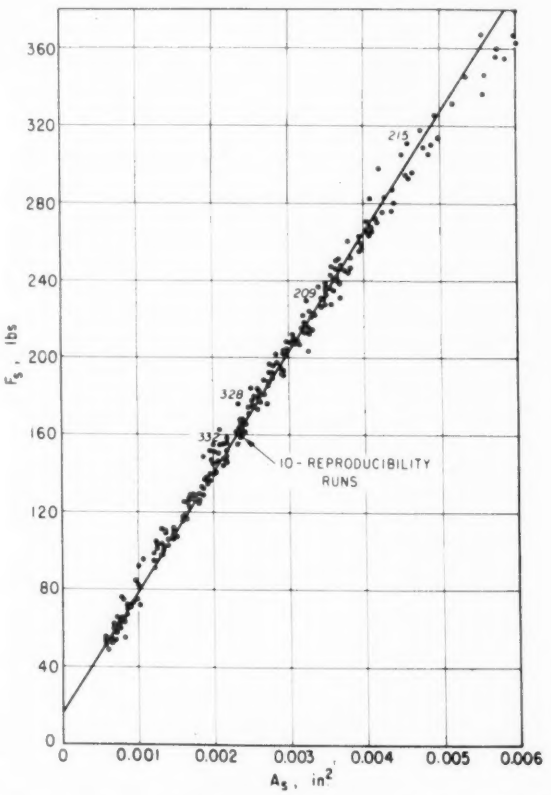

Fig. 3 Shear force, F_S, as function of shear-plane area, A_S, on which force acts for all SAE 1112 steel; cold-rolled and annealed

Cutting condition:

Tool = 18-4-1 high-speed steel, 3 deg end clearance
End cutting of tubular specimen
Mean cutting speeds = 33.7 – 170.8 fpm
Feed = 0.002 – 0.010 ipr
Rake angles = 5 – 40 deg
Width of cut = 0.200 in.
Cutting fluid = air

The reproducibility data points were obtained by keeping the cutting conditions constant. It must be concluded, therefore, that the scatter is nearly all due to experimental errors and that the shear force F_S is essentially a linear function of the shear area. It is even more startling to observe that all metal-cutting data points at three different speeds, ranging from 33.7 to 170.8 fpm, obtained with SAE 1112 annealed and cold-rolled steel, can be plotted on a single graph as shown in Fig. 3. It is again seen that the deviation from linearity is of the order of the scatter of the reproducibility runs.

These results, however, are no mere coincidence, because for the remainder of the alloys tested in this investigation, which are shown in Figs. 4 to 6, inclusive, the same linear relationship between F_S and A_S exists. The somewhat greater scatter of some of the data points observed here may be attributable to the greater tendency for chatter to occur. It is of interest again to note that the 2024-T4 aluminum alloy test data for two cutting speeds also fall on a single straight line as shown in Fig. 4.

To assure that these data are not peculiar to the present idiosyncracies of testing, additional data were taken from the literature and are shown in Figs. 7 to 9, inclusive. Again, straight lines are observed and, in fact, linearity remains even when the cutting speed is varied from 197 to 1186 fpm as occurred in Merchant's tests, the results of which are shown in Fig. 8.

Inasmuch as all F_S versus A_S graphs show positive intercept F_{S0} at zero A_S, Figs. 2–9, it is of interest to seek an explanation for this anomaly. Backer, et al. [9], proposed that the high forces observed at small feeds result from a size effect. These investigators apparently could show that for very thin chips such an effect existed, as for example, in grinding and in micromilling. When the chips are relatively thick, however, as in the present investigation, it is doubtful that a size effect is active. Another explanation was offered by Shaw and Finnie [10], who assumed that the shear-plane area is actually larger than that determined from chip measurements because of the fact that some bulging occurs at the free surface of the chip where the shear plane terminates. This bulging is described as flow ahead of the shear plane. The results of the present investigation could be interpreted as offering support for this hypothesis.

Another explanation might be offered by the fact that flank wear occurs on all cutting tools. It may be assumed, therefore, that this must be accompanied by frictional effects between the tool and the workpiece. This concept was suggested by Thomsen, et al. [11], who proposed that a certain force would be necessary

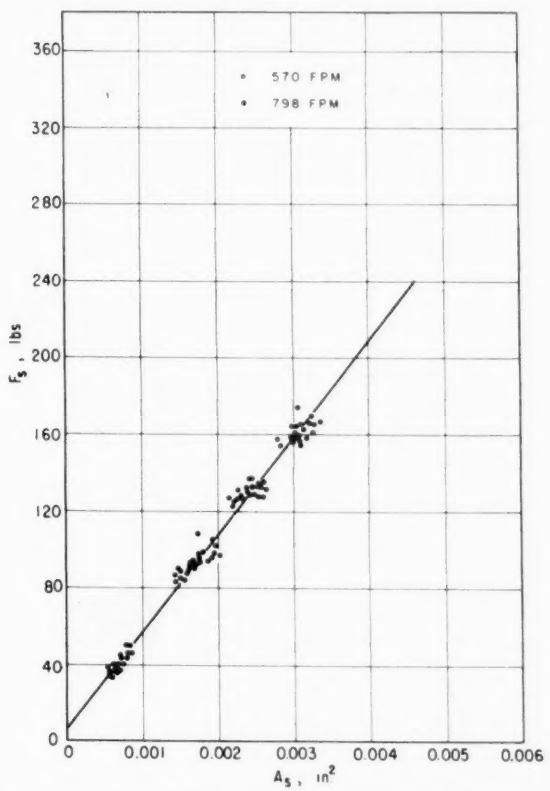

Fig. 4 Shear force, F_S, as function of shear-plane area, A_S, on which force acts for 2024-T4 aluminum alloy

Cutting condition:

Tool = 18-4-1 high-speed steel, 3 deg end clearance
End cutting of tubular specimen
Mean cutting speed = 570 – 798 fpm
Rake angle = 5 – 40 deg
Feed = 0.002 – 0.010 ipr
Width of cut = 0.200 in.
Cutting fluid = air

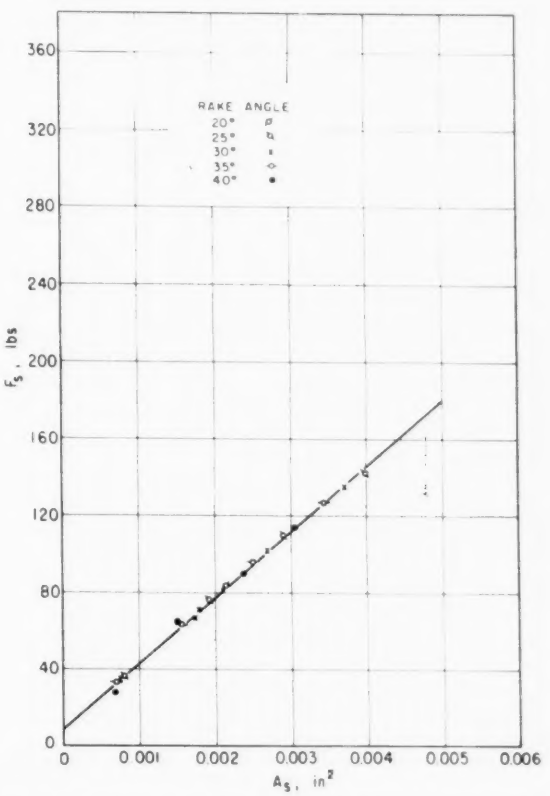

Fig. 5 Shear force, F_S, as function of shear-plane area, A_S, on which force acts for 6061-T6 aluminum alloy

Cutting condition:

Tool = 18-4-1 high-speed steel, 3 deg end clearance
End cutting of tubular specimen
Mean cutting speed = 573 fpm
Feed = 0.002 – 0.010 ipr
Width of cut = 0.200 in.
Cutting fluid = air

to overcome deformation and friction at the flank of the tool and, therefore, contributed nothing to chip deformation.

In order to test if the workpiece-deformation hypothesis might be used in explaining the intercept F_{S0}, which is nearly constant for a material and independent of rake angles and cutting speeds investigated, typical dynamometer forces F_H and F_V, as functions of feed, were plotted in Figs. 10 and 11. It is seen that all data points for a given rake angle α can be represented by straight lines except those for 5 deg at all feeds, and 10 and 15 deg at higher feeds. In the latter cases the deformation mechanism may differ from the remainder of the test conditions since the chips have a tendency to become discontinuous. It is of interest to note, however, that the shear forces still appear to be linear functions of A_S, even though F_H and F_V are not linear with feed.

It may be noted that all straight lines of Figs. 10 and 11 intersect at nearly the same force values. This fact, observed with their earlier data, led Thomsen, et al. [11], to the conclusion that this force at the intercept was not available for chip deformation, since in this case the feed is zero. This concept was discussed in their paper by Hahn [11] who showed that an instability occurs at low feeds (less than 0.001 ipr) and his observed force readings, it was claimed, actually decreased to zero as feed approached zero. This and similar interpretations of experimental data have led to the concept of size effect, as noted in the foregoing, since at small feeds the ratio of uncorrected shear force to shear-plane area, $F_S/A_S = \tau$, yields shearing stresses which assume unreasonable magnitudes at low feeds. If it is accepted, however, that at low feeds of the order of 0.001 ipr or less, as reported by Hahn [11], the mechanism of chip formation changes radically (since at these feeds the chips become discontinuous and disintegrate to metal powder), then the intercept concept for formation of continuous chips may be valid.

The actual intercepts taken from Figs. 10 and 11 were used to calculate the forces R_0 and F_{S0} shown in Fig. 12. It is at once evident that F_{S0} is, at least to a first approximation, constant and hence nearly independent of α.

If it is accepted that the intercept of F_S at zero A_S may be regarded as a constant force unavailable for chip deformation, owing to whatever cause, then the shearing force on the shearing plane can be written as follows:

$$F_S = F_{S0} + (F_S - F_{S0}) = F_{S0} + A_S\tau \qquad (4)$$

Hence the slope of each straight line of Figs. 2–9, inclusive, is given by $(F_S - F_{S0})/A_S = \tau$ and is the constant shearing stress or shearing flow stress on the shear plane.

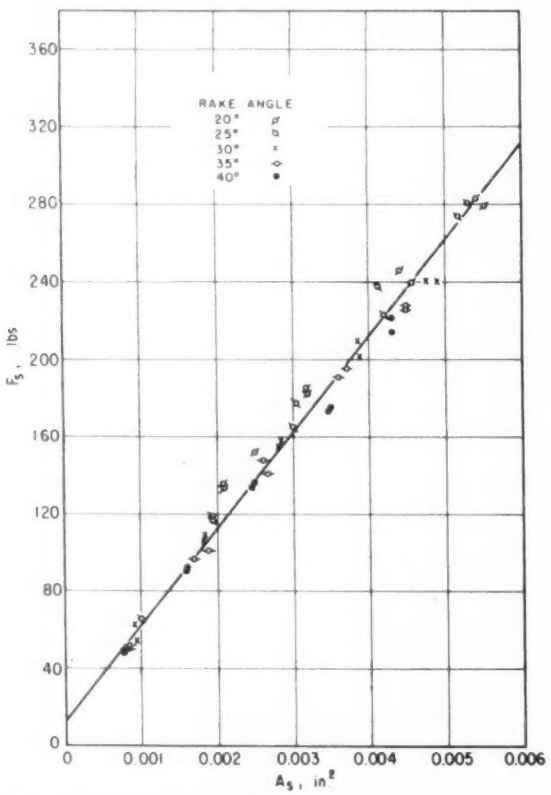

Fig. 6 Shear force, F_S, as function of shear-plane area, A_S, on which force acts for alpha-brass (85 per cent Cu, 15 per cent Zn)

Cutting condition:

Tool = 18-4-1 high-speed steel, 3 deg end clearance
End cutting of tubular specimen
Mean cutting speed = 472 fpm
Feed = 0.002 – 0.011 ipr
Width of cut = 0.181 in.
Cutting fluid = air

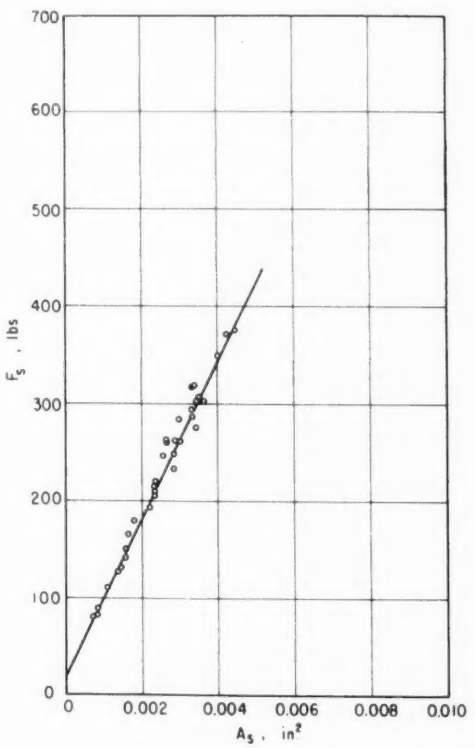

Fig. 7 Shear force, F_S, as function of shear-plane area, A_S, on which force acts for SAE 4135

Cutting condition:

Tool = 18-4-2 + 5Co high-speed steel, 3 deg end clearance
Mean cutting speed = 29.4 fpm
Rake angle = 25 – 40 deg
Feed = 0.002 – 0.010 ipr
Width of cut = 0.231 in.
Cutting fluids = CCl_4 and Lusol
Data from Creveling, et al. [5]

Normal Stress on Shear Plane

It also may be of interest to examine the normal forces on this same plane. Figs. 13 to 15, inclusive, show examples of the normal forces F_N as functions of shear-plane areas A_S, which were obtained in the present investigation. It is evident that no single line can be drawn and that the data points appear to align themselves into families of curves with angles α as parameters. It may be of interest to note further that occasional instabilities in the apparent operating conditions seem to occur as indicated by data points 209, 215, 328, and 332 in Fig. 14, which depart from the general trend of the F_N versus A_S relationship. No such departure from the general trend, however, is observed for the corresponding data points, F_S versus A_S, shown in Fig. 3. This anomaly may be explained by the fact that a sudden change in the friction mechanism on the tool face, as for example a small built-up edge, will affect the normal force on the shear plane and consequently the normal stress without necessarily affecting the shear mechanism on this same plane. It appears, therefore, that a unique solution for the unknown functional relationship of the normal stresses on the shear plane must incorporate the mechanism of friction on the tool face; it also appears, however, that the solution is independent of the shearing stresses on the shear plane. Hence the concept of independence of maximum shearing flow stress from normal stress for a given strain rate or strain, which is the common concept employed in the theory of plasticity, seems to apply to the process of chip formation in metal cutting.

Properties of Workpiece at Metal-Cutting Conditions

Accepting the concept of intercept correction for the shearing forces on the shear plane, it remains to be explained why the shearing stress is not a function of strain or strain rate. In order to do this it is profitable at this time to review present knowledge of the stress-strain relationships at high rates of strain and the strain rates to be expected in metal cutting.

A number of investigators have attempted to affix magnitudes to strain rates in metal cutting, but agreement here is poor and the only item on which agreement exists is that the metal-cutting strain rates are extremely high. This lack of a clear-cut estimate of magnitudes of shearing strain rates is, of course, due to the fact that the shearing strain rate depends on the size of the shear zone which, under present methods of measurement, cannot be determined accurately. Thus, for example, Kececioglu [12] for low-carbon steel with cutting speeds varying from 126–746 fpm estimates the strain-rates to vary from 2500–212,000 per sec; Drucker's [13] estimate is 40,000 per sec; Chao and Bisacre [3] believe they vary from 10^3–10^6 per sec; and Shaw's [14] estimate is that they are of the order of 10^6 per sec and higher. These strain rates are extremely high when compared with a static tension test where the strain rates are of the order of 10^{-3} per sec, or a rapid impact test with strain rates of about 10^3 per sec.

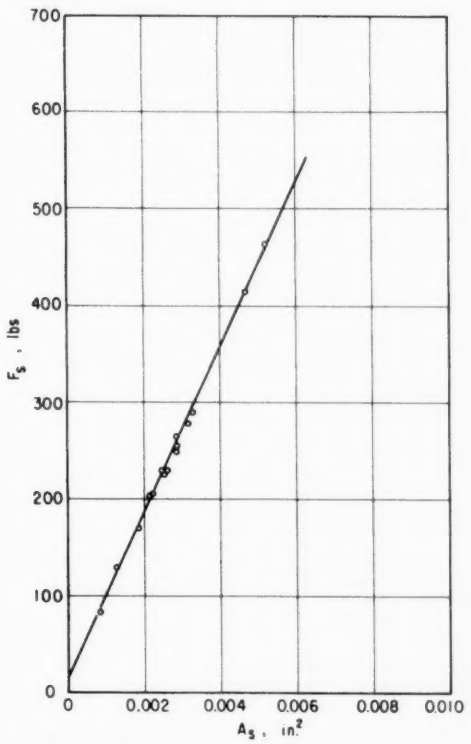

Fig. 8 Shear force, F_S, as function of shear-plane area, A_S, on which force acts for NE 9445 steel

Cutting condition:
Sintered-carbide tool
Mean cutting speed = 197–1186 fpm
Rake angle = +10 to −10 deg
Feed = 0.0037 − 0.0079 ipr
Width of cut = 0.25 in.
Data from Merchant [1]

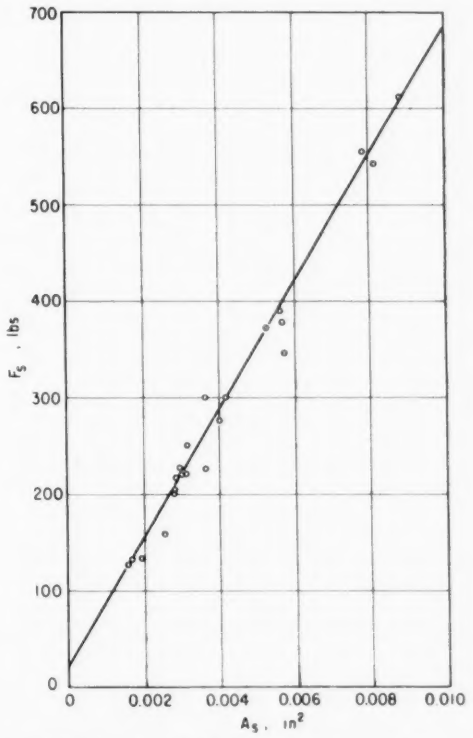

Fig. 9 Shear force, F_S, as function of shear-plane area, A_S, on which force acts for SAE 1015 steel (118 BH)

Cutting condition:
Carbide-tipped tool
Mean cutting speed = 126 − 746 fpm
Rake angle = −10 to 36.5 deg orthogonal cutting
Feed = 0.004–0.012 ipr
Width of cut = 0.169 in.
Cutting fluid = air
Data from Kececioglu [12]

Quantitative information on stress-strain properties at high rates of strain, approaching those of metal cutting, are not to be found in the literature. This is evidently because of the fact that test speeds are beyond the scope of ordinary laboratory equipment and metal-cutting strain rates apparently have not as yet been realized. This led Shaw [14] to the belief that, if we understand the mechanics of metal cutting thoroughly, it should become possible to use it as a property test. It must be realized, however, that this would not permit us to obtain complete stress-strain curves, but only mean shearing stresses or flow stresses.

The effect of strain rate on the flow stress of metals has been a subject of investigation for many years. Much time and effort have been expended on studying the behavior of metals in the creep range of deformation rates and it appears that an understanding of the mechanism is beginning to emerge. Dorn [15, 16] has recently given a comprehensive account of the theory. It appears that at least for high-purity aluminum alloys a single mechanism of creep is operative at high temperatures in the vicinity of the melting temperature of the metal. This mechanism of plastic flow appears to be that of a thermally activated dislocation climb process, in which the activation energies are those of self-diffusion. At higher stress levels for any given strain, however, which correspond to lower temperatures and higher strain rates, the mechanism of plastic flow apparently changes. It is suggested that more of the energy required for plastic flow now comes from the applied mechanical energy and less from thermal fluctuation alone. These observations generally agree with what is believed to occur at high rates of strain.

Cottrell [17] recently gave an interesting discussion of what might be a mechanism at high rates of strain. He assumes that the slip process in metals, as is now generally accepted, is that due to movement of dislocations. Dislocations are believed to be present in all metals and are called primary dislocations. These primary dislocations create secondary dislocations and have been called Frank-Read sources. These dislocations are believed to move and in the process create a large number of new ones by a mechanism originally suggested by Frank and Read [18]. Such sources have now actually been observed in real crystals. The dislocation is considered as a line of slightly displaced atoms on which terminates an extra so-called half plane of atoms in the crystal. Under the presence of a sufficient stress the line or edge dislocation can bow outward and in this movement from a dislocation loop. As the loop breaks away from its anchorage a new line source is created. Hence every new dislocation loop formed, which in essence is plastic deformation, creates at the same time a new Frank-Read source.

The formation and movement of these dislocation loops require both temperature and sufficient stress in varying degrees to overcome the obstacles in their paths. These obstacles may be in the form of stress fields formed by other dislocations (work-hardening), alloy precipitates (precipitation-hardening), and grain

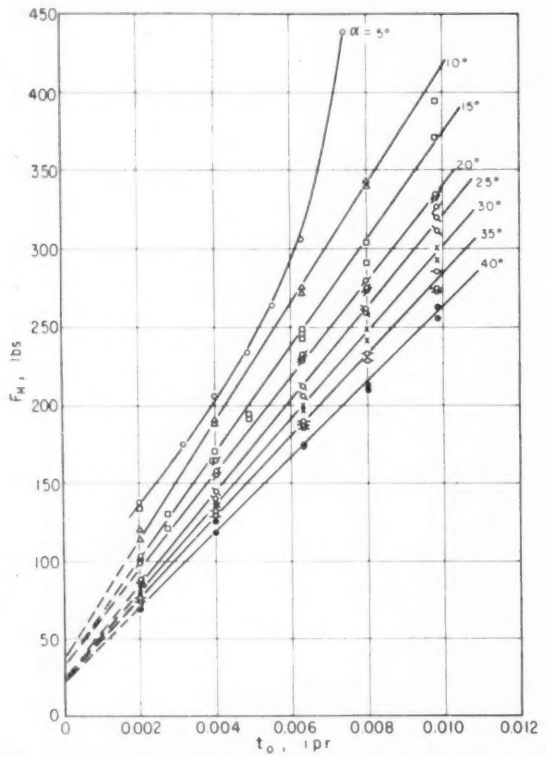

Fig. 10 Horizontal tool force, F_H (cutting force) as function of feed, t_o, for SAE 1112 steel in cold-rolled state

Cutting condition:
Tool = 18-4-1 high-speed steel, 3 deg end clearance
End cutting of tubular specimen
Mean cutting speed = 90.8 fpm
Feed = 0.002 – 0.010 ipr
Width of cut = 0.200 in.
Cutting fluid = air

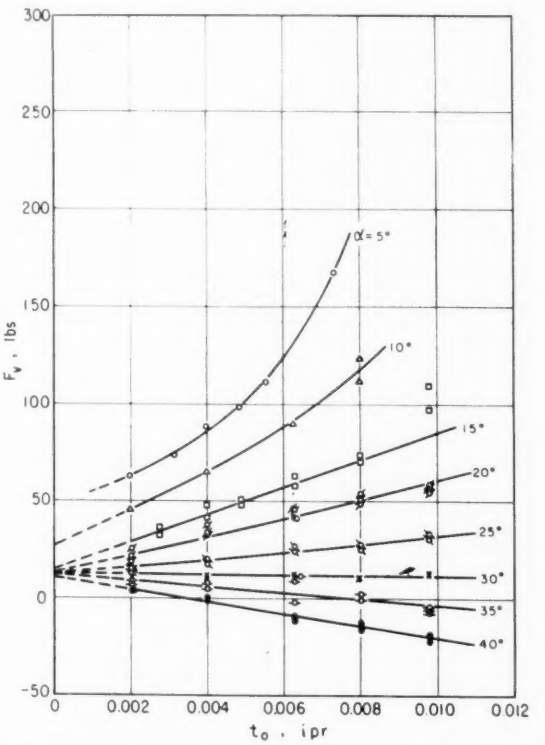

Fig. 11 Vertical tool force, F_V (thrust force) as function of feed, t_o, for SAE 1112 steel in cold-rolled state

Cutting condition:
Tool = 18-4-1 high-speed steel, 3 deg end clearance
End cutting of tubular specimen
Mean cutting speed = 90.8 fpm
Feed = 0.002 – 0.010 ipr
Width of cut = 0.200 in.
Cutting fluid = air

boundaries (polycrystalline effects). Such obstacles can be presented by an undulating stress field. When the applied stress is smaller than that of the internal or undulating stress field, the dislocation cannot pass the obstacle except by thermal fluctuations and therefore is temperature-dependent. If, however, the reverse is true, rapid slip will occur. It is believed, therefore, that at high rates of deformation the applied stress must reach a critical value greater than the internal stress in order to start deformation and that straining then is sudden and catastrophic. The contribution in this case due to thermal activation, which is of importance at lower strain rates and lower internal stress levels, would be insignificant. From this it can be concluded that, at very high rates of strain, the following observations might be made:

1 The initiation of yielding at high rates of strain is higher than that at lower rates; i.e., static yield point is below dynamic yield point.

2 The temperature effect due to generation of heat by plastic flow is essentially absent; hence the flow stress is not a function of strain rate.

3 The straining is sudden and catastrophic at any applied stress level; hence work-hardening effects cannot be observed. This implies that the stress-strain curve is flat topped.

Drucker [13] suggested earlier that the shear stress-shear strain curves of metals at the high rates of strain encountered in metal cutting must be essentially flat topped curves. He based these observations on results from tension impact tests by Manjoine [19] and Fehr, et al. [20], and these results apparently substantiate modern ideas on deformation by dislocation movement. Pugh and Watkins [21] in testing cylindrical slugs in a drop-forging test found that for aluminum the dynamic stress-strain curve at a mean strain rate of 50 per sec was higher and much flatter than the static stress-strain curve. They also tested copper, but the results are inconclusive, since the total strain achieved was limited. Cook [22] has reported compression test data for a number of steels, including low-carbon steel, which he obtained with a cam-type plastometer designed to give constant strain rates. He found that all curves are relatively flat and often drooping beyond small strains of the order of 0.5. Unfortunately, his results, at strain rates up to 100 per sec, were obtained at temperature ranges from 1650 to 2200 F and room-temperature tests were not included. While these results do not appear to apply directly to high-speed strain rates when the specimens are initially at room temperature, they confirm at least qualitatively modern thoughts on the behavior of metals at high rates of strain.

The fact that the shearing stresses on the shear plane, reported in the present investigation, appear to be constant and therefore are independent of strain rates and finite strains seems to be in qualitative agreement with the foregoing concepts on high rates of strain, providing the initial temperature of the metal just prior to entering the shear zone is at or near room temperature. In order to answer this question we might investigate the magnitude and temperature distributions at and near the shear zone.

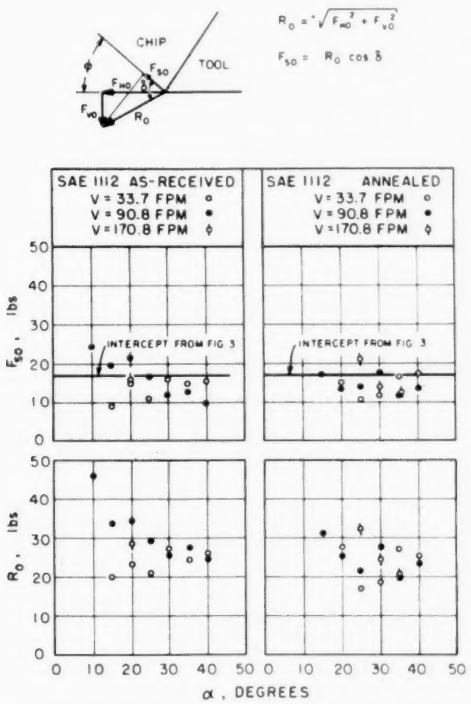

Fig. 12 Shear-force components, F_{So}, on shear plane and resultant force, R_o, as functions of rake angle α for SAE 1112 steel. Note: Forces F_{So} and R_o were obtained from intercepts of Figs. 10 and 11 at zero feed.

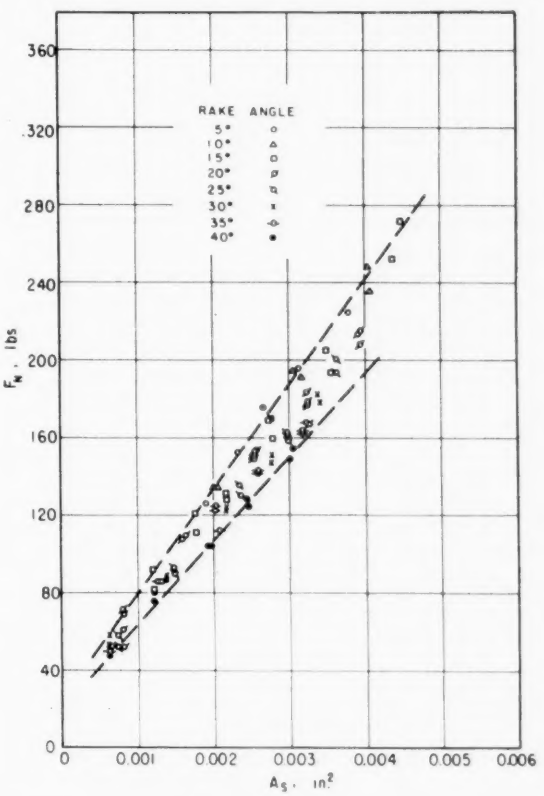

Fig. 13 Normal force, F_N, as function of shear-plane area, A_S, on which force acts for SAE 1112 steel as-received

Cutting condition:
Tool = 18-4-1 high-speed steel, 3 deg end clearance
End cutting of tubular specimen
Mean cutting speed = 90.8 fpm
Feed = 0.002 – 0.010 ipr
Width of cut = 0.200 in.
Cutting fluid = air

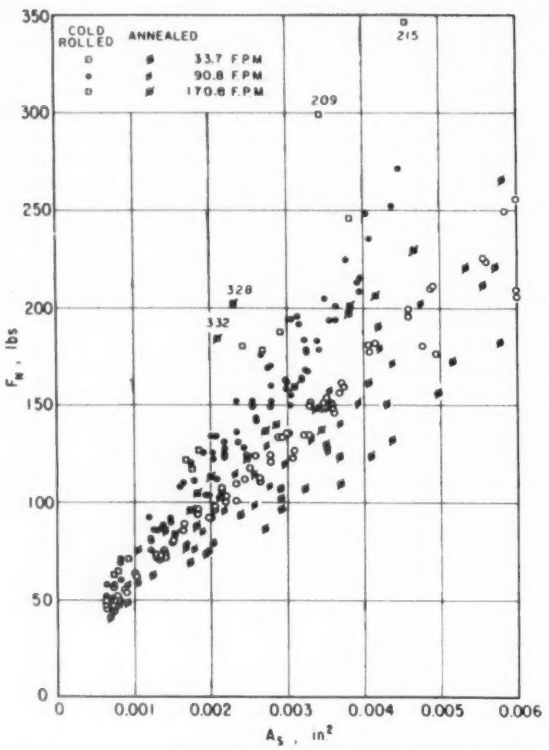

Fig. 14 Normal force, F_N, as function of shear-plane area, A_S, on which force acts for SAE 1112 steel cold-rolled and annealed

Cutting condition:

Tool = 18-4-1 high-speed steel, 3 deg end clearance
End cutting of tubular specimen
Mean cutting speed = 33.7 – 170.8 fpm
Feed = 0.002 – 0.010 ipr
Rake angle = 5–40 deg
Width of cut = 0.200 in.
Cutting fluid = air

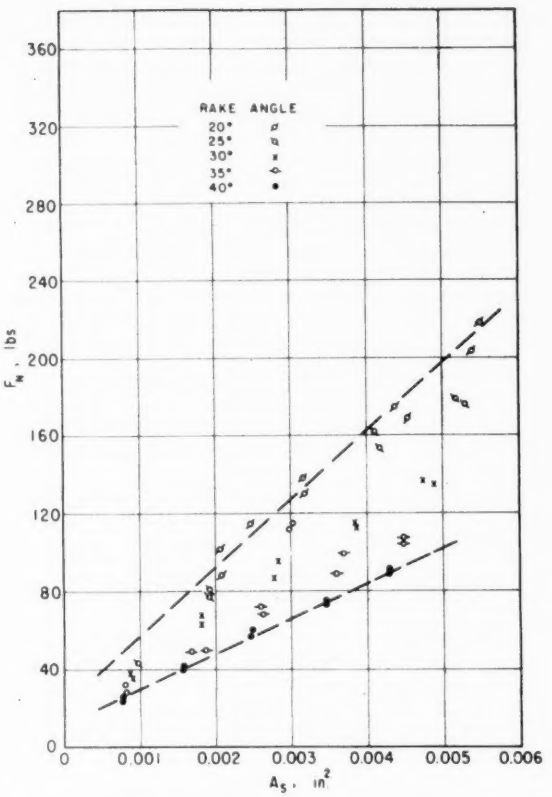

Fig. 15 Normal force, F_N, as function of shear-plane area, A_S, on which force acts for alpha-brass

Cutting condition:

Tool = 18-4-1 high-speed steel, 3 deg end clearance
End cutting of tubular specimen
Mean cutting speed = 472 fpm
Feed = 0.002 – 0.011 ipr
Width of cut = 0.181 in.
Cutting fluid = air

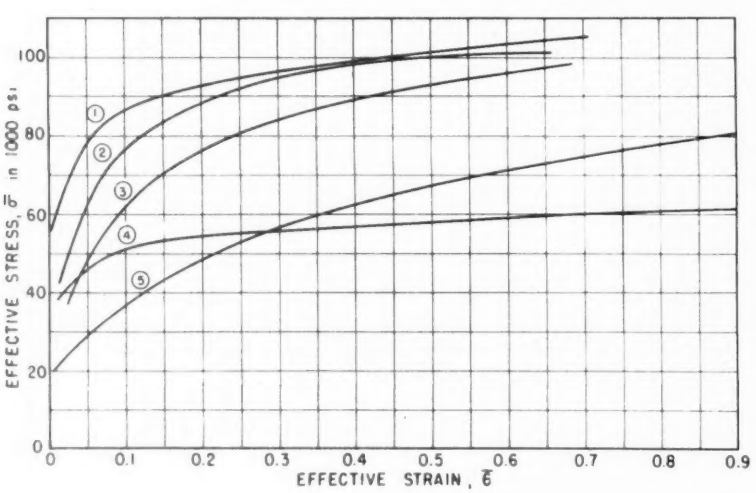

Fig. 16 Effective-stress versus effective-strain curves for materials used in metal-cutting tests. Data evaluated in compression tests using solid cylindrical specimens with grooved and lubricated ends compressed between flat polished dies.

Test curves are as follows:

(1) SAE 1112 steel as-received (cold-rolled), 0.750 in. diam × 1 in. long
(2) 2024-T4 aluminum alloy, 0.375 in. diam × 1/2 in. long
(3) SAE 1112 steel annealed, 0.750 in. diam × 1 in. long
(4) 6061-T6 aluminum alloy, 0.375 in. diam × 1/2 in. long
(5) Alpha-brass (85 Cu, 15 Zn), 0.200 in. diam × 1/4 in. long

A number of investigators [23, 24, 25, 26] have tackled the problem of estimating the shear-plane temperature analytically by treating the shear plane as a moving heat source. The resulting temperatures thus found are relatively high and are highest at the tool point. The additional friction on the tool as the chip slides over its face increases the interface to still higher temperatures. Thus, for example, Chao and Trigger [24] when cutting NE 9445 annealed steel at a cutting speed of 300 fpm, and with a (0-4-7-7-6-0-3/64) triple-carbide tool, calculated an average shear-plane temperature of 748 F and, measured by a work-tool thermocouple technique, a temperature of 1300 F on the tool-chip interface. While this high tool-chip interface temperature of 1300 F exists it probably will affect the friction mechanism without affecting the shear-plane temperature, since it occurs only in a narrow and somewhat removed zone.

Vieregge [26] has determined a temperature distribution ahead of the shear plane and it was thought that this temperature might affect the initial temperature with which the material enters the shear zone and hence its initial properties. Vieregge determined, for example, that at a cutting speed of 200 fpm the average temperature rises from 200 F in a distance of less than 0.001 in. to a shear-plane temperature of about 800 F. While this temperature gradient could affect the initial shear properties of the material, it is doubtful that it is a factor here since the shear plane actually is a zone of finite thickness, possibly of the same order of magnitude as the short distance in which the steep temperature gradient exists. Furthermore, the ripples readily observable on the air side of the chip indicate that the shearing process is not uniform and that it must consist of an intermittent slip process, in which the initial temperature of the metal just entering the shear zone may be considered to be essentially at room temperature. A similar conclusion was reached by Chao, et al. [3, 4].

A set of experiments substantiating the foregoing conclusions is supplied by Krabacher and Merchant [27]. These investigators hot-machined SAE 3145, by raising the initial temperature of the workpiece and found that the cutting force F_H and F_V decreased linearly with increasing initial workpiece temperature at constant cutting speeds. Thus it appears that from the standpoint of modern solid-state physics, the shearing stress on the shear plane in metal cutting should be independent of strain and strain rate.

Correlation of Metal-Cutting Data With Properties of Workpiece

It remains now to correlate the shear stresses observed in metal cutting with property tests. It has been pointed out already that no such high-speed data at the metal-cutting strain rates are available. It is, therefore, of interest to compare metal-cutting data with static tests. This already has been done by Lapsley, Grassi, and Thomsen [28] and more recently by Weisz [29], who found that the shear stresses correlated approximately with the tensile properties at the same finite strains. Their dynamometer forces, however, were not corrected for possible

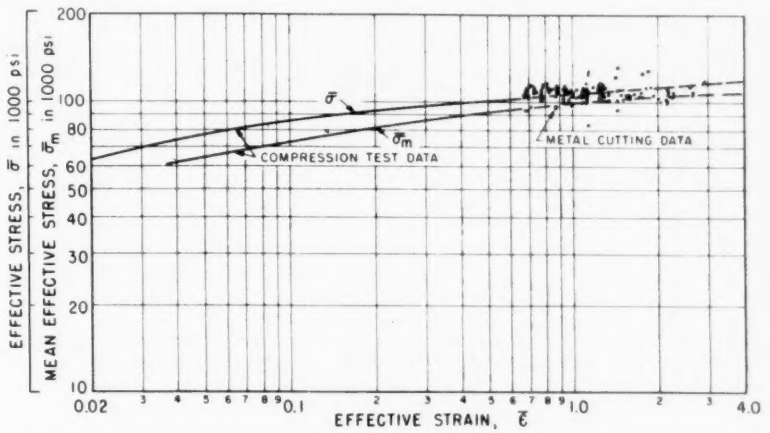

Fig. 17 Comparison of effective-stress $\bar{\sigma}$ and mean effective-stress $\bar{\sigma}_m$—effective-strain curves from compression tests with all metal-cutting data points of SAE 1112 steel as-received

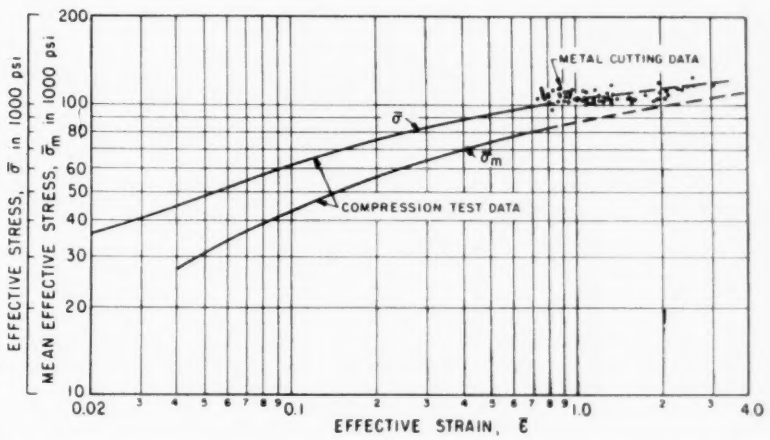

Fig. 18 Comparison of effective-stress $\bar{\sigma}$, and mean effective-stress $\bar{\sigma}_m$—effective-strain curves from compression tests with all metal-cutting data points of SAE 1112 steel annealed

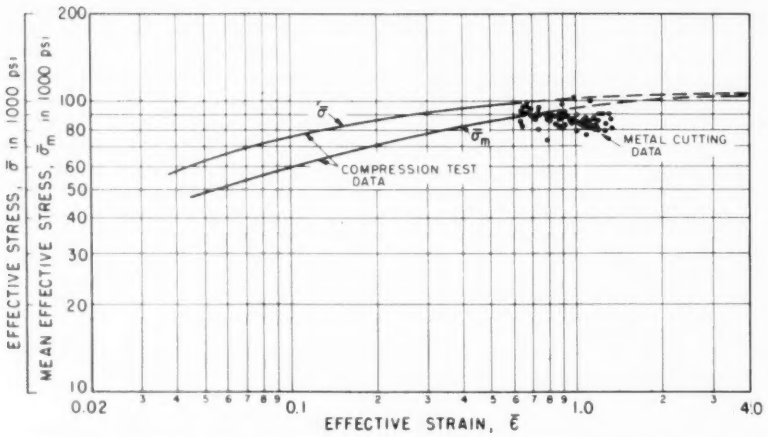

Fig. 19 Comparison of effective-stress $\bar{\sigma}$ and mean effective-stress $\bar{\sigma}_m$—effective-strain curves from compression tests with all metal-cutting data points of 2024-T4 aluminum alloy

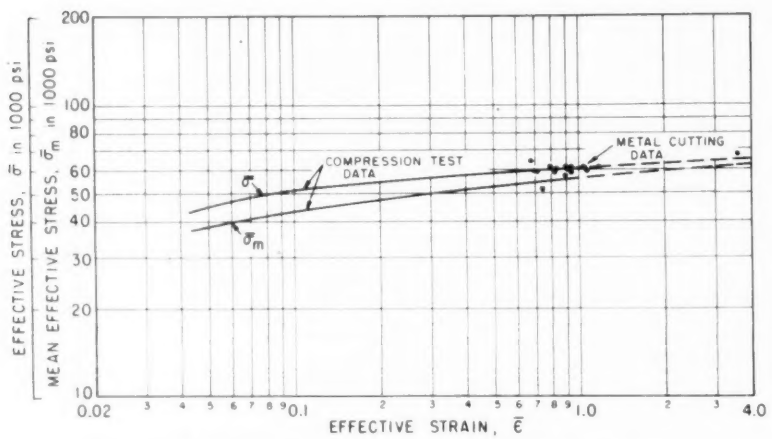

Fig. 20 Comparison of effective-stress $\bar{\sigma}$ and mean effective-stress $\bar{\sigma}_m$—effective-strain curves from compression tests with all metal-cutting data points of 6061-T6 aluminum alloy

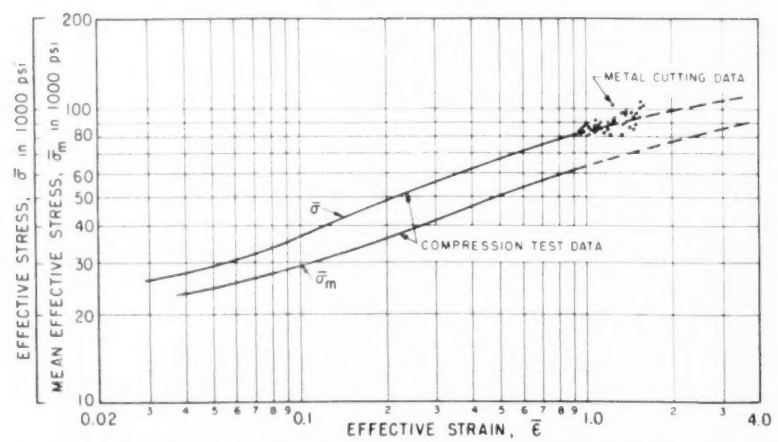

Fig. 21 Comparison of effective-stress $\bar{\sigma}$ and mean effective-stress $\bar{\sigma}_m$—effective-strain curves from compression tests with all metal-cutting data points of alpha-brass (85 Cu, 15 Zn)

workpiece deformation with a consequence that the small feeds fell above the stress-strain curve.

The plastic-flow properties for the materials investigated are shown in Fig. 16. The effective stress-effective strain curves shown in this figure were obtained with compression tests assuming the distortion energy or Levy-Mises theory to hold. The effective stress $\bar{\sigma}$ is proportional to the quadratic invariant of the deviator stresses and reduces in a compression test to the axial stress σ_x. In the case of metal cutting, however, the value of $\bar{\sigma} = \sqrt{3}\,\tau$, where τ is the shearing stress on the shear plane. The corresponding finite effective strain $\bar{\epsilon}$ is also simply given by the true axial strain when stress ratios remain constant, which is defined as $\bar{\epsilon} = \epsilon_x = \ln(l/l_0) = 2\ln(d_0/d)$, where l, l_0 and d, d_0 are final and initial lengths and diameters of the test pieces, respectively. The effective strain $\bar{\epsilon}$ is related to the shearing strain γ in metal cutting by the formula $\bar{\epsilon} = \gamma/\sqrt{3}$. It should be noted that the specimens, whose stress-strain curves are given in Fig. 16, were cut from the tube walls of the specimens (or solid end of SAE 1112) and their flat ends were provided with shallow spiral grooves to aid in lubrication to reduce barreling of the specimens. All tests were made in a hydraulic testing machine at low speeds with the specimens being deformed between flat polished anvils. It may be observed that the materials investigated were selected to give a reasonable range in instantaneous flow stresses and work-hardening characteristics.

The comparison between metal-cutting data points and compression test curves (solid curves) is made in Figs. 17 to 21, inclusive, for all materials. The metal-cutting data points were obtained by correcting the shear forces F_S by subtracting the average intercept values, F_{S0}; i.e., $\tau = \bar{\sigma}/\sqrt{3} = (F_S - F_{S0})/A_S$. It should be noted that it was necessary to extrapolate the compression curves to higher values of effective strain $\bar{\epsilon}$, since the test equipment did not permit obtaining large reductions. It is at once evident that the correlation is good, except for 2024-T4 aluminum alloy, where the metal-cutting data points fell below the compression test curve. In order to compare also mean effective stresses $\bar{\sigma}_m$ in compression tests with the metal-cutting data points, which is equivalent to comparing energies of deformation, the additional curves are shown. The average effective stresses $\bar{\sigma}_m$ for these curves were obtained by taking the area under the stress-strain curves of Fig. 16 for any value $\bar{\epsilon}$ and dividing this area by $\bar{\epsilon}$; i.e.

$$\bar{\sigma}_m = \frac{1}{\bar{\epsilon}} \int_0^{\bar{\epsilon}} \bar{\sigma} d\bar{\epsilon}$$

It is seen that the $\bar{\sigma}_m$ versus $\bar{\epsilon}$ curves fall below the metal-cutting data points except those of 2024-T4 aluminum alloy of Fig. 19, which now are in approximate agreement.

From the foregoing comparison it appears that static-property test data can be correlated with metal-cutting data points, but the reason for correlation is obscure. There appears to be no simple mechanism by which it can be explained that the flow stresses in metal cutting and compression tests must take on unique values at the same finite strains.

Conclusions

1 The shearing stresses on the shear plane for SAE 1112 free-cutting steel and for the test conditions investigated appear to be independent of normal stress, finite strain, strain rate, and initial state of cold work.

2 The shearing stresses for the remainder of the alloys, i.e., 2024-T4 and 6061-T6 aluminum alloys and alpha-brass, also were constant, but the range of cutting conditions was not as extensive as that for SAE 1112.

3 The normal stresses on the shear plane appear to be related to the friction processes on the face of the tool, but the functional relationship is not as yet known.

4 The shear-flow stresses in metal cutting and those obtained in a static compression test correlate well, except for 2024-T4 aluminum alloy. The reason for correlation at a unique strain has not been determined as yet.

Acknowledgments

The authors wish to express their thanks to the Rock Island Arsenal without whose support this investigation could not have been carried out. The authors further wish to express their appreciation to the University of California, especially the Division of Industrial Engineering, for permitting the use of laboratory equipment and facilities. They also wish to thank Miss Matsumoto for typing the report and Mr. Kot for preparing the figures.

References

1 M. E. Merchant, "Mechanics of the Metal Cutting Process," *Journal of Applied Physics*, vol. 16, 1945, pp. 267–324.

2 P. W. Bridgman, "On Torsion Combined With Compression," *Journal of Applied Physics*, vol. 14, 1943, pp. 273–283.

3 B. T. Chao and G. H. Bisacre, "The Effect of Speed and Feed of the Mechanics of Metal Cutting," *Proceedings of The Institution of Mechanical Engineers*, vol. 165, (WEP No. 63), 1951, pp. 1–13.

4 B. T. Chao, K. J. Trigger, and L. B. Zylstra, "Thermophysical Aspects of Metal Cutting," TRANS. ASME, vol. 74, 1952, pp. 1039–1054.

5 J. H. Creveling, T. F. Jordan, and E. G. Thomsen, "Some Studies of Angle Relationships in Metal Cutting," TRANS. ASME, vol. 79, 1957, pp. 127–138.

6 D. Kececioglu, "Shear-Zone Temperature in Metal Cutting and Its Effects on Shear-Flow Stress," TRANS. ASME, vol. 80, 1958, pp. 541–546.

7 S. Kobayashi, R. Herzog, D. M. Eggleston, and E. G. Thomsen, "An Application of Plastic Flow Analysis to Orthogonal Metal Cutting," Final report to Rock Island Arsenal issued by the Institute of Engineering Research, University of California, no. 117, Berkeley, Calif., May, 1958.

8 D. M. Eggleston, R. Herzog, and E. G. Thomsen, "Some Additional Studies of the Angle Relationships in Metal Cutting," published in this issue, pp. 263–279.

9 W. R. Backer, E. R. Marshall, and M. C. Shaw, "The Size Effect in Metal Cutting," TRANS. ASME, vol. 74, 1952, pp. 61–72.

10 M. C. Shaw and I. Finnie, "The Shear Stress in Metal Cutting," TRANS. ASME, vol. 77, 1955, pp. 115–125.

11 E. G. Thomsen, J. T. Lapsley, Jr., and R. C. Grassi, "Deformation Work Absorbed by the Workpiece During Metal Cutting," TRANS. ASME, vol. 75, 1953, pp. 591–603.

12(*a*) D. Kececioglu, "Force Components, Chip Geometry, and Specific Cutting Energy in Orthogonal and Oblique Machining of SAE 1015 Steel," TRANS. ASME, vol. 80, 1958, pp. 149–157.

12(*b*) D. Kececioglu, "Shear-Strain Rate in Metal Cutting and Its Effects on Shear-Flow Stress," TRANS. ASME, vol. 80, 1958, pp. 158–168.

13 D. C. Drucker, "An Analysis of the Mechanics of Metal Cutting," *Journal of Applied Physics*, vol. 20, 1949, pp. 1013–1021.

14 M. C. Shaw, "A Quantized Effect of Strain-Hardening as Applied to the Cutting of Metals," *Journal of Applied Physics*, vol. 21, 1950, pp. 599–606.

15 J. E. Dorn, "The Spectrum of Activation Energies for Creep," ASM, *Creep and Recovery*, 1957, p. 255.

16 T. A. Trozera, O. D. Sherby, and J. E. Dorn, "Effect of Strain-Rate and Temperature on the Plastic Deformation of High Purity Aluminum," *Trans. ASM*, vol. 49, 1957.

17 A. H. Cottrell, "Deformation of Solids at High Rates of Strain," advance copy of paper presented to Conference on the Properties of Materials at High Rates of Strain, sponsored by The Institution of Mechanical Engineers, London, England, April-May, 1957.

18 F. C. Frank and W. T. Read, Jr., "Multiplication Processes for Slow Moving Dislocations," *Physical Review*, vol. 79, second series, 1950, p. 722.

19 M. J. Manjoine, "Influence of Rate of Strain and Temperature on Yield Stresses of Mild Steel," *Journal of Applied Mechanics*, vol. 11, TRANS. ASME, vol. 66, 1944, pp. A-211–218.

20 R. O. Fehr, E. R. Parker, and D. J. DeMicheal, "Measurement of Dynamic Stress and Strain in Tensile Test Specimens," *Journal of Applied Mechanics*, vol. 11, TRANS. ASME, vol. 66, 1944, pp. A-65–71.

21 H. Ll. D. Pug and M. T. Watkins, "Some Strain-Rate Effects in Drop Forging Tests," advance copy of paper presented to Conference on the Properties of Materials at High Rates of Strain, sponsored by The Institution of Mechanical Engineers, London, England, April-May, 1957.

22 P. M. Cook, "True Stress-Strain Curves for Steel in Compression at High Temperature and Strain-Rates, For Application to the Calculations of Load and Torque in Hot Rolling," advance copy of paper presented to Conference on the Properties of Materials at High Rates of Strain, sponsored by The Institution of Mechanical Engineers, London, England, April-May, 1957.

23 E. G. Loewen and M. C. Shaw, "On the Analysis of Cutting-Tool Temperature," TRANS. ASME, vol. 76, 1954, pp. 217–231.

24 B. T. Chao and K. J. Trigger, "Temperature Distribution at the Tool-Chip Interface in Metal Cutting," TRANS. ASME, vol. 77, 1955, pp. 1107–1121.

25 J. H. Weiner, "Shear-Plane Temperature Distribution in Orthogonal Cutting," TRANS. ASME, vol. 77, 1955, pp. 1331–1341.

26 G. Vieregge, "Temperaturfeld und Wärmebilanz des Schervorganges bei der Zerspanung," *Werkstatt und Betrieb*, vol. 88, 1955, pp. 227–230.

27 E. J. Krabacher and M. E. Merchant, "Basic Factors in Hot-Machining of Metals," TRANS. ASME, vol. 73, 1951, pp. 761–769.

28 J. T. Lapsley, Jr., R. C. Grassi, and E. G. Thomsen, "Correlation of Plastic Deformation During Metal Cutting With Tensile Properties of the Work Material," TRANS. ASME, vol. 72, 1950, pp. 979–986.

29 M. Weisz, "Etude Metallographique de la Formation du Copeau d'Usinage," PhD thesis, Publication de l'institute de Recherches de la Sidérurgie, series A, no. 142, Paris, France, 1957.

D. M. EGGLESTON

Graduate Student in Mechanical Engineering, University of California, Berkeley, Calif.

R. HERZOG

Student in Mechanical Engineering, University of California, Berkeley, Calif.

E. G. THOMSEN

Professor of Metal Processing, University of California, Berkeley, Calif. Mem. ASME

Observations on the Angle Relationships in Metal Cutting[1]

Orthogonal-cutting experiments using SAE 1112 free-cutting steel, 2024-T4 and 6061-T6 aluminum alloys, and alpha-brass (85 Cu–15 Zn) at feeds of 0.002 to 0.010 ipr, were performed on a lathe with 18-4-1 high-speed-steel cutting tools. The mean cutting speeds and rake angles for SAE 1112 varied from 33.7 to 170.8 fpm and 5 to 40 deg, respectively, while the remainder of the alloys were tested at conditions yielding a continuous chip without a built-up edge at speeds ranging from approximately 470 to 790 fpm. It was found that the angle λ between the shear plane and the resultant tool force R was only approximately constant for each test condition and varied with cutting speed. Hence the equation $\lambda = \phi + \beta - \alpha = const$ and the linear relationship between ϕ and $\beta - \alpha$ are only approximately satisfied. Furthermore, neither the Ernst and Merchant minimum-energy criterion, nor the Lee and Shaffer nor the Hill ideal plastic-solid solution, is in agreement with all the experimental observations.

THE basic problem of establishing a universal relationship among the metal-cutting variables has apparently not been solved. This is despite the fact that attempts to analyze the mechanics of this process began more than one hundred years ago and coincided with the development of machine tools, some of which have retained their essential shape to this day. Scientific progress in the analysis of metal-cutting processes at first went hand in hand with the development of some of our modern tools but was soon outstripped by new developments introduced by the machine-tool builders which brought these tools and processes to near perfection. It appears that scientific achievements, as measured by the understanding of the mechanics of metal cutting, never again were in step with the practical know-how of the art of metal cutting. This was brought out by Finnie [1][2] in a recent survey of the metal-cutting literature, in which he made the startling revelation that by 1900 the analysis of cutting forces had become almost as well developed as it is today.

Mechanics of Metal Cutting

The model for orthogonal or two-dimensional [2] metal cutting, to which the present investigation will be restricted, is shown in Fig. 1. Here the layer t_0 of the workpiece in the form of a continuous chip without built-up edge is seen to be removed by shearing along the shear plane. This is analogous to a process of stacking of cards on this plane in which small regions of the metal undergo plastic deformation. Subsequently, the chip of thickness t flows along the face of the tool where it encounters friction on the tool-chip interface. The width of the chip remains essentially constant; i.e., $w_0 = w$, and hence the problem is usually treated as one in plane strain. The angle ϕ can be calculated from chip measurements by the equation

$$\phi = \tan^{-1}\left(\frac{r \cos \alpha}{1 - r \sin \alpha}\right) \tag{1}$$

where r is the chip ratio and may be determined by a number of methods as will be shown later. The force system shown in Fig. 1 is required to deform the layer t_0 as it is removed from the workpiece by shearing along the shear plane and to overcome friction as the chip slides up the tool face. The two forces F_H and F_V, which determine the force vector R, may be obtained with a two-component dynamometer. A more comprehensive view of the force system is given by the force circle of Fig. 2, where it is shown that the angle between the resultant force R and the shear plane is given by

$$\lambda = \phi + \beta - \alpha \tag{2}$$

Creveling, Jordan, and Thomsen [2] recently reported that λ of equation (2) appeared to be constant for a given material and speed as rake angle and feed were varied.

A number of attempts have been made to derive the functional angle relationship, $f(\phi, \beta, \alpha) = 0$ from first principles. It appears, however, as noted by Hill [3] that only two of these have any real theoretical significance. These are the so-called Ernst and Merchant [4] solution, which is based on minimum energy, and the Lee and Shaffer [5] solution, which was derived by considering that a portion of the chip behaves like an ideal plastic solid. These solutions are as follows:

Ernst and Merchant solution is

$$\left.\begin{aligned} \phi &= 45 + \alpha/2 - \beta/2 \\ \text{or} \\ \lambda &= 45 - \alpha/2 + \beta/2 \end{aligned}\right\} \tag{3}$$

and Lee and Shaffer solution is

$$\left.\begin{aligned} \phi &= 45 + \alpha - \beta \\ \text{or} \\ \lambda &= 45 = \phi + \beta - \alpha \end{aligned}\right\} \tag{4}$$

It should be mentioned that equation (3) was already considered

[1] The paper is taken in part from the report entitled, "An Application of Plastic Flow Analysis to Orthogonal Metal Cutting," May, 1958, which was the result of an investigation sponsored by the Machinability program located at Rock Island Arsenal, Ill., under Contract DA-11-070-508-ORD-605, with the University of California.

[2] Numbers in brackets indicate References at end of paper.

Contributed by the Metal Process Section of the Production Engineering Division and presented at the Annual Meeting, New York, N. Y., November 30–December 5, 1958, of THE AMERICAN SOCIETY OF MECHANICAL ENGINEERS.

NOTE: Statements and opinions advanced in papers are to be understood as individual expressions of their authors and not those of the Society. Manuscript received at ASME Headquarters, August 4, 1958. Paper No. 58—A-138.

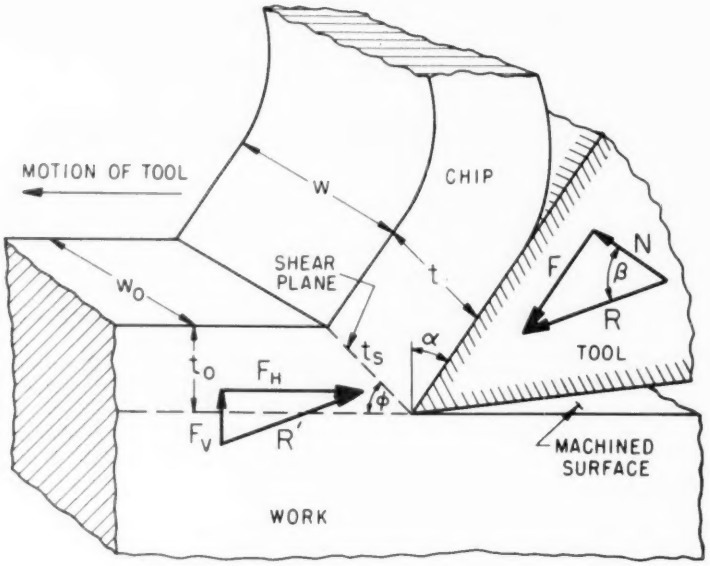

Fig. 1 Model for orthogonal metal cutting

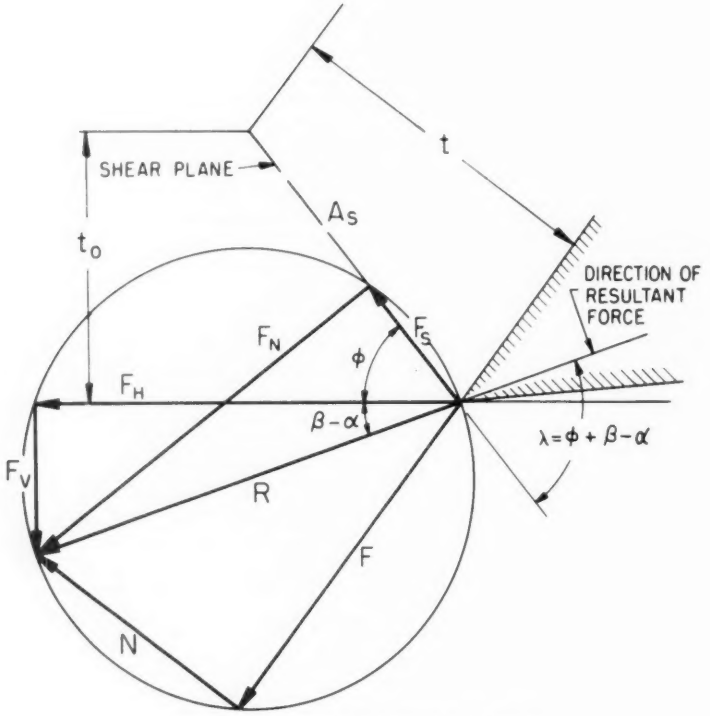

Fig. 2 Force system in orthogonal metal cutting

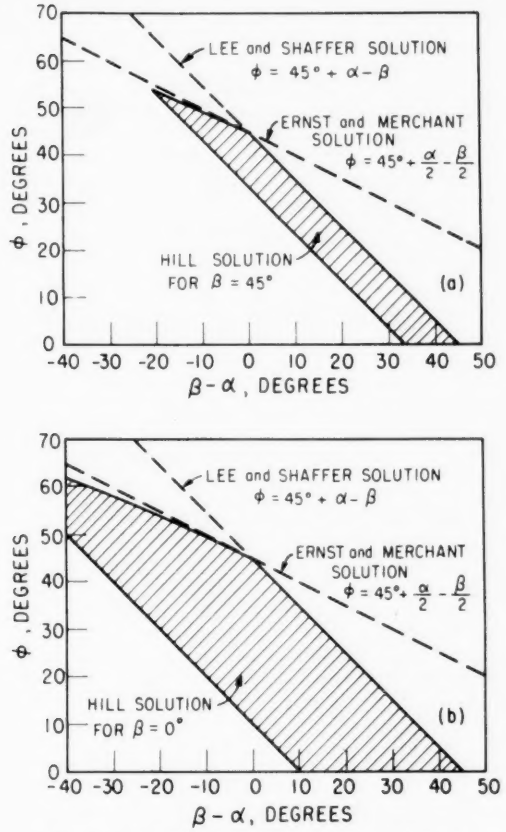
LEE and SHAFFER SOLUTION
$\phi = 45° + \alpha - \beta$
ERNST and MERCHANT SOLUTION
$\phi = 45° + \frac{\alpha}{2} - \frac{\beta}{2}$
HILL SOLUTION FOR $\beta = 45°$
(a)
ϕ, DEGREES
$\beta - \alpha$, DEGREES
LEE and SHAFFER SOLUTION
$\phi = 45° + \alpha - \beta$
ERNST and MERCHANT SOLUTION
$\phi = 45° + \frac{\alpha}{2} - \frac{\beta}{2}$
HILL SOLUTION FOR $\beta = 0°$
(b)
ϕ, DEGREES
$\beta - \alpha$, DEGREES

Fig. 3 Three possible solutions for angle relationship
Lower boundaries for varying α not shown

by Zvorykin [6] of Russia as early as 1893, and was later rediscovered by others [7, 8]. This fact, however, should not have the effect of depreciating the contributions made by Ernst and Merchant [4] and later by Merchant [9], since their work was done independently and certainly has had the effect of reviving the interest of scientists and engineers for work in the field of metal cutting. In addition, Merchant [9] has derived certain fundamental relationships such as shear strain, velocity components, stress components, and others which may be referred to as the basic equations of the mechanics of metal cutting.

The solutions given by equations (3) and (4) are shown by straight lines on the graph of Fig. 3, and have the Cartesian coordinates ϕ and $\beta - \alpha$. The experimental points available in the published literature do not, in general, fall on either of these curves and hence do not agree with equations (3) or (4). This apparent lack of uniqueness has prompted a number of investigators to seek explanations for the nonconformity of real materials with the foregoing theories [9, 10, 11].

Hill [3], in his recent analysis of the mechanics of metal cutting, criticized the solutions represented by equations (3) and (4), in that he states they are incomplete solutions, since the entire state of stress was not examined. Hill [12] then proceeded to analyze the state of stress and using a new principle "on the limits set by plastic yielding to the intensity of singularities of stress," came to the conclusion that it may be fruitless to search for a unique solution. In fact, he proved that for $\beta = 45$ deg and $\beta = 0$ deg as shown in Figs. 3(*a* and *b*), respectively, the angle ϕ of the shear zone may be anywhere in the shaded areas. From this he argued that the actual angle ϕ in a valid steady state cannot be determined unless the complete solution is known. Since complete solutions have not been proposed as yet, it must be assumed that the problem of metal cutting is still unsolved.

Inasmuch as real metals do not necessarily behave like ideal plastic solids, however, it is not certain whether Hill's arguments are valid. A case in point is the data which were observed by Creveling, Jordan, and Thomsen [2], who found that SAE 4135 yielded results which fell outside the limit zones specified by Hill. Thus it appears that no solution on metal cutting is presently in complete agreement with the limited experimental data now available and that the success of obtaining a satisfactory solution probably will not come until more data are published with which any proposed solution may be compared. It is the purpose, therefore, of the present investigation to increase the number of data points now known and to examine the constancy of λ as reported by Creveling, Jordan, and Thomsen [2].

Experimental Procedure

The materials investigated and test conditions are shown in Table 1. All specimens were cut from the same bar or tube to avoid the effects on the cutting conditions of variation in structure and composition. The materials were tested in the as-received condition, except SAE 1112, which also was tested in the annealed condition. The test specimens were finish-turned in an engine lathe before mounting in the four-jaw chuck of a 14-in. × 30-in. American Pacemaker lathe. All tubular specimens were provided with plugs at the chucking end of the specimens to assure rigid mounting. In addition, all specimens were centered accurately (within 0.001 in. fir) before commencing any given test by end cutting.

The dynamometer employed was of the beam type and was equipped with temperature-compensating SR-4 resistance gages, whose response to beam deflection was recorded on a two-channel Brush oscillograph.

The single-point cutting tools consisted of commercial $^5/_8$-in. high-speed-steel tool bits (18-4-1 HSS), which were ground all over. The tools were prepared for each rake angle by grinding the flank so that the tool when mounted in the dynamometer was provided with a 3-deg primary clearance angle. The grinding was performed on a Cincinnati tool and cutter grinder using a carborundum 4-in. × $1^1/_2$-in. AA46-K8-V40 cupped grinding wheel. A secondary clearance angle also was ground on the flank and was approximately 10 deg, leaving a land of about $^3/_{16}$-in. width. The primary clearance angle was redressed on the Cincinnati grinder between each test. The face of the tool also was refinished between each test by hand honing with a hard synthetic Arkansas honing stone. The honing strokes were maintained parallel with the shank of the tool and hence the lay was

Table 1 Materials and test conditions

Material	Dimension of test specimens OD, in.	Wall, in.	Rake-angle range, deg	t_0, feed range, ipr	Average cutting-speed range, fpm
SAE 1112, as-received (cold-rolled)	2.875	0.201	5–40	0.002–0.0098	33.7–170.8
SAE 1112, annealed	2.875	0.201	5–40	0.002–0.0098	33.7–170.8
2024—T4, (24S-T)	4.171	0.200	5–40	0.002–0.0098	570–789
6061—T6, (61S-T)	4.169	0.200	20–40	0.002–0.0098	573
Brass, 85 Cu + 15 Zn, cold drawn	3.462	0.181	20–40	0.002–0.0111	472

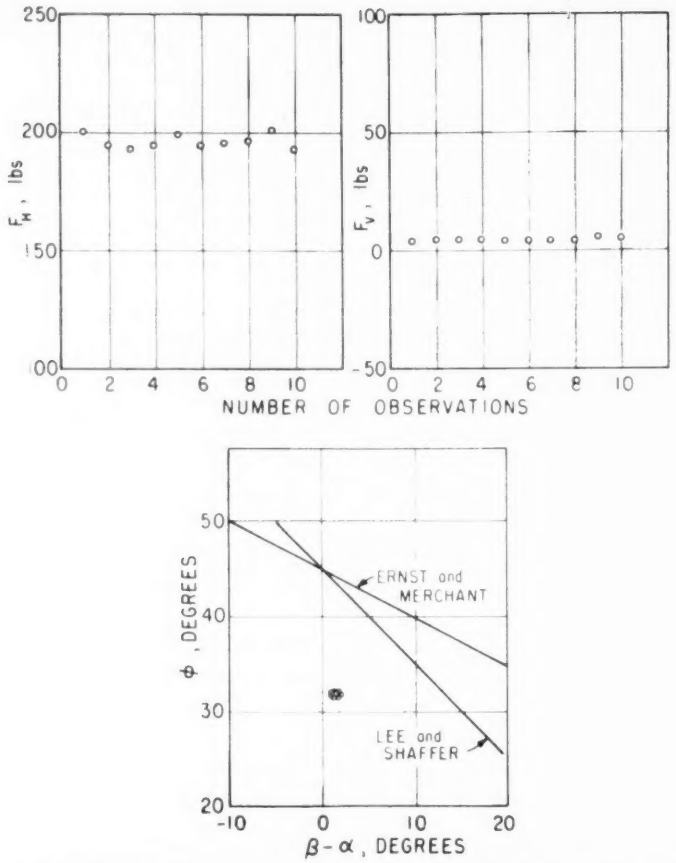

Fig. 4 Reproducibility tests-tool forces and shear angle as function of $(\beta - \alpha)$. Orthogonal cutting; material cut SAE 1112 as-received; speed 33.7 fpm; rake angle 30 deg, feed 0.0063 ipr; cutting fluid air; tool 18-4-1 HSS with 3 deg end clearance.

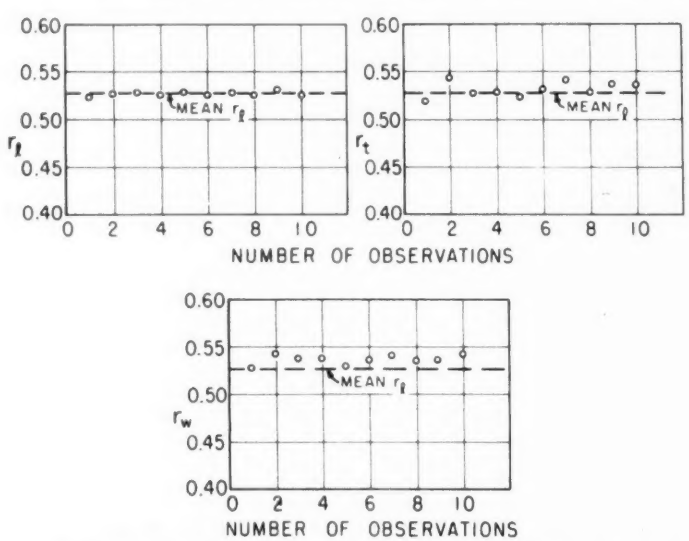

Fig. 5 Reproducibility tests-chip ratios. Orthogonal cutting; material cut SAE 1112 as-received; speed 33.7 fpm; rake angle 30 deg; feed 0.0063 ipr; cutting fluid air; tool 18-4-1 HSS with 3 deg end clearance.

parallel with the direction of chip flow. All tools were finished with a surface finish of better than 5 microin., as determined on an RMS type profilometer.

The limits of feed, speed, and rake angle were dictated in the main by the absence of built-up edge, vibration, tendency for tool to dig in, and formation of segmental or discontinuous type of chips. Thus, for example, segmental chips with each segment still attached to its neighbor to form a continuous ribbon were observed with SAE 1112 at rake angles of less than 5 deg and occasionally even with rake angles equal to 5 deg. Conditions leading to vibration appeared to be present with all nonferrous alloys tested, but the tendency appeared to be least at the cutting speeds indicated in the table.

In order to determine the chip ratios, three methods were used for all continuous chips. They were:

(*a*) $r_l = l/l_0$ = length chip ratio
(*b*) $r_t = t_0/t$ = thickness chip ratio
(*c*) $r_w = wpt_0l_s/W$ = weight-length chip ratio

where the symbols have the following meaning:

l = final length of center line of chip consisting of 5 revolutions of workpiece, as determined from a longitudinal reference slot cut into the test tube. Measurements were made on a special chip-length measuring device.

l_0 = original length of chip when still in workpiece; it is equal to length of center line in mid-point of wall of tube corresponding to 5 revolutions of workpiece.

t_0 = feed on lathe, accurately determined by calibrating actual advance of tool per revolution of workpiece.

t = average thickness at center of 5 representative chips. The thickness was measured in a supermicrometer having modified hardened ball anvils ($^1/_{16}$ in. on smooth or tool side of chip and $^3/_{16}$ in. on rough or air side of chip) and was corrected by subtracting 1.4 times the sum of the surface finishes on both sides of the chip. It was assumed that the roughness profiles were of sinusoidal shape. Least count on micrometer = 0.0001 in.

l_s = length of 10 short flattened chips each approximately 0.3 in. long. The lengths were determined on a Bausch and Lomb contour projector equipped with a graduated sector on its viewing screen corresponding to the curvature of the chips at a magnification of 25:1. Approximate deviation from true length = ±1 per cent.

W = weight of 10 short chips of combined length l_s which was determined in a chainomatic balance having a least count of 0.0001 gram.

ρ = density of materials as determined from a representative sample in chainomatic balance. The densities were as follows:

SAE 1112 as-received	ρ = 127.3 g per cu in. (specific gravity = 7.78)
SAE 1112 annealed	ρ = 127.3 g per cu in. (specific gravity = 7.78)
2024—T4 (24S-T)	ρ = 45.5 g per cu in. (specific gravity = 2.79)
6061—T6 (61S-T)	ρ = 44.4 g per cu in. (specific gravity = 2.71)
Alpha-brass, 85 Cu + 15 Zn cold drawn	ρ = 142.7 g per cu in. (specific gravity = 8.70)

w_0 = width of chip before removal and is equal to wall thickness of tubular specimens. Determination was made with a micrometer with ball-point anvils to an accuracy of 0.001 in.

w = final width of chip. It was determined on flattened chips in a toolmaker's microscope. Measurements were made to 0.0001 in. but rounded off to 0.001 in. in view of the fact that the edges become rough as a result of slight side flow, and the original tube walls were measured with an ordinary micrometer. It was found that the width of the chip may be considered to be constant and that plane-strain conditions evidently prevail. Slight increase in thickness for larger chips was evidently due to edge flow only.

In order to test the reproducibility of all components of the system, ten runs were made with all independent variables held constant. The results are shown in Figs. 4 and 5. It is seen that generally the results reproduce quite well and that the experimental values of F_H are within an estimated accuracy of ±2 per cent. The points representing the calculated shear angle ϕ and difference of angle $(\beta - \alpha)$ group themselves in a small cluster as shown in Fig. 4. The scatter of these points is in good agreement with that calculated from estimated probable errors in F_H, F_V, and r_l.

The chip ratios obtained by three chip-measuring methods are shown in Fig. 5. It is seen that the correlation between methods is generally good. For continuous chips the r_l method was found to have a much smaller probable error than the other methods, presumably because measuring the length of the entire chip tends to average variations in thickness. For discontinuous chips the r_w-method shows a slightly smaller probable error than the r_l-method, the latter being, on the other hand, easier and faster. The correction for roughness in the r_t-method is very important for small feeds where the depth of valleys on the air side of the chip may be a significant fraction of the total chip thickness. For these reasons all calculations for continuous chips were based on r_l and those for discontinuous chips were based on r_w.

Experimental Results and Discussion

The experimental results of the present investigation are given in Tables 3 to 12, inclusive, in the Appendix. In order to conserve space only the original data are shown; all quantities derived from these data are shown only in graphical form. The formulas and experimental variables used to determine all quantities which appear in this paper are summarized in Table 2.

The results of ϕ as a function of $\beta - \alpha$ for SAE 1112 steel in the as-received (cold-rolled) state are shown in Figs. 6 to 8, inclusive, for three cutting speeds varying from 33.7–170.8 fpm,

Table 2 Nomenclature and equations

α = rake angle, deg
$\beta = \tan^{-1}\left\{\dfrac{F_V + F_H \tan \alpha}{F_H - F_V \tan \alpha}\right\}$, friction angle, deg
$\phi = \tan^{-1}\left\{\dfrac{r \cos \alpha}{1 - r \sin \alpha}\right\}$, shear angle, deg
$\lambda = \phi + \beta - \alpha$, deg
r = chip ratio, subscripts, l, t, w, refer to method of determination (see text)
t_0 = thickness of layer of metal removed, in.
t = thickness of chip, in.
w_0 = wall thickness of workpiece, in.
w = width of chip, in.
F_H = force component in direction of motion, lb
F_V = force component normal to direction of motion, lb
$R = (F_H^2 + F_V^2)^{1/2}$, resultant force, lb
$F = R \sin \beta = F_H \sin \alpha + F_V \cos \alpha$, force component parallel to tool face, lb
$N = R \cos \beta = F_H \cos \alpha - F_V \sin \alpha$, force component normal to tool face, lb

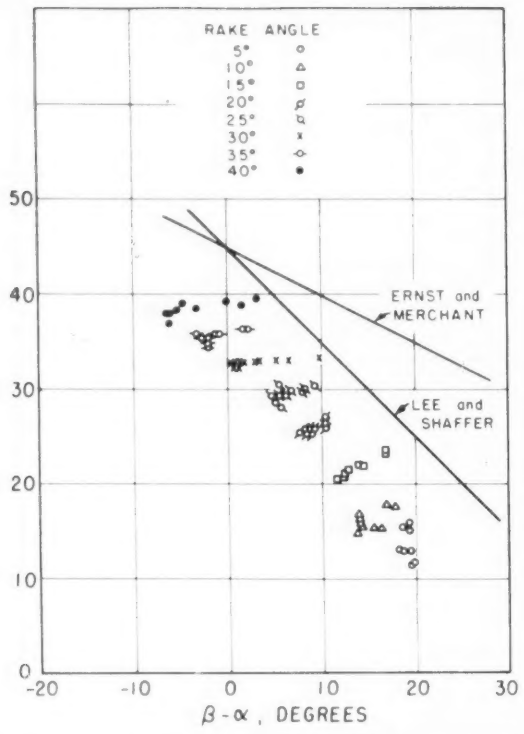

Fig. 6 Shear angle as function of ($\beta - \alpha$) for SAE 1112 as-received at 33.7 fpm. Orthogonal cutting; feeds 0.0020 to 0.0098 ipr; cutting fluid air; tool 18-4-1 HSS with 3 deg end clearance.

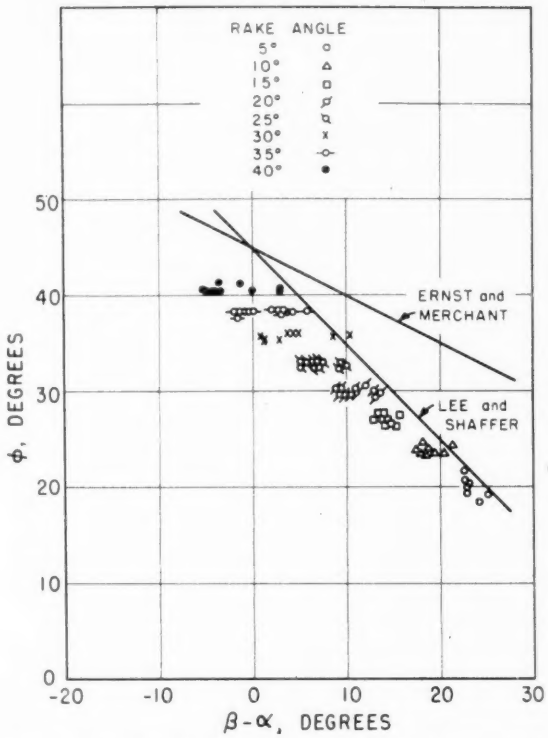

Fig. 7 Shear angle as function of ($\beta - \alpha$) for SAE 1112 as-received at 90.8 fpm. Orthogonal cutting; feeds 0.0020 to 0.0098 ipr; cutting fluid air; tool 18-4-1 HSS with 3 deg end clearance.

feeds from 0.002 to 0.010 ipr, and rake angles from 5 to 40 deg. In addition, all data points obtained with SAE 1112 steel in the as-received and annealed states are shown superimposed for the three speeds investigated in Figs. 9 and 10. In order that $\lambda = \phi + \beta - \alpha$ remain constant, for any particular range of rake angles and feeds, it is necessary that the experimental points fall on a line parallel to the Lee and Shaffer line. It is seen by observation that this condition is not satisfied completely. It appears, in fact, that the average slope of the experimental curves is somewhere between the slopes of the Lee and Shaffer curve and the Ernst and Merchant curve. It should be noted that the data points for the small feeds are generally farthest away from the mean grouping of the data points. This phenomenon may be associated with a size effect [13], as has often been suggested, or possibly with workpiece deformation [14]. It also should be noted that the scatter of data points given in any particular figure is no greater than that which Merchant [9] presented in his original paper and on which he based his proof of the minimum-energy criterion.

Examining Figs. 9 and 10 it may be noted that the data points approach the Lee and Shaffer curve more closely, i.e., $\phi = 45$ deg, as the cutting speed is increased. This fact is more clearly seen in Figs. 11 and 12, where λ has been plotted as a function of cutting speed for SAE 1112 steel in the as-received and annealed states. The data points at each speed have been plotted as functions of α in order to spread out the points.

The remaining data for the aluminum alloys 2024-T4 and 6061-T6 and the alpha-brass are given in Figs. 13 to 15, inclusive. It is seen that the data points of the 2024-T4 aluminum alloys fall above the Lee and Shaffer curve, which is the limiting curve bounding Hill's possible domain for a solution, while the data points of brass have a slope of their own which is even smaller than that of the Ernst and Merchant curve.

From the foregoing it is evident that λ is only approximately constant and that its magnitude appears to depend on cutting speed and material or, perhaps, variables not yet determined. In addition, the functional relationship between ϕ and $\beta - \alpha$, while approximately linear, follows neither the minimum-energy nor the ideal plastic-solid solutions. This agrees with observations recently reported by Pugh [15] and Chisholm [16]. It is evident, therefore, that no single criterion is applicable to the angle relationship in metal cutting and no satisfactory theory is as yet available to account for all the experimental observations.

Conclusions

1 For the materials and cutting conditions investigated, it was found that the angle λ between the resultant force R and the shear plane is constant only to a first approximation; hence $\lambda =$ const is not a unique solution for any given material.

2 The functional relationships between the shear angle, ϕ, and the difference in friction angle and rake angle, $\beta - \alpha$, are only approximately linear.

3 Neither the Ernst and Merchant minimum-energy criterion, nor the ideal plastic-solid solution of Lee and Shaffer, nor that of Hill is in agreement with all the experimental observations.

Acknowledgments

The authors wish to express their thanks to the Rock Island Arsenal without whose support this investigation could not have been carried out. The authors further wish to express their appreciation to the University of California, especially the

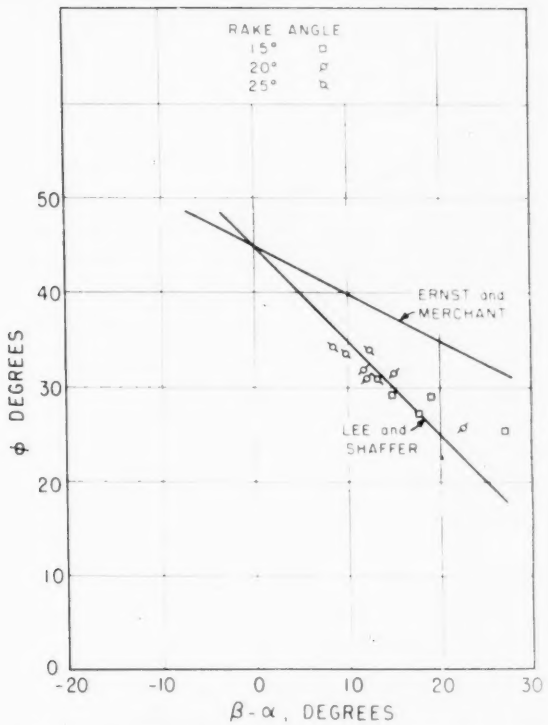

Fig. 8 Shear angle as function of $(\beta - \alpha)$ for SAE 1112 as-received at 170.8 fpm. Orthogonal cutting; feeds 0.0020 to 0.0098 ipr; cutting fluid air; tool 18-4-1 HSS with 3 deg end clearance.

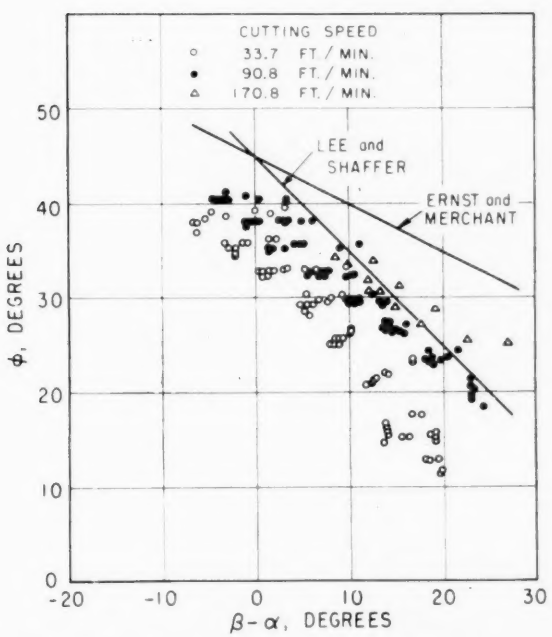

Fig. 9 Shear angle as function of $(\beta - \alpha)$ for SAE 1112 as-received. Orthogonal cutting; rake angles 5–40 deg; feeds 0.0020 to 0.0098 ipr; cutting fluid air; tool 18-4-1 HSS with 3 deg end clearance.

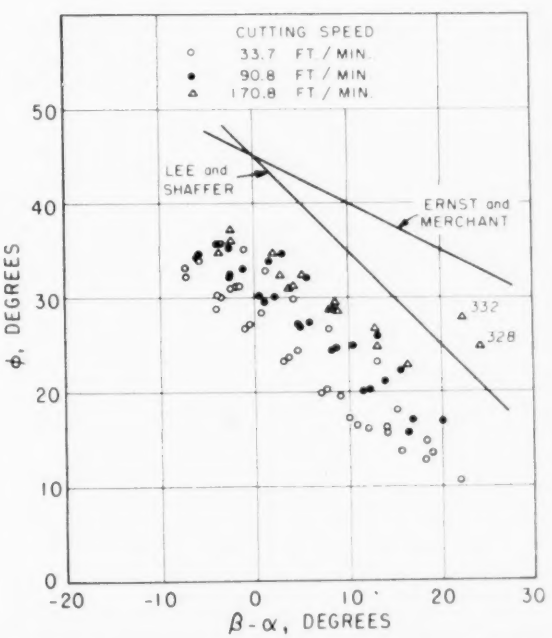

Fig. 10 Shear angle as function of $(\beta - \alpha)$ for SAE 1112 annealed. Orthogonal cutting; rake angles 5–40 deg; feeds 0.0020 to 0.0098 ipr; cutting fluid air; tool 18-4-1 HSS with 3 deg end clearance.

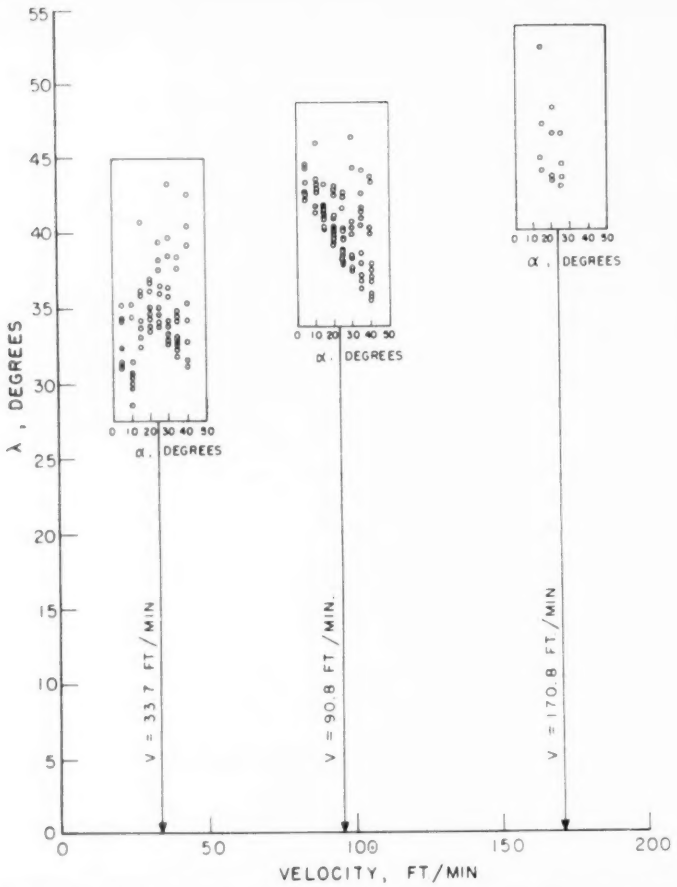

Fig. 11 Angle λ as function of cutting speeds for SAE 1112 as-received. Orthogonal cutting; feeds 0.0020 to 0.0098 ipr; cutting fluid air; tool 18-4-1 HSS with 3 deg end clearance.

Division of Industrial Engineering, for permitting the use of laboratory equipment and facilities. They also wish to thank Miss Matsumoto for typing the paper; Mr. Kot for preparing final graphs; Messrs. Lockrem, Gohl, and Petersen for assisting in the laboratory; Messrs. Schlegel, Dailey, Leontie, Thometz, Kuykendall, students in Engineering, for assisting with the experimental phase of the project.

References

1 I. Finnie, "A Review of the Metal-Cutting Analyses of the Past Hundred Years," *Mechanical Engineering*, vol. 78, 1956, p. 715.

2 J. H. Creveling, T. F. Jordan, and E. G. Thomsen, "Some Studies of Angle Relationships in Metal Cutting," TRANS. ASME, vol. 79, 1957, pp. 127–138.

3 R. Hill, "The Mechanics of Machining: A New Approach," *Journal of the Mechanics and Physics of Solids*, vol. 3, 1954, pp. 47–53.

4 H. Ernst and M. E. Merchant, "Chip Formation, Friction, and High Quality Machined Surfaces," from "Surface Treatment of Metals," *Trans. ASM*, vol. 29, 1941, pp. 299–328.

5 E. H. Lee and B. W. Shaffer, "The Theory of Plasticity Applied to a Problem of Machining," *Journal of Applied Mechanics*, vol. 18, TRANS. ASME, vol. 73, 1951, pp. 405–413.

6 K. A. Zvorykin, "Rabota i Usilie Neobkhodimyya dlya Oteleniya Metallischeskikh Struzhek," Moscow, Russia, 1893.

7 H. Weisbach, editor, "Ingenieur und Maschinenmechanik," part 3, first half, second edition, 1896, p. 825; section written by G. Hermann.

8 Väino Piispanen, "Lastunmuodostumisen Teoriaa," *Teknillinen Aikakauslehti*, vol. 27, 1937, pp. 315–322.

9 M. E. Merchant, "Mechanics of the Metal Cutting Process," *Journal of Applied Physics*, vol. 16, 1945, pp. 267–324.

10 H. Hucks, "Plastizitätsmechanische Grundlagen und Kenngrössen der Zerspannung," Dissertation, Technische Hochschule, Aachen, Germany, February, 1951.

11 Toshio Sata, "Friction Process on Cutting Tool and Cutting Mechanism," *Proceedings* of the Fourth Japan National Congress for Applied Mechanics, 1954.

12 R. Hill, "On the Limits Set by Plastic Yielding to the Intensity of Singularities of Stress," *Journal of the Mechanics and Physics of Solids*," vol. 2, 1954, pp. 278–285.

13 W. R. Backer, E. R. Marshall, and M. C. Shaw, "The Size Effect in Metal Cutting," TRANS. ASME, vol. 74, 1952, pp. 61–72.

14 E. G. Thomsen, J. T. Lapsley, Jr., and R. C. Grassi, "Deformation Work Absorbed by the Workpiece During Metal Cutting," TRANS. ASME, vol. 75, 1953, pp. 591–603.

15 H. Ll. D. Pugh, "Mechanics of the Cutting Process," presented at Conference on Technology of Engineering Manufacture, The Institution of Mechanical Engineers, London, England, March 1958, advance copy, paper 53.

16 A. W. J. Chisholm, "A Review of Some Basic Research on the Machining of Metals," presented at Conference on Technology of Engineering Manufacture, The Institution of Mechanical Engineers, London, England, March 1958, advance copy, paper 58.

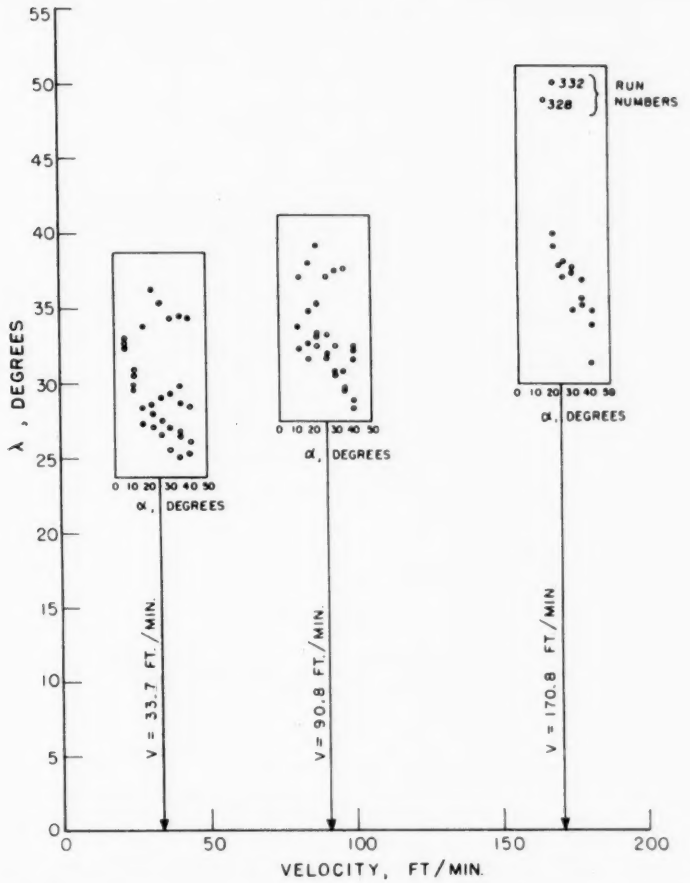

Fig. 12 Angle λ as function of cutting speeds for SAE 1112 annealed. Orthogonal cutting; feeds 0.0020 to 0.0098 ipr; cutting fluid air; tool 18-4-1 HSS with 3 deg end clearance.

APPENDIX

Meaning of Symbols used in Tables 3 to 12

α = rake angle, deg
F_H = force component in direction of motion, lb
F_V = force component normal to direction of motion, lb
t_0 = feed, thousandths of an inch per revolution
r_l = length chip ratio
r_t = thickness chip ratio
r_w = weight chip ratio
w_0 = wall thickness = initial width of chip, in.
w = final width of chip, in.
ϕ = shear angle, deg
l_T = tool-chip contact length, in.

Chip finish —roughness in root-mean-square values, microinches
Tool—refers to measurements on tool side of chip
Air—refers to measurements in center on rough or air side of chip

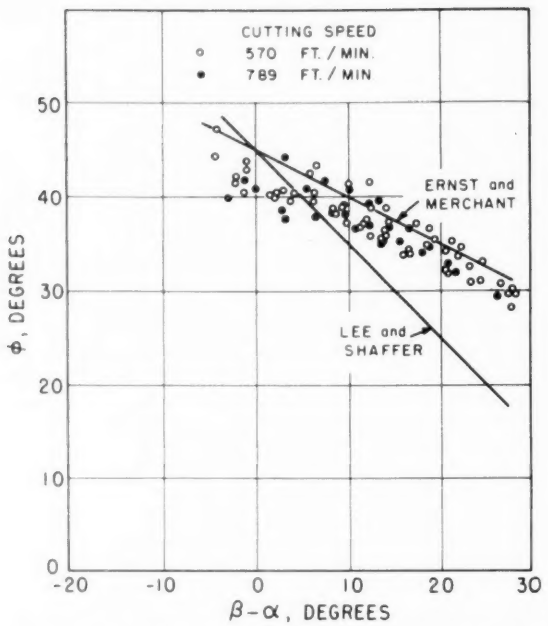

Fig. 13 Shear angle as function of $(\beta - \alpha)$ for aluminum 2024-T4. Orthogonal cutting; rake angles 5–40 deg; feeds 0.0020 to 0.0098 ipr; cutting fluid air; tool 18-4-1 HSS with 3 deg end clearance.

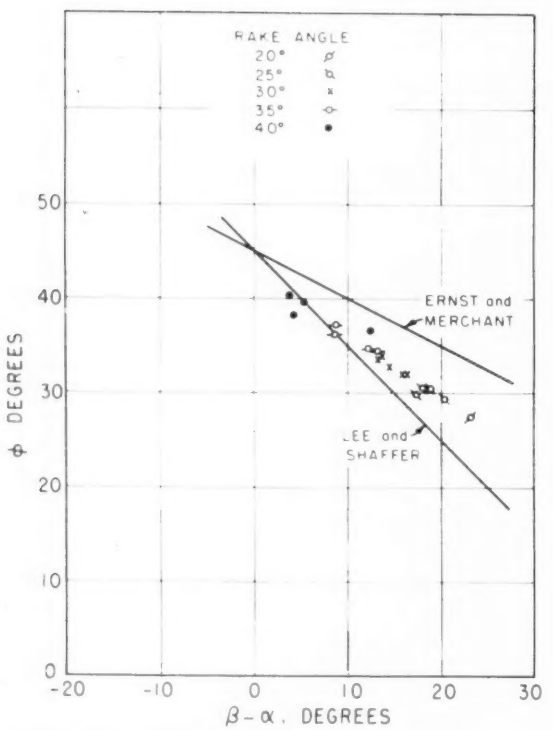

Fig. 14 Shear angle as function of $(\beta - \alpha)$ for aluminum 6061-T6. Orthogonal cutting; speed 573 fpm; feeds 0.0020 to 0.0098 ipr; cutting fluid air; tool 18-4-1 HSS with 3 deg end clearance.

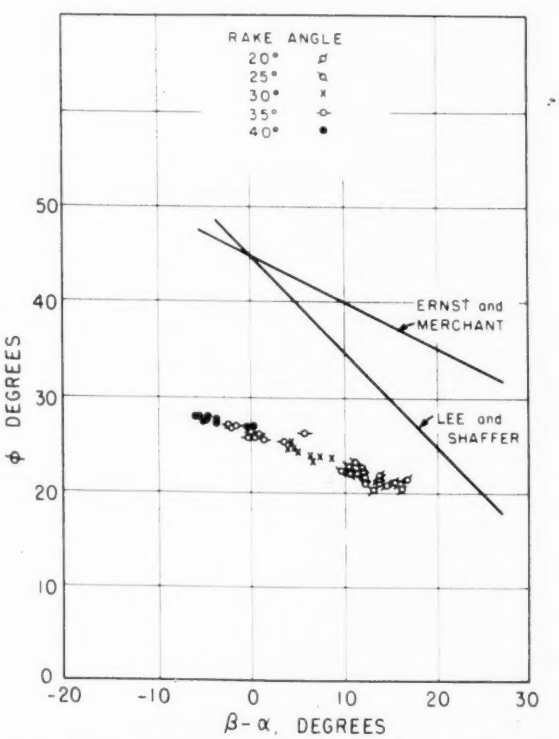

Fig. 15 Shear angle as function of $(\beta - \alpha)$ for alpha-brass. Orthogonal cutting; speed 472 fpm; feeds 0.0020 to 0.0111 ipr; cutting fluid air; tool 18-4-1 HSS with 3 deg end clearance.

Table 3 Cutting data

Work material: SAE 1112 as-received
Tool material: HSS (18-4-1); 3-deg end clearance
Cutting fluid: Air
Outside diameter of tube: 2.875 in.
Mean cutting speed: 33.7 fpm

Run No.	α	F_H	F_v	t_o	Chip Ratios r_l	r_t	r_w	w_o	w	ϕ	l_T Min.	Max.	Chip Finish Tool	Air
26	5	166	60	1.99	0.202	0.189	0.193	0.202	0.201	11.6	0.010	0.013	30	180
27	5	170	60	1.99	0.200	0.191	0.202	0.202	0.202	11.5	0.010	0.014	10	217
29	5	269	89	4.01	0.224	0.224	0.233	0.202	0.200	12.8	0.021	0.026	19	160
30	5	274	90	4.01	0.228	0.218	0.234	0.202	0.201	13.0	0.017	0.027	19	170
33	5	270	95	4.01	0.225	0.214	0.224	0.202	0.201	12.8	0.016	0.022	16	206
31	5	354	124	6.31	0.263	0.251	0.262	0.202	0.202	15.0	0.017	0.031	17	362
32	5	353	123	6.31	0.265	0.256	0.268	0.202	0.201	15.1	0.019	0.035	27	364
34	5	410	143	8.02	0.279	0.269	0.284	0.202	0.201	15.9	0.021	0.034	17	430
35	5	435	145	8.02	0.272	0.266	0.284	0.202	0.201	15.5	0.018	0.032	20	410
36	10	114	36	1.99	0.303	0.278	0.296	0.202	0.201	17.5	0.013	0.017	12	154
37	10	120	36	1.99	0.303	0.286	0.299	0.202	0.202	17.6	0.010	0.011	15	204
38	10	235	65	4.01	0.263	0.254	0.262	0.202	0.202	15.2	0.016	0.020	8	140
40	10	233	68	4.01	0.266	0.258	0.258	0.202	0.201	15.4	0.016	0.020	11	127
41	10	360	88	6.31	0.262	0.259	0.266	0.202	0.200	15.1	0.021	0.029	12	163
42	10	355	90	6.31	0.256	0.241	0.256	0.202	0.200	14.8	0.025	0.031	21	142
44	10	405	103	8.02	0.267	0.259	0.266	0.202	0.202	15.5	0.033	0.038	17	143
45	10	410	103	8.02	0.269	0.260	0.268	0.202	0.201	15.7	0.034	0.036	14	140
46	10	470	118	9.81	0.284	0.273	0.287	0.202	0.200	16.4	0.029	0.043	20	167
47	10	479	119	9.81	0.289	0.280	0.291	0.202	0.201	16.6	0.036	0.042	16	193
48	15	94	29	1.99	0.404	0.392	0.396	0.202	0.200	23.5	0.004	--	14	126
50	15	90	28	1.99	0.397	0.391	0.389	0.202	0.201	23.1	0.008	--	12	133
51	15	178	40	4.01	0.369	0.366	0.374	0.202	0.201	21.5	0.012	0.015	14	136
52	15	178	45	4.01	0.376	0.366	0.370	0.202	0.201	21.9	0.012	0.016	11	157
53	15	173	43	4.01	0.377	0.370	0.377	0.202	0.201	22.0	0.010	0.014	14	140
54	15	273	60	6.31	0.362	0.362	0.372	0.202	0.201	21.1	0.017	0.022	14	183
56	15	267	58	6.31	0.364	0.364	0.371	0.201	0.200	21.2	0.017	0.023	18	163
57	15	405	88	9.81	0.354	0.350	0.365	0.201	0.200	20.7	0.025	0.030	20	137
58	15	412	85	9.81	0.352	0.354	0.364	0.201	0.200	20.6	0.026	0.030	20	170
59	20	87	16	1.99	0.448	0.433	0.437	0.201	0.200	26.5	0.006	0.007	11	117
60	20	88	16	1.99	0.451	0.435	0.445	0.201	0.200	26.6	0.007	0.008	12	137
61	20	158	29	4.01	0.445	0.438	0.445	0.201	0.200	26.3	0.010	0.012	11	157
62	20	155	28	4.01	0.440	0.428	0.436	0.201	0.200	26.0	0.010	0.011	12	147
63	20	234	36	6.31	0.435	0.435	0.446	0.201	0.200	25.7	0.014	0.018	14	147
64	20	230	38	6.31	0.435	0.436	0.448	0.201	0.201	25.7	0.015	0.018	14	153
65	20	290	40	8.02	0.430	0.425	0.432	0.201	0.201	25.4	0.018	0.021	14	140
66	20	285	43	8.02	0.435	0.434	0.449	0.201	0.201	25.7	0.017	0.023	16	160
67	20	348	51	9.81	0.429	0.430	0.430	0.201	0.200	25.4	0.022	0.029	21	160
68	20	351	54	9.81	0.430	0.438	0.452	0.201	0.201	25.4	0.018	0.027	35	180
69	25	79	11.5	1.99	0.501	0.480	0.485	0.201	0.200	29.9	0.008	0.009	14	123
71	25	83	13.5	1.99	0.505	0.486	0.491	0.201	0.201	30.1	0.007	0.008	17	120
72	25	143	17	4.01	0.497	0.493	0.499	0.201	0.201	29.7	0.008	0.010	15	137
73	25	145	20	4.01	0.494	0.490	0.495	0.201	0.201	29.5	0.008	0.011	11	140
74	25	213	17	6.31	0.487	0.491	0.496	0.201	0.201	29.1	0.012	0.015	12	153
75	25	212	20	6.31	0.492	0.491	0.499	0.201	0.201	30.4	0.012	0.014	20	143
77	25	260	27	8.02	0.487	0.490	0.496	0.201	0.201	29.1	0.016	0.020	13	160
78	25	268	25	8.02	0.490	0.480	0.487	0.201	0.200	29.2	0.014	0.018	15	160
79	25	325	28	9.81	0.486	0.500	0.508	0.201	0.200	29.0	0.016	0.021	21	147
80	25	325	32	9.81	0.473	0.485	0.494	0.201	0.201	28.2	0.016	0.020	53	152
81	25	318	28	9.81	0.480	0.483	0.495	0.201	0.201	28.7	0.022	0.033	20	150
82	30	81	14	1.99	0.551	0.530	0.553	0.201	0.200	33.4	0.007	0.008	18	107
83	30	75	7	1.99	0.545	0.515	0.525	0.201	0.201	33.0	0.006	0.007	16	107
84	30	77	9	1.99	0.544	0.522	0.519	0.201	0.201	33.0	0.006	0.007	18	117
85	30	133	8	4.01	0.544	0.535	0.535	0.201	0.202	33.0	0.009	0.011	12	148
86	30	137	7	4.01	0.541	0.534	0.541	0.201	0.202	32.8	0.008	0.010	12	132
87	30	197	6	6.31	0.539	0.536	0.547	0.201	0.200	32.6	0.010	0.014	14	137
88	30	185	1	6.31	0.539	0.540	0.543	0.201	0.200	32.6	0.012	0.015	14	142
89	30	196	5	6.31	0.541	0.544	0.550	0.201	0.200	32.8	0.010	0.012	14	143
90	30	249	3	8.02	0.539	0.526	0.540	0.201	0.201	32.6	0.018	0.021	15	140
91	30	246	6	8.02	0.536	0.534	0.545	0.201	0.200	32.4	0.019	0.021	16	127
92	30	286	5	9.81	0.536	0.538	0.547	0.201	0.201	32.4	0.020	0.027	20	150
93	30	298	5	9.81	0.533	0.544	0.541	0.201	0.201	32.2	0.019	0.031	20	130
94	35	79	2	1.99	0.590	0.545	0.565	0.201	0.201	36.1	0.007	0.007	19	103
95	35	78	3	1.99	0.590	0.533	0.576	0.201	0.200	36.1	0.006	0.006	20	100
96	35	128	-3	4.01	0.586	0.571	0.584	0.201	0.200	35.9	0.008	0.010	17	135
97	35	133	-4	4.01	0.585	0.569	0.578	0.201	0.201	35.8	0.008	0.009	16	130
100	35	125	-2	4.01	0.584	0.583	0.591	0.201	0.201	35.7	0.008	0.009	16	123
98	35	185	-9	6.31	0.579	0.581	0.589	0.201	0.200	35.4	0.012	0.015	15	140
99	35	186	-9	6.31	0.579	0.583	0.589	0.201	0.201	35.4	0.012	0.015	17	160
101	35	230	-13	8.02	0.572	0.565	0.580	0.201	0.201	34.9	0.015	0.020	23	130
102	35	229	-9	8.02	0.578	0.594	0.586	0.201	0.201	35.3	0.013	0.021	22	127
103	35	279	-11	9.81	0.568	0.559	0.567	0.201	0.201	34.6	0.022	0.034	48	157
104	35	280	-11	9.81	0.566	0.572	0.583	0.201	0.201	34.4	0.023	0.032	40	140
105	40	75	4	1.99	0.634	0.603	0.616	0.201	0.200	39.4	0.008	0.009	32	110
106	40	70	0	1.99	0.630	0.598	0.618	0.201	0.200	39.1	0.007	--	28	110
107	40	69	2	1.99	0.625	0.602	0.618	0.201	0.200	38.8	0.007	0.009	33	103
108	40	125	-7	4.01	0.624	0.638	0.612	0.201	0.201	38.5	0.010	0.011	33	130
109	40	124	-10	4.01	0.627	0.609	0.613	0.201	0.200	38.8	--	--	18	130
110	40	178	-17	6.31	0.617	0.638	0.636	0.201	0.200	38.1	0.015	--	23	120
111	40	179	-16	6.31	0.613	0.622	0.615	0.201	0.200	37.8	0.014	0.015	26	127
112	40	210	-24	8.02	0.613	0.620	0.615	0.201	0.200	37.8	0.015	0.018	20	140
113	40	212	-23	8.02	0.613	0.626	0.635	0.201	0.201	37.8	0.015	0.017	22	143
114	40	258	-30	9.81	0.613	0.625	0.629	0.201	0.201	37.8	0.017	0.023	27	150
115	40	260	-26	9.81	0.598	0.603	0.609	0.201	0.201	36.7	0.019	0.023	48	127

Table 4 Cutting data

Work material: SAE 1112 as-received
Tool material: HSS (18-4-1); 3-deg end clearance
Mean cutting speed: 90.8 fpm

Cutting fluid: Air
Outside diameter of tube: 2.875 in.

Run No.	α	F_H	F_v	t_o	Chip Ratios r_l	r_t	r_w	w_o	w	ϕ	l_T Min.	l_T Max.	Chip Finish Tool	Chip Finish Air
220	5	138	62	1.99	--	0.261	0.322	0.200	0.201	18.3	0.006	0.007	19	170
224	5	133	63	1.99	--	0.211	0.342	0.200	0.201	19.3	0.008	0.014	--	--
221	5	173	73	3.14	0.340	0.292	0.344	0.200	0.201	19.2	0.015	0.018	29	261
225	5	205	88	4.01	0.356	0.330	0.358	0.200	0.201	20.1	0.014	0.019	22	178
222	5	233	98	4.89	0.382	0.342	0.377	0.200	0.201	21.5	0.020	--	31	193
223	5	263	111	5.51	0.364	0.346	0.362	0.200	0.201	20.5	0.018	0.022	38	208
226	5	306	130	6.31	0.344	0.326	0.339	0.200	0.202	19.5	0.015	0.024	73	163
228	10	114	45	1.99	--	0.420	0.428	0.200	0.201	24.5	0.010	0.018	11	160
242	10	120	44	1.99	--	0.414	0.413	0.201	0.201	23.7	0.008	0.010	11	117
230	10	187	64	4.01	0.412	0.364	0.407	0.200	0.201	23.7	0.012	0.025	16	150
243	10	190	65	4.01	0.400	0.350	0.395	0.201	0.201	22.9	0.013	0.017	17	177
231	10	271	90	6.31	0.429	0.418	0.425	0.200	0.201	24.5	0.022	0.025	18	180
244	10	275	89	6.31	0.410	0.396	0.411	0.201	0.201	23.5	0.017	0.024	21	173
229	10	344	123	8.02	0.408	0.397	0.403	0.200	0.201	23.4	0.025	0.028	55	182
245	10	340	111	8.02	0.407	0.406	0.415	0.201	0.202	23.3	0.021	0.025	45	163
196	15	119	32	2.75	0.455	0.390	0.445	0.201	0.200	26.5	0.009	0.010	17	140
246	15	130	37	2.75	0.466	0.434	0.460	0.201	0.201	27.2	0.009	0.011	22	177
195	15	164	41	4.01	0.462	0.429	0.452	0.201	0.200	26.9	0.011	0.016	13	166
247	15	170	48	4.01	0.468	0.441	0.473	0.201	0.202	27.3	0.011	0.013	20	163
197	15	189	48	4.89	0.459	0.455	0.458	0.201	0.200	26.7	0.014	0.017	14	136
233	15	193	51	4.89	0.459	0.421	0.454	0.201	0.202	26.7	0.014	0.016	12	157
201	15	242	57	6.31	0.460	0.459	0.468	0.200	0.201	26.8	0.019	0.021	14	147
202	15	245	63	6.31	0.472	0.452	0.473	0.200	0.201	27.5	0.020	0.023	18	140
248	15	249	63	6.31	0.467	0.450	0.474	0.201	0.201	27.3	0.017	0.020	18	175
198	15	305	74	8.02	0.474	0.460	0.478	0.201	0.201	27.5	--	--	27	153
234	15	291	70	8.02	0.461	0.462	0.472	0.201	0.202	26.8	0.018	0.020	19	173
199	15	372	97	9.81	0.459	0.467	0.475	0.201	0.200	26.7	0.023	0.024	29	160
235	15	395	110	9.81	0.446	0.432	0.452	0.201	0.201	26.1	0.030	0.035	43	183
140	20	100	24	1.99	0.493	0.465	0.467	0.201	0.201	29.1	0.009	--	16	125
141	20	103	25	1.99	0.499	0.442	0.476	0.201	0.201	29.5	0.008	--	15	115
203	20	74	18	1.99	0.499	0.469	0.495	0.200	0.200	29.5	0.007	--	17	123
249	20	87	21	1.99	0.500	0.470	0.487	0.201	0.201	29.6	0.008	0.009	15	120
142	20	158	37	4.01	0.504	0.482	0.495	0.201	0.200	29.7	0.012	--	18	150
143	20	165	33	4.01	0.500	0.498	0.502	0.201	0.201	29.6	0.011	--	11	147
236	20	155	34	4.01	0.514	0.502	0.514	0.201	0.201	30.3	0.011	0.012	28	150
144	20	230	45	6.31	0.503	0.520	0.520	0.201	0.200	29.7	0.015	0.017	13	163
145	20	233	45	6.31	0.500	0.499	0.507	0.201	0.201	29.6	0.015	0.016	18	170
200	20	232	41	6.31	0.506	0.495	0.499	0.200	0.201	29.9	0.015	0.016	18	147
250	20	229	41	6.31	0.502	0.503	0.501	0.201	0.202	29.7	0.014	0.018	12	163
146	20	280	53	8.02	0.502	0.497	0.507	0.201	0.200	29.7	0.017	0.019	17	158
147	20	260	45	8.02	0.500	0.503	0.513	0.201	0.201	29.6	0.016	0.018	15	160
148	20	275	48	8.02	0.499	0.493	0.501	0.201	0.201	29.5	0.020	0.021	18	148
251	20	274	51	8.02	0.500	0.500	0.518	0.201	0.202	29.6	0.017	0.018	17	170
149	20	333	58	9.81	0.505	0.507	0.518	0.201	0.201	29.8	0.020	0.021	35	173
151	20	335	55	9.81	0.506	0.505	0.518	0.201	0.201	29.9	0.019	0.021	27	187
237	20	327	54	9.81	0.505	0.505	0.515	0.201	0.201	29.8	0.020	0.021	22	163
152	25	84	15	1.99	0.540	0.529	0.523	0.201	0.201	32.4	0.008	--	22	117
153	25	85	15	1.99	0.539	0.511	0.528	0.201	0.201	32.3	0.008	--	20	127
204	25	78	13	1.99	0.536	0.532	0.528	0.200	0.200	32.1	0.008	--	20	123
154	25	139	19	4.01	0.544	0.552	0.552	0.201	0.200	32.6	0.011	--	25	150
155	25	144	18	4.01	0.545	0.537	0.534	0.201	0.201	32.7	0.012	0.014	16	170
205	25	139	18	4.01	0.545	0.526	0.554	0.200	0.201	32.7	0.010	0.011	15	127
156	25	212	26	6.31	0.542	0.551	0.554	0.201	0.201	32.5	0.014	0.015	26	150
157	25	205	24	6.31	0.541	0.547	0.545	0.201	0.200	32.4	0.014	0.015	21	153
158	25	262	27	8.02	0.544	0.548	0.563	0.201	0.201	32.6	0.017	0.019	22	163
159	25	259	26	8.02	0.542	0.542	0.552	0.201	0.202	32.5	0.016	0.017	19	140
206	25	258	25	8.02	0.541	0.535	0.549	0.200	0.201	32.4	0.017	--	14	147
160	25	312	30	9.81	0.545	0.541	0.558	0.201	0.201	32.7	0.020	0.021	22	157
161	25	320	34	9.81	0.545	0.563	0.559	0.201	0.201	32.7	0.020	0.021	25	165
162	30	76	12	1.99	0.580	0.534	0.562	0.201	0.200	35.3	0.007	--	25	123
163	30	79	15	1.99	0.583	0.571	0.571	0.201	0.200	35.6	0.007	0.008	28	117
164	30	135	11	4.01	0.583	0.576	0.582	0.201	0.201	35.6	0.009	--	27	130
165	30	135	10	4.01	0.583	0.565	0.570	0.201	0.201	35.6	0.010	0.011	27	147
238	30	134	12	4.01	0.584	0.575	0.580	0.201	0.201	35.6	0.010	0.011	25	153
166	30	200	11	6.31	0.578	0.575	0.575	0.201	0.201	35.2	--	--	21	137
167	30	198	10	6.31	0.580	0.567	0.579	0.201	0.201	35.3	0.013	0.015	22	140
168	30	248	10	8.02	0.578	0.583	0.581	0.201	0.201	35.2	0.017	0.018	17	153
169	30	242	10	8.02	0.578	0.582	0.592	0.201	0.201	35.2	0.016	0.017	15	140
170	30	300	12	9.81	0.581	0.575	0.584	0.201	0.201	35.4	0.019	0.022	24	150
171	30	293	13	9.81	0.577	0.579	0.580	0.201	0.201	35.1	0.021	0.023	33	137
172	35	74	6	1.99	0.617	0.568	0.600	0.202	0.200	38.0	0.007	0.008	28	110
173	35	76	8	1.99	0.619	0.568	0.603	0.202	0.200	38.1	0.007	0.008	35	120
174	35	129	8	4.01	0.620	0.609	0.617	0.202	0.200	38.2	0.010	0.011	25	120
175	35	132	5	4.01	0.621	0.597	0.605	0.202	0.200	38.3	0.011	--	48	127
176	35	189	11	6.31	0.617	0.615	0.623	0.202	0.201	38.0	0.013	--	37	120
177	35	188	9	6.31	0.619	0.622	0.623	0.202	0.201	38.1	0.013	0.014	40	130
240	35	185	-2	6.31	0.611	0.610	0.601	0.201	0.201	37.6	0.013	0.017	40	143
178	35	233	-1	8.02	0.617	0.630	0.625	0.202	0.201	38.0	0.018	0.020	28	150
179	35	228	2	8.02	0.618	0.603	0.608	0.202	0.201	38.1	0.016	0.019	17	127
181	35	273	-5	9.81	0.617	0.615	0.635	0.202	0.201	38.0	0.019	0.020	26	127
182	35	285	-7	9.81	0.611	0.624	0.630	0.202	0.201	37.5	0.019	0.020	19	123
183	35	272	-6	9.81	0.617	0.620	0.621	0.201	0.201	38.0	0.018	0.019	23	147
184	40	69	4	1.99	0.647	0.600	0.633	0.201	0.200	40.4	0.008	0.009	58	100
185	40	69	4	1.99	0.644	0.570	0.629	0.201	0.200	40.1	0.007	--	43	112
192	40	126	0	4.01	0.648	0.559	0.640	0.201	0.200	40.3	0.012	--	44	128
194	40	118	-2	4.01	0.655	0.650	0.655	0.201	0.200	40.9	0.009	0.010	47	117
190	40	173	-10	6.31	0.648	0.645	0.653	0.201	0.200	40.3	0.014	0.015	53	133
191	40	174	-11	6.31	0.648	0.646	0.652	0.201	0.200	40.3	0.014	0.015	28	120
241	40	173	-9	6.31	0.647	0.650	0.648	0.201	0.201	40.4	0.016	0.019	50	112
188	40	212	-16	8.02	0.645	0.642	0.655	0.201	0.201	40.2	0.020	0.025	33	117
189	40	210	-12	8.02	0.651	0.660	0.652	0.201	0.200	41.2	0.019	0.021	50	110
186	40	263	-19	9.81	0.644	0.645	0.661	0.201	0.201	40.1	0.030	0.035	38	138
187	40	256	-22	9.81	0.646	0.648	0.657	0.201	0.201	40.4	0.025	0.027	38	120

Table 5 Cutting data

Work material: SAE 1112 as-received
Tool material: HSS (18-4-1); 3-deg end clearance
Cutting fluid: Air
Outside diameter of tube: 2.875 in
Mean cutting speed: 170.8 fpm

Run No.	α	F_H	F_v	t_o	Chip Ratios r_l	r_t	r_w	w_o	w	ϕ	l_T Min.	Max.	Chip Finish Tool	Air
208	15	95	30	1.99	--	0.446	0.470	0.200	0.201	27.3	0.010	0.015	43	120
207	15	168	45	4.01	0.499	0.494	0.494	0.200	0.201	29.0	0.011	0.013	16	165
210	15	233	81	5.51	0.479	0.477	0.478	0.200	0.201	27.9	0.017	--	137	140
209	15	336	171	7.35	0.434	0.422	0.445	0.200	0.201	25.3	0.016	--	200	143
211	20	85	23	1.99	0.528	0.521	0.511	0.200	0.201	31.2	0.010	--	29	113
212	20	179	38	4.89	0.535	0.521	0.531	0.200	0.201	31.6	0.012	0.014	27	127
213	20	265	58	7.35	0.525	0.524	0.527	0.200	0.201	30.9	0.014	0.017	35	147
215	20	429	179	9.81	0.432	0.411	0.449	0.200	0.202	25.5	0.040	0.050	93	168
216	25	84	19	1.99	0.559	0.550	0.564	0.200	0.201	33.6	0.007	0.008	54	117
217	25	170	26	4.89	0.569	0.558	0.580	0.200	0.201	34.2	0.012	0.014	46	147
218	25	256	45	7.35	0.557	0.546	0.566	0.200	0.201	33.5	0.016	0.018	103	163
219	25	355	85	9.81	0.521	0.509	0.528	0.200	0.201	30.8	0.020	0.022	75	160

Table 6 Cutting data

Work material SAE 1112 annealed
Tool material: HSS (18-4-1); 3-deg end clearance
Cutting fluid: Air
Outside diameter of tube: 2.875 in.
Mean cutting speed: 33.7 fpm

Run No.	α	F_H	F_v	t_o	Chip Ratios r_l	r_t	r_w	w_o	w	ϕ	l_T Min.	Max.	Chip Finish Tool	Air
291	5	178	71	1.99	0.191	0.173	0.194	0.201	0.202	10.8	0.013	0.014	8	210
292	5	333	115	4.89	0.237	0.216	0.227	0.201	0.205	13.5	0.022	0.024	10	383
293	5	443	147	7.35	--	0.232	0.257	0.201	0.204	14.7	--	--	12	308
294	10	165	53	1.99	0.214	0.183	0.192	0.201	0.205	12.7	0.013	0.014	12	207
296	10	313	88	4.89	0.241	0.224	0.241	0.201	0.204	13.9	0.025	0.027	10	190
295	10	410	104	7.35	0.266	0.259	0.268	0.201	0.204	15.6	0.029	0.032	10	210
297	10	518	132	9.81	--	0.275	0.286	0.201	0.205	16.5	0.036	0.038	13	230
298	15	110	30	1.99	0.312	0.299	0.321	0.201	0.203	18.1	0.009	0.011	12	160
299	15	266	57	4.89	0.278	0.262	0.274	0.201	0.203	16.2	0.020	0.023	10	180
300	15	366	71	7.35	0.285	0.275	0.293	0.201	0.203	16.5	0.029	0.031	10	200
301	15	459	83	9.81	0.294	0.284	0.295	0.201	0.205	17.1	0.037	0.039	13	220
302	20	98	23	1.99	0.394	0.368	0.375	0.201	0.201	23.1	0.008	0.009	11	160
303	20	218	35	4.89	0.333	0.320	0.329	0.201	0.203	19.5	0.016	0.017	9	170
304	20	316	44	7.35	0.344	0.327	0.340	0.201	0.202	20.1	0.024	0.027	11	210
305	20	396	50	9.81	0.340	0.337	0.350	0.201	0.203	19.9	--	--	10	180
306	25	85	12	1.99	0.450	0.417	0.436	0.201	0.201	26.7	0.007	0.008	15	150
307	25	190	16	4.89	0.411	0.378	0.410	0.201	0.203	24.3	0.014	0.015	9	190
308	25	269	18	7.35	0.401	0.382	0.405	0.201	0.203	23.7	0.021	0.023	11	190
309	25	349	20	9.81	0.394	0.378	0.395	0.201	0.202	23.2	0.026	0.028	10	170
310	30	78	6	1.99	0.497	0.453	0.485	0.201	0.202	29.9	0.007	0.008	12	140
311	30	160	3	4.89	0.476	0.450	0.468	0.201	0.202	28.5	0.012	0.014	10	160
312	30	238	-1	7.35	0.456	0.432	0.451	0.201	0.202	27.2	0.016	0.017	13	180
313	30	305	-5	9.81	0.450	0.442	0.466	0.201	0.202	26.7	0.021	0.023	14	200
325	35	79	2	1.99	0.545	0.480	0.530	0.201	0.201	33.0	0.007	0.008	19	160
324	35	156	-6	4.89	0.515	0.481	0.515	0.201	0.202	30.9	0.012	0.013	15	147
315	35	148	-6	4.89	0.520	0.505	0.517	0.201	0.202	31.3	0.011	0.012	14	150
323	35	225	-13	7.35	0.503	0.488	0.510	0.201	0.203	30.0	0.016	0.017	16	168
317	35	214	-14	7.35	0.506	0.488	0.507	0.201	0.203	30.3	0.017	0.018	14	137
322	35	289	-19	9.81	0.487	0.491	0.495	0.201	0.202	28.9	0.021	0.023	22	206
318	40	72	-1	1.99	0.577	0.535	0.562	0.201	0.201	35.2	0.007	0.008	20	110
319	40	144	-14	4.89	0.564	0.541	0.546	0.201	0.201	34.1	0.012	0.013	17	160
320	40	195	-24	7.35	0.550	0.531	0.556	0.201	0.203	33.1	0.017	0.018	15	180
321	40	254	-31	9.81	0.539	0.526	0.541	0.201	0.202	32.3	--	--	21	163

Table 7 Cutting data

Work material: SAE 1112 annealed
Tool material: HSS (18-4-1); 3-deg end clearance
Mean cutting speed: 90.8 fpm

Cutting fluid: Air
Outside diameter of tube: 2.875 in.

Run No.	α	F_H	F_v	t_o	Chip Ratios r_l	r_t	r_w	w_o	w	ϕ	l_T Min.	Max.	Chip Finish Tool	Air
272	10	131	48	1.99	--	0.218	0.295	0.201	0.203	17.0	0.013	0.017	--	--
273	10	256	77	4.89	0.294	0.272	0.310	0.201	0.203	17.0	0.021	0.022	12	280
274	10	392	115	7.35	--	0.253	0.276	0.201	0.204	16.0	0.032	0.035	56	223
256	15	118	33	1.99	--	0.330	0.384	0.201	0.202	22.4	0.010	0.012	28	160
257	15	218	53	4.89	0.362	0.339	0.360	0.201	0.202	21.1	0.020	0.022	16	263
258	15	319	69	7.35	0.350	0.330	0.347	0.201	0.202	20.4	0.023	0.024	9	240
259	15	414	84	9.81	0.345	0.335	0.356	0.201	0.203	20.1	0.033	0.035	14	263
260	20	90	21	1.99	0.440	0.395	0.427	0.201	0.201	26.0	0.007	0.008	18	170
261	20	195	36	4.89	0.422	0.409	0.422	0.201	0.202	24.9	0.014	0.015	15	214
262	20	275	40	7.35	0.412	0.400	0.417	0.201	0.202	24.3	0.020	0.021	13	223
286	20	286	43	7.35	0.416	0.406	0.420	0.201	0.202	24.6	--	--	16	197
263	20	364	56	9.81	0.415	0.400	0.416	0.201	0.202	24.5	--	--	68	238
264	25	82	12	1.99	0.482	0.396	0.465	0.201	0.202	28.8	0.008	0.009	17	173
265	25	174	18	4.89	0.460	0.294	0.466	0.201	0.202	27.4	0.012	0.013	12	223
266	25	251	22	7.35	0.453	0.674	0.455	0.201	0.202	27.0	0.018	0.020	15	200
267	25	326	26	9.81	0.456	0.447	0.461	0.201	0.203	27.1	0.025	0.026	15	233
268	30	82	8	1.99	0.529	0.444	0.495	0.201	0.202	31.9	0.007	0.008	22	137
269	30	159	6	4.89	0.504	0.486	0.504	0.201	0.203	30.3	0.012	0.013	16	215
270	30	235	5	7.35	0.494	0.498	0.501	0.201	0.202	29.6	0.017	0.018	21	203
271	30	295	3	9.81	0.502	0.488	0.488	0.201	0.202	30.2	0.028	0.032	18	180
276	35	72	4	1.99	0.566	0.527	0.563	0.201	0.202	34.5	0.007	0.008	29	127
277	35	145	-3	4.89	0.545	0.530	0.545	0.201	0.201	33.0	0.013	0.014	20	167
278	35	220	-10	7.35	0.535	0.516	0.528	0.201	0.202	32.3	0.016	0.017	16	173
279	35	283	-13	9.81	0.533	0.540	0.543	0.201	0.203	32.2	0.022	0.023	15	173
280	40	68	2	1.99	--	0.570	0.562	0.201	0.200	34.0	0.008	--	--	150
281	40	144	-9	4.89	0.585	0.559	0.595	0.201	0.202	35.8	0.012	0.014	25	153
284	40	148	-10	4.89	0.584	0.584	0.566	0.201	0.202	35.6	0.011	0.012	26	147
282	40	213	-10	7.35	0.576	0.562	0.569	0.201	0.202	35.1	0.018	0.026	28	153
285	40	201	-20	7.35	0.570	0.555	0.580	0.201	0.202	34.6	0.018	0.019	18	173
283	40	266	-27	9.81	0.564	0.572	0.581	0.201	0.202	34.1	0.022	0.033	28	160

Table 8 Cutting data

Work material: SAE 1112 annealed
Tool material: HSS (18-4-1); 3-deg end clearance
Cutting speed: 170.8 fpm

Cutting fluid: Air
Outside diameter of tube: 2.875 in.

Run No.	α	F_H	F_v	t_o	Chip Ratios r_l	r_t	r_w	w_o	w	ϕ	l_T Min.	Max.	Chip Finish Tool	Air
328	15	245	110	4.89	0.425	0.383	0.416	0.201	0.204	24.8	.040	--	85	210
332	20	224	92	4.89	0.471	0.427	0.471	0.201	0.202	27.8	0.020	0.035	70	200
334	20	193	45	4.89	0.455	0.437	0.454	0.201	0.202	26.8	0.019	--	75	220
331	20	303	90	7.35	0.386	0.374	0.407	0.201	0.203	22.7	0.025	0.040	90	210
336	25	184	28	4.89	0.494	0.481	0.484	0.201	0.202	29.5	0.016	0.019	28	200
337	25	261	39	7.35	0.481	0.469	0.480	0.201	0.202	28.8	0.021	0.022	35	172
338	25	364	84	9.81	0.422	0.428	0.438	0.201	0.203	24.9	0.025	0.050	95	217
340	30	169	16	4.89	0.537	0.505	0.484	0.201	0.201	32.4	0.013	0.018	45	183
341	30	244	16	7.35	0.516	0.483	0.526	0.201	0.202	31.1	0.018	0.020	33	160
342	30	336	54	9.81	0.472	0.471	0.474	0.201	0.202	28.2	0.022	0.024	200	190
344	35	161	6	4.89	0.570	0.543	0.558	0.201	0.202	34.8	0.013	0.015	45	170
345	35	239	12	7.35	0.536	0.532	0.554	0.201	0.203	32.4	0.018	0.019	33	170
346	35	319	25	9.81	0.521	0.492	0.524	0.201	0.203	31.3	0.021	0.035	75	180
348	40	143	-6	4.89	0.605	0.605	0.614	0.201	0.200	37.2	0.012	0.013	20	140
349	40	222	-8	7.35	0.589	0.539	0.574	0.201	0.202	36.0	0.017	0.018	45	150
350	40	264	-16	9.81	0.574	0.608	0.578	0.201	0.203	34.8	0.022	0.024	66	170

Table 9 Cutting data

Work material: 2024-T4 aluminum alloy
Tool material: HSS (18-4-1); 3-deg end clearance
Mean cutting speed: 570 fpm

Cutting fluid: Air
Outside diameter of tube: 4.171 in

Run No.	α	F_H	F_v	t_o	Chip Ratios r_l	r_t	r_w	w_o	w	ϕ	l_T Min.	l_T Max.	Chip Finish Tool	Chip Finish Air
432	5	84	50	1.99	0.521	0.550	0.523	0.200	0.200	28.8	--	--	47	140
503	5	79	51	1.99	0.512	0.533	0.536	0.200	0.202	28.1	--	--	18	123
431	5	144	75	4.01	0.517	0.501	0.543	0.200	0.200	28.4	0.008	0.009	11	233
433	5	159	84	4.89	0.548	0.527	0.552	0.200	0.203	29.8	0.013	0.015	5	257
504	5	166	85	4.89	0.550	0.523	0.555	0.200	0.202	29.9	0.013	0.014	8	162
434	5	216	87	7.35	--	0.621	0.636	0.200	0.203	33.8	0.016	0.018	6	300
505	5	215	88	7.35	--	0.635	0.655	0.200	0.202	34.7	0.016	0.017	7	232
435	5	277	89	9.81	--	0.682	0.720	0.200	0.203	37.4	0.018	0.020	19	312
506	5	269	88	9.81	--	0.649	0.740	0.200	0.203	38.2	0.018	0.019	--	325
436	10	74	37	1.99	0.547	0.561	0.529	0.200	0.200	30.7	--	--	33	123
507	10	72	38	1.99	0.537	0.547	0.537	0.200	0.201	30.3	0.011	0.012	24	118
437	10	153	69	4.89	0.551	0.550	0.568	0.200	0.201	31.0	0.014	0.015	9	200
508	10	166	71	4.89	0.548	0.532	0.588	0.200	0.202	30.8	0.015	0.016	6	218
438	10	206	73	7.35	--	0.596	0.642	0.200	0.203	35.4	0.017	0.018	6	217
509	10	209	72	7.35	--	0.578	0.638	0.200	0.202	35.2	0.018	0.019	5	208
510	10	212	70	7.35	--	0.594	0.625	0.200	0.202	34.7	0.018	0.019	4	218
439	10	263	67	9.81	--	0.651	0.680	0.200	0.203	37.2	0.018	0.019	8	290
511	10	254	69	9.81	--	0.650	0.685	0.200	0.203	35.6	0.019	0.020	10	180
440	15	68	31	1.99	0.573	0.587	0.554	0.200	0.200	33.0	--	--	30	152
512	15	70	30	1.99	0.564	0.552	0.547	0.200	0.200	32.6	0.010	0.012	34	117
441	15	148	55	4.89	0.555	0.524	0.555	0.200	0.202	32.1	0.014	0.015	23	213
513	15	144	54	4.89	0.552	0.540	0.559	0.200	0.201	31.9	0.015	0.016	11	165
442	15	203	60	7.35	--	0.576	0.600	0.200	0.203	34.5	0.016	0.017	8	207
514	15	198	56	7.35	--	0.594	0.623	0.200	0.202	35.7	0.016	0.017	5	195
443	15	243	49	9.81	--	0.596	0.650	0.200	0.204	37.0	0.018	0.019	11	243
515	15	239	49	9.81	--	0.616	0.654	0.200	0.202	37.3	0.018	0.019	15	210
444	20	68	26	1.99	0.600	0.624	0.636	0.200	0.200	35.3	0.012	0.014	38	130
516	20	63	24	1.99	0.585	0.630	0.582	0.200	0.200	34.5	0.008	0.009	25	115
445	20	145	43	4.89	0.578	0.567	0.560	0.200	0.200	34.1	0.016	0.020	21	193
517	20	138	40	4.89	0.573	0.562	0.587	0.200	0.200	33.8	--	--	19	165
446	20	195	47	7.35	--	0.580	0.607	0.200	0.203	35.7	0.017	0.018	6	227
447	20	200	48	7.35	0.605	0.594	0.638	0.200	0.202	35.6	0.017	0.018	4	192
518	20	194	48	7.35	--	0.590	0.612	0.200	0.202	36.0	0.019	0.020	12	192
448	20	239	38	9.81	--	0.632	0.666	0.200	0.202	39.0	0.017	0.018	3	197
519	20	234	39	9.81	--	0.638	0.666	0.200	0.202	39.1	0.021	0.022	4	177
449	25	62	21	1.99	0.613	0.628	0.605	0.200	0.200	36.8	0.007	0.009	36	130
520	25	61	19	1.99	0.616	0.612	0.630	0.200	0.200	37.1	0.007	0.008	17	132
450	25	138	34	4.89	0.606	0.588	0.610	0.200	0.200	36.5	0.012	0.013	21	147
521	25	133	29	4.89	0.598	0.592	0.586	0.200	0.201	35.9	0.014	0.015	24	162
451	25	195	39	7.35	0.613	0.595	0.615	0.200	0.201	36.8	0.017	0.018	10	135
522	25	195	33	7.35	--	0.626	0.617	0.200	0.201	37.1	0.016	0.017	19	182
452	25	235	26	9.81	--	0.641	0.671	0.200	0.203	40.4	0.018	0.019	7	185
523	25	234	25	9.81	--	0.631	0.661	0.200	0.202	39.7	0.018	0.019	9	187
453	30	61	18	1.99	--	0.579	0.592	0.200	0.200	36.1	0.013	0.014	30	70
524	30	61	15	1.99	0.631	0.653	0.668	0.200	0.200	38.6	0.006	0.008	20	110
454	30	129	28	4.89	0.633	0.637	0.629	0.200	0.200	38.7	0.014	0.015	22	137
525	30	126	19	4.89	0.625	0.627	0.610	0.200	0.200	38.2	0.014	0.015	52	170
455	30	183	27	7.35	0.634	0.632	0.648	0.200	0.202	38.7	0.016	0.017	8	137
526	30	180	19	7.35	--	0.647	0.654	0.200	0.202	40.1	0.016	0.017	16	192
456	30	226	12	9.81	--	0.628	0.665	0.200	0.202	40.8	0.018	0.020	8	150
527	30	219	14	9.81	--	0.645	0.645	0.200	0.202	39.5	0.019	0.020	8	192
457	35	58	10	1.99	0.665	0.674	0.650	0.200	0.200	41.4	--	--	27	63
528	35	60	13	1.99	0.666	0.668	0.667	0.200	0.200	41.5	0.004	0.005	20	122
458	35	123	7	4.89	0.650	0.631	0.658	0.200	0.200	40.3	0.008	0.013	28	133
529	35	119	9	4.89	0.649	0.657	0.645	0.200	0.200	40.2	0.011	0.013	36	132
459	35	175	4	7.35	0.648	0.624	0.668	0.200	0.201	40.2	0.013	0.016	14	132
530	35	169	5	7.35	0.647	0.636	0.651	0.200	0.201	40.2	0.013	0.015	26	160
460	35	211	-4	9.81	--	0.633	0.651	0.200	0.203	40.4	0.014	0.016	9	147
531	35	210	-3	9.81	--	0.633	0.699	0.200	0.201	43.7	0.017	0.018	14	192
461	40	58	6	1.99	0.676	0.638	0.611	0.200	0.200	42.5	0.010	0.013	20	88
532	40	52	6	1.99	0.689	0.662	0.689	0.200	0.200	43.4	0.005	0.006	20	132
462	40	111	-2	4.89	0.681	0.676	0.714	0.200	0.201	42.8	0.018	0.022	24	110
533	40	115	-2	4.89	0.680	0.671	0.695	0.200	0.200	42.8	0.011	0.013	20	145
463	40	164	-6	7.35	0.661	0.664	0.676	0.200	0.201	41.4	0.017	0.018	21	113
534	40	160	-6	7.35	0.670	0.678	0.665	0.200	0.201	42.1	0.015	0.017	33	135
464	40	214	-14	9.81	--	0.656	0.639	0.200	0.201	39.7	0.019	0.020	14	147
535	40	205	-15	9.81	--	0.670	0.700	0.200	0.201	44.3	0.018	0.019	25	162

Table 10 Cutting data

Work material: 2024-T4 aluminum alloy
Tool material: HSS (18-4-1); 3-deg end clearance
Cutting fluid: Air
Outside diameter of tube: 4.171 in.
Mean cutting speed: 789 fpm

Run No.	α	F_H	F_v	t_o	Chip Ratios r_l	r_t	r_w	w_o	w	ϕ	l_T Min.	l_T Max.	Chip Finish Tool	Chip Finish Air
537	10	77	38	1.99	0.518	0.556	0.543	0.200	0.200	29.2	0.004	0.005	41	143
536	10	151	58	4.89	0.584	0.570	0.590	0.200	0.201	33.0	0.014	0.015	8	258
538	10	205	58	7.35	--	0.625	0.660	0.200	0.204	36.3	--	0.017	14	255
539	10	244	54	9.81	--	0.679	0.724	0.200	0.205	39.4	0.017	0.018	--	--
540	15	78	31	1.99	0.553	0.638	0.506	0.200	0.200	31.9	--	0.005	23	138
541	15	148	49	4.89	0.590	0.583	0.602	0.200	0.202	33.9	--	0.014	8	203
542	15	193	43	7.35	--	0.620	0.649	0.200	0.202	37.0	0.017	0.018	13	257
543	15	235	36	9.81	--	0.657	0.690	0.200	0.203	38.8	0.018	0.019	15	230
544	20	64	22	1.99	0.588	0.626	0.576	0.200	0.200	34.6	0.006	0.008	29	128
545	20	159	39	4.89	0.590	0.600	0.579	0.200	0.201	34.8	0.014	0.015	17	193
548	20	137	39	4.89	0.596	0.590	0.595	0.200	0.201	35.2	--	--	14	190
546	20	189	33	7.35	--	0.639	0.648	0.200	0.203	38.1	0.017	0.017	8	222
547	20	225	23	9.81	--	0.678	0.703	0.200	0.202	41.0	0.018	0.019	10	230
549	25	68	18	1.99	0.615	0.594	0.559	0.200	0.200	37.0	0.008	0.010	27	135
550	25	136	26	4.89	0.607	0.608	0.611	0.200	0.201	36.6	0.013	0.014	20	187
551	25	188	24	7.35	--	0.609	0.695	0.200	0.201	41.7	0.018	0.019	10	207
552	25	218	11	9.81	--	0.659	0.680	0.200	0.201	40.9	0.020	0.021	8	222
553	30	53	13	1.99	0.649	0.646	0.654	0.200	0.200	39.7	0.008	0.009	25	80
554	30	124	15	4.89	0.622	0.637	0.629	0.200	0.021	38.0	0.010	0.012	21	150
555	30	175	10	7.35	--	0.651	0.627	0.200	0.201	38.4	0.010	0.014	7	160
557	35	54	10	1.99	--	0.661	0.655	0.200	0.200	40.6	0.008	0.010	28	103
558	35	123	7	4.89	--	0.430	0.608	0.200	0.200	37.6	0.014	--	15	197
559	35	168	1	7.35	--	0.623	0.652	0.200	--	40.5	0.015	0.016	13	227
560	35	205	-10	9.81	--	0.745	0.642	0.200	0.201	39.8	0.017	0.018	14	183
561	40	51	3	1.99	0.700	0.704	0.683	0.200	0.200	44.2	--	--	28	103
562	40	118	-2	4.89	0.666	0.680	0.673	0.200	0.200	41.7	--	--	123	147

Table 11 Cutting data

Work material: 6061-T6 aluminum alloy
Tool material: HSS (18-4-1); 3-deg end clearance
Cutting fluid: Air
Outside diameter of tube: 3.169 in.
Mean cutting speed: 573 fpm

Run No.	α	F_H	F_v	t_o	Chip Ratios r_l	r_t	r_w	w_o	w	ϕ	l_T Min.	l_T Max.	Chip Finish Tool	Chip Finish Air
484	20	120	51	4.89	0.467	0.437	0.490	0.200	0.201	27.5	--	--	10	115
488	25	51	16	1.99	0.499	0.486	0.495	0.200	0.200	29.8	0.025	0.031	10	102
485	25	110	36	4.89	0.512	0.491	0.523	0.200	0.201	30.6	0.006	0.008	7	117
486	25	159	54	7.35	0.511	0.513	0.507	0.200	0.201	30.6	0.016	0.020	8	125
487	25	206	77	9.81	0.495	0.496	0.499	0.200	0.202	29.5	0.021	0.032	6	138
489	30	50	15	1.99	0.531	0.594	0.523	0.200	0.200	32.1	0.009	0.011	7	93
490	30	95	23	4.89	0.560	0.573	0.575	0.200	0.200	33.9	0.016	0.018	10	120
493	30	101	24	4.89	0.556	0.543	0.586	0.200	0.200	33.8	--	--	10	102
491	30	145	37	7.35	0.544	0.538	0.570	0.200	0.200	32.9	0.024	0.029	10	130
492	30	193	55	9.81	0.532	0.543	0.544	0.200	0.201	32.1	0.028	0.032	6	117
494	35	47	11	1.99	0.563	0.633	0.583	0.200	0.200	34.3	0.012	0.014	5	78
495	35	89	14	4.89	0.604	0.608	0.627	0.200	0.201	37.1	0.015	0.018	9	113
496	35	133	20	7.35	0.589	0.580	0.603	0.200	0.200	36.1	0.021	0.026	6	107
497	35	180	39	9.81	0.570	0.570	0.594	0.200	0.201	34.6	0.021	0.028	9	97
498	40	41	9	1.99	0.599	0.618	0.597	0.200	0.200	36.6	0.007	0.009	6	97
499	40	89	6	4.89	0.645	0.676	0.639	0.200	0.200	40.2	0.016	0.018	7	105
500	40	120	9	7.35	0.621	0.689	0.643	0.200	0.200	38.4	0.024	0.026	7	108
501	40	159	15	9.81	0.632	0.603	0.635	0.200	0.200	39.8	0.025	0.029	8	107

Table 12 Cutting data

Work material: brass (85 Cu + 15 Zn) cold drawn
Tool material: HSS (18-4-1); 3-deg end clearance
Mean cutting speed: 472 fpm

Cutting fluid: Air
Outside diameter of tube: 3.462 in.

Run No.	α	F_H	F_v	t_o	Chip Ratios r_l	r_t	r_w	w_o	w	ϕ	l_T Min.	Max.	Chip Finish Tool	Air
564	20	162	48	4.01	0.353	0.345	0.362	0.181	0.184	20.7	--	--	6	103
591	20	155	36	4.01	0.349	0.363	0.374	0.181	0.184	20.4	--	--	5	90
563	20	183	53	4.89	0.358	0.362	0.374	0.181	0.182	20.9	--	--	3	110
565	20	223	62	6.31	0.362	0.364	0.391	0.181	0.183	21.2	--	--	3	100
592	20	215	56	6.31	0.359	0.351	0.371	0.181	0.186	21.0	--	--	4	100
566	20	294	73	8.84	0.368	0.388	0.376	0.181	0.184	21.5	--	--	5	97
593	20	284	71	8.84	0.363	0.383	0.389	0.181	0.186	21.3	--	--	7	127
567	20	340	102	11.10	0.368	0.399	0.378	0.181	0.184	21.5	--	--	3	100
594	20	339	83	11.10	0.375	0.392	0.389	0.181	0.187	22.0	--	--	5	113
577	25	77	17	1.99	0.362	0.367	0.363	0.181	0.181	21.2	--	--	5	77
595	25	75	18	1.99	--	0.435	0.378	0.181	0.181	22.1	--	--	5	70
568	25	140	30	4.01	0.376	0.380	0.377	0.181	0.181	22.1	--	--	3	83
596	25	138	28	4.01	0.377	0.376	0.379	0.181	0.182	22.1	--	--	2	92
569	25	195	41	6.31	0.382	0.381	0.397	0.181	0.182	22.4	--	--	4	103
597	25	208	39	6.31	0.380	0.378	0.412	0.181	0.183	22.3	--	--	7	107
570	25	282	55	8.84	0.392	0.384	0.394	0.181	0.183	23.1	--	--	2	103
598	25	265	56	8.84	0.384	0.387	0.392	0.181	0.185	22.6	--	--	3	113
571	25	327	55	11.10	0.383	0.404	0.786	0.181	0.184	22.5	--	--	4	107
599	25	322	59	11.10	0.390	0.401	0.409	0.181	0.188	22.9	--	--	5	110
576	30	64	12	1.99	0.385	0.372	0.384	0.181	0.181	22.4	--	--	8	73
600	30	73	9	1.99	0.405	0.405	0.402	0.181	0.181	23.7	--	--	8	32
572	30	125	15	4.01	0.400	0.398	0.419	0.181	0.182	23.4	--	--	3	97
601	30	124	19	4.01	0.403	0.385	0.395	0.181	0.181	23.6	--	--	5	95
573	30	176	16	6.31	0.411	0.405	0.386	0.181	0.181	24.1	--	--	6	97
602	30	182	24	6.31	0.406	0.406	0.416	0.181	0.183	23.7	--	--	8	100
574	30	239	17	8.84	0.418	0.417	0.427	0.181	0.181	24.6	--	--	7	113
603	30	229	19	8.84	0.417	0.424	0.436	0.181	0.183	24.6	--	--	2	107
575	30	274	24	11.10	0.416	0.424	0.440	0.181	0.181	24.4	--	--	5	97
604	30	275	22	11.10	0.428	0.436	0.446	0.181	0.183	25.2	--	--	5	105
578	35	59	4	1.99	0.433	0.418	0.426	0.181	0.181	25.2	--	--	5	67
605	35	60	6	1.99	0.433	0.408	0.425	0.181	0.181	26.1	--	--	7	70
579	35	112	1	4.01	0.441	0.435	0.447	0.181	0.181	25.9	--	--	2	78
606	35	108	3	4.01	0.437	0.423	0.433	0.181	0.181	25.5	--	--	5	88
580	35	164	0	6.31	0.446	0.442	0.449	0.181	0.181	26.2	--	--	2	77
607	35	156	0	6.31	0.443	0.426	0.417	0.181	0.181	25.9	--	--	5	90
581	35	210	-7	8.84	0.453	0.444	0.460	0.181	0.181	26.6	--	--	2	90
608	35	219	4	8.84	0.442	0.450	0.458	0.181	0.182	25.9	--	--	5	103
582	35	249	-8	11.10	0.454	0.469	0.466	0.181	--	26.7	--	--	2	78
609	35	251	-7	11.10	0.456	0.453	0.462	0.181	0.183	26.8	--	--	3	100
583	40	53	0	1.99	0.464	0.436	0.455	0.181	0.181	26.8	--	--	3	68
610	40	56	0	1.99	0.463	0.437	0.452	0.181	0.181	26.8	--	--	5	67
584	40	99	-6	4.01	0.468	0.456	0.464	0.181	0.181	27.1	--	--	5	77
611	40	100	-5	4.01	0.467	0.442	0.460	0.181	0.181	27.1	--	--	3	80
585	40	147	-9	6.31	0.472	0.465	0.476	0.181	0.181	27.5	--	--	7	80
612	40	144	-11	6.31	0.476	0.477	0.491	0.181	0.181	27.7	--	--	8	83
586	40	188	-14	8.84	0.475	0.475	0.488	0.181	0.181	27.7	--	--	4	85
613	40	188	-16	8.84	0.473	0.482	0.495	0.181	0.181	27.5	--	--	4	97
587	40	230	-23	11.10	0.481	0.488	0.498	0.181	0.181	28.0	--	--	4	82
614	40	238	-23	11.10	0.481	0.483	0.488	0.181	0.181	28.0	--	--	7	93

Journal of ENGINEERING FOR INDUSTRY

Information for Authors

• Manuscripts should be submitted in final form to the Editor. Each manuscript must be accompanied by a statement that it has not been published elsewhere nor has it been submitted for publication elsewhere. A paper which would occupy more than 8 pages of the Journal may be returned to the author for abridgment.

• The author should state his business connection, the title of his position, and his mailing address. A short abstract (50 to 100 words) should be included on the first page immediately preceding the introductory paragraph of the paper.

Three copies of the manuscript are required. One of these must be a carefully prepared printer's copy, typed in double spacing, on one side of the page only, with wide margins, on $8^1/_2$ by 11-in. opaque white paper. Mimeographed manuscripts, if prepared with exceptional care, can be accepted provided they are completely edited.

• As far as possible, all mathematical expressions should be typewritten. Greek letters and other symbols not available on the typewriter should be carefully inserted in ink. Care should be taken to distinguish between capital and lowercase letter, between zero (0) and the letter (*O*), between the numeral (1) and the letter (*l*), etc. A letter representing a vector cannot be printed with an arrow above or below it. The letter should be underscored with a single wavy line, wherever it appears in the text, to designate boldface type.

• A list of symbols carefully marked for the use of the editor (thus: κ, Greek l.c. kappa), if it has not been included in the body of the paper, should accompany the manuscript on a separate page.

• Before preparing a manuscript the author should study printed articles in the Journal, with special attention to the form and style of mathematical expressions, tables, footnotes, references, and abstract. Numbers that identify mathematical expressions should be enclosed in parentheses. Numbers that identify references at the end of the paper should be enclosed in brackets. Care should be taken to arrange all tables and mathematical expressions in such a way that they will fit into a single column when set in type. Equations that might extend beyond the width of one column (fractions that should not be broken or long expressions enclosed in parentheses) should be rephrased to go on two or more lines within column width. Fractional powers are preferred to root signs and should always be used in more elaborate formulas. The solidus should be used instead of the horizontal line for fractions wherever possible.

• A normal paper should not exceed 8 pages in the Journal. It is about 8000 words or 20 double-spaced typewritten pages exclusive of drawings. A Technical Brief should not exceed 750 words or about one page in the Journal inclusive of drawings.

• Originals and two copies of figures must accompany the manuscript. Line drawings should not be larger than $8^1/_2 \times 11$ in. and should be planned for reduction to column width. Lettering should be large enough to be clearly legible when the illustration is reduced. The originals of line drawings must be in India ink on white or pale blue tracing paper or tracing cloth. Photographs of equipment or test specimens must be glossy prints and should be used sparingly. Captions for figures should be typed double-spaced and included as the last page of the manuscript. The figure number and author's name should be written in the margin or on the back of each illustration.

• Titles of papers should be brief.

• Authors can obtain copies of the ASME Manual MS-4, "An ASME Paper," from the Editor and are urged to do so before drafting their papers in final form.

• Papers published in Journals of the Transactions of the ASME must be presented at a Meeting, either in person or by title. Scheduling of papers is in the hands of the Publications Committee.

• An author is entitled to 25 preprints free of charge (in the case of two authors, 15 each; three or more authors, 10 each). Larger quantities of preprints or reprints can be ordered from Editorial Department, The American Society of Mechanical Engineers, 29 West 39th Street, New York 18, N. Y. Quotations will be sent on request.

ASME Publications Committee

Please address all communications to:

Editor, ASME,

29 West 39th Street,

New York 18, N. Y.